December 2015

Ediacaran ocean redox evolution

Swapan Kumar Sahoo
University of Nevada, Las Vegas, sahoos@unlv.nevada.edu

EDIACARAN OCEAN REDOX EVOLUTION

By

Swapan Kumar Sahoo

Master's of Science – Geology
Tulane University
2006

Master's of Science – Geology
University of Calcutta, Kolkata, India
2003

Bachelor's of Science – Geology
University of Calcutta, Kolkata, India
2001

A dissertation submitted in partial fulfilment
of the requirements for the

Doctor of Philosophy – Geoscience

Department of Geoscience
College of Science
The Graduate College

University of Nevada, Las Vegas
December 2014

UNLV | GRADUATE COLLEGE

Dissertation Approval

The Graduate College
The University of Nevada, Las Vegas

November 14, 2015

This dissertation prepared by

Swapan Kumar Sahoo

entitled

Ediacaran Ocean Redox Evolution

is approved in partial fulfillment of the requirements for the degree of

Doctor of Philosophy – Geosciences
Department of Geoscience

Ganqing Jiang, Ph.D.
Examination Committee Chair

Kathryn Hausbeck Korgan, Ph.D.
Graduate College Interim Dean

Steven Rowland, Ph.D.
Examination Committee Member

Michael Wells, Ph.D.
Examination Committee Member

Timothy Lyons, Ph.D.
Examination Committee Member

Brian Hedlund, Ph.D.
Graduate College Faculty Representative

ABSTRACT

Ediacaran ocean redox evolution

By

Swapan Kumar Sahoo

Dr. Ganqing Jiang, Examination Committee Chair
Professor of Geology
University of Nevada, Las Vegas

The relative role that environmental versus intrinsic biological factors played in shaping the history of life on Earth is a fundamental but unanswered question in the natural sciences. Most famously, it has been heavily debated if the emergence and diversification of early animals during the Ediacaran Period (ca. 635–541 Ma) was tied to a rise in atmospheric-oceanic oxygen levels. Temporally discontinuous geochemical data and patchy fossil record in literature are inadequate to chart the Ediacaran redox history and its causal relationship with the biotic evolution. My PhD study aims for a multi-proxy geochemical record within a well-established stratigraphic framework of the Ediacaran (ca. 635–541 Ma) succession in South China. This succession is particularly suited for obtaining a high-resolution redox record based on redox-sensitive trace elements (RSEs) and pyrite sulfur isotopes due to the availability of organic-rich black shales. Modern-level RSE enrichments in black shales immediately overlying the Marinoan-age glacial diamictites reveal, for the first time, a pervasive ocean oxygenation event in the aftermath of the Earth's extreme cold. This oxygenation event may have triggered the first appearance of primitive animals in Earth history. Following this oxygenation, RSE concentrations returned back to crustal and near-crustal values until

the middle Ediacaran (ca. 580 Ma), implying significant ocean anoxia. Low RSE values appear again after spikes at ca. 580 Ma and ca. 550 Ma. The rises and falls of RSEs and pyrite sulfur isotopes document a dynamic Ediacaran (and likely including Cambrian) ocean redox state: multiple oxygenation events in the overall anoxic Ediacaran ocean. The brief (<5–10 Ma) oxygenation events may have triggered staged biotic innovations separated by long-term evolutionary stasis.

ACKNOWLEDGEMENTS

There is a Chinese proverb that “to know the road ahead, ask those coming back.” I’ve been fortunate enough to be surrounded by a great group of intellects who have guided me to the path, I am walking today. Among all those great mentors, who have inspired, advised, yet taught me to be challenged, I am most thankful to my mentor-adviser Ganqing Jiang. I would also like to extend my heartfelt gratitude to Michael Wells, Steve Rowland, Timothy Lyons and Brian Hedlund for their immense support and guidance. I’m also indebted to Dhrubojyoti Mukhopadhayay and Tapas Bhattacharjee for inspiring me in pursuing geology in the first place.

I’ve also been extremely fortunate to be surrounded by a great group of people in the University of Riverside Laboratory (The Lyon’s Lab). Perhaps, well it can’t be measured, but I owe many thanks to every member of the lab for teaching and helping me with the smallest lab issues to the greatest achievements. I owe to Jeremy Owens, Steve Bates, Chris Reinhart, Clint Scott, Noah Planavsky, Natascha Riedinger, and all of those in Tim’s lab. I also thank Nigel Hughes, Ryan McKenzie, Clara Lee, Lidya Tarhan and Noah Planavsky for their kindness and always making me feel welcome. I am also thankful to Brian Kendall for growing my interest in metal geochemistry.

I also need to thank the Department of Geosciences at University of Nevada, Las Vegas, especially Maria and Liz for their constant effort to make every graduate students’ life easier, and I was a hard one. All these years in Las Vegas would not have been possible without the support of so many friends, here at UNLV, as well as countless more around the world – most notably Laura Eaton, Bobby Henry, Lindsey Clark, Jeevan

Jayakody, Kelly Robertson, Dev Maharjan, Leon Taufani, Derek Adams, Michael Barrett, Merethe Lindanger and last but not the least Geoff Gilleaudeau.

I want to thank the friends in China University of Geocience (Beijing), particularly Xinqiang Wang. Without his support I couldn't have completed my field work and honestly, every walking step in China. My regards also goes to Professor Xiaoying Shi for his financial support when I did the field work in China and helps from his students, particularly Dongjie Tang (Peter).

Finally, I am grateful to have the ultimate trust and unconditional loyalty from my family -my mother, brother and my beloved wife through all the highs and lows. They gave me the support to bear the entire burden with patience, love, and courage which helped me to make it happen to this end. Thank you everyone, I express my gratitude to all of them who have kept me focused, and helped me to finally reach my goal.

DEDICATION

Clouds come floating into my life,

no longer to carry rain or usher storm,

but to add color to my sunset sky.

You can't cross the sea merely by standing and staring at the water.

—Rabindranath Tagore

Since my childhood days, I have always been dreaming of a simple life and blending into the nature. I still remember how I was taught to sit on a cow and plough the farms, go fishing all afternoon and perhaps all the minimalisms of life you can think about. Those ethics have ever since been embedded into my heart and soul and I still cherish them. Whatever I am today, is because of the lessons that I have got from my grandmother along with the nourishment and care of my mother. No matter how big of a storm was there, we survived, we were strong together and saw the sunlight in the foresight. Now, I want to build those in the future with the love of my life, my wife.

For those three amazing women in my life

– my grandmother, mother and my beloved wife.

TABLE OF CONTENTS

ABSTRACT ..... **iii**

ACKNOWLEDGEMENTS ..... **v**

DEDICATION ..... **vii**

CHAPTER 1 INTRODUCTION **1**

Introduction 1

References 4

CHAPTER 2 AN OXYGEN WINDOW IN THE WAKE OF THE MARINOAN GLACIATION **7**

1. Introduction 7

2. Main Article 8

3. References 19

CHAPTER 3 OXYGENATION EVENTS IN THE EDIACARAN OCEAN **30**

Abstract 30

1. Introduction 31

2. Stratigraphy, sampling, and analytical methods 34

3. Redox proxies 35

4. Results 36

5. Discussion 37

6. Conclusion 40

7. References 42

CHAPTER 4 METAL DISTRIBUTION IN EDIACARAN DOUSHANTUO BLACK SHALES: AN EXAMPLE TO TEST IRON SPECIATION AND METAL SEQUESTRATION UNDER EUXINIC CONDITIONS **47**

Abstract 47

1. Introduction 48

2. Background 52

2.1 Generalized stratigraphy 52

2.2 Depositional environments and age constraints 54

2.2.1 Member II black shales 56

2.2.2 Member IV black shales 57

3. Methods 58

3.1 Sample collection and preparation 58

3.2 Analytical methods 59

3.2.1 MicroProbe and SEM Analysis 59
3.2.2 XANES Experimental analysis 60
4. Results 61
4.1 Organic carbon and pyrite sulfur 61
4.2 Iron Speciation 62
4.2.1 Member II black shales 62
4.2.2 Member IV black shales 63
4.3 Molybdenum and other RSEs 64
4.4 Pyrite sulfur isotope 64
4.5 Pyrite framboid analysis 65
4.6 XANES Analysis of V oxidative state 66
5. Discussion 69
5.1 The origin of RSE variations in Member II black shales 69
5.2 Fe_T/Al ratios and the provenance of Member II and Member IV shales 72
6. Conclusion 77
7. References 78
APPENDIX A CHAPTER 2 86
1. Supplementary Inforamtion 86
1.1 Stratigraphy and paleogeographic reconstruction of the Doushantuo Formation 86
1.2 Sequence stratigraphic interpretation of the lower Doushantuo Formation 89
1.3 Sample location, paleobathymetric estimation, and age constraints 90
1.4 Notes on the Cryogenian–early Ediacaran paleontological record 92
1.5 Analytical methods 94
1.6 Trace elements as a redox tracer of ocean oxygenation 95
1.7 Iron speciation and redox fluctuations 97
1.8 Temporal Mo, V, U variations and redox fluctuations 100
1.9 The drop of RSE enrichments after the basal Doushantuo Formation shales 100
1.10 Molybdenum and Vanadium mass balance model 102
1.10.1 Overview of the modern Mo cycle 102
1.10.2 Overview of the modern V cycle 104
1.10.3 Mass balance equations and time-dependent modeling results 105
1.11 Secular trends in sulphur isotopes and Mo, V concentrations 109

1.11.1 Sulphur isotopes 109
1.11.2 Secular Mo, Mo/TOC variations 110
APPENDIX B CHAPTER 3 152
1. Data Repository 152
1.1 Depositional ages of the stratigraphic units in the Wuhe section, Guizhou Province, South China 152
1.2 Sampling 154
1.3 Analytical methods 154
APPENDIX C CHAPTER 4 174
CURRICULUM VITA 194

LIST OF TABLES

APPENDIX A CHAPTER 2

Supplementary Table S1 Iron speciation, TOC, and trace elemental data from the lower Doushantuo Formation: 112

Taoying section, Guizou Province, South China (Upper Slope) 112

Wuhe section, Guizou Province, South China (Lower Slope) 113

Yuanjia Section, Hunan Province, South China—(Basinal) 114

Supplementary Table S2 Reference list used for the compilation of the secular trends of Mo, Mo/TOC, V, and V/TOC, as used in Figure 3: 115

Supplementary Table S3A Data used for the compilation of the secular trends of Mo, Mo/TOC, V, and V/TOC: 117

Supplementary Table S3B Additional new data used for the compilation of the secular trends of Mo, Mo/TOC, V, and V/TOC: 151

APPENDIX B CHAPTER 3

Table DR1: Geochemical data from the Wuhe section 156

Table DR2: Summary of redox-sensitive trace element data of the Ediacaran-Early Cambrian (ca. 635–520 Ma) euxinic shales..... 160

APPENDIX C CHAPTER 4

Table 1: Geochemical data from the early Ediacaran and late Ediacaran black shales (ca. ~632 and ~551 Ma)..... 174

Member II, Wang'an section, Guizou Province, South China-Inner Shelf..... 174

Member II, Rongxi section, Hunan Province, South China-Shelf Margin..... 175

Member II, Taoying section, Guizou Province, South China-Upper Slope 176

Member II, Wuhe section, Guizou Province, South China-Lower Slope..... 178

Member II, Yuanjia Section, Hunan Province, South China-Basinal 180

Member II, Jiulongwan Section, Yangtze Geroges, South China-Inner Shelf 182

Member II, Zhongling Section, Yangtze Geroges, South China-Shelf Margin 183

Member IV, Rongxi section, Hunan Province, South China-Shelf 184

Member IV, Taoying section, Guizou Province, South China-Upper Slope..... 186

Member IV, Wuhe section, Guizou Province, South China-Lower Slope 187

Member IV, Jiulongwan Section, Yangtze Geroges, South China-Inner Shelf 178

Member IV, Zhongling Section, Yangtze Geroges, South China-Shelf Margin..... 189

Table 2: Micro Probe data for two selected Member II samples. 189

Table 3: Molybdenum concentration sensitivity test……..……....190

LIST OF FIGURES

CHAPTER 2

Figure 1 Locality maps and stratigraphy: 11

Figure 2 Trace metal abundance of Mo, Mo/TOC, V, V/TOC, U, U/TOC and pyrite sulphur isotopes ($\delta^{34}S_{pyrite}$) from the lower Doushantuo Formation black shales..... 16

Figure 3 Summary of redox sensitive trace elements and evolution of the ocean-atmosphere redox state..... 18

CHAPTER 3

Figure 1 Location map and paleogeographic location of the Wuhe section..... 33

Figure 2 Geochemical profiles of the Ediacaran–Early Cambrian strata in Wuhe section, South China..... 38

Figure 3 Compilation of RSE data from the Wuhe section and other Ediacaran–Early Cambrian euxinic shales 41

CHAPTER 4

Figure 1 The general patterns of Mo and Mo/TOC from the basal Doushantuo Member II and Member IV black shales 49

Figure 2 Locality maps and stratigraphic correlations..... 53

Figure 3 Shelf-to-basin transects 55

Figure 4 The pyrite sulfur isotope ($\delta^{34}S_{Py}$) gradient 65

Figure 5 V K-edge XANES spectra..... 68

Figure 6 Total iron (FeT) plotted versus aluminum (Al) for the Doushantuo Member II and Member IV black shales..... 73

Figure 7 Plots of TiO_2 vs. Al_2O_3 for Member II and Member IV black shales..... 76

APPENDIX A CHAPTER 2

Figure S1 Paleogeographic reconstruction of the Ediacaran Yangtze platform during the deposition of the Doushantuo Formation..... 87

Figure S2 Iron speciation data of the lower Doushantuo Formation:..... 99

Figure S3 Model results for seawater Mo and V changes through time: 108

Figure S4 Sulfur isotope composition of sedimentary sulphide ($\delta^{34}S_{Pyrite}$) and carbonate associated sulfate ($\delta^{34}S_{CAS}$) through time. time:..... 110

APPENDIX C CHAPTER 4

Figure S1 Iron speciation, Mo abundances and pyrite sulfur isotopes ($\delta^{34}S_{pyrite}$) of the Doushantuo Member II black shales..... 169

Figure S2 Iron speciation, Mo abundances and pyrite sulfur isotopes ($\delta^{34}S_{pyrite}$) of the Doushantuo Member IV black shales..... 171

Figure S3 Backscattered electron (BSE) images of framboids from Member II..... 173

CHAPTER 1

Introduction

Earth's ocean-atmosphere system was devoid of O_2 until very early in the Proterozoic Eon (pO_2 << 1% present atmospheric level [PAL]; Holland et al., 2006, Canfield, 2005; Shen et al., 2003), restricting eukaryotic evolution and primary productivity, and limiting organic–carbon burial (Anbar and Knoll, 2002). The protracted oxygenation of the ocean–atmosphere system is believed to have proceeded in two major steps. First, the early Proterozoic 'Great Oxidation Event' (GOE, ~2.4 Ga) marked the onset of sustained oxidative weathering on land (Holland 2006, Bekker et al., 2004). Atmospheric O_2 levels may have remained critically low, however, until a second significant rise in O_2 occurred during the late Neoproterozoic (~632–542 Ma), to near modern PAL (Canfield et al., 2007; Scott et al., 2008; Och and Shields-Zhou, 2012; Sahoo et al., 2012), finally paving the way for metazoan diversification.

Evidence for such protracted oxidation events are from direct geochemical studies—well established by carbon isotope record from carbonates, with sharp negative excursions (Halverson et al., 2005, Fike et al., 2006, McFadden et al., 2008), and redox-sensitive elements (RSE) record from sulfidic shales, where jumps in RSE (Mo, V and U) portrait expansion of the oceanic metal inventory, likely in response to a widely oxygenated ocean towards the end of the Proterozoic (~551 Ma, Scott et al., 2008; Bristow et al., 2009; Li et al., 2010). This link has further been supported by depleted pyrite sulfur isotopes ($\delta^{34}S_{Py}$) suggesting an overall increase in sulfate concentrations [SO_4^{2-}] in the deep ocean (Gorjan et al., 2000; Fike et al., 2006; Halverson and Hurtgen, 2007, McFadden et al., 2008, Li et al., 2010; Sahoo et al., 2012).

In South China, exceptionally well-preserved multicellular eukaryotes, including early animal embryos, algae, bilaterians, and morphologically differentiated benthic macrofossils has been reported vigorously from the Doushantuo and Lantian Formation (McFadden et al., 2008, Li et al., 2010, Yuan et al., 2011). It is important, however, to note that although metazoans certainly had evolved and diversified in the early Ediacaran (Yuan et al., 2011, Yin et al., 2007), animals with energetically expensive and O_2-demanding lifestyles (e.g., locomotion, carnivory, burrowing) appeared much later in the fossil record (< 590–558 Ma, Liu et al., 2010)—more than 40 million years after pervasive early Ediacaran (ca. 635–630 Ma) ocean oxygenation (Sahoo et al., 2012).

Chapter 2 represents geochemical studies from early Ediacaran black shales, which documents an increase in abundance of RSEs and the growth of the marine sulfate reservoir, immediately following the Marinoan glaciation. This study reveals evidence for an O_2 increase that may have promoted the appearance of early animals in the wake of the glaciation (c.a, 632 Ma; Sahoo et al., 2012). This oxygenation event places the Ediacaran oxidation more than 50 million years earlier from previous estimates of 580—551 Ma (Canfield and Teske, 1996, Fike et al., 2006, Canfield et al., 2007, McFadden et al., 2008).

Oxygenation in the latter half of the Ediacaran (551 Ma) was associated with major carbon cycle perturbations recorded in the marine carbon isotope record in South China (McFadden et al., 2008; Li et al., 2010) and the Shuram excursion in Oman (Fike et al., 2006). This oxygenation event is also marked by significant enrichments in redox sensitive trace metals, particularly molybdenum (Scott et al., 2008; Sahoo et al., 2012). Furthermore, both the early and late Ediacaran oxygenation events were associated with

biotic innovations—the appearance of primitive animals and oxygen-demanding animals (Xiao et al., 1998; Narbonne, 2003, 2005; McFadden et al., 2008).

The view from the mid-Ediacaran period between these two oxygenation events, however, is considerably more complex and implies unique ocean chemistry and is the primary focus of Chapter 3. The unusually low RSE values from a slope section at Wuhe either record pervasively anoxic/euxinic oceans (ferruginous ocean; Canfield, 1998; Canfield et al., 2008, Li et al., 2010) or signal of a restricted sedimentary basin. Sedimentological and isotope record from the Ediacaran Yangtze platform in general and sulfur isotope record of the Wuhe section do not support interpretation of a restricted basin. Instead, the rise and falls of RSEs most likely record temporal redox fluctuations of the Ediacaran ocean. This implies that oxygenation of the Ediacaran (and possibly Cambrian) ocean was not a unidirectional process as previously thought.

Significant spatial variations in RSE concentration are observed among time-equivalent "euxinic" shales of the Doushantuo Formation. Taking the face values of RSE concentration from a single section may lead to misinterpretations about the Ediacaran ocean chemistry. In chapter 4, I discuss various possibilities for RSE variability at stratigraphical intervals. Variable RSE values from stratigraphically correlatable black shales demonstrate local environmental controls on RSE concentrations across the shelf-to-basin transects.

References

Anbar, A. D. & Knoll, A. H., 2002, Proterozoic ocean chemistry and evolution: A bioinorganic bridge?: Science, v. 297, p. 1137–1142.

Bekker, A., Holland, H.D., Wang, P.-L., Rumble, D., III, Stein, H.J., Hannah, J.L., Coetzee, L., and Beukes, N.J., 2004, Dating the rise of atmospheric oxygen: Nature, v. 427, p. 117-120.

Bristow, T.F., and Kennedy, M.J., 2008, Carbon isotope excursions and the oxidant budget of the Ediacaran atmosphere and ocean: Geology, v. 36, p. 863-866.

Canfield, D.E., 2005, The early history of atmospheric oxygen: Homage to Robert M. Garrels: Annual Review of Earth and Planetary Sciences, v. 33, no. 1, p. 1-36.

Canfield, D.E. & Raiswell, R., Narbonne, G. M., 2007, Late-Neoproterozoic deep-ocean oxygenation and the rise of animal life: Science, v. 315, p. 92-95.

Canfield, D.E., Poulton, S.W., Knoll, A.H., Narbonne, G.M., Ross, G., Goldberg, T., and Strauss, H., 2008, Ferruginous Conditions Dominated Later Neoproterozoic Deep-Water Chemistry: Science, v. 321, no. 5891, p. 949-952.

Canfield, D.E., 1998, A new model for Proterozoic ocean chemistry: Nature, v. 396, p. 450-453.

Fike, D.A., Grotzinger, J.P., Pratt, L.M., and Summons, R.E., 2006, Oxidation of the Ediacaran Ocean: Nature, v. 444, p. 744–747.

Gorjan, P., Veevers, J., Walter, M., 2000. Neoproterozoic sulfur isotope variation in Australia and global implications: Precambrian Research, v. 100, p. 151–179.

Halverson, G.P., Hoffman, P.F., Schrag, D.P., Maloof, A.C., Rice, A.H.N., 2005. Toward

a Neoproterozoic composite carbon-isotope record: Geological Scoiety of America Bulletin, v. 117, p. 1181-1207.

Halverson, G.P., and Hurtgen, M.T., 2007, Ediacaran growth of the marine sulfate reservoir: Earth and Planetary Science Letters, v. 263, no. 1–2, p. 32-44.

Holland, H.D., 2006. The oxygenation of the atmosphere and oceans: Philos. T. Roy. Soc. B, v. 361, p. 903-915.

Li, C., Love, G.D., Lyons, T.W., Fike, D.A., Sessions, A.L., and Chu, X., 2010, A Stratified Redox Model for the Ediacaran Ocean: Science, v. 328, no. 5974, p. 80-83.

Liu, A. G., McLlroy, D., & Brasier, M. D., 2010, First evidence for locomotion in the Ediacara biota from the 565 Ma Mistaken Point Formation, Newfoundland: Geology, v. 38, p. 123–126.

McFadden, K.A., Huang, J., Chu, X., Jiang, G., Kaufman, A.J., Zhou, C., Yuan, X., and Xiao, S., 2008, Pulsed oxidation and biological evolution in the Ediacaran Doushantuo Formation: Proceedings of the National Academy of Sciences, USA, v. 105, p. 3197–3202.

Narbonnne, G., Gehling, J., 2003, Life after snowball: the oldest complex Ediacaran fossils: Geology, v. 31, p. 27–30.

Narbonne, G.M., 2005. The Ediacaran biota: Neoproterozoic origin of animals and their Ecoystems: Annual Reviews in Earth and Planetary Science, v. 33, p. 421-442.

Och, L.M., and Shields-Zhou, G.A., 2012, The Neoproterozoic oxygenation event: Environmental perturbations and biogeochemical cycling: Earth-Science Reviews, v. 110, p. 26-57.

Sahoo, S.K., Planavsky, N.P., Kendall, B., Wang, X., Shi, X., Scott, C., Anbar, A.D., Lyons, T.W., and Jiang, G., 2012, Ocean oxygenation in the wake of the Marinoan glaciation: Nature, v. 489, p. 546-549.

Scott, C., Lyons, T.W., Bekker, A., Shen, Y., Poulton, S.W., Chu, X., and Anbar, A.D., 2008, Tracing stepwise oxygenation of the Proterozoic ocean: Nature, v. 452, p. 456-459.

Shen, Y., Knoll, A.H., Walter, M.R., 2003. Evidence for low sulphate and anoxia in a mid-Proterozoic marine basin: Nature, v. 423, p. 632-635.

Xiao, S., Zhang, Y., Knoll, A.H., 1998. Three-dimensional preservation of algae and animal embryos in a Neoproterozoic phosphorite: Nature, v. 391, p. 553–558.

Yin, L., Zhu, M., Knoll, A.H., Yuan, X., Zhang, J., and Hu, J., 2007, Doushantuo embryos preserved inside diapause egg cysts: Nature, v. 446, p. 661–663.

Yuan, X., Chen, Z., Xiao, S., Zhou, S., Hua, H., 2011. An early Ediacaran assemblage of macroscopic and morphologically differentiated eukaryotes: Nature, v. 470, p. 390–393.

CHAPTER 2

An Oxygen Window in the Wake of the Marinoan Glaciation*

1. Introduction

Metazoans likely have their roots in the Cryogenian (Love et al., 2009; Maloof et al., 2010; Erwin et al., 2011), but there is a marked increase in the appearance of novel animal and algae fossils shortly after the termination of the late Cryogenian (Marinoan) glaciation about 635 million years ago (Ma) (Yin et al., 2007; McFadden et al., 2008; Yuan et al., 2011). It has been hypothesized that an oxygenation event in the wake of the severe Marinoan glaciation was the driving factor behind this early diversification of metazoans and shift in ecosystem complexity (Hoffman and Schrag, 2002; Planavsky et al., 2010), but there is little evidence for increase in ocean-atmosphere O_2 following the Marinoan glaciation and for a direct link between early animal and redox evolution in general (Och and Shields-Zhou, 2012). As such, models linking trends in early biological evolution to shifts in Earth system processes remain controversial (Butterfield, 2009). Here we report new geochemical data from early Ediacaran organic-rich black shales (~635–630 Ma) of the basal Doushantuo Formation in South China. High enrichments of molybdenum and vanadium and low pyrite sulphur isotope values ($\Delta^{34}S$ values $\geq$ 65‰) in these shales record expansion of the oceanic inventory of redox-sensitive metals and the growth of the marine sulphate reservoir in response to a widely oxygenated ocean. The data provide evidence for an early Ediacaran

* This chapter has been published in Nature: Sahoo, S. K., Planavsky, N. J., Kendall, B., Wang, X., Shi, X., Scott, C., Anbar, A. D., Lyons, T. W., and Jiang, G., 2012, Ocean oxygenation in the wake of the Marinoan glaciation: Nature, v. 489, no. 7417, p. 546-549.

oxygenation event, which predates the previous estimates for post-Marinoan oxygenation (Fike et al., 2006; Canfield et al., 2007; Scott et al., 2008) by more than 50 million years (Myr). Our findings seem to support a link between the most severe glaciations in Earth's history, the oxygenation of the Earth's surface environments, and the earliest diversification of animals.

2. Main Article

The rise of oxygen in Earth surface environments was protracted and is thought to have proceeded in two major steps. The ocean-atmosphere system was essentially devoid of oxygen until very early in the Proterozoic Eon, when atmospheric oxygen rose to > 1% of the present atmospheric level (PAL) (Holland, 2006; Canfield, 2005). The timing and dynamics of this initial oxygenation are under active investigation, but there is little doubt that a major atmospheric transition, the so-called "Great Oxidation Event" (GOE), occurred about 2.4 billion years ago (Ga) (Holland, 2006; Canfield, 2005). It is commonly assumed that there was a second significant rise to near modern atmospheric oxygen levels during the late Neoproterozoic (~750–542 Ma) (Holland, 2006; Canfield, 2005); however, the timing and magnitude of this second oxygenation event remain elusive (Och and Shields-Zhou, 2012; Canfield, 2005).

The appearance of metazoan fossils has traditionally been used as a minimum estimate for the timing of the late Neoproterozoic oxygenation event (Knoll and Caroll, 1999). Molecular clock estimates place the origin of crown-group animals in the Cryogenian Period (850–635 Ma) (Erwin et al., 2011). There are also sponge biomarkers (Love et al., 2009) and sponge-like fossils (Maloof et al., 2010) in Cryogenian or older rocks, but these are only simple metazoans with limited oxygen demands (see

supplementary information). Novel micro-and macrofossils interpreted as early metazoans appear immediately above Marinoan-age (~635 Ma) glacial deposits in South China (Yin et al., 2007; McFadden et al., 2008; Yuan et al., 2011) (see supplementary information). Further, there is a radiation in marine algae following the Marinoan glaciation, which is likely linked to a metazoan-driven shift in trophic structure and ecosystem complexity (Peterson and Butterfield, 2005). It has been proposed that this biological innovation is linked to an oxygenation event following the extensive Marinoan glaciation (Hoffman and Schrag, 2002; Planavsky et al., 2010). However, there is no direct geochemical evidence for an increase in ocean oxygenation in the immediate aftermath of the Marinoan glaciation. The predominance of existing geochemical evidence for late Neoproterozoic redox shift are much younger (~580–550 Ma), controversial, or record a local shift in redox conditions that may not be globally representative (Och and Shields-Zhou, 2012; Fike et al., 2006; Canfield et al., 2007; Scott et al., 2008).

Trace metal enrichments in black shales can record information about the global ocean redox state (Scott et al., 2008; Emerson and Huested, 1991; Hastings et al., 1996; Algeo and Lyons, 2006). Following the establishment of pervasive oxidative weathering after the GOE at ~2.4 Ga (Holland, 2006; Canfield, 2005), the size of the global marine reservoir of redox-sensitive elements (RSEs) is primarily controlled by the spatial extent of anoxic versus oxic marine conditions (Emerson and Huested, 1991; Hastings et al., 1996). In reducing marine environments, the burial fluxes of many RSEs, notably molybdenum (Mo) and vanadium (V), exceed those in oxygenated settings by several orders of magnitude. Hence, it follows that when oxic conditions are more widespread

the global seawater concentrations of these RSEs will be higher (Emerson and Huested, 1991). For example, in today's predominantly oxygenated oceans, Mo is the most abundant transition metal (~105 nM; Emerson and Huested, 1991), despite its very low crustal abundance (~1 ppm; Wadepohl, 1995). Because the residence time of Mo (800–440 kyrs) (Emerson and Huested, 1991; Miller et al., 2011) and V (~50 kyrs) (Emerson and Huested, 1991; Hastings et al., 1996) in seawater is much longer than the ocean mixing time (~1.5 kyrs), Mo and V in marine basins track the global average conditions (Emerson and Huested, 1991; Hastings et al., 1996; Algeo and Lyons, 2006; Miller et al., 2011). This concept is well-grounded in an understanding of the modern Mo and V global mass balances (Emerson and Huested, 1991; Hastings et al., 1996).

The magnitude of RSE enrichments in anoxic marine sediments reflect dissolved RSE concentrations in seawater (Algeo and Lyons, 2006; Lyons et al., 2009). In general, RSE enrichments also scale with the organic carbon flux because reduced, particle reactive metal species (e.g., thiomolybdate or vanadyl ions) are bound by organic particles, resulting in strong correlations between the metal and total organic carbon (TOC) contents in modern anoxically deposited sediments and black shales (Algeo and Lyons, 2006; Lyons et al., 2009). Therefore, authigenic enrichments are commonly normalized to TOC concentrations (e.g., Mo/TOC and V/TOC) (Lyons et al., 2009). RSE enrichments in anoxic shales may also depend on other factors, such as sedimentation rates and sulphide levels. However, studies in modern anoxic basins with access to the open ocean (Emerson and Huested, 1991; Hastings et al., 1996; Algeo and Lyons, 2006; Lyons et al., 2009) have shown that the dissolved metal concentrations exert a first order control on the degree of the enrichment (see supplementary information). This

relationship sets the stage for using RSE enrichments in anoxic shales to track Earth's oxygenation history and specifically the extents of anoxia in the ocean (Och and Shields-Zhou, 2012; Scott et al., 2008; Lyons et al., 2009).

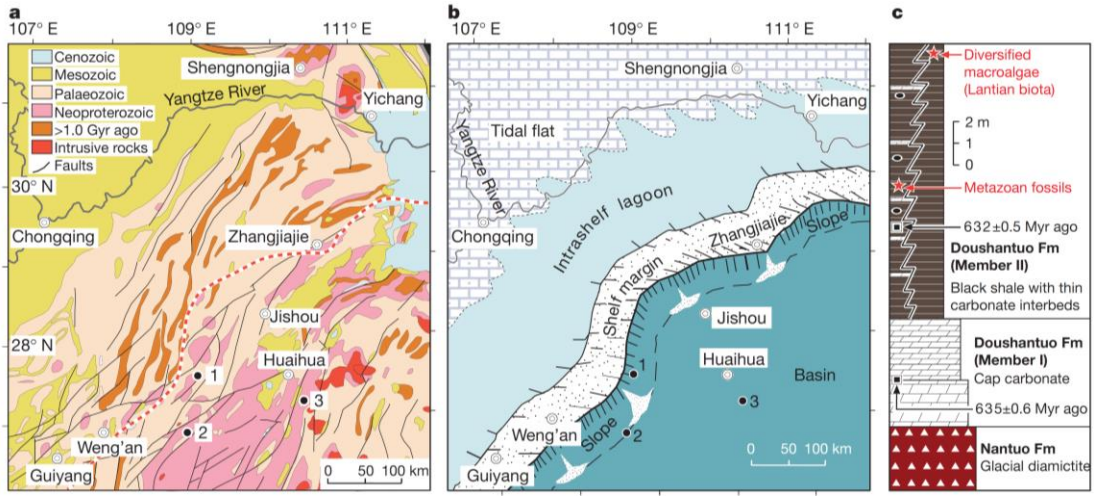

Figure 1 Locality maps and stratigraphy. a, Simplified geological map with location of sections (1–Taoying, 2–Wuhe, 3–Yuanjia). **b,** Paelogeographic model for the Doushantuo Formation (simplified from Jiang et al., 2011). **c,** Stratigraphy of the lower Doushantuo Formation with radiometric ages (Condon et al., 2005) and important fossil horizons marked (Yin et al., 2007; McFadden et al., 2008; Yuan et al., 2011).

The temporal record of RSE enrichments in shales deposited beneath an anoxic water column currently provides the least controversial and most direct geochemical signal for a significant redox shift in the late Neoproterozoic (Scott et al., 2008; Och and Shields-Zhou, 2012). However, the existing data only show a jump in RSE enrichments to Phanerozoic values near the end of the Ediacaran Period (~551 Ma) (Scott et al., 2008; Och and Shields-Zhou, 2012; Li et al., 2010), long after the radiation of complex metazoans including triploblastic animals (Yin et al., 2007; McFadden et al., 2008; Yuan et al., 2011; Pecoits et al., 2012). There is a pronounced data gap between this time and 663 Ma in previous analyses due to the lack of suitable open-marine, deep-water black

shale samples (Scott et al., 2008; Och and Shields-Zhou, 2012). Here, we fill this gap by analyzing organic-rich black shales of the basal Doushantuo Formation in South China that were likely deposited between 635 and 630 Ma (see supplementary information). We found very high, Phanerozoic-like RSE enrichments within a few Myrs after the Marinoan glaciation, coincident with the appearance of the earliest non-poriferan metazoan fossils (Yin et al., 2007; McFadden et al., 2008).

In South China, Marinoan-age glacial diamictites of the Nantuo Formation are overlain by a 3-to-6-m thick, 635.2±0.6 Myr old (Condon et al., 2005) cap-carbonate commonly referred to as Member I of the Doushantuo Formation (Fig. 1) (Jiang et al., 2011). The cap carbonate is conformably overlain by organic-rich black shales (Member II of the Doushantuo Formation), with subordinate carbonate layers and phosphorite-chert nodules in shelf and upper slope environments (Jiang et al., 2011) (see supplementary information). Putative metazoan fossils were found 6 meters above the Doushantuo cap carbonate in the Yangtze Gorges area (Yin et al., 2007; McFadden et al., 2008), less than two meters above an ash bed that has been dated as 632.5±0.5 Myr old (Condon et al., 2005). Morphologically complex macroscopic fossils of the Lantian biota (Yuan et al., 2011) were reported from slope-basinal black shales, approximately 15 meters above the cap carbonate (Fig. 1). Our geochemical analyses focus on the basal Member II black shales, which are roughly equivalent or slightly below these fossil horizons.

The basal Member II black shales have a transitional contact with the underlying cap carbonate (Jiang et al., 2010). Their widespread occurrence across the basin and lack of event beds (e.g., turbidites and olistostromes) suggest that they were deposited during

the latest stage of postglacial transgression or sea-level highstand, with the shelf-to-basin topography inherited from the Cryogenian (Jiang et al., 2011) (see supplementary information). We focused on deepwater Member II samples collected from three sections in an open-marine, slope-deep basin setting (Fig. 1). The black shales in the lower slope and basin sections contain an average of ~2.0 wt % of both pyrite iron (Fe_{Pyrite}) and total organic carbon (TOC) contents. The upper slope section has comparatively lower Fe_{Pyrite} (~0.3 wt% in average) and higher TOC (2.3 wt% in average) (Supplementary Table S1).

Slope and basin post-glacial black shales of Member II show strong Mo and V enrichments (Fig. 2). Mo enrichments in these sections commonly exceed the average Phanerozoic euxinic (anoxic and sulphidic) shale concentration of ~100 parts per million (ppm) and the Phanerozoic average Mo/TOC ratio (ppm/wt %) of ~25 (Scott et al., 2008; Och and Shields-Zhou, 2012). These high Mo enrichments constrain that the local water column was not only anoxic but also had free dissolved sulphide (euxinia) (Lyons et al., 2009). Vanadium enrichments of several thousand ppm are common and equivalent to the largest values observed in the Phanerozoic anoxic shale record (Och and Shields-Zhou, 2012) (Fig. 3). Similarly, uranium (U) in the lower Doushantuo Formation (Fig. 2) exceeds 30 ppm—equivalent to the largest enrichments observed in modern anoxic basins (Calvert and Pederson, 1993). Therefore, the magnitude of RSE enrichments used previously to argue for a late Neoproterozoic oxygenation event at ca. 551 Ma (Scott et al., 2008; Och and Shields-Zhou, 2012) are now found in > 630-Myr-old, early Ediacaran black shales (Fig. 3). It is well established that basin restriction, if anything, decreases the extent of RSE enrichment (Algeo and Lyons, 2006; Lyons et al., 2009), ruling out the possibility that the large enrichments have only local significance (see Supplementary

Information). Also, other factors, such as persistent or transient occurrences of oxygen in overlying waters, consistently mute the magnitude of RSE enrichment (Lyons et al., 2009). Hence, the large RSE enrichments in the lower Doushantuo Formation provide strong evidence for a significant global marine oxygenation event in the aftermath of the Marinoan glaciation.

Simple mass balance calculations confirm that the observed Mo and V enrichments in the lower Doushantuo Formation require a well-oxidized ocean (see Supplementary Information). Building from the global Mo and V cycles (Emerson and Huested, 1991; Hastings et al., 1996), it is possible to estimate the effects of increasing the riverine RSE flux on the marine Mo and V reservoirs. Even with a very elevated riverine flux of Mo and V, the marine redox landscape will control RSE reservoir sizes and thus RSE enrichments. For instance, based on mass balance calculations, even a doubling of the riverine Mo or V flux can be compensated for by relatively small growth in the extent of euxinia (e.g., 1-2% of the seafloor area; see Supplementary Fig. S3). Although continental Mo and V fluxes may have been elevated for short periods (thousands of years) during the most rapid stages of glacial retreat, glacially elevated fluxes are not expected during deposition of the examined black shales, which span a period of millions of years after glacial retreat. Mass balance calculations also indicate that even a relatively small areal increase (e.g., 2-3%) in anoxic seafloor would crash the Mo and V reservoirs at a time scale of $\leq$0.5 Myr (see Supplementary Information). Thus, the observed Mo and V enrichments in lower Doushantuo Formation black shales suggest that oxic waters bathed the vast majority of the ocean. Oxygen-deficient conditions must

have been spatially limited and only located where high organic matter loading caused oxygen depletion along ocean margins, such as in the Doushantuo basin.

Large variability in the magnitude of RSE enrichments in lower Doushantuo Formation black shales suggests locally variable redox conditions. There are intervals with high RSE enrichments adjacent (< 0.2 m) to intervals with near crustal, un-enriched RSE concentrations, despite apparently constant physical conditions (i.e., absence of wave-, storm-, and gravity-generated beds) well below the storm wave base (see Supplementary Information). These variations suggest significant redox shifts in environments and thus deposition of the units under mixed oxic, suboxic-ferruginous, and euxinic conditions. Redox fluctuations in deep-water environments well below the mixed layer, including those at an estimated depth of >1,000 meters in the basinal section (Jiang et al., 2010; Jiang et al., 2011) (see Supplementary Information), is consistent with a well-oxygenated global ocean-atmosphere system.

Intriguingly, all Mo, V, and U shift to lower values in the upper part of the basal Doushantuo black shales (Fig. 2). Given the observed variability in RSE enrichments within the basal unit, this drop in RSE enrichments may record a local environmental shift toward less reducing conditions that are not conducive to redox sensitive metal sequestration (see Supplementary Information). Alternatively, the drop of RSE values may record a shift back to more reducing ocean conditions typical of the mid-Proterozoic (~1800–700 Ma)—implying that the early Ediacaran oxygenation was not a unidirectional process (see Supplementary Information). This tantalizing possibility, however, requires a more comprehensive test in broader paleogeographic settings of the Nanhua basin and in other global successions.

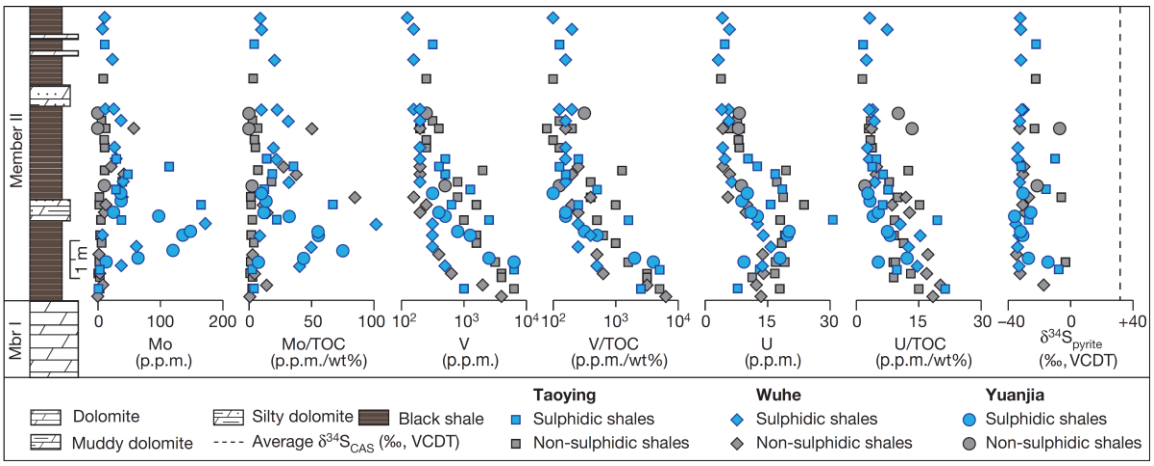

Figure 2 Trace metal abundance of Mo, Mo/TOC, V, V/TOC, U, U/TOC and pyrite sulphur isotopes ($\delta^{34}S_{pyrite}$) from the lower Doushantuo Formation black shales. The shape of data symbols indicates sample locations, including Taoying (upper slope section; square), Wuhe (lower slope section; diamond), and Yuanjia (basin section; circle). The color of data symbols is used to distinguish sulphidic (Fe_{Pyrite}/Fe_{HR} > 0.8; gray) from non-sulphidic (Fe_{Pyrite}/Fe_{HR} <0.8; light green) shales. The dashed line in the $\delta^{34}S_{pyrite}$ panel marks the average $\delta^{34}S_{CAS}$ value of the analyzed stratigraphic interval (McFadden et al., 2008; Li et al., 2010). Sulphur isotope data are reported as per mil (‰) deviations from the isotope composition of Vienna Cañon Diablo Troilite (VCDT).

Highly negative pyrite sulphur isotope ($\delta^{34}S_{pyrite}$) values down to –35‰ from the basinal samples (Fig. 2; Supplementary Table S1) further support our interpretation of an oxygenated ocean-atmosphere system following Marinoan deglaciation. Coeval (~635–630 Ma) carbonate-associated sulphur isotope ($\delta^{34}S_{CAS}$) values from shelf sections (McFadden et al., 2008; Li et al., 2010) have an average of ~34‰. In this framework, the calculated isotope fractionation between pyrite and coeval sulphate in the deep basin section is > 65‰—equivalent to maximum fractionations by modern sulphate reducing bacteria (Sim et al., 2011) and the maximum pyrite-coeval sulphate offset observed in the Phanerozoic rock record (Och and Shields-Zhou, 2012; Canfield and Raiswell, 1999) (Supplementary Fig. S4). An increase in the isotopic offset between pyrite and seawater sulphate in the late Neoproterozoic has been commonly linked to growth of the global

marine sulphate reservoir and surface oxidation (Och and Shields-Zhou, 2012; Canfield and Raiswell, 1999). The large sulphur isotope fractionation in the basal Member II shales, therefore, point toward a pervasively oxygenated ocean with lower associated pyrite burial, consistent with the conclusion drawn from RSE enrichments.

The shift to pervasively oxygenated oceans and, by inference, higher atmosphere O_2 conditions following the Marinoan glaciation may be linked to high nutrient availability (Planavsky et al., 2010). It has been proposed that there was a large marine phosphate reservoir during and following the Cryogenian glacial events (Hoffman and Schrag, 2002; Planavsky et al., 2010). Phosphate is commonly considered as the ultimate limiting nutrient on geological timescales, since nitrogen (N) can be supplied by biological nitrogen fixation from an essentially limitless atmospheric supply. Therefore, glacially induced perturbations to the phosphorous cycle may have triggered an organic carbon burial event (Jiang et al., 2010) that induced a shift toward higher oxygen levels.

This model, however, overlooks the potential for persistent N stress linked to trace metal biolimitation (Anbar and Knoll, 2002). In a broadly anoxic ocean chalcophilic trace metals (e.g., Mo, Cu, Cd) may be co-limiting nutrients and inhibit efficient N fixation—just as in the modern oxic marine system Fe stress limits N fixation over broad swaths of the ocean (Anbar and Knoll, 2002). Significant Mo biolimitation may have limited the organic carbon production and stabilized the redox state of the oceans through the mid-Proterozoic (Anbar and Knoll, 2002). In this light, a jump in sulphidic black shale Mo enrichments at the Cryogenian-Ediacaran transition likely records a shift in nutrient regimes as well as in global redox conditions.

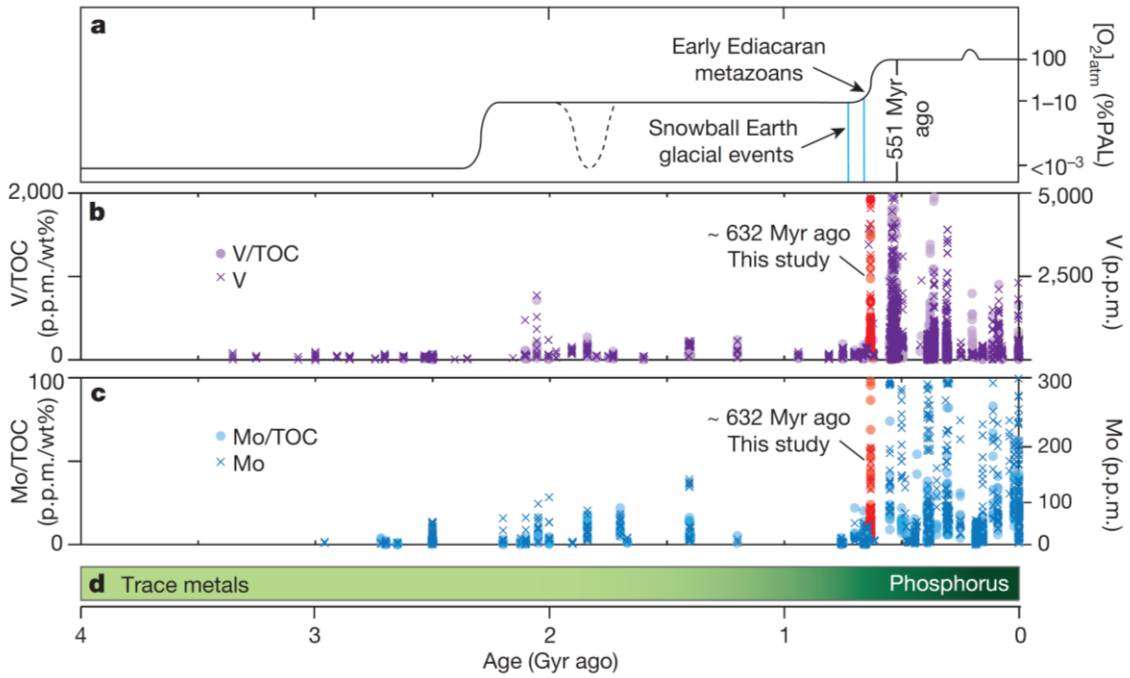

Figure 3. Summary of redox sensitive trace elements and evolution of the ocean-atmosphere redox state. a, Atmospheric oxygen levels compared with present atmospheric level (PAL). The early Ediacaran metazoans (Yin et al., 2007; McFadden et al., 2008) appeared shortly after the Marinoan glaciation, during an increase in ocean-atmosphere oxygen level (modified from Planavsky et al., 2010). **b,** Temporal trends in V enrichments (crosses) and V/TOC ratios (circles) in euxinic black shales (Supplementary Table S2). **c,** Temporal trends in Mo enrichments (crosses) and Mo/TOC ratios (circles) in euxinic black shales (Supplementary Table S2). The spikes of V, V/TOC, Mo, Mo/TOC, from the lower Doushantuo black shales (this study) are marked. **d,** Potential shift in nutrient limiting factor from trace metals to phosphorous after the Marinoan glaciation (Planavsky et al., 2010; Anbar and Knoll, 2002). Data compilation, stratigraphic and chronological details are provided in the Supplementary Information. The Mo and V records indicate that the ocean experienced a late Neoproterozoic growth in the inventory of redox-sensitive trace elements, which can be linked to ocean ventilation. This redox shift was previously thought to have occurred at ~551 Ma (Scott et al., 2008; Och and Shields-Zhou, 2012). Our study provides evidence for an oxygenation event associated with elevated seawater Mo–V enrichments and Mo/TOC–V/TOC ratios in the aftermath of the Marinoan glaciation, synchronous or slightly predating the earliest non-poriferan metazoan fossil record at ~632 Ma.

Marine chalcophilic trace metal levels following glacial retreat must have been sufficient to allow for significant organic carbon burial and the switch to a more pervasively oxygenated ocean. Dissolved marine Mo may have built up to critical levels

needed to move out of a marine system with chronic Mo-induced N stress during glaciation. A brief episode (e.g., thousands of years) of elevated Mo delivery associated with high rates of postglacial weathering prior to the deposition of the Doushantuo Member II shales may have also helped to provide the perturbation needed to overcome persistent Mo biolimitation. Mitigating coupled Mo-N stress would have allowed for efficient utilization of a large marine phosphate reservoir (Hoffman and Schrag, 2002; Planavsky et al., 2010) —ultimately promoting organic carbon burial and oxygen release. Ventilating the ocean would lead to significant growth of the Mo reservoir (and other RSE reservoirs) as manifest in the Member II shales deposited several million years after glacial retreat. The formerly enigmatic association of the "Snowball Earth" glaciations and early metazoan and algal diversification could thus be linked to shifts in nutrient availability, burial of organic carbon, and ultimately the shift to a more oxygenated ocean-atmosphere system that favored the early diversification of metazoan life and ecosystems.

3. References

Algeo, T.J., and Lyons, T.W., 2006, Mo-total organic carbon covariation in modern anoxic marine environments: Implications for analysis of paleoredox and paleohydrographic conditions: Paleoceanography, v. 21, no. 1.

Anbar, A. D. & Knoll, A. H., 2002, Proterozoic ocean chemistry and evolution: A bioinorganic bridge?: Science, v. 297, p. 1137–1142.

Brain, C. K., Prave, A. R., Hoffmann, K.-H., Fallick, A. E., Botha, A., Herd, D. A.,

Sturrock, C., Young, I., Condon, D. J. and Allison, S. G., 2012. The First Animals: ca. 760-million-year-old Sponge-like fossils from Namibia: South African Journal of Science, 108, Art. # 658, 8 pages.

Bristow, T.F., and Kennedy, M.J., 2008, Carbon isotope excursions and the oxidant budget of the Ediacaran atmosphere and ocean: Geology, v. 36, p. 863-866.

Brucker R. L. P., McManus J., Severmann S. and Berelson W. M., 2009, Molybdenum behavior during early diagenesis: insights from Mo isotopes. Geochem. Geophys. Geosyst. 10, Q06010.

Butterfield, N. J, 2009, Oxygen, animals and oceanic ventilation: an alternative view: Geobiology, v. 7, p. 1-7.

Calvert, S.E., and Pedersen, T.F., 1993, Geochemistry of Recent oxic and anoxic marine sediments: Implications for the geological record: Marine Geology, v. 113, no. 1-2, p. 67-88.

Canfield, D.E., 2005, The early history of atmospheric oxygen: Homage to Robert M. Garrels: Annual Review of Earth and Planetary Sciences, v. 33, no. 1, p. 1-36.

Canfield, D.E., Farquhar, J., & Zerkle, A.L., 2010, High isotope fractionations during sulfate reduction in a low-sulfate euxinic ocean analog: Geology, v. 38, p. 415-418.

Canfield, D.E. & Raiswell, R., Narbonne, G. M., 2007, Late-Neoproterozoic deep-ocean oxygenation and the rise of animal life: Science, v. 315, p. 92-95.

Canfield, D.E. & Raiswell, R., 1999, The evolution of the sulfur cycle: American Journal of Science, v. 299, p. 697-723.

Canfield, D.E. & Farquhar, J., 2009, Animal evolution, bioturbation, and the sulfate concentration of the oceans. : Proceedings of the National Academy of Sciences, USA, v. 106, p. 8123-8127.

Condon, D., Zhu, M., Bowring, S., Wang, W., Yang, A., and Jin, Y., 2005, U-Pb Ages from the Neoproterozoic Doushantuo Formation, China: Science, v. 308, p. 95-98.

Emerson, S.R., and Huested, S.S., 1991, Ocean anoxia and the concentrations of molybdenum and vanadium in seawater: Marine Chemistry, v. 34, p. 177-196.

Erwin, D.H., Laflamme, M., Tweedt, S.M., Sperling, E.A., Pisani, D., and Peterson, K.J., 2011, The Cambrian Conundrum: Early Divergence and Later Ecological Success in the Early History of Animals: Science, v. 334, p. 1091-1097.

Fike, D.A., Grotzinger, J.P., Pratt, L.M., and Summons, R.E., 2006, Oxidation of the Ediacaran Ocean: Nature, v. 444, p. 744–747.

Holland, H.D., 2006. The oxygenation of the atmosphere and oceans: Philos. T. Roy. Soc. B, v. 361, p. 903-915.

Halverson, G.P., and Hurtgen, M.T., 2007, Ediacaran growth of the marine sulfate reservoir: Earth and Planetary Science Letters, v. 263, no. 1–2, p. 32-44.

Hastings, D.W., Emerson, S.R., Erez, J., and Nelson, B.K., 1996, Vanadium in foraminiferal calcite: Evaluation of a method to determine paleo-seawater vanadium concentrations: Geochimica et Cosmochimica Acta, v. 60, no. 19, p. 3701-3715.

Hoffman, P.F., Halverson, G.P., Domack, E.W., Husson, J.M., Higgins, J.A., and Schrag, D.P., 2007, Are basal Ediacaran (635 Ma) post-glacial “cap dolostones” diachronous?: Earth and Planetary Science Letters, v. 258, no. 1–2, p. 114-131.

Hoffman, P.F., and Li, Z., 2009, A palaeogeographic context for Neoproterozoic glaciation: Palaeogeography, Palaeoclimatology, Palaeoecology, v. 277, no. 3–4, p. 158-172.

Hoffman, P.F., and Schrag, D.P., 2002, The snowball Earth hypothesis: testing the limits of global change: Terra Nova, v. 14, no. 3, p. 129-155.

Helz, G.R., Bura-Nakić, E., Mikac, N., and Ciglenečki, I., 2011, New model for molybdenum behavior in euxinic waters: Chemical Geology, v. 284, no. 3-4, p. 323-332.

Huldtgren, T., Cunningham, J.A., Yin, C., Stampanoni, M., Marone, F., Donoghue, P.C.J., and Bengtson, S., 2011, Fossilized Nuclei and Germination Structures Identify Ediacaran "Animal Embryos" as Encysting Protists: Science, v. 334, no. 6063, p. 1696-1699.

Ivantsov, A.Y., 2009, New reconstruction of Kimberella, problematic Vendian metazoan: Paleontology Journal, v. 43, p. 601–611.

Jiang, G., Shi, X., Zhang, S., Wang, Y., and Xiao, S., 2011, Stratigraphy and paleogeography of the Ediacaran Doushantuo Formation (ca. 635–551 Ma) in South China: Gondwana Research, v. 19, p. 831-849.

Jiang, G., Kennedy, M.J., and Christie-Blick, N., 2003a, Stable isotopic evidence for methane seeps in Neoproterozoic postglacial cap carbonates: Nature, v. 426, p. 822-826.

Jiang, G., Kennedy, M.J., Christie-Blick, N., Wu, H., and Zhang, S., 2006. Stratigraphy,

Sedimentary Structures, and Textures of the Late Neoproterozoic Doushantuo Cap Carbonate in South China: Journal of Sedimentary Research, v. 76, p. 978-995.

Jiang, G., Wang, X., Shi, X., Zhang, S., Xiao, S., and Dong, J., 2010, Organic carbon isotope constraints on the dissolved organic carbon (DOC) reservoir at the Cryogenian–Ediacaran transition: Earth and Planetary Science Letters, v. 299, no. 1–2, p. 159-168.

Jiang, S., Yang, J., Ling, H., Chen, Y., Feng, H., Zhao, K., and Ni, P., 2007, Extreme enrichment of polymetallic Ni–Mo–PGE–Au in Lower Cambrian black shales of South China: An Os isotope and PGE geochemical investigation: Palaeogeography, Palaeoclimatology, Palaeoecology, v. 254, no. 1–2, p. 217-228.

Jiang, G., Sohl, L.E., Christie-Blick, N., 2003a. Neoproterozoic stratigraphic comparison of the Lesser Himalaya (India) and Yangtze Block (South China); paleogeographic implications: Geology, v. 31, p. 917–920.

Kendall, B., Creaser, R.A., Calver, C.R., Raub, T.D., and Evans, D.A.D., 2009, Correlation of Sturtian diamictite successions in southern Australia and northwestern Tasmania by Re–Os black shale geochronology and the ambiguity of “Sturtian”-type diamictite–cap carbonate pairs as chronostratigraphic marker horizons: Precambrian Research, v. 172, no. 3–4, p. 301-310.

Kendall B., Reinhard C.T., Lyons T.W., Kaufman A.J., Poulton S.W. and Anbar A.D., 2010, Pervasive oxygenation along Late Archaean ocean margins: Nature Geoscience, v. 3, p. 647-652.

Knoll, A.H. and Carroll, S.B., 1999, Early animal evolution: emerging views from

comparative biology and geology: Science, v. 284, p. 2129–2137.

Li, C., Love, G.D., Lyons, T.W., et al., 2012, Evidence for a redox stratified Cryogenian marine basin, Datangpo Formation, South China: Earth and Planetary Science Letters, v. 331–332, no. 0, p. 246-256.

Li, C., Love, G.D., Lyons, T.W., Fike, D.A., Sessions, A.L., and Chu, X., 2010, A Stratified Redox Model for the Ediacaran Ocean: Science, v. 328, no. 5974, p. 80-83.

Li, Z.X., Bogdanova, S.V., Collins, A.S., et al., 2008, Assembly, configuration, and break-up history of Rodinia: A synthesis: Precambrian Research, v. 160, no. 1–2, p. 179-210.

Liu, P.J., Yin, C.Y., Gao, L.Z., Tang, F., Chen, S.M., 2009. New material of microfossils from the Ediacaran Doushantuo Formation in the Zhangcunping area, Yichang, Hubei Province and its zircon SHRIMP U–Pb age: Chinese Science Bulletin, v. 54, p. 1058–1064.

Liu, A. G., McLlroy, D., & Brasier, M. D., 2010, First evidence for locomotion in the Ediacara biota from the 565 Ma Mistaken Point Formation, Newfoundland: Geology, v. 38, p. 123–126.

Liu, B., Xu, X., Pan, X., Huang, H., Xu, Q., 1993. Paleocontinental Sediments, Crust Evolution and Ore Deposits of South China: Science Press, Beijing, pp. 1–236.

Love, G.D., Grosjean, E., Stalvies, C., Fike, D.A., Grotzinger, J.P., Bradley, A.S., Kelly, A.E., Bhatia, M., Bowring, S.A., Condon, D.J., and Summons, R.E., 2009, Fossil steroids record the appearance of Demospongiae during the Cryogenian period: Nature v. 457, p. 718-722.

Lyons, T.W., Anbar, A.D., Severmann, S., Scott, C., and Gill, B.C., 2009, Tracking euxinia in the ancient ocean: A multiproxy perspective and Proterozoic case study: Annual Review of Earth and Planetary Sciences, v. 37, p. 507-534.

Lyons, T.W., and Severmann, S., 2006, A critical look at iron paleoredox proxies: New insights from modern euxinic marine basins: Geochimica et Cosmochimica Acta, v. 70, no. 23, p. 5698-5722.

Maloof AC, Rose CV, Beach R, Samuels BM, Calmet CC. 2010, Possible animal-body fossils in pre-Marinoan limestones from South Australia: Nature Geoscience, v. 3, p. 653-659.

Morford, J.L., Emerson, S.R., Breckel, E.J., and Kim, S.H., 2005, Diagenesis of oxyanions (V, U, Re, and Mo) in pore waters and sediments from a continental margin: Geochimica et Cosmochimica Acta, v. 69, no. 21, p. 5021-5032.

McFadden, K.A., Huang, J., Chu, X., Jiang, G., Kaufman, A.J., Zhou, C., Yuan, X., and Xiao, S., 2008, Pulsed oxidation and biological evolution in the Ediacaran Doushantuo Formation: Proceedings of the National Academy of Sciences, USA, v. 105, p. 3197–3202.

McManus, J., Berelson, W.M., Severmann, S., Poulson, R.L., Hammond, D.E., Klinkhammer, G.P., and Holm, C., 2006, Molybdenum and uranium geochemistry in continental margin sediments: Paleoproxy potential: Geochimica et Cosmochimica Acta, v. 70, no. 18, p. 4643-4662.

Miller, C.A., Peucker-Ehrenbrink, B., Walker, B.D., and Marcantonio, F., 2011, Re-assessing the surface cycling of molybdenum and rhenium: Geochimica et Cosmochimica Acta, v. 75, no. 22, p. 7146-7179.

Mills, D., Ward L. M. & Canfield D. E, 2012, Oxygen constraints on the origin of metazoans: Astrobiology Science Conference, Atlanta, Georgia, Abstract # 1244.

Neuweiler, F., Turner, E.C., Burdige, D.J., 2009, Early Neoproterozoic origin of the metazoan clade recorded in carbonate rock texture: Geology, v. 37, p. 475–478.

Och, L.M., and Shields-Zhou, G.A., 2012, The Neoproterozoic oxygenation event: Environmental perturbations and biogeochemical cycling: Earth-Science Reviews, v. 110, p. 26-57.

Pecoits, E., Konhauser, K.O., Aubet, N.R., Heaman, L.M., Veroslavsky, G., Stern, R.A., and Gingras, M.K., 2012, Bilaterian Burrows and Grazing Behavior at > 585 Million Years Ago: Science, v. 336, p. 1693-1696.

Peterson, K.J., & Butterfield, N.J., 2005, Origin of the Eumetazoa: Testing ecological predictions of molecular clocks against the Proterozoic fossil record: Proceedings of the National Academy of Sciences, USA, v. 102, p. 9547-9552.

Planavsky, N., 2009, Early Neoproterozoic origin of the metazoan clade recorded in carbonate rock texture: Comment. Geology, v. 37, e195.

Planavsky, N.J., Rouxel, O.J., Bekker, A., Lalonde, S.V., Konhauser, K.O., Reinhard, C.T., Lyons, T.W., 2010. The evolution of the marine phosphate reservoir: Nature, v. 467, p. 1088–1090.

Poulton, S.W., Fralick, P.W. & Canfield, D.E., 2004, The transition to a sulphidic ocean ~1.84 billion years ago: Nature, v. 431, p. 173-177.

Poulton, S.W., and Canfield, D.E., 2005, Development of a sequential extraction procedure for iron: implications for iron partitioning in continentally derived particulates: Chemical Geology, v. 214, no. 3–4, p. 209-221.

Poulson, R.L., Siebert, C., McManus, J., & Berelson, W.M., 2006, Authigenic molybdenum isotope signatures in marine sediments: Geology, v. 34, p. 617-620.

Raiswell, R. & Canfield, D.E., 1998, Sources of iron for pyrite formation in marine sediments. American Journal of Science, v. 298, p. 219-245.

Rose, C.V., and Maloof, A.C., 2010, Testing models for post-glacial 'cap dolostone' deposition: Nuccaleena Formation, South Australia: Earth and Planetary Science Letters, v. 296, no. 3–4, p. 165-180.

Schiffbauer, J.D., Xiao, S., Sen Sharma, K., Wang, G., 2012. The origin of intracellular structures in Ediacaran metazoan embryos: Geology, v. 40, p. 223-226.

Scott, C., Lyons, T.W., Bekker, A., Shen, Y., Poulton, S.W., Chu, X., and Anbar, A.D., 2008, Tracing stepwise oxygenation of the Proterozoic ocean: Nature, v. 452, p. 456-459.

Severmann, S., Lyons, T. W., Anbar, A., McManus, J., and Gordon, G., 2008, Modern iron isotope perspective on the benthic iron shuttle and the redox evolution of ancient oceans: Geology, v. 36, p. 487–490.

Shields, G., Kimura, H., Yang, J., and Gammon, P., 2004, Sulphur isotopic evolution of Neoproterozoic-Cambrian seawater: new francolite-bound sulphate δ34S data and a critical appraisal of the existing record: Chemical Geology, v. 204, p. 163-182.

Sim, M.S., Bosak, T., & Ono, S., 2011, Large sulfur isotope fractionation does not require disproportionation: Science, v. 333, p. 74-77.

Smetacek, V., 2001, A watery arms race: Nature, v. 411, p. 745.

Tribovillard, N., Algeo, T.J., Lyons, T., and Riboulleau, A., 2006, Trace metals as paleoredox and paleoproductivity proxies: An update: Chemical Geology, v. 232, no. 1–2, p. 12-32.

Vernhet, E., Heubeck, C., Zhu, M.-., and Zhang, J.-., 2007, Stratigraphic reconstruction of the Ediacaran Yangtze platform margin (Hunan province, China) using a large olistolith: Palaeogeography, Palaeoclimatology, Palaeoecology, v. 254, no. 1–2, p. 123-139.

Wang, L., Shi, X., and Jiang, G., 2012, Pyrite morphology and redox fluctuations recorded in the Ediacaran Doushantuo Formation: Palaeogeography, Palaeoclimatology, Palaeoecology, v. 333–334, no. 0, p. 218-227.

Wedepohl, K., 1995, The composition of the continental crust: Geochimica et Cosmochimica Acta, v. 59, no. 7, p. 1217-1232.

Xiao, S., A. H. Knoll, J. D. Schiffbauer, C. Zhou, X. Yuan, 2012, Comment on Fossilized nuclei and germination structures identify Ediacaran animal embryos as encysting protists: Science, v. 335: p. 1169c.

Xiao, S., Zhang, Y., Knoll, A.H., 1998. Three-dimensional preservation of algae and animal embryos in a Neoproterozoic phosphorite: Nature, v. 391, p. 553–558.

Xiao, S., McFadden, K.A., Peek, S., Kaufman, A.J., Zhou, C., Jiang, G., and Hu, J., 2012, Integrated chemostratigraphy of the Doushantuo Formation at the northern Xiaofenghe section (Yangtze Gorges, South China) and its implication for Ediacaran stratigraphic correlation and ocean redox models: Precambrian Research, v. 192–195, no. 0, p. 125-141.

Yin, L., Zhu, M., Knoll, A.H., Yuan, X., Zhang, J., and Hu, J., 2007, Doushantuo

embryos preserved inside diapause egg cysts: Nature, v. 446, p. 661–663.

Yuan, X., Chen, Z., Xiao, S., Zhou, S., Hua, H., 2011. An early Ediacaran assemblage of macroscopic and morphologically differentiated eukaryotes: Nature, v. 470, p. 390–393.

Zhang, S., Jiang, G., Han, Y., 2008c. The age of the Nantuo Formation and Nantuo glaciation in South China: Terra Nova, v. 20, p. 289–294.

Zhou, C., Xie, G., Mcfadden, K., Xiao, S., Yuan, X., 2007. The diversification and extinction of Doushantuo-Pertatataka acritarchs in South China: causes and biostratigraphic significance: Geological Journal, v. 42, p. 229–262.

Zhou, C., Bao, H., Peng, Y., Yuan, X., 2010. Timing the deposition of ^{17}O-depleted barite at the aftermath of Nantuo glacial meltdown in South China: Geology, v. 38, p. 903–906.

Zhu, M., Zhang, J., and Yang, A., 2007, Integrated Ediacaran (Sinian) chronostratigraphy of South China: Palaeogeography, Palaeoclimatology, Palaeoecology, v. 254, no. 1–2, p. 7-61.

CHAPTER 3

Oxygenation Events in the Ediacaran Ocean*

Abstract

The late Neoproterozoic ocean is envisioned to have gone through a unidirectional oxygenation during the earliest (ca. 635 Ma), middle (ca. 580 Ma), or late (ca. 560 Ma) Ediacaran, but temporally discontinuous geochemical data and the metazoan fossil record fail to document a progressively oxygenated Ediacaran ocean, particularly for the early Ediacaran (ca. 635–580 Ma). To better understand marine redox evolution during this interval we carried out a multi-proxy paleoredox study in a deep-water section in South China that spans the Ediacaran Period. Iron speciation and pyrite morphology indicate locally euxinic environments throughout the Ediacaran in this section. In the same rocks, sulfur isotope data and enrichment patterns of redox sensitive elements provide evidence for multiple oxygenation events in an overall anoxic Ediacaran-Early Cambrian ocean. The duration of these oxygenation events may be comparable to those of the anoxic events in oxygenated Phanerozoic oceans. While anoxic events caused mass extinctions followed by fast recovery in biologically diversified Phanerozoic oceans, oxygenation events in ecologically monotonous anoxic Ediacaran-Early Cambrian oceans may have stimulated biotic innovations followed by prolonged evolutionary stasis.

* This chapter has been submitted to a journal for review for publication.

1. Introduction

The Ediacaran Period (635–541 Ma) is generally thought to mark a fundamental shift in Earth's surface redox state and encompasses the emergence of complex ecosystems (Och and Shields-Zhou, 2012; Xiao, 2014). Metazoans first appeared in the earliest Ediacaran (Yin et al., 2007) or during the Cryogenian (Love et al., 2009; Erwin et al., 2011), yet evidence of animals with energy-expensive and O_2-demanding lifestyles, such as motility and predation, appear much later in the fossil record (< 590–558 Ma; Erwin et al., 2011; Pecoits et al., 2012). This pattern of an early appearance but late ecological diversification may be tied to shifts in the oxidizing capacity of Earth's surface throughout the Ediacaran (e.g., Erwin et al., 2011; Sperling et al., 2013).

Currently, there are seemingly contradictory views of Ediacaran marine redox evolution. Several records suggest ocean oxygenation around 580 Ma, the time period following the last of the major Neoproterozoic glaciations (Fike et al., 2006; Canfield et al., 2007; McFadden et al., 2008; Scott et al., 2008). More recently, it has been argued that there were well-oxygenated oceans in the early Ediacaran (ca. 635–630 Ma), in the immediate aftermath of the Marinoan glaciation (Sahoo et al., 2012). Both of these views seemly conflict with evidence for widespread anoxic conditions and with a lack of evidence of ocean ventilation in some Ediacaran basins (e.g., Johnston et al., 2013). Further, most of the Ediacaran seems to be a time period during which Fe was common in anoxic water columns, instead of sulfide. This is a common feature in Earth's early history (Poulton and Canfield, 2011), when generally reducing conditions prevailed, but is extremely rare in well-oxygenated, sulfate-rich Phanerozoic oceans.

A new, stratigraphically continuous window into Ediacaran marine redox conditions is needed to reconcile apparently conflicting views about the Ediacaran redox evolution. In this paper we report a multi-proxy study that constrains local and global redox conditions of the Ediacaran ocean from a deep-water section at Wuhe, South China (Fig. 1). The Wuhe section is ideally suited for tracking the Ediacaran ocean redox evolution because (1) it was paleogeographically located in the slope of the Ediacaran Yangtze platform (Fig. 1B; Jiang et al., 2011), a passive margin developed in the southeastern side of the Yangtze Block (YB) that was well connected with the open ocean during the Ediacaran-Early Cambrian (Fig. 1A; Zhang et al., 2013, 2014) and (2) relatively complete Ediacaran strata in this section are dominated by organic-rich black shales that allow currently available redox proxies to capture the paleoceanographic signal.

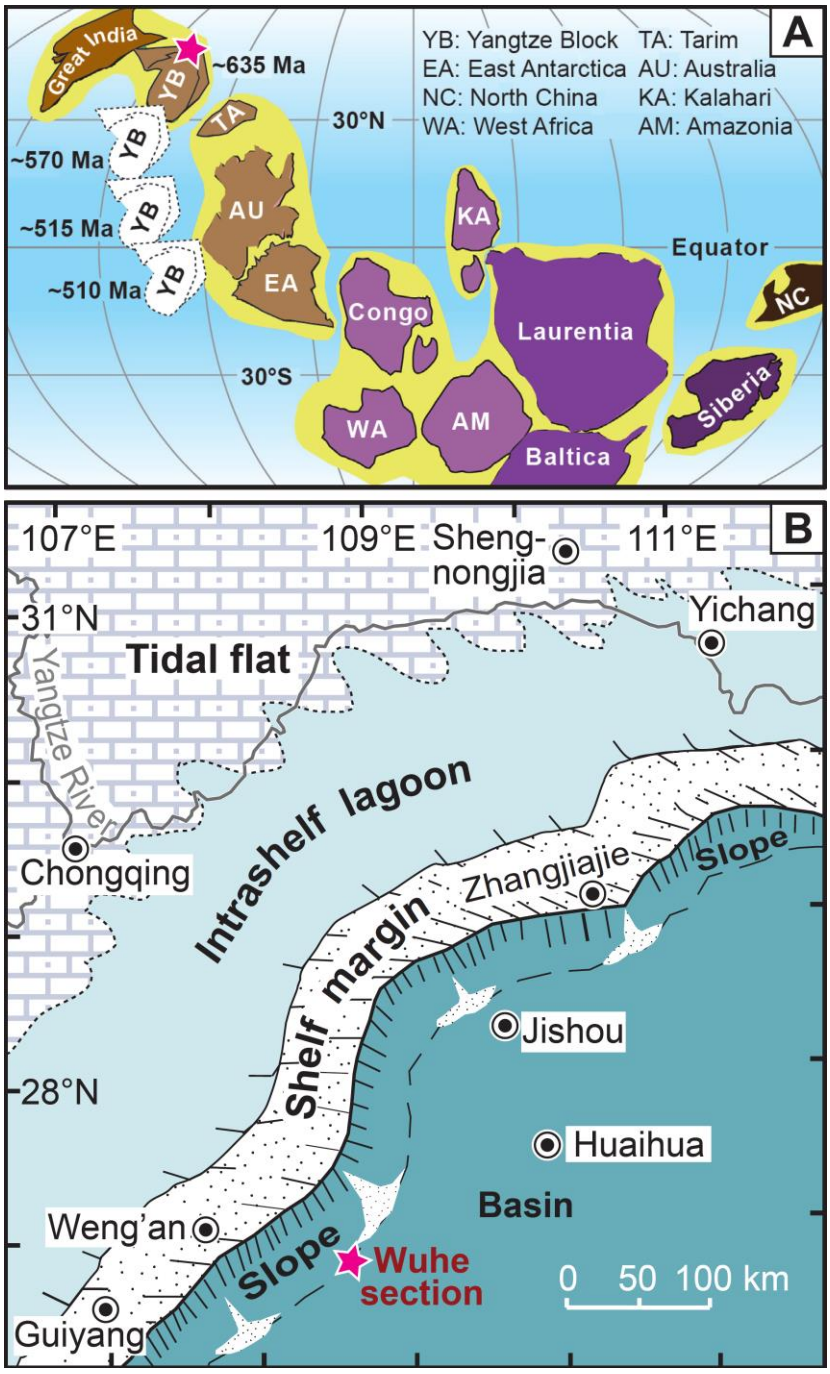

Figure 1. Location map and paleogeographic location of the Wuhe section. A: Location of the Yangtze Block (YB) in global reconstruction at ca. 635 Ma (Zhang et al., 2013) and its latitudinal change from ca. 635 Ma to ca. 510 Ma (dashed outlines; Zhang et al., 2014). Existing paleomagnetic data indicate that the YB was most likely an isolated continent block well connected with the open ocean during the Ediacaran-Early Cambrian (Zhang et al., 2014). **B:** Paleogeographic location of the Wuhe section on the Ediacaran Yangtze platform, along the southeast margin of the YB (after Jiang et al., 2011).

2. Stratigraphy, sampling, and analytical methods

Well-exposed strata at the Wuhe section include the Doushantuo (DST; 120 m), Dengying (DY; 12 m), Liuchapo (LP; 40 m) formations and a few meters of the basal Niutitang (NTT) Formation. The DST Formation can be divided into four members (Members I–IV; Fig. 2) that are roughly correlative to those in the Yangtze Gorges area (Jiang et al., 2011). The DST Formation is dominated by laminated black shales with subordinate dolostone beds. The DY Formation is composed of microcrystalline dolostone with chert beds or nodules. The overlying LP Formation consists of black cherts with thin black shale interbeds, which is in turn overlain by organic-rich black shale of the NTT Formation.

Based on the distinctive marker beds and regional stratigraphic correlation, the base and top of the DST Formation are reasonably assigned as ca. 635 Ma and ca. 551 Ma, respectively, and the Member II-Member III transition might be time-equivalent with the Gaskiers glaciation at ca. 580 Ma (Data Repository). The LP-NTT boundary is traditionally considered as the Ediacaran-Cambrian (E-C) boundary, but a recent U-Pb age of 522.7 ± 4.9 Ma (Wang et al., 2012a) from the base of the NTT in an adjacent section suggests that the E-C boundary may be located within the LP Formation (Fig. 2). Thus, we are confident that the measured section covers the entire Ediacaran Period.

Black shale samples were collected at an average spacing of 20-50 cm. Geochemical analyses were completed at the University of California, Riverside (UCR) and Arizona State University (ASU), following published methods (see Data Repository).

3. Redox proxies

We use the well-established, empirically calibrated iron (Fe) speciation proxy data to identify local water column redox conditions. These inferred local conditions then provide the background for our interpretations of regional/global marine redox based on redox sensitive element (RSE) and sulfur isotope (δ34S) geochemistry. Black shales with FeHR/FeT > 0.38 are indicative of Fe scavenging under an anoxic water column (Poulton and Canfield, 2011). Similarly, FeT/Al ratios greater than 0.5 in continental margin sediments is an indicator of water column anoxia (Lyons and Severmann, 2006). Anoxic shales with FePY/FeHR > 0.7 are considered to represent deposition under euxinic conditions, whereas FePY/FeHR < 0.7 represents ferruginous conditions (Poulton and Canfield, 2011). Independent evidence of euxinic conditions are pyrite framboid diameters (PFD) of less than 10 μm (e.g., Wilkin et al., 1996).

If black shales can be independently determined to have been deposited under locally euxinic conditions, the degree of RSE enrichments (Mo, U, Re, V, Cr) can be used to track first order shifts in the global marine redox state (Emerson and Huested, 1991; Lyons et al., 2009). This idea builds from two key principles: (1) the global marine redox landscape is the primary control on the size of the dissolved ocean RSE reservoir (Emerson and Huested, 1991) and (2) the RSE reservoir exerts a first order control on RSE enrichments in euxinic sediments (Lyons et al., 2009). This approach is most clearly illustrated in euxinic sections that capture Phanerozoic Ocean Anoxic Events: large drops in RSE enrichments correspond to the peak of anoxic conditions on a global scale (Hetzel et al., 2009). Sulfur isotopes complement the Fe and RSE proxies by providing a means

to track the global redox controlled sulfur (pyrite) burial fluxes and local sulfur redox transformations (Lyons et al., 2009).

4. Results

At the Wuhe section (Fig. 2 and Table DR1), the DST Formation shows a marked enrichment in Fe_{HR}/Fe_T ratios (0.72 ± 0.19) and extremely low levels of ferric oxides (0.07 ± 0.18). Through most of the section, Fe_T/Al ratios (0.52 ± 0.21) are elevated relative to typical continental margin sediments. The Fe_{PY}/Fe_{HR} ratios (0.87 ± 0.13) are consistently high, and there is a strong correlation (R^2 = 0.91) between Fe_{HR} and Fe_{PY}. Further, the entire succession is characterized by abundant small diameter pyrite framboids (mean PFD = 5.4 ± 0.6 μm; n = 5274; Wang et al., 2012b).

There are three discrete intervals (ca. 635 Ma basal Member II, ca. 580 Ma basal Member III, and ca. 551 Ma Member IV) with high Mo, V, Cr, Re, and U enrichments (Fig. 2). High RSE values (1–172 ppm of Mo, 10^2–10^4 ppm of V, 3-16 ppm of U, 4–700 ppb of Re, and 25–201 ppm of Cr) and $\delta^{34}S_{PY}$ values down to –34.6‰ (Fig. 2; Zone A) occur in basal Member II, followed by a progressive shift to low, crustal RSE concentrations (2–5 ppm of Mo, 80–100 ppm of V, 3–5 ppm of U, 3–46 ppb of Re, and 34–88 ppm of Cr) and a shift to high $\delta^{34}S_{PY}$ values (from –35‰ to +6‰) spanning from 10 m to 60 m. At the base of Member III, we again observe high RSE values (7–15 ppm of Mo, 10^2–10^4 ppm of V, 16–19 ppm of U, 10–10^3 ppb of Re, and 230–1422 ppm of Cr) and low $\delta^{34}S_{PY}$ values down to –21.5‰ (Fig. 2; Zone B). Shortly after this enrichment zone, RSE values again decrease up section to near crustal levels, and $\delta^{34}S_{PY}$ increases up to +6‰ in middle-upper Member III. Lastly, in Member IV there is a third positive shift

(Fig. 2; Zone C) of RSE enrichments (2–126 ppm of Mo, 10^1–10^4 ppm of V, 3–32 ppm of U, 10–10^3 ppb of Re, and 28–508 ppm of Cr) and a decrease of $\delta^{34}S_{PY}$ down to –23.3‰. The overlying LP Formation witnesses another drop in RSE values and increase in $\delta^{34}S_{PY}$.

5. Discussion

Based on the Fe proxies and PFDs, the Wuhe section was deposited under near persistent euxinic conditions throughout the Ediacaran. Further, the abundance of small diameter framboidal pyrites and a lack of Fe oxides indicate limited late stage sulfide mineralization or oxic alteration. This environmental context, coupled with the lack of evidence for shifts in the degree of basin isolation (Jiang et al., 2011; Zhang et al., 2014), sets the stage for using the degree of RSE enrichments to track the evolution of Ediacaran global marine redox landscape.

The periods with substantial RSE enrichments indicate the presence of large marine RSE reservoirs and thus a well-oxygenated ocean. Again this idea builds from the notion that RSE reservoirs are controlled by the extent of anoxia on a global scale and that RSE enrichments in anoxic shales track the size of the oceanic RSE reservoir (Lyons et al., 2009; Reinhard et al., 2013). The RSE enrichments at ca. 635 Ma, ca. 580 Ma, and ca. 551 Ma are comparable to the levels found in Phanerozoic anoxic shales (Och and Shields-Zhou, 2012), which intuitively suggest comparable marine redox conditions—that is, widespread oxic conditions. Crustal (majority of Member II) or near crustal (majority of Member III) RSE values through most of the persistently anoxic Wuhe black shale section, however, indicate that the Ediacaran was also characterized, perhaps

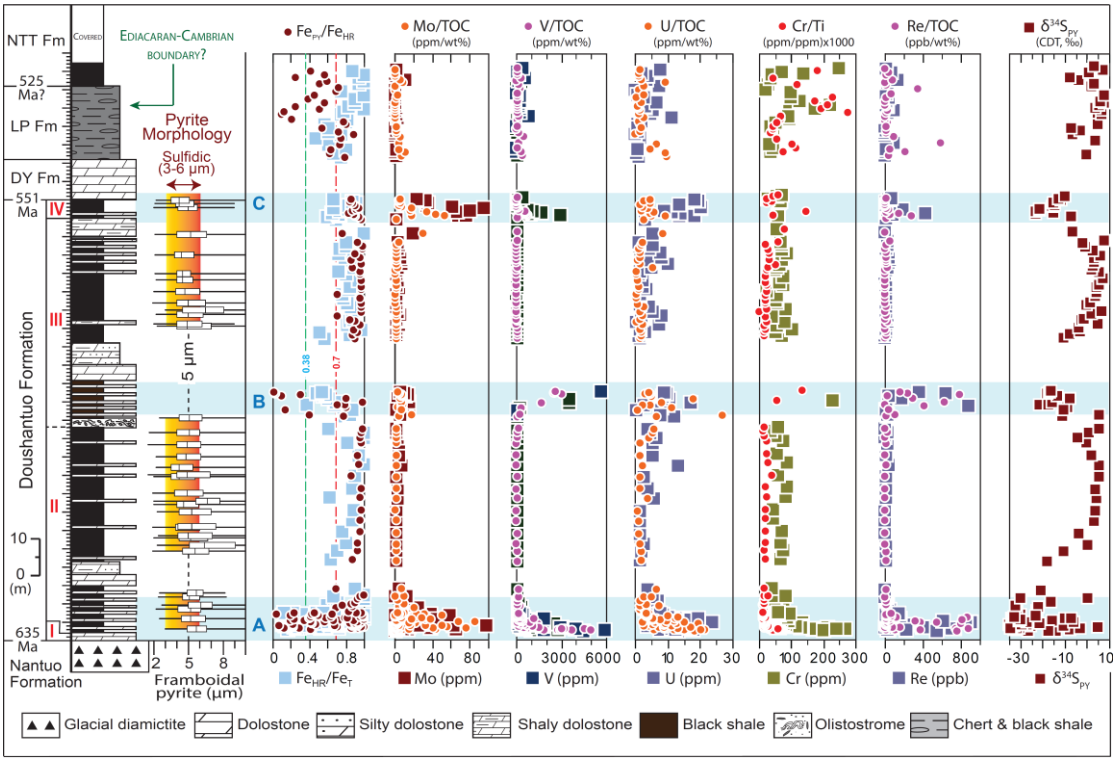

Figure 2. Geochemical profiles of the Ediacaran–Early Cambrian strata in Wuhe section, South China. The box-and-whisker plots of pyrite framboid diameters (PFD) show the median (5 μm), range, and 25th and 75th percentiles of framboidal diameter distributions (Wang et al., 2012b). The PFD and iron speciation data (Fe_{HR}/Fe_T > 0.38; Fe_{PY}/Fe_{HR} > 0.7) indicate persistent water-column euxinia during most of the Ediacaran, making this section ideal for tracking the global ocean redox evolution using RSE enrichments. Highly enriched RSE (Mo, V, U, Cr, Re) in the basal (Zone A), middle (Zone B), and uppermost (Zone C) Doushantuo Formation are interpreted as recording three distinctive oxygenation events at ca. 635 Ma, ca. 580 Ma, and ca. 560 Ma (see Data Repository for age discussions). Crustal-level RSE values between these events record a return to prolonged oceanic anoxia. This interpretation is supported by low $\delta^{34}S_{PY}$ values during oxygenation events and high $\delta^{34}S_{PY}$ values in between.

dominantly so, by intervals of expansive and persistent euxinia and potentially ferruginous conditions. Recent modeling efforts suggest that at least 1-10% seafloor euxinia and ≥ 30% seafloor anoxia are needed to crash the Mo and Cr seawater reservoirs, respectively, to levels that favour near crustal concentrations in euxinic shales (Reinhard et al., 2013). Thus, the coupled Fe proxy and RSE trends presented here document, for the first time, three oxygenation events in an overall anoxic Ediacaran ocean from a single stratigraphic succession, providing evidence for large-scale shifts in marine redox conditions.

The large $\delta^{34}S_{PY}$ variations at the Wuhe section, despite evidence for persistent water column pyrite formation from the Fe proxies and PFD record, also suggest dynamic Ediacaran redox conditions. Heavy $\delta^{34}S_{PY}$ values may be linked to decreases in the marine sulfate reservoir, which could be driven by widespread expansion of euxinic conditions and collectively increased global pyrite burial (Scott et al., 2014). Alternatively, shifts in $\delta^{34}S_{PY}$ could be tied to variations in the areal extent of oxic water-column present offshore of the Yangtze platform. A decrease in the extents of oxic water column respiration could increase microbial sulfate reduction rates. This shift in rates would ultimately decrease the $\Delta^{34}S$ value (see Leavitt et al., 2013, for a discussion). Both of these models for the $\delta^{34}S_{PY}$ record, which are potentially complementary, require temporally dynamic redox conditions.

Compilation of the RSE data from the Wuhe section and other Ediacaran-Early Cambrian (ca. 635–520 Ma) euxinic shales (Fig. 3 and Table DR2) reveals modern-level RSE enrichments at ca. 635 Ma, ca. 580 Ma, ca. 560 Ma, ca. 540 Ma, and ca. 530 Ma; each of them is followed by crustal or near crustal RSE values. This secular RSE pattern

highlights rises and falls in the surface oxidation state up to the Cambrian explosion. Of particular relevance, extremely low diversification rates (Xiao, 2014) and a drop in acritarch diversity (McFadden et al., 2009) seen in the fossil record between 630 and 580 Ma (Fig. 3) are potentially tied to significant global expansion of reducing conditions unfavourable for animals and other complex organisms. A precise estimation on the duration of each oxygenation event requires additional efforts, but it is reasonably within a range of 5–10 Ma. The frequency of RSE peaks increases during the late Ediacaran-Early Cambrian, which may record a transient redox state towards a fully oxygenated Phanerozoic ocean.

6. Conclusion

Coupled data for Fe, S isotopes, and redox-sensitive elements from euxinic shales of a deep-water slope section in the Yangtze platform, South China, document multiple oxygenation events with suggestions of increasing frequency in an overall anoxic Ediacaran ocean. While Phanerozoic anoxic events in dominantly oxic oceans caused mass extinctions followed by fast recovery, Precambrian oxygenation events may have stimulated biotic innovations followed by prolonged evolutionary stasis. The highly dynamic Ediacaran redox history presented here provides a potential explanation for seemingly conflicting estimates for the timing of Ediacaran ocean oxygenation. Dynamic oxygenation may also help explain the delay between the initial appearance of metazoans and the much later appearance and diversification of most metazoan groups and complex metazoan ecosystems in the Early Cambrian.

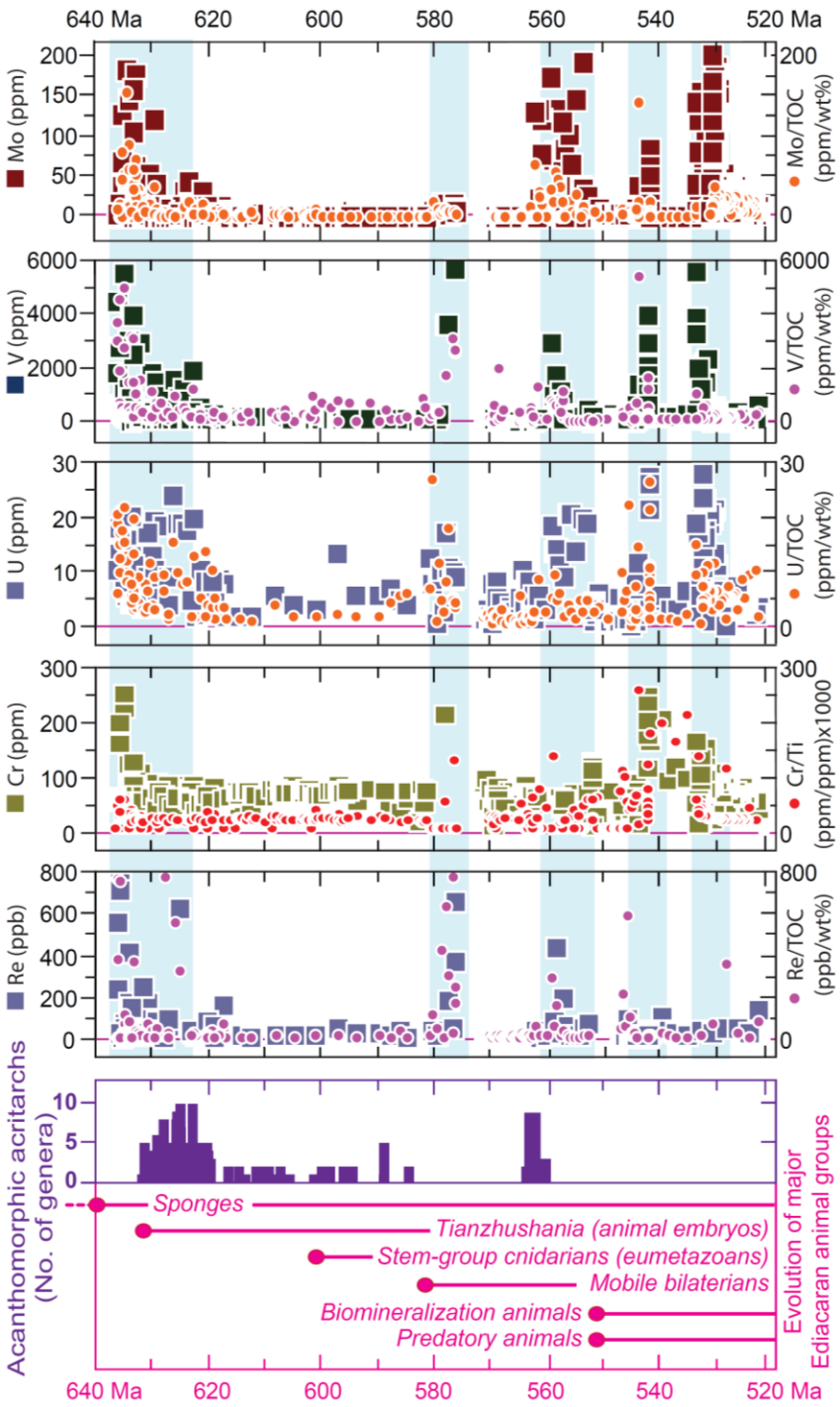

Figure 3. Compilation of RSE data from the Wuhe section and other Ediacaran–Early Cambrian euxinic shales (see Table DR2) showing multiple oxygenation events in an overall anoxic Ediacaran-Early Cambrian ocean. Prolonged anoxia between ca. 630 and ca. 580 Ma corresponds with a low diversity of acanthomorphic acritarchs (McFadden et al., 2009) and delayed diversification of major Ediacaran animal groups (Xiao et al., 2014).

7. References

Canfield, D.E., Poulton, S.W., and Narbonne, G.M., 2007, Late-Neoproterozoic deep-ocean oxygenation and the rise of animal life: Science, v. 315, p. 92-95.

Condon, D., Zhu, M., Bowring, S., Wang, W., Yang, A., Jin, Y., 2005, U–Pb ages from the Neoproterozoic Doushantuo Formation, China: Science, v. 308, p. 95–98.

Emerson, S.R., and Huested, S.S., 1991, Ocean anoxia and the concentrations of molybdenum and vanadium in seawater: Marine Chemistry, v. 34, p. 177-196.

Erwin, D.H., Laflamme, M., Tweedt, S.M., Sperling, E.A., Pisani, D., and Peterson, K.J., 2011, The Cambrian Conundrum: Early Divergence and Later Ecological Success in the Early History of Animals: Science, v. 334, p. 1091-1097.

Fike, D.A., Grotzinger, J.P., Pratt, L.M., and Summons, R.E., 2006, Oxidation of the Ediacaran Ocean: Nature, v. 444, p. 744–747.

Hetzel, A., Böttcher, M.E., Wortmann, U.G., and Brumsack, H., 2009, Paleo-redox conditions during OAE 2 reflected in Demerara Rise sediment geochemistry (ODP Leg 207): Palaeogeography, Palaeoclimatology, Palaeoecology, v. 273, p. 302-328.

Jiang, G., Kaufman, A.J., Christie-Blick,N., Zhang, S.,Wu,H., 2007. Carbon isotope variability across the Ediacaran Yangtze platformin South China: implications for a large surface-to-deep ocean $\delta^{13}C$ gradient: Earth and Planetary Science Letters, v. 261, p. 303–320.

Jiang, G., Shi, X., Zhang, S., Wang, Y., and Xiao, S., 2011, Stratigraphy and paleogeography of the Ediacaran Doushantuo Formation (ca. 635–551 Ma) in South China: Gondwana Research, v. 19, p. 831-849.

Jiang, G., Kennedy, M.J., Christie-Blick, N., Wu, H., and Zhang, S., 2006, Stratigraphy, Sedimentary Structures, and Textures of the Late Neoproterozoic Doushantuo Cap Carbonate in South China: Journal of Sedimentary Research, v. 76, p. 978-995.

Johnston, D.T., Poulton, S.W., Tosca, N.J., O'Brien, T., Halverson, G.P., Schrag, D.P., and Macdonald, F.A., 2013, Searching for an oxygenation event in the fossiliferous Ediacaran of northwestern Canada: Chemical Geology, v. 362, p. 273-286.

Kendall, B., Reinhard, C.T., Lyons, T.W., Kaufman, A.J., Poulton, S.W., and Anbar, A.D., 2010, Pervasive oxygenation along late Archaean ocean margins: Nature Geoscience, v. 3, p. 647-652.

Li, C., Love, G.D., Lyons, T.W., Fike, D.A., Sessions, A.L., and Chu, X., 2010, A Stratified Redox Model for the Ediacaran Ocean: Science, v. 328, p. 80-83.

Leavitt, W.D., Halevy, I., Bradley, A.S., and Johnston, D.T., 2013, Influence of sulfate reduction rates on the Phanerozoic sulfur isotope record: Proceedings of the National Academy of Sciences, USA, v. 110, p. 11244-11249.

Love, G.D., Grosjean, E., Stalvies, C., Fike, D.A., Grotzinger, J.P., Bradley, A.S., Kelly, A.E., Bhatia, M., Bowring, S.A., Condon, D.J., and Summons, R.E., 2009, Fossil steroids record the appearance of Demospongiae during the Cryogenian period: Nature v. 457, p. 718-722.

Lyons, T.W., Anbar, A.D., Severmann, S., Scott, C., and Gill, B.C., 2009, Tracking euxinia in the ancient ocean: A multiproxy perspective and Proterozoic case study: Annual Review of Earth and Planetary Sciences, v. 37, p. 507-534.

Lyons, T.W., and Severmann, S., 2006, A critical look at iron paleoredox proxies: New insights from modern euxinic marine basins: Geochimica et Cosmochimica Acta, v. 70, p. 5698-5722.

McFadden, K.A., Huang, J., Chu, X., Jiang, G., Kaufman, A.J., Zhou, C., Yuan, X., and Xiao, S., 2008, Pulsed oxidation and biological evolution in the Ediacaran Doushantuo Formation: Proceedings of the National Academy of Sciences, USA, v. 105, p. 3197–3202.

McFadden, K.A., Xiao, S., Zhou, C., and Kowalewski, M., 2009, Quantitative evaluation of the biostratigraphic distribution of acanthomorphic acritarchs in the Ediacaran Doushantuo Formation in the Yangtze Gorges area, South China: Precambrian Research, v. 173, p. 170-190.

Och, L.M., and Shields-Zhou, G.A., 2012, The Neoproterozoic oxygenation event: Environmental perturbations and biogeochemical cycling: Earth-Science Reviews, v. 110, p. 26-57.

Pecoits, E., Konhauser, K.O., Aubet, N.R., Heaman, L.M., Veroslavsky, G., Stern, R.A., and Gingras, M.K., 2012, Bilaterian Burrows and Grazing Behavior at > 585 Million Years Ago: Science, v. 336, p. 1693-1696.

Poulton, S.W., and Canfield, D.E., 2005, Development of a sequential extraction procedure for iron: implications for iron partitioning in continentally derived particulates: Chemical Geology, v. 202, p. 79-94.

Poulton, S.W., and Canfield, D.E., 2011, Ferruginous Conditions: A dominant feature of the ocean through Earth's history: Elements, v. 7, p. 107-112.

Reinhard, C.T., Planavsky, N.J., Robbins, L.J., et al., 2013, Proterozoic ocean redox and biogeochemical stasis: Proceedings of the National Academy of Sciences, USA, v. 110, p. 5357-5362.

Sahoo, S.K., Planavsky, N.P., Kendall, B., Wang, X., Shi, X., Scott, C., Anbar, A.D., Lyons, T.W., and Jiang, G., 2012, Ocean oxygenation in the wake of the Marinoan glaciation: Nature, v. 489, p. 546-549.

Scott, C., Lyons, T.W., Bekker, A., Shen, Y., Poulton, S.W., Chu, X., and Anbar, A.D., 2008, Tracing the stepwise oxygenation of the Proterozoic ocean: Nature, v. 452, p. 456-459.

Scott, C., Wing, B.A., Bekker, A., Planavsky, N.J., Medvedev, P., Bates, S.M., Yun, M., and Lyons, T.W., 2014, Pyrite multiple-sulfur isotope evidence for rapid expansion and contraction of the early Paleoproterozoic seawater sulfate reservoir: Earth and Planetary Science Letters, v. 389, p. 95-104.

Sperling, E.A., Frieder, C.A., Raman, A.V., Girguis, P.R., Levin, L.A., and Knoll, A.H., 2013, Oxygen, ecology, and the Cambrian radiation of animals: Proceedings of the National Academy of Sciences, USA, v. 110, p. 13446-13451.

Wang, X., Shi, X., Jiang, G., and Zhang, W., 2012a, New U–Pb age from the basal Niutitang Formation in South China: Implications for diachronous development and condensation of stratigraphic units across the Yangtze platform at the Ediacaran–Cambrian transition: Journal of Asian Earth Sciences, v. 48, no. 0, p. 1-8.

Wang, L., Shi, X., and Jiang, G., 2012b, Pyrite morphology and redox fluctuations recorded in the Ediacaran Doushantuo Formation: Palaeogeography, Palaeoclimatology, Palaeoecology, v. 333–334, p. 218-227.

Wilkin, R.T., Barnes, H.L., and Brantley, S.L., 1996, The size distribution of framboidal pyrite in modern sediments: An indicator of redox conditions: Geochimica et Cosmochimica Acta, v. 60, p. 3897-3912.

Xiao, S., 2014, Oxygen and early animal evolution, in Farquhar, J., ed., Treatise on Geochemistry (2nd Edition), Volume 6: The Atmosphere History: Dordrecht, Elsevier, p. 231-250.

Yin, L., Zhu, M., Knoll, A.H., Yuan, X., Zhang, J., and Hu, J., 2007, Doushantuo embryos preserved inside diapause egg cysts: Nature, v. 446, p. 661–663.

Zhang, S., Evans, D.A.D., Li, H., Wu, H., Jiang, G., Dong, J., Zhao, Q., Raub, T.D., and Yang, T., 2013, Paleomagnetism of the late Cryogenian Nantuo Formation and paleogeographic implications for the South China Block: Journal of Asian Earth Sciences, v. 72, p. 164-177.

Zhang, S., Li, H., Jiang, G., Evans, D.A.D, Dong, J., Wu, H., Yang, T., Liu, P., and Xiao, Q., 2014, New Paleomagnetic results from the Ediacaran Doushantuo Formation in South China and their paleogeographic implications: Precambrian Research (in press).

Zhou, C., and Xiao, S., 2007, Ediacaran δ13C chemostratigraphy of South China: Chemical Geology, v. 237, p. 89-108.

CHAPTER 4

Metal distribution in Ediacaran Doushantuo black shales: An example to test iron speciation and metal sequestration under euxinic conditions

Abstract

Temporal enrichment patterns of redox sensitive elements (RSE) in reducing black shales provide a first order portrait for ocean oxygenation from Archean to Phanerozoic. However, because RSE enrichments in black shales may vary in response to local depositional environments and post-depositional diagenesis, confusions have been raised for the use of RSE as a global ocean redox proxy. In this chapter, I use a set of geochemical and petrological redox indicators to demonstrate the pros and cons of using RSE as a global redox indicator through a comparative study of two critical Ediacaran black shales – the ca. 630 Ma Member II and ca. 551 Ma Member IV black shales of the Doushantuo Formation in South China, both of which have been linked to Ediacaran oxygenation and increase in oceanic RSE inventory.

Significant spatial variations in RSE concentration are observed among time-equivalent "euxinic" shales of the Doushantuo Formation. Taking the face values of RSE concentration from a single section may lead to misinterpretations about the Ediacaran ocean chemistry. For example, the Doushantuo Member II black shales of the Weng'an section are deemed "euxinic" by iron speciation and the near crustal RSE values from these shales may be misinterpreted as recording low oxidative weathering, strong basin restriction, or an unusually small oceanic RSE reservoir similar to that of the Archean ocean. Pyrite morphological study, however, reveals large (> 10 μm) pyrite framboids indicative of pore-water euxinia or euhedral pyrites (diagenetic origin) with enriched $\delta^{34}S$

values. In this case, the Weng'an black shales were not deposited from euxinic water column and the RSE values from this section cannot be used as a global ocean redox proxy. Similarly, for the late Ediacaran interval (Doushantuo Member IV, ca. 551 Ma), RSEs are muted in the upper slope sections (pseudo-euxinic) but are highly enriched in inner shelf and basinal euxinic sections. These examples demonstrate that, in many cases, iron speciation alone cannot identify oxic/anoxic/euxinic environments, particularly when total iron enrichments are low and Fe/Al ratios are significantly lower than the average crustal Fe/Al ratio (~0.5). In such cases, a comprehensive multi-proxy study across shelf-to-basin environments is needed to document the global ocean redox signature.

1. Introduction

Over the last decade, there has been an explosive growth in transition metal geochemistry, adding to our understanding of biogeochemical cycling of bioessential metals, such as Fe, Mo, Zn, Co, Ni, and Cu (Anbar and Knoll, 2002). Over broad geological times, bioessential metals are important buffers for primary productivity and controls the availability of metal-micronutrients, and hence the long-term evolution of life forms on our planet (Zerkle et al., 2005; Falkowski and Goldfrey, 2008). Seawater inventory of bioessential elements is controlled by the riverine input from oxidative weathering and the sink from anoxic versus oxic water column (Emerson and Huested, 1999; Anbar, 2008). Therefore, temporal variations in redox sensitive element (RSE) concentration may record the first-order changes in the oceanic RSE inventory and track the earth's oxygenation over geologic timescales (Anbar & Knoll 2002; Falkowski et al., 2004; Saito et al., 2003; Scott et al., 2008; Lyons et al., 2009).

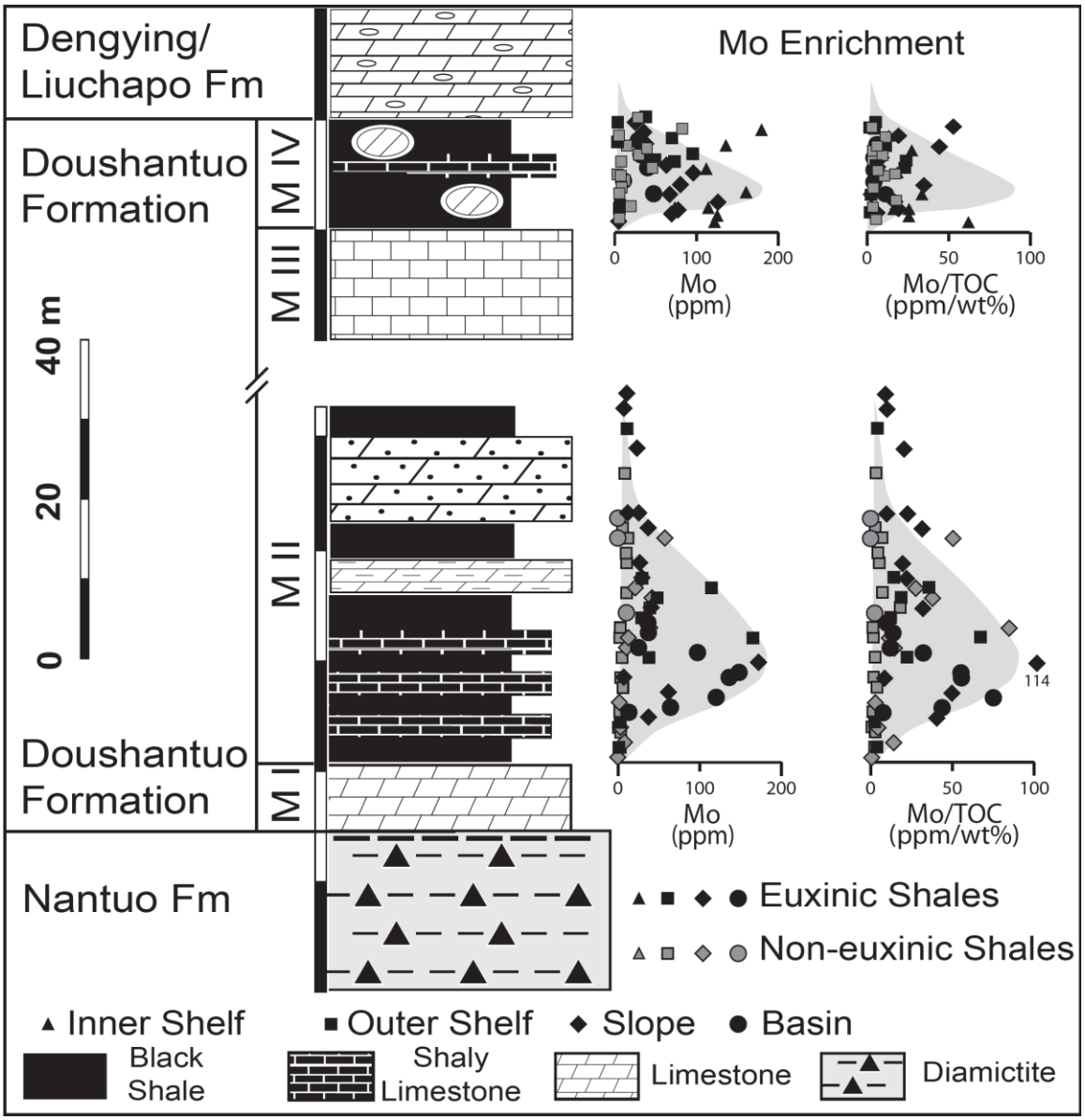

Figure 1 The general patterns of Mo and Mo/TOC from the basal Doushantuo Member II and Member IV black shales. High Mo enrichments from these shales may record expansion of the oceanic Mo inventory in response to ocean oxygenation but this "oxygenation" signature can only be recorded in sections with appropriate local redox conditions (i.e., depositional environments with water-column euxinia). This chapter focuses on spatial Mo (and other redox sensitive element (RSE) such as V, U, and Re) variations in Doushantuo Member II and Member IV black shales across the shelf-to-basin transects.

The high RSE concentrations in oxic ocean seawater, however, are not always recorded in sediments and sedimentary rocks. In modern environments, only euxinic (anoxic + H_2S-rich) shales deposited in the few anoxic basins such as the Black Sea capture the large oceanic RSE reservoir (Emerson and Huested, 1991; Hastings et al., 1996; Miller et al., 2011; Partin et al., 2013). Shales deposited from oxic water column or isolated basins without connection to the open ocean may have low RSE values. Therefore, using RSE values from black shales to infer ancient ocean geochemistry requires comprehensive comparison and evaluation. While high RSE values comparable with those of the modern anoxic shales record most likely a large RSE reservoir in an oxygenated ocean, low RSE values from a single stratigraphic section may result from (1) oxic depositional environment, (2) basin restriction (Algeo and Lyons et al., 2006) or (3) significant shrink of the RSE reservoir in response to increased ocean anoxia (Scott et al., 2008; Lyons et al., 2009; Hetzel et al., 2009; Sahoo et al., 2012; Owens et al., 2012; Reinhard et al., 2013). Thus, independent information about the water column chemistry and paleogeographic analyses are needed to ensure the proper use of RSE enrichment data.

The water column chemistry of the depositional environments is commonly determined by iron (Fe) speciation, which distinguishes biogeochemically highly reactive iron (Fe_{HR}) from total iron (Fe_T). The Fe_{HR} is defined as pyrite iron (Fe_{pyrite}) plus other iron phases that are potentially reactive with hydrogen sulphide on diagenetic time scales: carbonate-associated iron (Fe_{Carb}), ferric oxides (Fe_{Ox}), and magnetite (Fe_{Mag}) so that highly reactive iron $Fe_{HR} = Fe_{pyrite} + Fe_{Carb} + Fe_{Ox} + Fe_{Mag}$ (Poulton and Canfield, 2005). Black shales with $Fe_{HR}/Fe_T > 0.38$ are indicative of Fe scavenging under an anoxic water

column and anoxic shales with $Fe_{PY}/Fe_{HR} > 0.7$ are considered to represent deposition under euxinic conditions (Poulton and Canfield, 2011).

The Fe speciation, however, could be compromised by certain factors such as post-depositional weathering (e.g., through weathering and oxic fluid interaction) and diagenesis (e.g., diagenetic pyrite formation). It could also be influenced by increase in sedimentation rate over a short period of time (e.g., gravity flow) that may dilute highly reactive iron contents (Raiswell and Canfield, 1998; Lyons and Severmann, 2006). This information is sometimes overlooked when interpreting the RSE enrichments in "euxinic" shales calibrated by Fe speciation data.

In this chapter I present a comparative study on the spatial RSE variations of two distinctive stratigraphic intervals: the basal Doushantuo black shales (ca. 635-630 Ma) and the black shales at the top of the Doushantuo Formation (ca. 551 Ma). Both intervals have recorded high RSE enrichments indicative of oxygenated oceans and expansion of the oceanic RSE reservoir (Fig. 1; Scott et al., 2008; Sahoo et al., 2012), but low RSE values have also been found in coeval "euxinic" shales in shallow-water or upper slope sections (e.g., Bristow et al., 2009; Li et al., 2010). Using multiple petrographic and geochemistry redox indicators, this study demonstrates the conditions of using RSE enrichments as a global redox indicator. The data presented here explain the lack of oxygenation signature at ca. 635 Ma and ca. 551 Ma in some sections of the Ediacaran Yangtze platform in South China and in other sedimentary basins.

2. Background

2.1. Generalized stratigraphy

South China hosts the most extensive and complete Ediacaran-Early Cambrian stratigraphic and biological record in the world (McFadden et al., 2008; Li et al., 2010; Jiang et al., 2011). Exceptionally well-preserved multicellular eukaryotes, including early metazoan/animal embryos, algae, bilaterians, and morphologically differentiated benthic macrofossils have been reported from the Doushantuo Formation and its time-equivalent Lantian Formation (McFadden et al., 2008, Li et al., 2010, Yuan et al., 2011). In our measured sections, the Ediacaran succession consists of the Doushantuo and Dengying formations. The Doushantuo Formation, which overlies the late Cryogenian glaciogenic Nantuo Formation (ca. 654–635 Ma; Condon et al., 2005; Zhang et al., 2008), is divided into four distinct members (marked as I to IV in Fig. 2) in the Yangtze Gorges area and in Guizhou Province (McFadden et al., 2008; Jiang et al., 2011). Member I refers to the 2–5-m-thick cap carbonate, conformably overlain by Member II, which consists of 10–55-m-thick organic-carbon rich black shales interbedded with thin carbonate layers and minor phosphorite-chert nodules in upper slope environments (Jiang et al., 2011). This Member was likely deposited during the late stage of the Nantuo deglaciation and transgression. Member III in the shelf sections is composed mainly of carbonates with minor shales but in the lower slope sections such as the Wuhe in Guizhou province it consists of predominately shales, with minor carbonates and thin bedded chert layers. The transition from Member II to III is marked by exposed platform margin evidenced by abundance of slump blocks and olistostrome carbonates in the slope environments

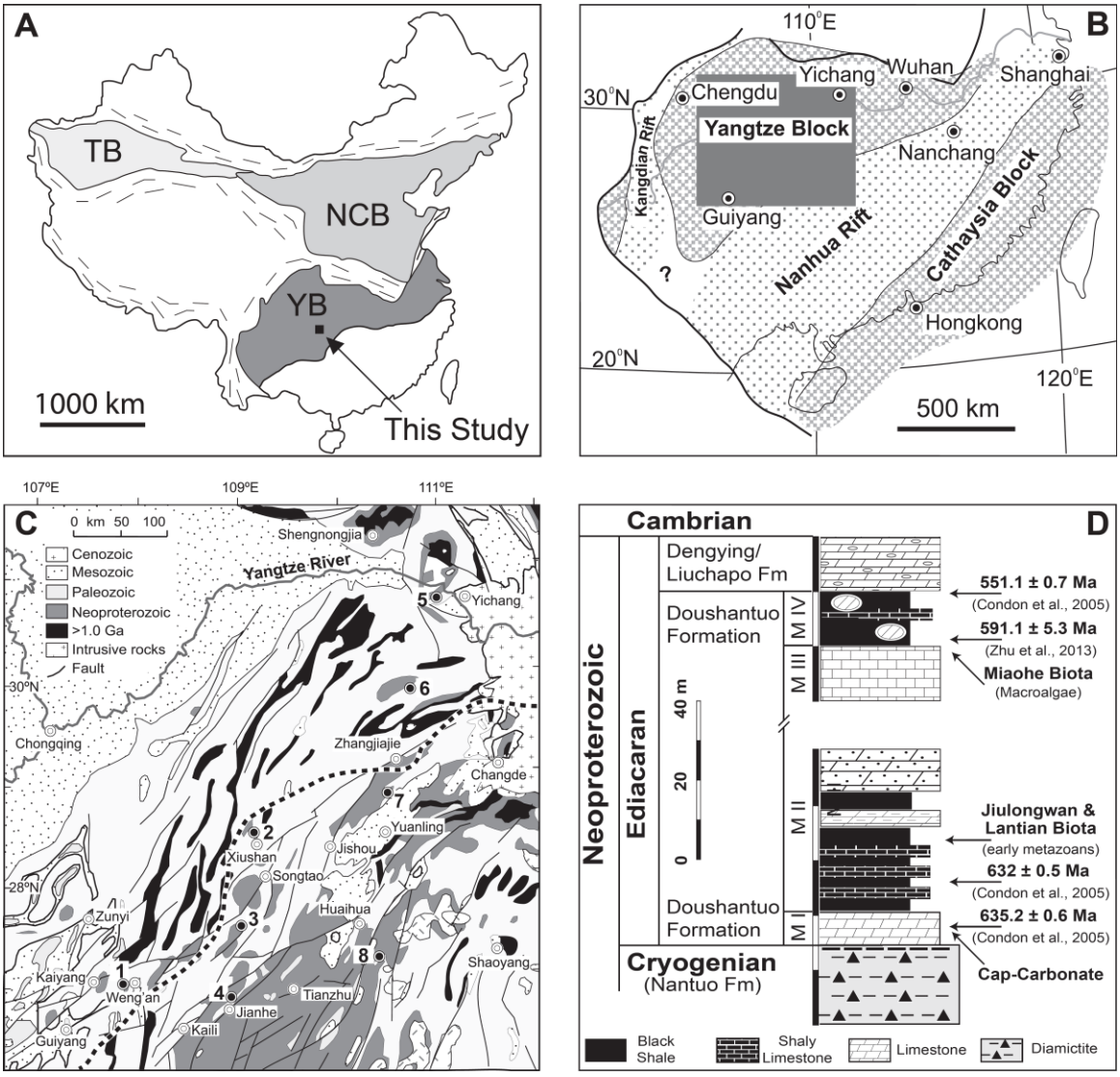

Figure 2 Locality maps and stratigraphic correlations. (**A**) Yangtze Block (YB) in relation to North China Block (NCB) and Tarim Block (TB). (**B**) Neoproterozoic tectonic framework of South China, highlighting inferred continental rift systems at c. 800 Ma (modified from Jiang et al., 2003). (**C**) Simplified geological map showing exposure of the Neoproterozoic strata in the Yangtze platform of South China and position of the sections in this study and from literature. Location of sections: 1–Weng'an; 2–Rongxi; 3–Taoying; 4–Wuhe; 5–Jiulongwan (The Yangtze Gorges area); 6–Zhongling; 7–Siduping; 8–Yuanjia. (**D**) Simplified stratigraphic column showing the Doushantuo Member II and Member IV shales and their age constraints.

(Jiang et al., 2007; 2010). Member IV refers to the <10-m-thick organic-rich black shale interval at the top of the Doushantuo Formation. Black shales from Member II and IV are thinly laminated, without wave- or storm-generated coarse-grained beds or turbidites (Jiang et al., 2010), suggesting their deposition well below the storm wave base. In the lower slope, Member IV is overlain by a 12-m-thick carbonate interval (Dengying Formation), followed by bedded cherts and siliceous shales of the Liuchapo Formation (Jiang et al., 2011).

2.2. Depositional environments and age constraints

On the basis of sedimentological stacking pattern and facies analysis, the Doushantuo Formation was interpreted as deposition from a passive continental margin developed in the southeast side of the Yangtze Block (Jiang et al., 2003). Volcanic ash beds were found at the base (635.2±0.6 Ma), middle (614 ± 7.6 Ma) and top (551.1 ± 0.7 Ma) of the Doushantuo Formation (Condon et al., 2005; Liu et al., 2009). The Precambrian-Cambrian boundary in measured sections, however, is less certain, but quite likely within the Liuchapo Formation (Jiang et al., 2012; Wang et al., 2012). The U-Pb zircon ages of 635.2 ± 0.6 Ma from the base of the Doushantuo and 551.1 ± 0.7 Ma from the top of the Doushantuo Formation (Condon et al., 2005) provide a maximum and minimum depositional age for the studied interval.

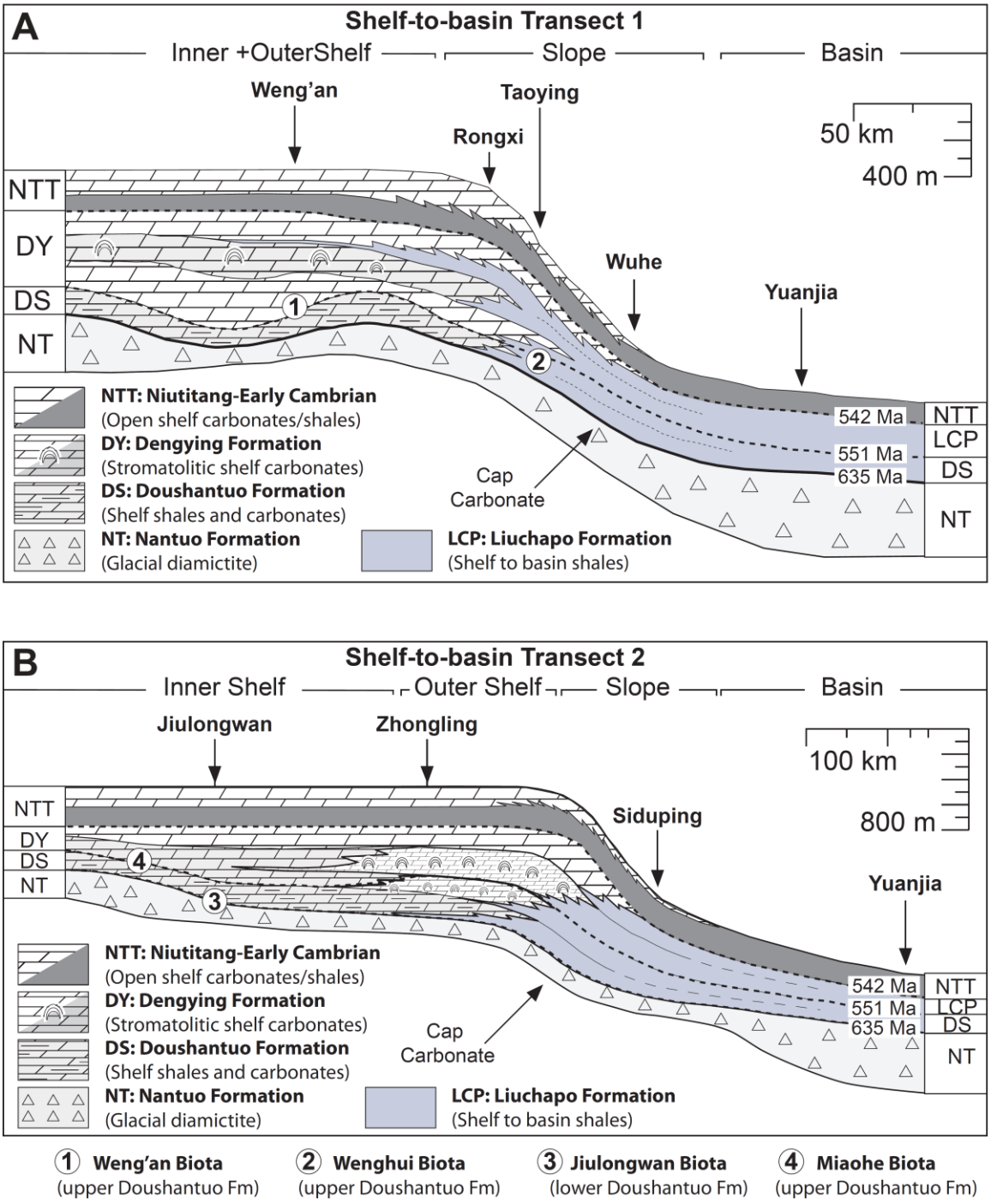

Figure 3 Shelf-to-basin transects. (**A**) Shelf-to-basin transect 1 showing location of sampled sections in Weng'an (inner shelf), Rongxi (shelf-margin to upper slope), Taoying (upper slope), Wuhe (lower slope), and Yuanjia (basin). (**B**) Transect 2 from the Yangtze Gorges area to basin showing location of sections in Jiulongwan (inner shelf) and Zhongling (outer shelf-shelf margin), Siduping (upper slope) and Yuanjia (basin).

2.2.1. Member II black shales

The Doushantuo Member II consists of a less than 55-m-thick organic-carbon rich black shale overlying the cap-carbonate, which has been dated 635.2 ± 0.6 Ma (Condon et al., 2005). In the Yangtze Gorges area (close to loc. 5 in Fig. 2C), less than two meters above the cap-carbonate layer, an ash bed that has been dated as 632.5 ± 0.5 Ma (Condon et al., 2005). From the Zhangcunping section, north of the type section in Jiulongwan (loc. 5 in Fig. 2C and Fig. 3B), Liu et al., (2009) reported a SHRIMP U–Pb zircon age of 614 ± 7.6 Ma from an ash bed overlying the Member II black-shales. Although there is no volcanic-ash beds preserved in the studied sections, these two ages constrain the Member II deposition between 635.2 ± 0.6 Ma and 614 ± 7.6 Ma.

Metazoan and morphologically complex fossils (Lantian Biota and Jiulongwan Biota) were reported from the Yangtze Gorges area (Yin et al., 2007) and the Anhui Province (Yuan et al., 2011) 2–15 m above the Doushantuo cap carbonate. The samples analyzed here focus on the basal Member II black shales that covers the metazoans of the Yangtze Gorges area but predates the Lantian biota, as used in the study by Sahoo et al., (2012). Fresh samples were collected from four sections to cover the inner shelf, outer shelf/upper slope, lower-slope, and basin facies (Fig. 3 A). The inner shelf section at Weng'an, Guizhou province is well known for animal embryos and red algal fossils (Xiao et al., 1998; 2014; Zhou et al., 2007). In this section the basal Member II consists of laminated black shales with dolomitic phosphorite interbeds. The outer shelf to upper slope section at Rongxi is characterized by laminated black shales with thin dolostone layers. The upper slope section at Taoying, Guizhou province (27°50'01.5"N, 109°01'03.9"E) is dominated by dark-black shales, with subordinate carbonates. In the

lower slope section at Wuhe, Guizhou province (26°45’93.6”N, 108°25’00.5”E), the basal Doushantuo Member II consists of mainly black shales with thin carbonate interbeds. Member II in the basinal section at Yuanjia, Hunan province (27°29’23”N, E110°14’37.4”E) is composed of primarily dark black-shales with minor calcareous marlstone beds (Fig. 3).

2.2.2. Member IV black shales

Member IV of the Doushantuo Formation was deposited on a passive margin continental shelf in the Nanhua Basin of South China (McFadden et al., 2008; Jiang et al., 2011). Although the thickness varies, Member IV (< 10 m thick) is widespread across the Yangtze platform and represents a marker for the uppermost Doushantuo Formation. This black shale interval also defines the lithological boundary between the Doushantuo Formation and the overlying Dengying Formation (Figs. 2 and 3). Radiometric (U-Pb zircon) ages from an ash bed indicate a depositional age ≥ 551.1 ± 0.7 Ma (Condon et al., 2005). Recently Zhu et al. (2013) suggested a Re–Os age of 595 ± 22 Ma from the basal Member IV black shales in the Three Gorges area. A subset of these samples delineates a more precise isochron age of 591.1 ± 5.3 Ma. If this age is considered, the duration of the Doushantuo Member IV may be as long as 35 million years, given the top Member IV age of 551.1 ± 0.7 Ma (Condon et al., 2005). Although these new dates build issues surrounding the timing of oxygenation events, these correlations are not central to our argument.

Fossil rich Member IV, also known as the Miaohe Member, is heavily studied in the Yangtze Georges area where a marked increase in Mo concentrations in black shale (Fig. 1), with values comparable to Phanerozoic euxinic shales has been suggested for

terminal Proterozoic oxygenation (Scott et al., 2008; Li et al., 2010; Partin et al., 2013). I focused on the interval where the boundary with Denying Formation is considered as the upper limit for Member IV. The outer shelf-to-upper slope section in Rongxi is characterized by laminated dark-black shales. The upper slope section in Taoying is also dominated by dark-black shales, with abundant microfossil assemblage of the Wenghui Biota (Wang and Wang, 2006). The lower slope section in Wuhe consists of mainly black shales with sparse pyrite nodules. Literature data from other sections on the Yangtze platform were also compiled and compared for better understanding of the spatial variations in iron speciation and RSE enrichments.

3. Methods

3.1. Sample collection and preparation

Samples of the basal Member II and Member IV black shales were collected at an average spacing of 20 cm from Weng'an, Rongxi, Taoying, Wuhe, and Yuanjia sections (Fig. 3A). In combination with well-documented sections and data from Jiulongwan and Zhongling sections (Bristow et al., 2009; Li et al., 2010; Huang et al., 2013), the final dataset covers two shelf-to-basin transects (Fig. 3A and 3B). The basal Doushantuo Member II and Member IV black shales are correlatable among these sections. Because the upper limit for the Member II interval is variable, we placed the datum to the top of the cap carbonate for geochemical analysis. Accordingly, we placed the datum for Member IV to the base of Dengying Formation.

Samples were cleaned, chipped, and powdered with special care at the University of Nevada, Las Vegas. A chip of each representative sample was further utilized for

petrographic analysis. Pyrite morphology was analyzed under scanning electron and reflected microscopes. Pyrite morphology study of the Wuhe section samples was conducted by Wang et al. (2012) at the China University of Geosciences (Beijing). Geochemical analyses include iron speciation, trace metal abundance, pyrite sulfur isotopes, organic carbon content, ion micro-probe analysis and vanadium X-edge absorption spectra (K-edge peaks).

3.2. Analytical methods

Analytical methods for iron-speciation, total organic carbon, sulphur isotopes and trace metal are discussed heavily in Chapter 1 and 2. Here I am only adding the additional analysis those were not discussed before.

3.2.1 MicroProbe and SEM Analysis

Four Member II shale samples from Taoying, Wuhe and Yuanjia were selected for analysis based on the presence of high RSE enrichments. Scanning electron microscopy (SEM) and energy dispersive X-ray analysis (EDS) was performed on a JEOL 5600 SEM and an Oxford ISIS EDS at UNLV. Sample preparation involved probe quality thin-sections as well as fresh cut samples. Samples were resized appropriately to fit in the SEM, attached to a brass cylinder with carbon-coated tape, and sputtered for 30s with a gold/palladium coating using a Model 3 Pelco Sputter Coater. Petrographic thin-sections were viewed in SEM, EDS and backscattered mode at 2500×magnification to determine pyrite content and micromorphology, and when present, the size distribution of pyrite grains within the clay matrix. EDS analysis was used to detect the co-existence of sulfur, molybdenum, aluminum and iron to distinguish pyrites from other clay constituents (Figs 7). Wang et al. (2012) used a Camscan to test the same suite of samples

from Taoying and Wuhe to detail the framboidal pyrite size distribution and at least 100 framboids were measured from each sample. A more detailed discussion of this technique is presented elsewhere (Wignall and Newton, 1998; Bond et al., 2004; Bond and Wignall, 2005). In addition to SEM/EDS, electron probe micro analyzer (EPMA) or commonly known as electron microprobe was also performed on a JEOL JXA-8530F (FEG) at Department of Geology and Geophysics, Yale University.

3.2.2. XANES Experimental analysis

To probe the vanadium (V) oxidation state we collected K-edge X-ray absorption near edge structure (XANES) spectra, because the energy required to excite 1s electrons from the V core (edge energy) will depend on the oxidation state of the V. It is important to note that XANES is a bulk characterization technique; therefore it only provides information on the average electronic properties of the entire sample (Wong et al., 1984). V K-edge XANES spectroscopy was performed on selected samples at Sector 5 of the Advanced Photon Source, Argonne National Laboratory, on the Dupont-Northwestern-Dow Collaborative Access Team (DND-CAT) bending magnet D beam-line. The beam energy was controlled by a Si (111) mono-chromator with resolution of 10^{-4}eV. Incident and transmitted intensities were measured with Canberra ionization chambers. Energies were calibrated in transmission mode against a V foil, setting the first inflection point at the known edge energy of V^0 (5465 eV). Absorption intensities were normalized in Athena. V-enriched samples were brushed onto Kapton tape and mounted at an incident angle of $\theta = 45 \pm 5°$ with respect to beam and fluorescence detector. Spectra for the samples were collected in fluorescence mode using a four-channel SII Vortex-ME4 detector.

4. Results

Major (Fe, Al, Ti) and trace element (Mo, V, U, Cr, and Re) concentrations, as well as Fe speciation and pyrite sulfur isotopic data were summarized in Tables 1 and 2. When it is possible, geochemical data from previous publications across the shelf-to-basin transect 2 (Fig. 3B) are also included for comparison. XANES analysis was performed only on samples of the lower slope Wuhe section (n = 10) with high and low V concentration. Selected samples were analyzed for micro-probe analysis as well as SEM imagery. Results of microprobe and XANES analyses are summarized in Table 2.

4.1. Organic carbon and pyrite sulfur

TOC concentrations range from 0.1 to 4.5 wt.% (average 1.47 ± 1%) and S_P concentrations range from 0 to 4 wt.% (average 0.95 ± 1%) at Member II (Table 1). The TOC concentrations of Member IV black shales range from 0.1 to 15.3 wt.% (average 5.8 ± 3.5%) and S_P concentrations vary from 0.05 to 2.8 wt.% (average 1.1 ± 0.9%) (Table 1). In detail, during early Ediacaran Member II, the inner shelf section at Weng'an is enriched in S_P (average = 1.6 ± 0.27%) but has low TOC (average = 0.26 ± 0.11). The outer shelf to upper slope section in Rongxi has higher values (TOC = 2.34 ± 0.85%) but only minor pyrites (average Sp = 0.48 ± 0.69%). The upper slope section in Taoying has comparable TOC values (average TOC = 2 ± 0.75%) with Rongxi but lacks any visible and acid-extractable pyrites (average Sp = 0.36 ± 0.46%). The lower slope Wuhe section has lower TOC (average TOC = 1 ± 0.27%) but abundant framboidal pyrites (average Sp = 1.55 ± 0.86%). The basinal section in Yuanjia has higher TOC (average TOC = 2.2 ± 1.06%) and abundant pyrites (average Sp = 1.89 ± 1.55%).

Member IV black shales of the outer shelf-to-upper slope section in Rongxi are highly enriched in TOC (average = 7.82 ± 4.1%) and S_P (average = 1.16 ± 0.8%). The upper slope section in Taoying has slightly lower TOC (average TOC = 5.11 ± 1.7%) but much lower S_P (average = 0.13 ± 0.04%). The lower slope section at Wuhe has lower TOC (average TOC = 4.79 ± 2.7%) but abundant framboidal pyrites (average = Sp = 1.59 ± 0.68%).

4.2. Iron Speciation

4.2.1 Member II black shales

Nearly all Member II black shale samples have $Fe_{HR}/Fe_T > 0.38$ and $Fe_P/Fe_{HR} > 0.7$, seemly recording euxinic conditions (Fig. S1). This is consistent with the traditional DOP redox indicator and high Fe_T/Al ratios (Fig. S1 and Table 1). The inner shelf Weng'an section represents the most proximal depositional setting in this study. Interestingly it has the highest Fe_{HR}/Fe_T values (0.97 ± 0.04) (Fig. S1A) and Fe_P/Fe_{HR} values (0.79 ± 0.10) (Fig. S1B), as well as high Fe_T/Al ratios (1.04 ± 0.7) (Fig. S1C) and DOP (0.89 ± 0.0). In contrast, the upper slope Taoying section have moderate Fe_{HR}/Fe_T and Fe_P/Fe_{HR} (average Fe_{HR}/Fe_T = 0.42 ± 0.3 and Fe_P/Fe_{HR} = 0.54 ± 0.3). Here, several Fe_{HR}/Fe_T values (average = 0.22 ± 0.08) are below 0.38, similar to modern sediments deposited under oxic water column (Raiswell and Canfield, 1998). These samples also have low Fe_P/Fe_{HR} (average = 0.41 ± 0.23) and extremely low Fe_T/Al ratios, consistent with deposition under oxic conditions (Fig. S1A, Fig. S1B). Some samples in this section have $Fe_{HR}/Fe_T > 0.38$ but low Fe_P/Fe_{HR} and DOP, indicating ferruginous conditions. Another group of samples in the Taoying section have both high Fe_{HR}/Fe_T (average=0.76 ± 0.22) and high Fe_P/Fe_{HR} (average=0.85 ± 0.06) indicative of water-column euxinia.

A few samples from the shelf margin-upper slope Rongxi section have Fe_{HR}/Fe_T < 0.38 and Fe_P/Fe_{HR} < 0.7, indicating oxic environments, but most samples have high Fe_{HR}/Fe_T (> 0.38) and Fe_P/Fe_{HR} (> 0.7) suggestive of euxinic conditions. The shelf margin (Rongxi) and upper slope (Taoying) seem to record fluctuating oxic/euxinic environments, probably resulted from chemocline instability (Poulton et al., 2010, Jiang et al., 2008).

4.2.2 Member IV black shales

Most Member IV black shales from inner shelf (Jiulongwan) and lower slope (Wuhe) section, have Fe_{HR}/Fe_T > 0.38 (average Fe_{HR}/Fe_T = 0.73 ± 0.23), and Fe_P/Fe_{HR} > 0.7 (average Fe_P/Fe_{HR} = 0.68 ± 0.28), as well as high Fe_T/Al (average Fe/Al = 0.89 ± 0.16), suggestive of bottom water euxinia (Fig. S2) and consistent with the traditional DOP redox indicator and high Fe_T/Al ratios (Fig. S2 and Table 1). Only a few samples from the Taoying section have Fe_{HR}/Fe_T < 0.38 and Fe_P/Fe_{HR} < 0.7 (average Fe_P/Fe_{HR} = 0.34 ± 0.26), suggesting alternating ferruginous and oxic conditions. In the Rongxi section, Fe_P/Fe_{HR} values are more scattered (average = 0.56 ± 0.21) than in Taoying and Wuhe (average Fe_P/Fe_{HR} = 0.9 ± 0.04). Interestingly, the Fe_T/Al ratios of the Taoying section samples are extremely low (average Fe/Al = 0.14 ± 0.06), even lower than the oxic threshold at Rongxi (average Fe/Al = 0.41 ± 0.23). In comparison with the data from the Three Georges area, Fe_{HR}/Fe_T values are close to or above 0.38 at Jiulongwan (average Fe_{HR}/Fe_T = 0.60 ± 0.17), and are significantly elevated at Zhongling (average Fe_{HR}/Fe_T = 0.93 ± 0.12). The $Fe_P/Fe_{HR,}$ values from both the Jiulongwan and Zhongling sections are all higher than 0.7, indicating persistent euxinia (This is consistent with the traditional DOP redox indicator and high Fe_T/Al ratios (Fig. S2A-S2C).

4.3. Molybdenum and other RSEs

Black shale samples from both Member II and Member IV have high but variable Mo, V, Re, and U values (Figs. S1D and S2D). Member II shales have 0–172 ppm of Mo, 10^1–10^4 ppm of V, 1.4-34 ppm of U and 0.4–3068 ppb of Re (Fig. S1). Black shales from Member IV have 0–180 ppm of Mo, 10^1–10^4 ppm of V, 2.5–32 ppm of U and 10–10^3 ppb of Re (Fig. S2). A particularly intriguing interval is the Member IV black shales from the Taoying section, where most RSEs are close to average crustal values (2–17 ppm of Mo, 10^1–10^2 ppm of V, 2.5–15 ppm of U and 2–23 ppb of Re).

4.4. Pyrite sulfur isotope

Pyrites from Member II shales show significant $\delta^{34}S_P$ variations (Fig. S2E and Fig. 4). In the slope and basin sections at Taoying, Wuhe and Yuanjia, negative $\delta^{34}S_P$ values down to –35.5‰ are observed, followed by a positive shift towards +10‰ within a few meters. In contrast, equivalent shale-units in Weng'an have positive $\delta^{34}S_P$ values up to +35.9‰. The $\delta^{34}S_P$ values from the Rongxi section fall between, ranging from -20‰ to +20‰ (Fig. 4). Member IV pyrites also exhibit a negative $\delta^{34}S_P$ anomaly in the Rongxi and Wuhe sections. In contrast, positive $\delta^{34}S_P$ values up to +40.6‰ are observed from the Taoying section. When plotted together with existing data from the Jiulongwan and Zhongling sections (McFadden et al., 2008; Li et al., 2010), $\delta^{34}S_P$ values of Member IV shales also display a large sulfur isotope gradient.

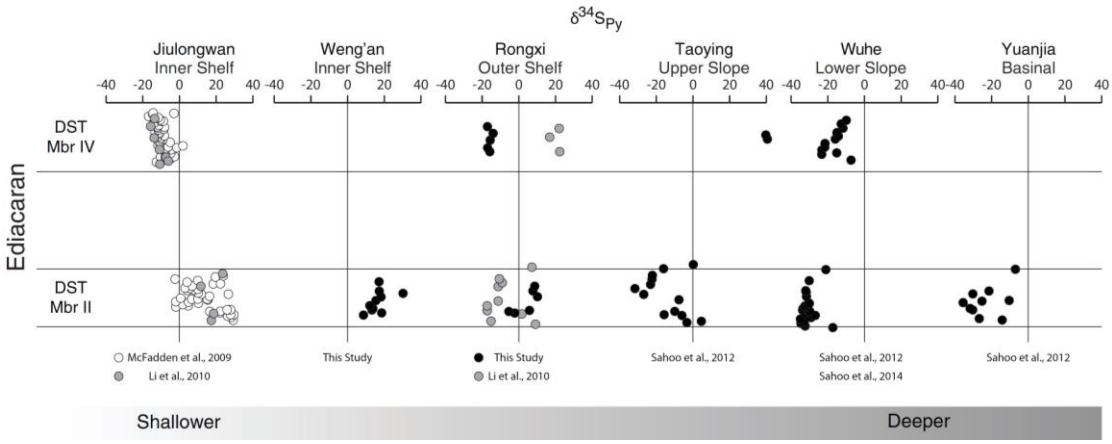

Figure 4 The pyrite sulfur isotope ($\delta^{34}S_{Py}$) gradient. Isotopic gradient from shallow to deep water sections, observed in Member II and Member IV black shales. Data of the Jiulongwan section in the Yangtze Georges are from McFadden et al. (2008) and Li et al. (2010).

4.5. Pyrite framboid analysis

There are abundant framboidal pyrites from the lower slope and basin section at Wuhe and Yuanjia (Wang et al., 2012). Pyrite framboids in these sections have average diameter < 10 μm, independently suggesting euxinic water column conditions (e.g., Bond and Wignall, 2005; Raiswell et al., 2008; Wignall et al., 2010). Framboidal pyrites are much less abundant in shelf-margin and upper slope sections at Rongxi and Taoying; when they are present, most of the pyrites have diameters > 10 μm, indicating partial diagenetic pyrite formation. In the shelf section at Weng'an, no framboidal pyrites are observed. Samples with abundant framboidal pyrites from the Wuhe (WH09-4.3) and Yuanjia (WHH 6.4) sections are chosen to do micro-probe analyses (Fig. S3 and Table 2).

Table 3 provides information about the Mo concentrations surrounding framboidal pyrites in samples WH09-4.3 and WHH-6.4, both of which have high bulk

Mo concentrations. The majority of Mo concentrations and the percentages of pyrite in whole rock sample analyses are from Sahoo et al., (2012). Pyrite-S contents were measured as part of earlier studies (see Table 1) and are based on wet chemical extraction via the chromium reduction method (Canfield et al., 1986). Mo concentrations measured within individual pyrite crystals from both the samples are much higher (0.7–16 times) than those in the equivalent shale matrix. Because pyrite represents only a small fraction of the bulk sample, it tells that the majority of Mo is hosted in pyrites.

4.6. XANES Analysis of V oxidative state

In the modern oxic water column, V is present as V (V) in the form of vanadate oxyanions (HVO_4^{2-} and HVO_4^-), while in mildly reducing conditions V (V) is reduced to V (IV) and present in the form of vanadyl ions (VO_2^-) and related hydroxyl species ($VO(OH)_3^-$) or hydroxides ($VO(OH)_2$) (Emerson, S. R. & Huested, 1991; Tribovillard et al., 2006). Because V exhibits a wide range of oxidation states (-1, to +5) and coordination geometries (octahedral, tetrahedral, square pyramid, trigonal bipyramidal and dodecahedral) with various ligands in its compounds (Wang et al., 1993), its variety in chemical structures provides an advantage to use V in the systematic study and understanding of the effect of bonding and coordination symmetry on the observed XANES spectra. A more detailed discussion of this technique is presented elsewhere (Wang et al., 1993, Heinrich et al., 1998). In this study we obtain high resolution K-edge XANES spectra of V in a series of selected shale samples from Member II of well-defined iron-proxies and known geochemical signatures. We used samples with the highest V enrichment (> 4000 ppm) as well as very low abundance (70-100 ppm).

In strongly reducing conditions with high dissolved sulfide (H_2S) concentrations, V (IV) will be further reduced to V (III), which may precipitate as V_2O_3 or $V(OH)_3$ (Tribovillard et al., 2006). V (IV) and V (III) can be scavenged by organic matter, leading to V enrichment in sediments deposited under an anoxic water column (Emerson, S. R. & Huested, 1991). Considering the fact that Member II shales with enriched V were deposited under strongly reducing conditions (euxinic), as evidenced by the Fe speciation data (Fig. S1), V(III) and V(IV) would be the major V species in those shale samples because V_2O_5 is the most abundant and stable form of V oxide.

Absorption intensity for the sample with very high V content (> 4000 ppm; sample number WH09-2.4) produced a well-resolved spectrum (Fig. 5B). Interestingly, samples with low V concentrations (e.g., WH09-119.5) from Member II and Member IV shales also produced identical spectrum shape (Fig. 5B), indicating that V-containing molecular or crystalline species in the shales record similar signature. Note that the location of the pre-edge peak (+4.5 eV) and 1s to 4p peak (+21.5 eV) are nearly identical to what has been previously observed from the standard Roscoelite (Wang et al., 1993). Roscoelite is one-layer monoclinic mica in which V_3^+ ions are substituted in octahedral sites by AlO_6 units (Wang et al., 1993; Heinrich et al., 1998). Spectral analysis of sample WH09-2.4 exhibits similarity with Roscoelite, and prominent peaks in the pre-edge region and 1s to 4p absorption onset region occur at +3.7 eV and +14.7 eV, respectively. From the spectral patterns (Fig 8 A), it is obvious that all analyzed shale samples contain V_3^+ species in octahedral coordination form, which is similar to that of illite.

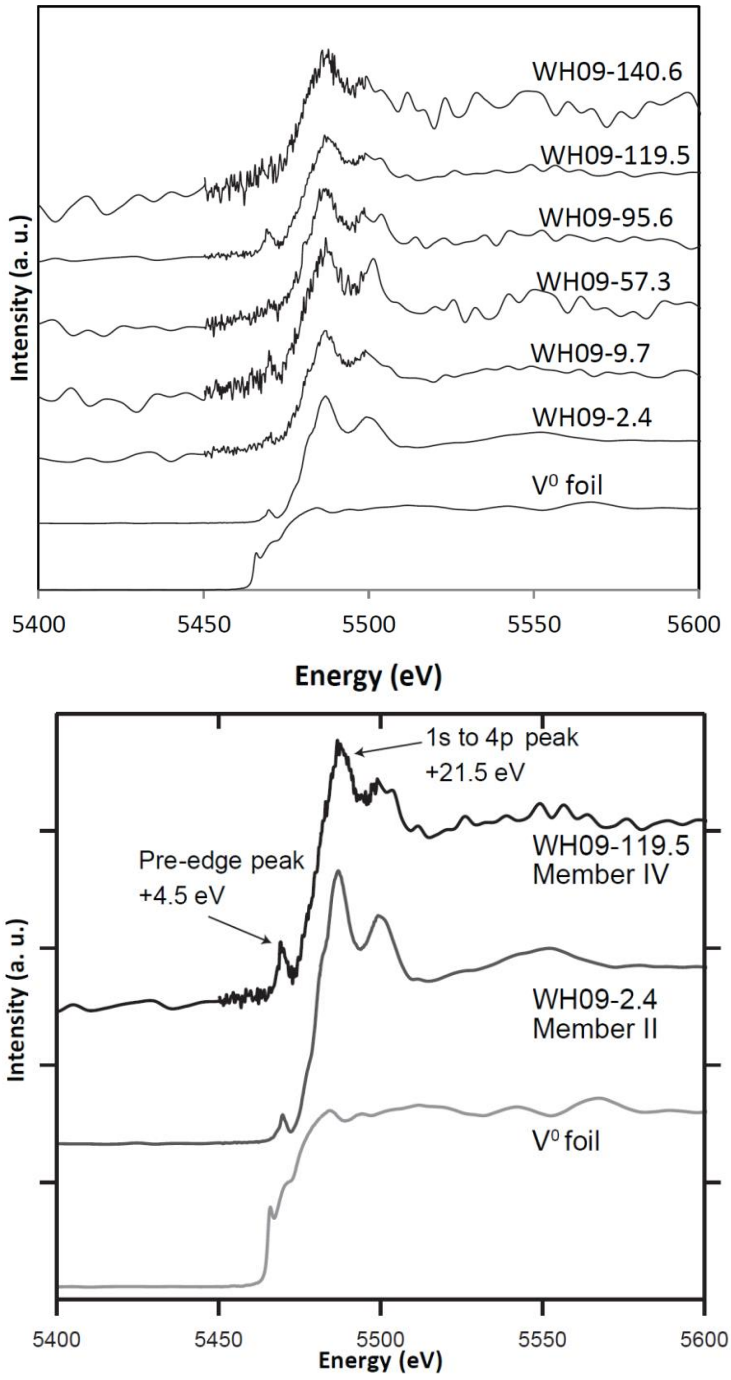

Figure 5 V K-edge XANES spectra. (**A**) Normalized XANES spectra for the V reference foil (V^0) and V-enriched samples through Member II to Member IV black shales of the Wuhe section. WH09-2.4 represents Member II whereas WH09-119.5 represents Member IV black shales. Note the presence of a pre-edge peak at +4.5 eV (relative to the edge of 5465 eV) and the strong 1s to 4p peak at +21.5 eV. Both suggest deposition under strong reducing conditions (B).

5. Discussion

5.1. The origin of RSE variations in Member II black shales

High RSE enrichments in the Doushantuo Member II shales deposited in the immediate aftermath of the Nantuo glaciation (~635–630 Ma) record a significant rise of the marine RSE inventory and an overall increase of seawater [SO_4^{2-}], marking an oxygenation event (Sahoo et al., 2012). However, the high RSE enrichments (and thus the oxidation event) documented from slope-basinal sections are not recorded in the shelf sections at Weng'an and Jiulongwan, and are only partially recorded in shelf-margin sections at Rongxi and Zhongling, despite the fact that iron speciation indicate seemly "euxinic" conditions in these sections (Figs. 4 and 5).

Possible interpretations for the lack of RSE enrichments in shelf sections at Weng'an and Jiulongwan may include (1) strongly restricted environments without connection to the open ocean (e.g., Bristow et al., 2009), (2) low seawater RSE concentrations in pervasively anoxic ocean, and (3) oxic-suboxic local depositional environments that did not capture the oceanic RSE signature. Partial restriction of the inner shelf from the open ocean during the deposition of basal Member II shales was possible, but a complete cut off from ocean seawater is unlikely because (1) the widespread occurrence of the Doushantuo cap carbonate (Member I) across the shelf-to-basin transects indicates seawater covered the entire Yangtze platform during the postglacial transgression; (2) the occurrence of acritarchs (some of them are interpreted as animal embryos) immediately above the cap carbonate (e.g., Yin et al., 2007) suggests marine environments with connections to the open ocean; and (3) the appearance of

phosphorites or phosphorite-chert nodules a few meters immediately above the cap carbonate also suggest phosphorus source from the open ocean.

The second possibility, i.e., low seawater RSE in pervasively anoxic ocean, could hold only if the basal Member II shales in Jiulongwan and Weng'an sections are much younger than those of the slope-basinal sections in Taoying, Wuhe, and Yuanjia where high RSE enrichments shift to near crustal/crustal values a few meters above the cap carbonate. It means that the RSE-enriched, basal Doushantuo black shales in slope-basinal sections pinches out towards the shelf. We cannot exclude this possibility but considering the overall depending-upward trend from the cap carbonate to its overlying shales in all shelf, slope and basinal sections, strong diachronous deposition of the basal Member II shales is less likely.

The most likely interpretation is that the local depositional environments at Weng'an and Jiulongwan did not capture the oceanic RSE enrichment signature and the "euxinic" redox conditions indicated by iron speciation data in these sections record a pore-water diagenetic signature. This is consistent with the lack of framboidal pyrites or the presence of only large-diameter (> 10 μm) pyrite framboids in the shelf sections, which indicates diagenetic pyrite formation. Therefore, the "euxinic" condition determined by $Fe_{HR}/Fe_T > 0.38$ and $Fe_T/Fe_{HR} > 0.7$ may actually record pore-water instead of water-column euxinia because iron speciation itself could not distinguish primary-secondary iron sulfides. Pore-water euxinia (therefore, oxic water column) is also supported by the strongly positive $\delta^{34}S_p$ values (≥ 45‰) in the Weng'an section (e.g, Gill et al., 2011).

The spatial variations of RSE enrichments of the basal Member II black shales confirms the requirement of water-column euxinia to capture the oceanic RSE signature, similar to the signature recorded in modern anoxic basins (Algeo and Lyons, 2006; Lyons et al., 2009). High RSE enrichments occur in slope-basinal sections in Taoying, Wuhe and Yuanjia where abundant framboidal pyrites are present. Microprobe analyses of Mo concentrations surrounding pyrite framboids reveal much higher Mo values in pyrite framboids than in shale matrix (Fig. 7), confirming the strong affinity of Mo (and other RSEs) with iron sulfide. Partial mobilization of RSEs during burial diagenesis would have been common, even in well-preserved black shales with measurable pyrite framboids. This may explain the presence of high and lower RSE values in adjacent samples of Member II black shales in slope-basinal sections (Figs. S1 and S2).

High RSE enrichments of the Member IV shales are found in shelf, slope and basinal sections but are muted in shelf-margin and upper slope sections (Zhongling and Taoying; Fig. S1 and S2). Unlike the case of Member II, low RSE values in Taoying is accompanied with moderate Fe_{HR}/Fe_T (< 0.58), DOP (~0.25), Fe_T/Fe_{HR} (< 0.34) and Fe_T/Al (~0.14) values indicative oxic-suboxic water column conditions. Although some Fe_{HR}/Fe_T values are higher than the anoxic threshold (0.38), unusually low Fe_T (0.9%; in comparison with crustal Fe abundance of ~5%) and low Fe_T/Al ratios (~0.14) may have exaggerated Fe_{HR}/Fe_T ratios. Therefore, the lack of RSE enrichment in shelf-margin and upper slope sections is most likely caused by oxic-suboxic water column conditions unfavorable for recording the oceanic RSE reservoir.

Sedimentological evidence indicates that the depositional environments of the upper slope were close to the chemocline of the stratified Nanhua basin (Jiang et al.,

2011), where chemocline instability may have caused redox fluctuations and variable Fe_{HR}/Fe_T and Fe_P/Fe_T values (Poulton et al., 2010). Fluctuating redox conditions may record moderate RSE jumps. Therefore, Fe speciation results document likely alternating oxic, suboxic, and short lived euxinic environments in the vicinity of the shelf margin and pervasive deep-water euxinia in lower slope during Member IV period, even though Fe-rich conditions appear to have been common in bottom waters during this time (Canfield et al., 2008, Li et al., 2010).

5.2. Fe_T/Al ratios and the provenance of Member II and Member IV shales

Fe_T/Al ratios may add to our understanding of past redox conditions (Lyons et al., 2003; Lyons and Severmann, 2006; Raiswell et al., 2011). In the modern ocean, anoxic marine sediments are enriched in reactive Fe (e.g., the Black Sea, Orca Basin, Effingham Inlet, and Cariaco Basin; Lyons et al., 2003; Lyons and Severmann, 2006), and their Fe/Al ratios (a mean of 0.53 ± 0.11; Raiswell et al., 2008) exceeds the average marine shale Fe_T/Al ratio of 0.5 (Taylor and McLennan, 1985). In ancient anoxic shales, reactive Fe is decoupled from the siliciclastic flux and they often have elevated Fe_T/Al ratios exceeding the oxic baseline (e.g., Kendall et al., 2009; Gill et al., 2011). In contrast to this prediction, shales from both Member II and Member IV of the Doushantuo Formation have a wide range of FeT/Al ratios, with the majority of samples falling below average shale values (Fig 6). The only exception are the shales from the inner shelf Jiulongwan section where most samples have elevated Fe_T/Al ratios (Li et al., 2010) close to the average shale value, which is consistent with deposition from shallow-water environments without significant authigenic Fe enrichment.

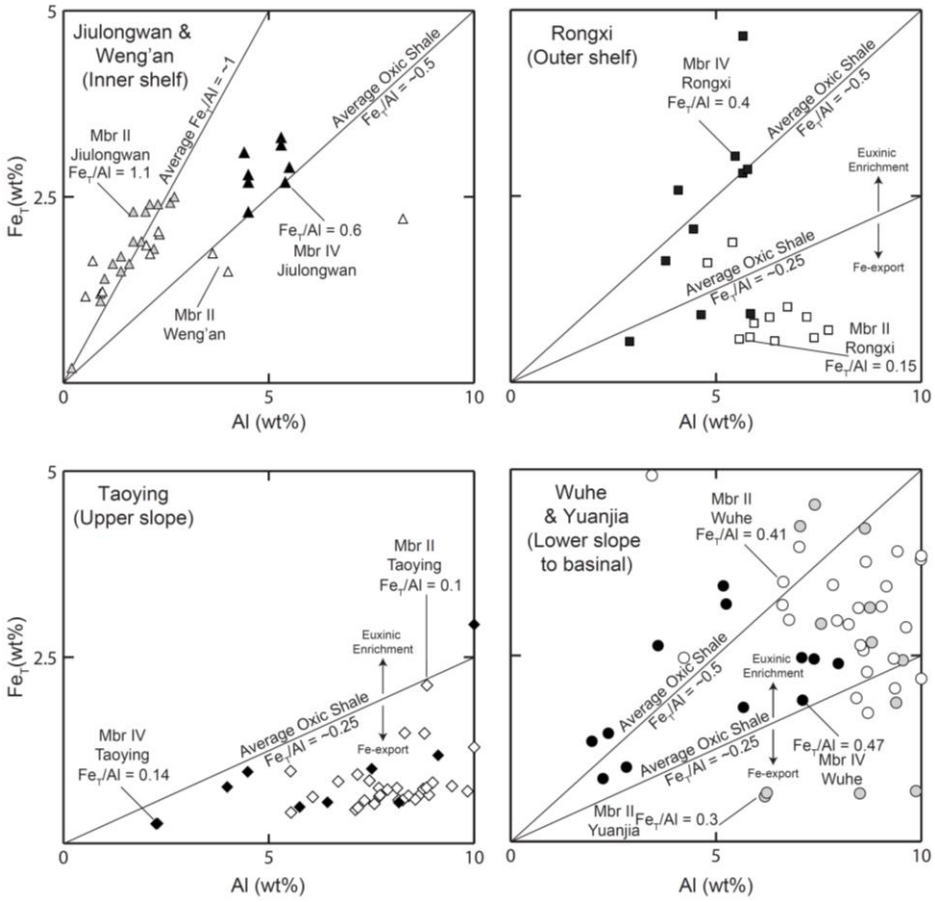

Figure 6 Total iron (Fe_T) plotted versus aluminum (Al) for the Doushantuo Member II and Member IV black shales. (**A**) In the shallow water inner shelf sections of the Yangtze platform and Weng'an, majority of the euxinic shale samples have higher Fe_T/Al ratios than average oxic shale (Taylor and McLennan, 1985; Raiswell et al., 2008). (**B**) In the outer shelf, oxic and ferruginous shale has a comparatively lower average Fe_T/Al ratio (0.15) than average oxic shale (Lyons and Severmann, 2006). However, for member IV, the ratio is close to oxic shelf (0.4). (**C**) In the upper slope Taoying section, both Member II and IV shales are predominantly oxic, and has a substantially lower average Fe_T/Al ratio (0.08 to 0.14) than average oxic shale. (**D**) Lower slope and basinal sections have scattered Fe_T/Al ratios, although most fall within the euxinic enrichment zone. During Member II, shales from outer slope and upper shelf sections are finer-grained than shale from inner shelf Weng'an and Jiulongwan, and the preferential concentration of Al in the clay sized sediment fraction is the most likely explanation for lower Fe_T/Al ratios of oxic shale Taoying (also see Figure 10). A similarly low oxic Fe_T/Al baseline is observed in the Member IV of Taoying section (0.14). Shale from Upper slope during Member IV is also clay-rich compared to inner shelf, likely explaining lower baseline Fe_T/Al values for oxic shale. Euxinic samples then show iron enrichment above this baseline in lower slope and basinal sections, both during Member II and IV, yet a handful of samples exhibit loss of iron below this baseline. This is tentatively attributed to iron reduction and export to the water column, which is seen in modern oxic shelf.

The shelf margin and upper slope shale samples have substantially low Fe_T/Al ratios. Member IV shales, on the other hand, have relatively more consistent Fe_T/Al ratios and are often elevated when reactive Fe is enriched. Samples with low Fe_{HR}/Fe_T ratios (< 0.38) have an average Fe_T/Al ratio of 0.27, and in these samples Al contents (average ~8 wt %) are higher than those of euxinic ($Fe_{HR}/Fe_T > 0.38$; $Fe_P/Fe_{HR} > 0.7$) shales (Fig. 5). Because Al is preferentially concentrated in the clay-sized fraction of siliciclastic sediments (Nesbitt et al., 1996; Mishra and Sen, 2011), it suggests that lower Fe_T/Al ratios from shelf-margin and upper slope sections (Taoying, Zhongling and Rongxi) may be related to higher clay content in black shales. Despite overall low Fe_T/Al ratios, euxinic shale samples ($Fe_{HR}/Fe_T > 0.38$ and $Fe_P/Fe_{HR} > 0.7$) from Member IV are generally enriched in Fe_T (Figs. 5 and 9), supporting authigenic pyrite enrichment under euxinic conditions. A subset of the samples, mostly from the upper slope Taoying section, are oxic ($Fe_{HR}/Fe_T < 0.38$) and have Fe_T/Al ratios lower than the oxic baseline of siliciclastic flux (e.g., Figs. 4 and 5). A reasonable speculation for such low Fe_T may be Fe remobilization during early oxic diagenesis (Raiswell and Canfield, 1998; Anderson and Raiswell, 2004).

The low Fe_T/Al ratios of the Doushantuo Formation could have been related to the sediment source and paleogeographic location of measured sections. Strong restriction and recycling may have led to the loss of Fe in clay minerals in some sections. Huang et al. (2012) suggested different sediment source for early and late Ediacaran shale units of the Nanhua basin. On the basis of major and trace elemental contents, particularly Al_2O_3/TiO_2 ratios, they suggested that the Doushantuo Member II shales had a sediment source from mafic igneous rocks. Because both Al and Ti are chemically

inert elements and have short resident time in seawater; their concentrations in sediments are mainly controlled by the composition of sediment source rocks (Maynard, 1992; McLennan et al., 1993). In general, feldspathic rocks host the majority of crustal Al, whereas Ti is more abundant in mafic rocks, associated with minerals such as olivine, pyroxene, biotite and ilmenite (Huang et al., 2012). Therefore, low Al_2O_3/TiO_2 ratios (e.g., 3–8) suggest sediment source from mafic igneous rocks and high Al_2O_3/TiO_2 ratios (e.g., 21-70) are suggestive of felsic source rocks (Huang et al., 2012).

The Al_2O_3/TiO_2 ratios from measured sections (Fig. 7) across the shelf-to-basin transect in Guizhou show drastically different patterns from that of the Jiulongwan section reported by Huang et al. (2012). Although Member II and Member IV shales show slightly different trajectories, the general Al_2O_3/TiO_2 slopes of both Member II and Member IV in all sections are similar to that of the Member IV black shales in the Jiulongwan section, which has been interpreted as recording Al_2O_3/TiO_2 ratios of open oceans sediments (Huang et al., 2012). The unusual Al_2O_3/TiO_2 pattern from Member II shales of the Jiulongwan section, which has been interpreted as resulting from mafic-ultramafic source rocks, is a much localized feature that occurs only in the Yangtze Gorges area (Fig. 7). Thus, the overall low Fe_T/Al ratios of the Doushantuo black shales were less likely controlled by the source rocks but quite possibly controlled by the type and concentration of clay minerals, which needs further investigation in the future.

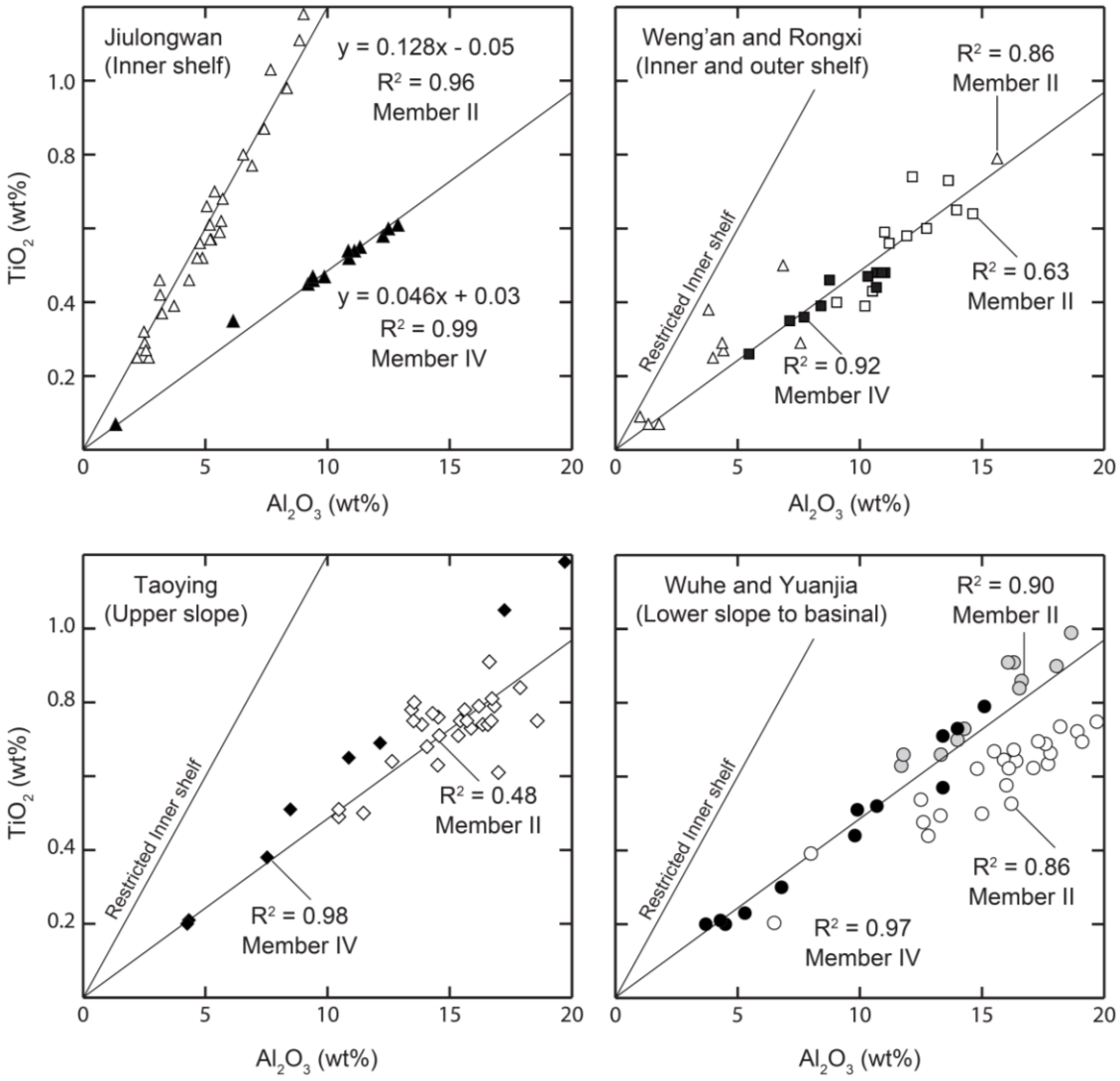

Figure 7 Plots of TiO_2 vs. Al_2O_3 for Member II and Member IV black shales. Al_2O_3/TiO_2 ratios range from 3 to 8 for mafic igneous rocks, 8 to 21 for igneous rocks of intermediate composition, and 21 to 70 for felsic igneous rocks (Hayashi et al., 1997). We used data from Huang et al., (2012) as a reference value for restricted and open ocean setting. (**A**) Member II shales from Jiulongwan (Yangtze Platform) have lower ratios (7 to 10), therefore, points towards dominantly mafic source and restricted environment. During Member IV, however, shales suggest a more open ocean felsic environment. (**B-D**) All the shales from Transect 2, both Member II and Member IV, have open ocean type settings and reflects higher Al_2O_3/TiO_2 ratios. Therefore the low Fe_T/Al ratios of the Doushantuo black shales and spatial RSE variations are not mainly resulted from basin restriction.

6. Conclusions

High redox sensitive element (RSE) enrichments in the basal Member II (ca. 635-630 Ma) and Member IV (ca. 551 Ma) black shales of the Ediacaran Doushantuo Formation in South China record ocean oxygenation events that expanded the marine RSE reservoirs. However, large spatial variations in RSE concentration are observed among time-equivalent shales of the Doushantuo Formation. For Member II black shales, near crustal RSE values are observed in inner shelf sections of the Yangtze platform (e.g., Weng'an and Jiulongwan), despite euxinic conditions indicated by iron speciation data. The absence of framboidal pyrites or presence of only large-diameter framboidal pyrites, plus strongly positive pyrite $\delta^{34}S$ (up to 45‰) in these sections, suggest pore-water euxinia instead of water-column euxinia. The lack of RSE enrichments in these sections is thus interpreted as controlled by local oxic-suboxic environments incapable of capturing the oceanic RSE signature. Member IV black shales show similar spatial RSE variations but in this case, the shelf-margin and upper slope sections did not capture the oceanic RSE signature due to fluctuating oxic-suboxic-anoxic local redox conditions likely close to the chemocline of the Nanhua basin. These examples demonstrate that, in many cases, iron speciation alone cannot definitively identify oxic/anoxic/euxinic water column redox chemistry and using RSE enrichments as a global redox indicator requires comprehensive multi-proxy study across different paleogeographic positions of sedimentary basins. This phenomenon partially explains the lack of RSE enrichments (and thus the lack of signature for ocean oxygenation) in many Doushantuo sections and other sections globally (for example, western Laurentia).

The Doushantuo Member II and Member IV black shales show variable Fe_T/AL ratios, some of which are significantly lower than the average crustal Fe_T/AL ratio of ~0.5. Previous interpretations ascribed the low Fe_T/AL ratios to changes in sedimentary source rocks. Compilation of Al_2O_3/TiO_2 ratios from measured sections and literature indicates open-ocean Al_2O_3–TiO_2 pattern in most Doushantuo sections and unusually low Al_2O_3/TiO_2 ratios documented from Member II shales in the Yangtze Gorges area represent a much localized phenomenon. Low Fe_T/Al ratios of the Doushantuo shales may be related to the type and concentration of clay minerals in shales that requires further investigation.

7. References

Algeo, T.J., and Lyons, T.W., 2006, Mo-total organic carbon covariation in modern anoxic marine environments: Implications for analysis of paleoredox and paleohydrographic conditions: Paleoceanography, v. 21, no. 1.

Anbar, A. D. & Knoll, A. H., 2002, Proterozoic ocean chemistry and evolution: A bioinorganic bridge?: Science, v. 297, p. 1137–1142.

Anbar, A. D., 2008, Elements and evolution: Science, v. 322, p. 1481–1483.

Anderson, T.F., Raiswell, R., 2004. Sources and mechanisms for the enrichment of highly reactive iron in euxinic Black Sea sediments. Am. J. Sci. 304, 203-233.

Bond, D.P.G., Wignall, P.B., 2005. Evidence for Late Devonian (Kellwasser) anoxic events in the Great Basin, western United States. In: Morrow, J., Over, J., Wignall, P.B. (Eds.), Understanding Late Devonian and Permian–Triassic biotic

and climatic events: towards an integrated approach. Developments in Palaeontology and Stratigraphy. Elsevier, pp. 225–261.

Bond, D., Wignall, P.B., Racki, G., 2004. Extent and duration of marine anoxia during the Frasnian–Famennian (Late Devonian) mass extinction in Poland, Germany, Austria and France. Geol. Mag. 141, 173–193.

Bristow, T.F., and Kennedy, M.J., 2008, Carbon isotope excursions and the oxidant budget of the Ediacaran atmosphere and ocean: Geology, v. 36, p. 863-866.

Canfield, D.E., Poulton, S.W., Knoll, A.H., Narbonne, G.M., Ross, G., Goldberg, T., and Strauss, H., 2008, Ferruginous Conditions Dominated Later Neoproterozoic Deep-Water Chemistry: Science, v. 321, no. 5891, p. 949-952.

Condon, D., Zhu, M., Bowring, S., Wang, W., Yang, A., and Jin, Y., 2005, U-Pb Ages from the Neoproterozoic Doushantuo Formation, China: Science, v. 308, p. 95-98.

Emerson, S.R., and Huested, S.S., 1991, Ocean anoxia and the concentrations of molybdenum and vanadium in seawater: Marine Chemistry, v. 34, no. 3-4, p. 177-196.

Falkowski, P.G., Katz, M.E., Knoll, A.H., Quigg, A., Raven, J.A., Schofield, O., and Taylor, F.J.R., 2004, The Evolution of Modern Eukaryotic Phytoplankton: Science, v. 305, no. 5682, p. 354-360.

Falkowski, P.G., and Godfrey, L.V., 2008, Electrons, life and the evolution of Earth's oxygen cycle: Philosophical Transactions of the Royal Society B: Biological Sciences, v. 363, p. 2705-2716.

Gill, B.C., Lyons, T.W., Young, S.A., Kump, L.R., Knoll, A.H., Saltzman, M.R. 2011.

Sulphur isotope evidence for widespread euxinia in the Later Cambrian ocean. Nature v. 469 p. 80-83.

Hastings, D.W., Emerson, S.R., Erez, J., and Nelson, B.K., 1996, Vanadium in foraminiferal calcite: Evaluation of a method to determine paleo-seawater vanadium concentrations: Geochimica et Cosmochimica Acta, v. 60, no. 19, p. 3701-3715.

Hayashi, K., Fujisawa, H., Holland, H.D., and Ohmoto, H., 1997, Geochemistry of ~1.9 Ga sedimentary rocks from northeastern Labrador, Canada: Geochimica et Cosmochimica Acta, v. 61, no. 19, p. 4115-4137.

Hetzel, A., Böttcher, M.E., Wortmann, U.G., and Brumsack, H., 2009, Paleo-redox conditions during OAE 2 reflected in Demerara Rise sediment geochemistry (ODP Leg 207): Palaeogeography, Palaeoclimatology, Palaeoecology, v. 273, no. 3–4, p. 302-328.

Huang, J., Chu, X., Lyons, T.W., Planavsky, N.J., and Wen, H., 2013, A new look at saponite formation and its implications for early animal records in the Ediacaran of South China: Geobiology, v. 11, no. 1, p. 3-14.

Jiang, G., Zhang, S., Shi, X., and Wang, X., 2008, Chemocline instability and isotope variations of the Ediacaran Doushantuo basin in South China: Science in China Series D-Earth Sciences, v. 51, p. 1560-1569.

Jiang, G., Shi, X., Zhang, S., Wang, Y., and Xiao, S., 2011, Stratigraphy and paleogeography of the Ediacaran Doushantuo Formation (ca. 635–551 Ma) in South China: Gondwana Research, v. 19, p. 831-849.

Jiang, G., Kennedy, M.J., and Christie-Blick, N., 2003a, Stable isotopic evidence for

methane seeps in Neoproterozoic postglacial cap carbonates: Nature, v. 426, p. 822-826.

Jiang, G., Wang, X., Shi, X., Zhang, S., Xiao, S., and Dong, J., 2010, Organic carbon isotope constraints on the dissolved organic carbon (DOC) reservoir at the Cryogenian–Ediacaran transition: Earth and Planetary Science Letters, v. 299, no. 1–2, p. 159-168.

Jiang, S., Yang, J., Ling, H., Chen, Y., Feng, H., Zhao, K., and Ni, P., 2007, Extreme enrichment of polymetallic Ni–Mo–PGE–Au in Lower Cambrian black shales of South China: An Os isotope and PGE geochemical investigation: Palaeogeography, Palaeoclimatology, Palaeoecology, v. 254, no. 1–2, p. 217-228.

Jiang, G., Sohl, L.E., Christie-Blick, N., 2003a. Neoproterozoic stratigraphic comparison of the Lesser Himalaya (India) and Yangtze Block (South China); paleogeographic implications: Geology, v. 31, p. 917–920.

Kendall, B., Creaser, R.A., Calver, C.R., Raub, T.D., and Evans, D.A.D., 2009, Correlation of Sturtian diamictite successions in southern Australia and northwestern Tasmania by Re–Os black shale geochronology and the ambiguity of “Sturtian”-type diamictite–cap carbonate pairs as chronostratigraphic marker horizons: Precambrian Research, v. 172, no. 3–4, p. 301-310.

Liu, P.J., Yin, C.Y., Gao, L.Z., Tang, F., Chen, S.M., 2009. New material of microfossils from the Ediacaran Doushantuo Formation in the Zhangcunping area, Yichang, Hubei Province and its zircon SHRIMP U–Pb age: Chinese Science Bulletin, v. 54, p. 1058–1064.

Li, C., Love, G.D., Lyons, T.W., Fike, D.A., Sessions, A.L., and Chu, X., 2010, A

Stratified Redox Model for the Ediacaran Ocean: Science, v. 328, no. 5974, p. 80-83.

Lyons, T.W., and Severmann, S., 2006, A critical look at iron paleoredox proxies: New insights from modern euxinic marine basins: Geochimica et Cosmochimica Acta, v. 70, no. 23, p. 5698-5722.

Lyons, T.W., Anbar, A.D., Severmann, S., Scott, C., and Gill, B.C., 2009, Tracking Euxinia in the Ancient Ocean: A Multiproxy Perspective and Proterozoic Case Study: Annual Review of Earth and Planetary Sciences, v. 37, no. 1, p. 507-534.

McFadden, K.A., Huang, J., Chu, X., Jiang, G., Kaufman, A.J., Zhou, C., Yuan, X., and Xiao, S., 2008, Pulsed oxidation and biological evolution in the Ediacaran Doushantuo Formation: Proceedings of the National Academy of Sciences, USA, v. 105, p. 3197–3202.

Mishra, M., Sen, S., 2011. Geochemical signatures for the grain size variation in the siliciclastics of Kaimur Group, Vindhyan Supergroup from Markundi Ghat, Sonbhadra District, (U.P.), India. Geochemistry Int. v. 49, p. 274-290.

Miller, C.A., Peucker-Ehrenbrink, B., Walker, B.D., and Marcantonio, F., 2011, Re-assessing the surface cycling of molybdenum and rhenium: Geochimica et Cosmochimica Acta, v. 75, no. 22, p. 7146-7179.

Nesbitt, H.W., Young, G.M., and Bosman, S.A., 2009, Major and trace element geochemistry and genesis of supracrustal rocks of the North Spirit Lake Greenstone belt, NW Ontario, Canada: Precambrian Research, v. 174, no. 1–2, p. 16-34.

Owens, J.D., Lyons, T.W., Li, X., et al., 2012, Iron isotope and trace metal records of iron cycling in the proto-North Atlantic during the Cenomanian-Turonian oceanic anoxic event (OAE-2): Paleoceanography, v. 27, no. 3, p. - PA3223.

Partin, C.A., Bekker, A., Planavsky, N.J., et al., 2013, Large-scale fluctuations in Precambrian atmospheric and oceanic oxygen levels from the record of U in shales: Earth and Planetary Science Letters, v. 369–370, no. 0, p. 284-293.

Poulton, S.W., and Canfield, D.E., 2005, Development of a sequential extraction procedure for iron: implications for iron partitioning in continentally derived particulates: Chemical Geology, v. 214, no. 3–4, p. 209-221.

Poulton, S., Fralick, P., Canfield, D., 2010. Spatial variability in oceanic redox structure 1.8 billion years ago: Nature Geoscience, v. 3, p. 486-490.

Poulton, S.W., and Canfield, D.E., 2011, Ferruginous Conditions: A Dominant Feature of the Ocean through Earth's History: Elements, v. 7, no. 2, p. 107-112.

Raiswell, R. & Canfield, D.E., 1998, Sources of iron for pyrite formation in marine sediments. American Journal of Science, v. 298, p. 219-245.

Raiswell, R., Reinhard, C.T., Derkowski, A., Owens, J., Bottrell, S.H., Anbar, A.D., Lyons, T.W., 2011. Formation of syngenetic and early diagenetic iron minerals in the late Archean Mt. McRae Shale, Hamersley Basin, Australia: New insights on the patterns, controls and paleoenvironmental implications of authigenic mineral formation:. Geochim. Cosmochim. Acta, v. 75, p. 1072-1087.

Raiswell, R., Newton, R., Bottrell, S.H., Coburn, P.M., Briggs, D.E.G., Bond, D.P.G.,

Poulton, S.W., 2008. Turbidite depositional influences on the diagenesis of Beecher's Trilobite Bed and the Hunsrück Slate; sites of soft tissue pyritazation: American Journal of Science, v. 308, p. 105-129.

Reinhard, C.T., Planavsky, N.J., Robbins, L.J., et al., 2013, Proterozoic ocean redox and biogeochemical stasis: Proceedings of the National Academy of Sciences, v. 110, no. 14, p. 5357-5362.

Sahoo, S.K., Planavsky, N.P., Kendall, B., Wang, X., Shi, X., Scott, C., Anbar, A.D., Lyons, T.W., and Jiang, G., 2012, Ocean oxygenation in the wake of the Marinoan glaciation: Nature, v. 489, p. 546-549.

Saito, M.A., Sigman, D.M., Morel, F.M.M., 2003. The bioinorganic chemistry of the ancient ocean: the co-evolution of cyanobacterial metal requirements and biogeochemical cycles at the Archean-Proterozoic boundary? Inorg. Chim. Acta 356, 308-318.

Scott, C., Lyons, T.W., Bekker, A., Shen, Y., Poulton, S.W., Chu, X., and Anbar, A.D., 2008, Tracing stepwise oxygenation of the Proterozoic ocean: Nature, v. 452, p. 456-459.

Taylor, S.R., McLennan, S.M., 1985. The continental crust: its composition and evolution. Blackwell Scientific Publications, Palo Alto, CA.

Tribovillard, N., Algeo, T.J., Lyons, T., and Riboulleau, A., 2006, Trace metals as paleoredox and paleoproductivity proxies: An update: Chemical Geology, v. 232, no. 1–2, p. 12-32.

Wong, F.W. Lytle, R.P. Messmer, D.H. Maylotte, 1984, K-edge absorption spectra of selected vanadium compounds, Physical Review B, v. 30, p. 5596-5610.

Wang, Y., Wang, X., 2006.,The holdfasts of macroalage in the Neoproterozoic Doushantuo Formation in northeastern Guizhou province and their environmental significance: Acta Micropalaeontologia Sinica, v. 23, p. 154–164.

Wang, L., Shi, X., and Jiang, G., 2012, Pyrite morphology and redox fluctuations recorded in the Ediacaran Doushantuo Formation: Palaeogeography, Palaeoclimatology, Palaeoecology, v. 333–334, no. 0, p. 218-227.

Wignall, P.B., Newton, R., 1998. Pyrite framboid diameter as a measure of oxygen deficiency in ancient mudrocks: American Journal of Science, v. 298, p. 537–552.

Xiao, S., Zhang, Y., Knoll, A.H., 1998. Three-dimensional preservation of algae and animal embryos in a Neoproterozoic phosphorite: Nature, v. 391, p. 553–558.

Yin, L., Zhu, M., Knoll, A.H., Yuan, X., Zhang, J., and Hu, J., 2007, Doushantuo embryos preserved inside diapause egg cysts: Nature, v. 446, p. 661–663.

Yuan, X., Chen, Z., Xiao, S., Zhou, S., Hua, H., 2011. An early Ediacaran assemblage of macroscopic and morphologically differentiated eukaryotes: Nature, v. 470, p. 390–393.

Zerkle, A.L., House, C.H., Cox, R.P., and Canfield, D.E., 2006, Metal limitation of cyanobacterial N_2 fixation and implications for the Precambrian nitrogen cycle: Geobiology, v. 4, no. 4, p. 285-297.

Zhang, S., Jiang, G., Han, Y., 2008c. The age of the Nantuo Formation and Nantuo glaciation in South China: Terra Nova, v. 20, p. 289–294.

Zhou, C., Xie, G., Mcfadden, K., Xiao, S., Yuan, X., 2007. The diversification and extinction of Doushantuo-Pertatataka acritarchs in South China: causes and biostratigraphic significance: Geological Journal, v. 42, p. 229–262.

APPENDIX A: CHAPTER 2

1. Supplementary Information

1.1 Stratigraphy and paleogeographic reconstruction of the Doushantuo Formation

The Ediacaran Doushantuo Formation (ca. 635–551 Ma) (Condon et al., 2005) in South China overlies the late Cryogenian Nantuo Formation (ca. 654–635 Ma) (Zhang et al., 2008). The type section of the Doushantuo Formation is defined in the Yangtze Gorges area where it is divided into four members (McFadden et al., 2008; Zhu et al., 2007; Zhou et al., 2007; Jiang et al., 2011). Member I refer to the 3-6-m-thick cap carbonate at the base of the Doushantuo Formation. Member II consists of alternating organic-rich shale and carbonates with abundant centimeter-scale chert nodules. Member III consists of predominately carbonates with bedded chert layers and minor shale laminae. Member IV refers to the ca. 10-m-thick black, organic-rich shale interval at the top of the Doushantuo Formation. The thickness of the Doushantuo Formation varies from 40 to 200 m and lateral facies change from shallow-water phosphatic dolostone to deeper-water black shale and siliceous shales (Zhu et al., 2007; Zhou et al., 2007; Jiang et al., 2011). The Doushantuo cap carbonate (Member I) (Jiang et al., 2003a; Jiang et al., 2006) and the organic-rich black shale of Member IV serve as the marker beds for the overall stratigraphic correlation across the basin (Jiang et al., 2011).

The Doushantuo Formation was deposited as part of a passive continental margin succession (Wang and Li, 2003; Jiang et al., 2003b; Liu et al., 1993). The paleogeographic reconstruction of the Doushantuo Formation (Fig. S1) was based on the facies analyses across the shelf-to-basin transects (Jiang et al., 2011). The uniform

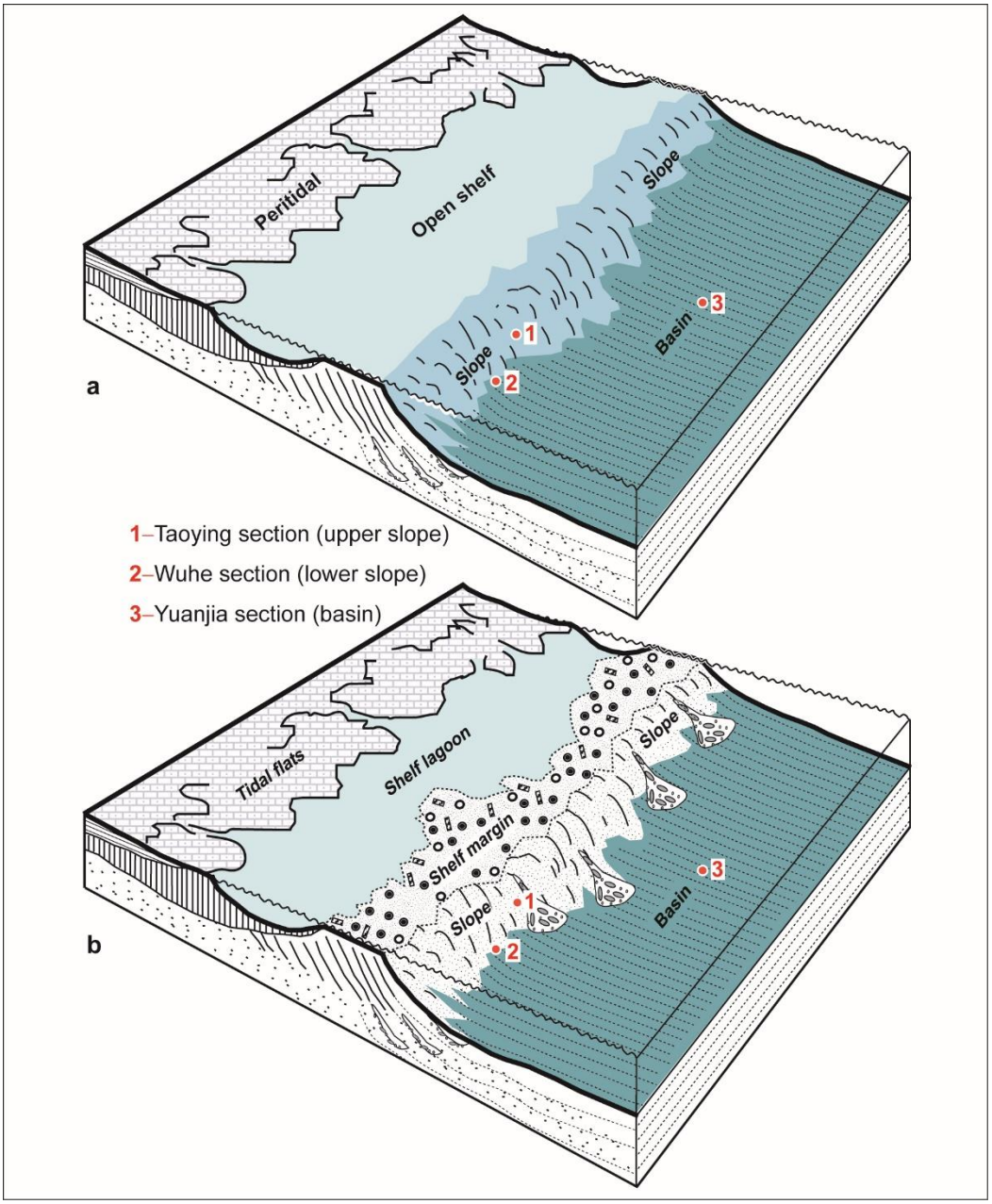

Figure S1 Paleogeographic reconstruction of the Ediacaran Yangtze platform during the deposition of the Doushantuo Formation (ca. 635-551 Myr) (Jiang et al., 2011). **a**, open shelf for the lower Doushantuo Formation. **b**, rimmed shelf for the middle and upper Doushantuo Formation. The depositional setting for the sampled interval (lower Doushantuo Formation) is illustrated in (**a**). Sampled sections are from the slope (loc. 1& 2) and basin (loc. 3) settings that were below the storm wave base and were well connected with the open ocean. Paleobathymetric estimation is based on the continental slope gradient (Liu et al., 1993) and accommodation space of Cambrian-early Silurian stratigraphic units (Jiang et al., 2006; Jiang et al., 2003b). The water depth of the basinal section (loc. 3) is estimated to have been greater than 1000 m.

thickness and similar facies of the Doushantuo cap carbonate (Member I) and its immediately overlying black shales (lower Member II) across the basin suggest an open shelf setting at the beginning of the Doushantuo deposition (Fig. S1a). The open shelf evolved into a rimmed shelf (Fig. S1b) after the Doushantuo cap carbonate deposition, from a topographic high inherited from the Nantuo glaciation and/or through preferential carbonate growth at the shelf margin (Jiang et al., 2011). This change is marked by the presence of shallow-water carbonate facies with exposure features in the shelf margin and by the abundance of olistostrome carbonates and slump blocks in the upper slope sections adjacent to the open ocean side of the platform margin (Fig. S1b) (Jiang et al., 2011).

Most of the existing geochemical studies of the Doushantuo Formation have been focused on the Yangtze Gorges or adjacent areas (e.g., ref. McFadden et al., 2008; Li et al., 2010; Bristow et al., 2009). Existing redox sensitive element (RSE) analyses of the lower Doushantuo Formation from this area (Li et al., 2010; Bristow et al., 2009) did not reveal high RSE enrichments or a signal for a large fractionation of microbial sulphate reduction indicative of high (> 1 mM) dissolved sulphate concentrations. Unusually low RSE values from this region have been ascribed to basin isolation from the open ocean (Bristow et al., 2009). Alternative interpretation of the low RSE values from the Yangtze Gorges area could be oxic-dysoxic water column conditions that did not capture the ocean dissolved RSE concentration and that sulphate reduction was restricted to porewaters (closed system behavior). This study focuses on deep-water sections in the open-ocean side of the platform (Fig. S1).

1.2 Sequence stratigraphic interpretation of the lower Doushantuo Formation

The 3–6-m-thick Doushantuo cap carbonate is the most widespread and distinctive stratigraphic unit across the Nanhua basin (Jiang et al., 2011; Jiang et al., 2003a; Jiang et al., 2006). The cap carbonate has a sharp contact with the underlying glacial diamictite of the Nantuo Formation, with no interbedded carbonate and diamictite at the transition. Instead, in most studied sections across the basin, there is an 8-to-20-cm thick claystone/siltstone layer separating the cap carbonate and diamictite (Zhang et al., 2008; Jiang et al., 2006). These features suggest that the Doushantuo cap carbonate was deposited during the late stage of postglacial transgression when continental ice sheets have largely disappeared in the Yangtze block (Zhang et al., 2008; Jiang et al., 2006). Diachronous cap carbonate deposition tracking glacioeustatic flooding, reported from the Keilberg cap dolostone in Namibia[14] and the Nuccaleena Formation in Australia (Rose et al., 2010), is not present in the Doushantuo cap carbonate and may have happened earlier, most likely during the deposition of the Nantuo Formation (Zhang et al., 2008; Jiang et al., 2006). Given the transitional facies change from the cap carbonate to its overlying black shales (Jiang et al., 2010), the deglacial isostatic rebound may have also happened before cap carbonate deposition, although it has been argued that the 'dissolution' features and barites atop the cap carbonate in some shelf sections may record ice-melting isostatic rebound (Zhou et al., 2010).

The basal Member II black shales have a transitional contact with the underlying cap carbonate across the basin (Jiang et al., 2006; Jiang et al., 2010) and were most likely deposited during latest transgression or early highstand of sea level. Subsequent sea-level fall formed exposure surfaces at the platform margin and slump blocks and olistostrome

carbonates in the upper slope environments (Zhu et al., 2007; Jiang et al., 2011; Vernhet et al., 2007), but these features are stratigraphically higher than our sampled intervals. The black shales are thinly laminated, without wave- or storm-generated coarse-grained beds and turbidites (Jiang et al., 2010), suggesting their deposition well below the storm wave base.

1.3 Sample location, paleobathymetric estimation, and age constraints

The lower Doushantuo Formation black shales were collected from recently excavated outcrop sections. Samples were collected at an average spacing of 20 cm and, for the present work, samples with macroscopic pyrites were avoided.

Three sections were chosen to cover the upper slope to basinal paleo-depositional environments (Jiang et al., 2011) (Fig. S1): (1) the upper slope section in Taoying, Guizhou province (27°50’01.5”N, 109°01’03.9”E), (2) the lower slope section in Wuhe, Guizhou province (26°45’93.6”N, 108°25’00.5”E), and (3) the basinal section in Yuanjia, Hunan province (27°29’23”N, E110°14’37.4”E).

Based on the basin reconstruction, the cap carbonate and the basal Member II shales were deposited from a passive continental margin that inherited the topographic gradient from the Cryogenian continental margin (Jiang et al., 2011; Jiang et al., 2006; Liu et al., 1993). Paleobathymetric estimation based on the continental slope gradient (Liu et al., 1993) and accommodation space inferred from the thickness of Cambrian–early Silurian stratigraphic units (backstripping analyses) (Jiang et al., 2006; Jiang et al., 2003b) suggest that the water depth of the basinal section (Yuanjia; section 3) were greater than ~1000 m.

Our samples cover the first 5–9-m-thick black shales above the Doushantuo cap carbonate (or 9.5 m to 13.7 m above the base of the Doushantuo Formation; Table S1). We estimated that the age of the sampled interval is likely between ca. 635 Ma and 630 Ma (or conservatively, no younger than ca. 614 Ma), based on the following evidence: (1) The Doushantuo cap carbonate has been dated in the Yangtze Gorges area (shelf section) as 635.2±0.6 Ma (Condon et al., 2005). This age was from an ash bed 2.3 m above the base of the Doushantuo Formation (within the cap carbonate). From an adjacent section in the same area, an ash bed 5 m above the Doushantuo cap carbonate (9.5 m above the base of the Doushantuo Formation) was dated as 632.5±0.5 Ma (Condon et al., 2005). Hence, the duration of the 7.2-m-thick strata at the lower Doushantuo Formation in the Yangtze Gorges area is ~3 Myr. Assuming approximately synchronous deposition of the distinctive cap carbonate member and its immediate overlying black shale during the late transgression and early highstand, the sampled intervals (9.5–13.7 m thick) could be > 635 Ma and < 630 Ma. (2) The sampled interval is within the depositional sequence associated with the postglacial transgression (Jiang et al., 2011). Olistostrome carbonates and slump blocks indicative of sea-level fall are found in slope sections, but they are above the sampled intervals. (3) Samples are within the carbon isotope excursion associated with the cap carbonate and its overlying strata (Jiang et al., 2010). (4) The overall thickness of the Doushantuo Formation in measured sections, constrained by two marker beds (the cap carbonate and Member IV organic-rich black shales), is consistent with the stratigraphic correlation that the basal Member II in slope–basinal sections may be time-equivalent with that in the Yangtze Gorges area (Jiang et al., 2011). For example, the thickness of the Doushantuo Formation in the

Yangtze Gorges area is 155 m thick, and in the Wuhe section (loc. 2; Fig. S1) it is 120 m thick. In the Yangtze Gorges area, an age of 614±7.6 Ma was obtained from the middle Doushantuo Formation (Liu et al., 2009), at a stratigraphic position much higher than the basal member II shales. Thus, even with a conservative estimation, the analyzed basal member II shales should be older than ca. 614 Ma. In summary, litho-, sequence and chemostratigrapic correlation of the well-dated cap carbonate and its overlying shale interval (in the Yangtze Gorges area) across the basin suggest that the age of our analyzed shales is likely ca. 635–630 Ma, but any U-Pb zircon ages and/or Re-Os ages from the basinal sections could provide additional support for this age assignment.

1.4 Notes on the Cryogenian–early Ediacaran paleontological record

Historically, the prevailing view was that metazoans first appeared during the early Ediacaran Period (McFadden et al., 2008; Xiao et al., 1998; Yin et al., 2007; Yuan et al., 2011), shortly after the termination of the late Cryogenian (Marinoan) 'Snowball Earth' glaciation (ca. 635 Ma). However, recent molecular clock estimates place the origin of crown-group animals in the Cryogenian Period, but these animals, if they existed, were likely detritus feeders with minimum oxygen requirements (Erwin et al., 2011). There are sponge-biomarkers (Love et al., 2009) and claims of sponge-like fossils in Cryogenian or older rocks (Maloof et al., 2010; Brian et al., 2012; Neuweiler et al., 2009), but some of these fossils are controversial (Planavsky et al., 2009). Again, even if they are correctly interpreted, Cryogenian animals are likely simple metazoans with very limited oxygen demand (Hoffmann et al., 2008).

Animal embryo-like fossils from the early-middle Ediacaran Doushantuo Formation (Xiao et al., 1998; Yin et al., 2007) have been challenged (Huldtgren et al.,

2011), but existing evidence seem to support that they more likely represent stem-group metazoans (Xiao et al., 2012; Schiffbauer et al., 2012). The Lantian biota contains an assemblage of morphologically differentiated microfossils (Yuan et al., 2011); some of them can be reasonably interpreted as non-poriferan metazoans (Yuan et al., 2011). Further, there is a radiation in marine algae following the Marinoan glaciation, which has been linked to shift in ecosystem complexity driven by metazoan increase in trophic levels (Peterson et al., 2005; Butterfield, 2009). In the modern ocean, algae morphology is driven by metazoan grazing pressure rather than light or nutrient demands (Smetacek, 2001). Therefore, it is likely that the appearance of novel morphologies in primary producers, after a billion year period of sluggish evolutionary innovation, is linked to a major change in ecosystem structure (Peterson et al., 2005). Thus, there is evidence for significant biological innovation in the earliest Ediacaran.

It is important, however, to note that although metazoans certainly had evolved and diversified in the early Ediacaran, animals with energetically expensive and oxygen-demanding lifestyles (e.g., locomotion, carnivory, burrowing) appeared much later in the fossil record (< 590–558 Ma) (Pecoits et al., 2012; Liu et al., 2010; Ivanstov, 2009)—more than 40 million years after pervasive early Ediacaran (ca. 635–630 Ma) ocean oxygenation documented in our work. Ocean ventilation could have certainly set the stage for early animals and their subsequent evolution, but it is not necessarily the direct trigger for bilaterian radiation.

1.5 Analytical methods

Major and trace elemental abundances, iron speciation, and total organic carbon (TOC) were analyzed at the W. M. Keck Foundation Laboratory for Environmental Biogeochemistry, Arizona State University (ASU) and at the Biogeochemistry lab at the University of California, Riverside (UCR), following previously published methods (Kendall et al., 2010; Poulton et al., 2004; Scott et al., 2008; Poulton et al., 2005). Powdered sample splits were ashed for 8-10 hours at 550°C and dissolved completely by HF-HNO_3-HCL acid digestion (Kendall et al., 2010). Trace and major element concentrations were determined on a TheroFinnigan X-Series (ASU) and Agilent 7500E (UCR) quadrupole ICP-MS (inductively coupled plasma mass spectrometry). Accuracy and precision were monitored with duplicate samples and the US Geological Survey Devonian black shale standard SDO-1, and reproducibility in individual runs was better than 95% for the presented elements. Iron speciation analyses were conducted at UCR, following published methods (Li et al., 2010). Biogeochemically highly reactive iron (Fe_{HR}) is defined as pyrite iron (Fe_{PY}) plus other iron phases that are potentially reactive with hydrogen sulphide on diagenetic time scales: carbonate-associated iron (Fe_{Carb}), ferric oxides (Fe_{Ox}), and magnetite (Fe_{Mag}). Hence highly reactive iron $Fe_{HR} = Fe_{PY} + Fe_{Carb} + Fe_{Ox} + Fe_{Mag}$ (ref. 42). Fe_{Py} was calculated (assuming a stoichiometry of FeS_2) from the weight percentage of sulphur extracted during a 2 hour hot chromous chloride distillation followed by iodometric titration(Poulton et al., 2004; Scott et al., 2008; Poulton et al., 2005). Other iron species including Fe_{Carb}, Fe_{Ox}, and Fe_{Mag} were extracted sequentially (Poulton et al., 2005) using sodium acetate solution (for Fe_{Carb}), dithionite solution (for Fe_{Ox}), and ammonium oxalate (Fe_{Mag}). The sequential extracts were

analyzed with an Agilent 7500ce ICP-MS. As mentioned above, total iron concentrations (Fe_T) were determined by HF-HNO_3-HCl acid digestion followed by ICP-MS analysis. Reproducibility of iron measurements, monitored by duplicate analyses within and between sample batches, was better than 94%. Total organic carbon (TOC) contents were determined by taking the difference between carbonate carbon liberated by 4M HCl and total carbon released by combustion at 1,400°C, both of which were measured with an ELTRA C/S determinator at UCR (Scott et al., 2008). Lastly, also at UCR, pyrite-S was extracted for isotope measurements using the same chromous chloride distillation but in this case, reprecipitating the pyrite-S as Ag_2S. Suphur isotope measurements were made with a ThermoFinnigan Delta V continuous-flow stable-isotope-ratio mass spectrometer. Sulphur isotope data are reported as per mil (‰) deviations from the isotope composition of Vienna Cañon Diablo Troilite (VCDT). Reproducibility was better than 0.2% on the basis of single-run and long-term standard monitoring.

1.6 Trace elements as a redox tracer of ocean oxygenation

Redox sensitive elements (RSE) (e.g. Mo, V, and U) can be used as a tracer of the Earth's oxygenation (Scott et al., 2008; Poulton et al., 2005; Och and Shileds-Zhou, 2012). They have minimum detrital influence relative to enrichments in anoxic settings (Tribovillard et al., 2006) and their enrichments in modern anoxic shales, in first order, scale with their dissolved concentration in seawater (Algeo and Lyons, 2006; Lyons et al., 2009). However, when applying RSE redox proxies to black shales of the geological successions, the following conditions need to be considered:

(1) Because RSEs are conservative (Mo and U) or quasi-conservative (V) under oxic conditions, their enrichments in shales deposited under oxic water column are

commonly low and close to their crustal values (except for sediments very rich in Fe-Mn oxyhydroxides) (Tribovillard et al., 2006; Emerson and Huested, 1991; Hastings et al., 1996; Morford et al., 2005). Thus 'oxic' or 'suboxic' shales do not effectively capture the high dissolved RSE concentrations in modern seawater.

(2) The high dissolved RSE concentrations in modern seawater are most effectively captured in shales deposited in anoxic basins. The long resident times of Mo (800–440 kyrs) (Emerson and Huested, 1991; Miller et al., 2011), V (~50 kyrs) (Emerson and Huested, 1991), and U (250-500 kyrs) (Emerson and Huested, 1991) relative to the ocean mixing time (~1-1.5 kyrs) warrant that Mo, V, and U in anoxic basins, even with some restricted access to the open ocean, track the global average RSE concentration. However, strong basin restriction (isolation) without open ocean seawater renewal would deplete water column RSE concentrations and result in low RSE enrichments in anoxic shales (Algeo and Lyons, 2006; Lyons et al., 2009). For example, in the Black Sea, the bottom water column Mo concentration is only 2-3% of the open ocean and the Mo/TOC values in black shales drop to 4.5±1, compared to the Mo/TOC values of 25±5 in shales of the Cariaco Basin, where water column Mo concentration is 70–85% of the open ocean (Algeo and Lyons, 2006; Lyons et al., 2009).

(3) RSE removal in suboxic environments is more efficient than oxic environments but at least one order of magnitude less effective compared to anoxic environments (Lyons et al., 2009). Thus shales deposited in suboxic environments may have variable RSE enrichments between crustal values and the low end of anoxic shale values (Emerson and Huested, 1991; McManus et al., 2006; Brucker et al., 2009). In addition, because Mo, V, and U behave differently in suboxic environments, their

enrichments in a particular ‘suboxic’ shale bed are not necessarily correlatable (Emerson and Huested, 1991; Hastings et al., 1996; Morford et al., 2005).

In the modern oxygenated ocean, only anoxic shales in marine basins with access to the open ocean effectively capture the high dissolved RSE concentration in seawater. When applying to the ancient record, high RSE enrichments comparable to those of the modern anoxic shales provide definitive evidence for high dissolved RSE in an oxygenated ocean; there is no other alternative sedimentary process to enrich RSEs to such high values. However, low RSE values from a particular stratigraphic unit would have much less definitive meaning. It could be resulted from strong basin restriction (isolation) in an oxygenated ocean (comparable to the Black Sea), low RSE enrichments in oxic/suboxic local environments (comparable to modern oxic/suboxic sediments), or low dissolved RSE concentrations in poorly oxygenated ocean. When RSE enrichments from a particular stratigraphic unit are low, it can be used to infer a less oxygenated ocean only when paleogeographic reconstruction and other geochemical and/or paleontological evidence exclude strong basin restriction, and independent geochemical data indicate persistent anoxia/euxinia (Scott et al., 2008).

1.7 Iron speciation and redox fluctuations

One of the intriguing finding, is that the lower Doushantuo Formation black shales has submeter-scale variations in Fe_{HR}/Fe_T and Fe_{Py}/Fe_T ratios (Fig. S2; Table S1). Post-depositional alteration (e.g., through weathering and oxic fluid interaction) could potentially result in changes in iron speciation, but very low iron oxides in most samples (Table S2; Fig. S2) exclude this possibility. Sudden increase in sedimentation rate (e.g., gravity flow) may dilute highly reactive iron contents, resulting in low Fe_{HR}/Fe_T values

(Raiswell and Canfield, 1998; Lyons and Severmann, 2006). However, field and petrographic observations did not find any coarse-grained layers or obvious turbidites, which would be indicative of rapid deposition within the lower Doushantuo black shales. Thus, it is likely that the submeter-scale variations in Fe_{HR}/Fe_T and Fe_{Py}/Fe_T recorded dynamic redox fluctuations characterized by alternating oxic, suboxic, and anoxic local environments.

Overall the Fe_T contents of the lower Doushantuo black shales increase from the shelf (Li et al., 2010) and upper slope sections towards the lower slope and basin sections (Table S1), consistent with Fe redox cycling and transportation towards deeper water environments (Lyons and Severmann, 2006). However, a large portion of the Doushantuo samples have unusually low Fe_T/Al ratios (< 0.1; Table S1), much lower than the average crustal value of 0.5 (Severmann et al., 2008; Wedepohl, 1995). The origin of such low Fe_T/Al ratios from the Doushantuo Formation in this study and from previous reports (Li et al., 2010; Bristow et al., 2009) is not well understood and the details remain as an ongoing task to investigate. However, these deviations from typical shales suggest that the Doushantuo black shales are not equivalent to average continental margin shales and sediments in which iron proxies are calibrated. Therefore, Fe speciation results (Fig. S2) should be viewed with caution. For instance, it may not be possible to use Fe_{HR}/Fe_T ratios of the Doushantuo black shales to delineate anoxia given deviations from typical continental margin major element chemistry. For this reason, we do not use Fe_{HR}/Fe_T ratios as a quantitative paleoredox proxy in this study. However, Fe_{Py}/Fe_{HR} ratios will still be a reliable gauge for the sulphide availability in the depositional environment.

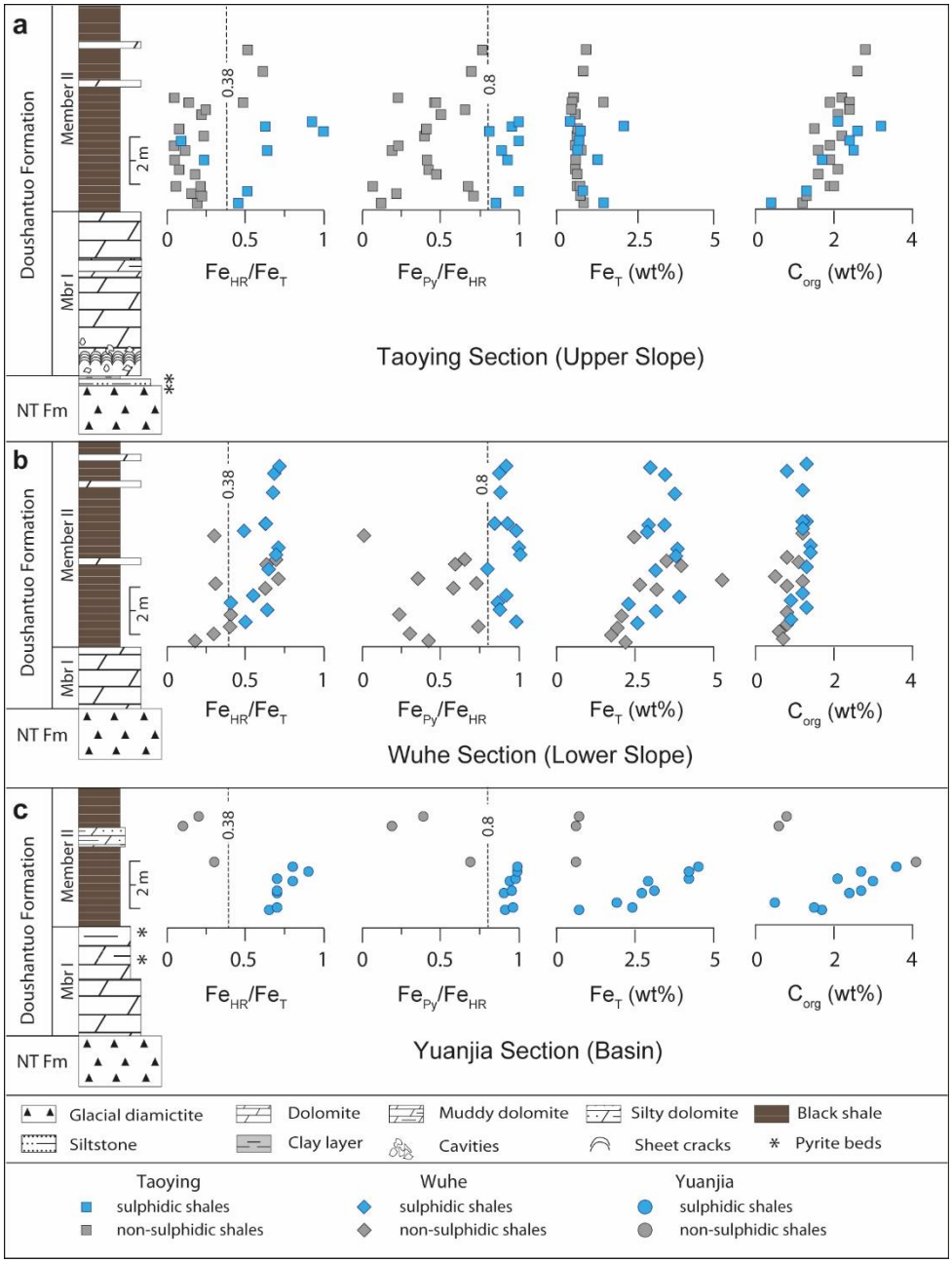

Figure S2 Iron speciation data of the lower Doushantuo Formation. a, Taoying section (upper slope). **b,** Wuhe section (lower slope). **c,** Yuanjia section (basin). Submeter-scale variations in Fe_{HR}/Fe_T and Fe_{Py}/Fe_T likely record dynamic redox fluctuations characterized by alternating oxic and anoxic local environments. However, when Fe_T values and Fe_T/Al ratios are significantly lower than average crustal values, using Fe_{HR}/Fe_T to distinguish anoxic vs. oxic environments needs to be done with caution. When Fe_T values are low, high Fe_{HR}/Fe_T (> 0.38) with low Fe_{Py}/Fe_{HR} (< 0.8) values indicative of ferruginous conditions may in fact record oxic conditions, while high Fe_{HR}/Fe_T (> 0.38) with high Fe_{Py}/Fe_{HR} (> 0.8) values could potentially record sulphidic conditions in porewaters.

1.8 Temporal Mo, V, U variations and redox fluctuations

Similar to the temporal variations in iron speciation, large variability in redox-sensitive element (RSE) enrichments has been observed in lower Doushantuo Formation black shales (Table S1; Fig. 2). Intervals with high Mo, V, and U enrichments are often adjacent (< 0.2 m) to intervals with near crustal, un-enriched values. Combined petrographic and geochemical evidence strongly suggest that variability in RSE enrichments within the lower Doushantuo Formation are linked to depositional processes. For instance, sulphides in examined samples, based on petrographic work, are present largely as framboidal or finely disseminated pyrites, which point towards minimal post-depositional sulphide alteration. Within sections of the Doushantuo Formation there are mm-thick laminae with macroscopic pyrites (Jiang et al., 2010), but such intervals have been carefully avoided in our sample preparation. With very limited exceptions, the shales were devoid of hematite, which could be indicative of oxic weathering or supergene alteration (Table S1). Processes that would alter RSE enrichments would also alter sulphides. Thus, the preservation of early diagenetic sulphide textures suggests that the shales host marine RSE signatures. The Phanerozoic-like RSE enrichments and the variability in enrichments are consistent with the presence of a globally well-oxygenated ocean but dynamic local redox conditions.

1.9 The drop of RSE enrichments after the basal Doushantuo Formation shales

In the basal Doushantuo Formation shales there is an apparent drop of Mo (Mo/TOC), V(V/TOC), and U(U/TOC) values after the first few meters (Table S1 and Fig. 2 in main text). While the high RSE enrichments at the basal interval unequivocally require a large oceanic RSE reservoir in response to a well-oxygenated ocean–

atmosphere system, low RSE values are much less definitive and could be derived from (1) strong basin restriction, (2) shift to less reducing, local environments, or (3) a decrease in the size of oceanic RSE reservoir.

Strong basin restriction (isolation) is a least likely option. Existing tectonic and paleogeographic reconstructions (Jiang et al., 2011; Jiang et al., 2003b; Li et al., 2008; Hoffman and Li, 2009) do not attach South China to the interior or margin of another major continent, and the low pyrite sulphur isotopes imply ready availability of sulphate in basinal waters, most likely in direct contact with the global ocean.

The most cautious interpretation for the drop of RSE enrichments is a local shift to less reducing environments on the basis of the following evidence and reasoning: (1) The sub-meter scale fluctuations in RSE enrichments at the basal few meters were unlikely caused by rapid contractions and expansion of marine RSE reservoirs. (2) Despite high RSE enrichments at the basal interval in slope-basin sections, coeval basal Doushantuo Formation shales from the shelf sections (Li et al., 2010; Bristow et al., 2009) did not have high RSE enrichments (despite that Fe proxies, given traditional interpretations, point toward anoxic conditions). The lack of high RSE enrichments in the shelf sections (Li et al., 2010; Bristow et al., 2009) is best explained by ineffective uptake of RSEs in less reducing (e.g., oxic-suboxic) environments rather than recording small oceanic RSE reservoirs. (3) The lack of RSE enrichments in shelf sections is consistent with our reasoning that the Fe speciation data from the Doushantuo Formation should be taken with caution. Because of the unusually low total Fe ((see Table S1 and references Li et al., (2010) and Bristow et al., (2009)) from the Doushantuo black shales in general, high Fe_{HR}/Fe_T (> 0.38) with low Fe_{PY}/Fe_{HR} (< 0.8) values indicative of ferruginous

conditions may record oxic conditions, while high Fe_{HR}/Fe_T (> 0.38) with high Fe_{PY}/Fe_{HR} (> 0.8) values could potentially record sulphidic conditions in porewaters.

The third interpretation, i.e., the drop of RSE enrichments after the basal Doushantuo shales record the shrink of the oceanic RSE reservoirs, is the most intriguing. It implies that the early Ediacaran oxygenation was not a unidirectional process. However, the drop of RSE enrichments down to near crustal values requires a shift back to reducing ocean conditions typical of mid-Proterozoic and Archean oceans (Scott et al., 2008; Och and Shileds-Zhou, 2012). This seems to be difficult in light of the trace metal biolimitation stabilizing feedback (Scott et al., 2008; Anbar and Knoll, 1999) and overall increasing biodiversity in early-middle Ediacaran (Erwin eta l., 20011; Peterson et al., 2005). However, given the scarcity of data from the Ediacaran successions, a comprehensive test in broader paleogeographic settings of the Nanhua basin and in other global successions is warranted.

1.10 Molybdenum and Vanadium mass balance model

1.10.1 Overview of the modern Mo cycle

In the modern ocean, Mo has a residence time of ~440–800 thousand years and an average seawater concentration of 105 nM (Emerson and Huested, 1991; Miller et al., 2011). Mo is enriched in sediments by adsorption onto organic matter under reducing conditions (Algeo and Lyons, 2006; Lyons et al., 2009), or by redox cycling of Mn-Fe-oxyhydroxides (Morford et al., 2005). In the modern oxygenated ocean, molybdenum (Mo) is present as Mo (VI) in the form of molybdate (MoO_4^{2-}) (Morford et al., 2005). Under reducing and sulphidic conditions, Mo is present in the form of Mo (IV) and often present as thiomolybdate ($MoOxS_{4-x}^{2-}$) (Morford et al., 2005). Conversion of molybdate

to particle reactive thiomolybdate requires the presence of free sulphide. Helz and others (2011) recently proposed that Mo is removed into anoxic settings as Fe-Mo(IV)-S particles, which may also be scavenged by sinking organic matter. However, this mineral phase has not been identified in any natural setting.

Oxic, suboxic and euxinic environments are important burial sinks for Mo, but their burial rates are markedly different from each other (Emerson and Huested, 1991; Morford et al., 2005; Miller et al., 2011; McManus et al., 2006; Brucker et al., 2009). Oxic marine sediments tend to have low crustal average (1-2 ppm), if not measuring ferromanganese oxides, where molybdate ions are adsorbed onto ferromanganese rich crusts (Morford et al., 2005; McManus et al., 2006). Mo can be removed faster (~10 times the crustal average) under suboxic environment, where mild reducing conditions (sulphidic pore waters) prevail below sediment-water interface (Lyons et al., 2009; Poulson et al., 2006). Mo burial in sediments deposited under an anoxic water column is typically several orders of magnitude higher than in suboxic sediments. Although the removal mechanisms are slightly different in each individual setting, the modern oceanic Mo budget is balanced by oxic, suboxic and euxinic settings, which collectively constitute ~35%, ~50% and ~15% of the total riverine flux of Mo into the ocean (Scott et al., 2008; Emerson and Huested, 1991). The modern Mo cycle is assumed to be in steady state.

1.10.2 Overview of the modern V cycle

In the modern ocean, V has a residence time of 50-100 thousand years and an average seawater concentration of 36 nM (Emerson and Huested, 1991; Hastings et al., 1996). In oxic water, vanadium is present as V(V) in the form of vanadate oxyanions (HVO_4^{2-} and HVO_4^-), while in mildly reducing conditions V(V) is reduced to V(IV) and present in the form of vanadyl ions (VO^{2-}) and related hydroxyl species ($VO(OH)_3^-$) or hydroxides ($VO(OH)_2$) (Tribovillard et al., 2006; Emerson and Huested, 1991). In strongly reducing conditions with high dissolved sulphide (H_2S) concentrations, V(IV) will be further reduced to V(III), which may precipitate as V_2O_3 or $V(OH)_3$ (Tribovillard et al., 2006). V(IV) and V(III) can be scavenged by organic matter, leading to V enrichment in sediments deposited under an anoxic water column (Emerson and Huested, 1991). Under oxic conditions, similar to Mo, V is only removed in significant quantities associated with Mn and Fe oxides (Tribovillard et al., 2006; Emerson and Huested, 1991; Hastings et al., 1996). One significant difference between the Mo and V global mass balances is the ratio of riverine particulate to dissolved flux, which for V (100) is much higher than Mo (2.5) (Emerson and Huested, 1991; Hastings et al., 1996). Another difference is that in mildly reducing (i.e., a subset of 'suboxic') conditions, V are diffusively released from sediments. This process is tightly coupled with the redox cycle of Mn (Hastings et al., 1996). Thus, suboxic seafloor is considered as a source for V but a sink for Mo in mass balance calculations (Hastings et al., 1996). It is possible that the modern V cycle is not currently fully in steady state and is adjusting from the last glacial maximum (Hastings et al., 1996). However, for geochemical modeling we have assumed a steady state.

1.10.3 Mass balance equations and time-dependent modeling results

The effects of perturbations to Mo and V geochemical cycles can be estimated using a first order model based on modern element mass balances (Emerson and Huested, 1991; Hastings et al., 1996). We modeled a simple time-dependent sensitivity of seawater concentration of Mo and V to their areal extent of different reducing conditions over time (Fig. S3). Using the modern mass balance of each metal, an instantaneous change is assumed at t = 0 using modern seawater source and sink fluxes. The mass balance is controlled by the difference of input and output fluxes of the particular element in the ocean so that:

$$\mathbf{(dC_{(RSE)}/dt) = F_{source} - F_{sinks}}$$

For the modern Mo cycle:

$$\mathbf{Vo(dC_{(Mo)}/dt) = Jr-(Aso*Fso)-(Ao*Fo)-(Aex*Fex)}$$

For the modern V cycle:

$$\mathbf{Vo(dC_{(V)}/dt) = Jr+(Aso*Fso)-(Ao*Fo)-(Aa*Fa)-(Aex*Fex)-Jh}$$

Where, Vo is the volume of the ocean; $C_{(Mo)}$ and $C_{(V)}$ are the concentrations of Mo and V in seawater, respectively. Jr is the riverine flux; Ao is the area of oxic sediments; Aa is the area of anoxic sediments; Aso is the area of the suboxic environments (oxic water column with reducing sediments); Aex is the area of euxinic sediments; Fo is the oxic flux; Fa is the anoxic flux; Fso is the 'suboxic' source flux (see above); and Jh is the hydrothermal burial flux. The equations are solved for time t (Hastings et al., 1996).

Modern mass balances of Mo and V (Emerson and Huested, 1991; Hastings et al., 1996) are summarized as below:

RSE	Riverine Flux	Ocean Conc.	Hydrothermal Flux	Environment	Oxic (O)	Suboxic (SO)	Anoxic (A)	Euxinic (EX)
V	5.4 x 10^8 mol/yr	36 nmol/L	5.5 x 10^8 mol/yr	**Seafloor fraction**	0.97	0.025	0.003	0.0005
				Burial Rate (nmol/cm^2 yr)	0.12	6.1	4.3	38.0
Mo	1.8 x 10^8 mol/yr	105 nmol/L	-	**Seafloor fraction**	0.9	0.01	-	0.0005
				Burial Rate (nmol/cm^2 yr)	0.021	2.61	-	12.51
Seafloor area: (3.5-3.61) x 10^8 km^2, Ocean volume: (1.3-1.37) x 10^{18} m^3								

The output fluxes are strongly dependent on the redox environment (Emerson and Huested, 1991; Hastings et al., 1996; Morford et al., 2005) and therefore we assumed that burial rates (*b*) in individual sink (i) scale with RSE inventory [Mo]. RSE removal fluxes (F) in each sink are also scaled to their respective seafloor coverage (A)—a first order or direct feedback model:

$$b_i = b_{i(today)} \bullet [Mo/Mo_{(today)}]$$

$$F_i = A_i \bullet b_i$$

A simple first order differential equation can be derived as (Hastings et al., 1996):

$$(dC_{(RSE)}/dt) = \lambda - \gamma \bullet RSE \qquad \text{where } \lambda = F_{source} \text{ and } \gamma = F_{sinks}$$

For time series, the exponentially derived end concentration (RSE_{term}) after time (t) is given by:

$$\mathbf{RSE_t = RSE_{term} + (RSE_{t=0} - RSE_{term}) \bullet \exp(-\gamma t)}$$

Where $RSE_{term} = F_{source}/F_{sinks} = (\lambda/\gamma)$

We modeled the change in seawater concentration of Mo and V through time by (1) increasing the riverine flux of Mo and V with increased weathering, and (2) increasing the extent of anoxic/euxinic environments in the ocean. The results show that doubling the riverine flux of Mo and V can be easily compensated for by a small increase (~2%) in anoxic marine seafloor (Emerson and Huested, 1991) (Fig. S3). More importantly, a small areal increase in euxinic seafloor can crash the ocean Mo and V reservoirs on a time scale much shorter than the response time to doubling the riverine flux (Fig. S3). For example, a 2–3% increase in euxinic seafloor would crash the Mo and V reservoirs at a time scale of < 0.5 Myr and 0.04 Myr, for Mo and V respectively. Therefore, we consider that the sudden increase in Mo and V (and other redox sensitive elements such as U) to Phanerozoic levels in the post-cap-carbonate black shales was a result of changes in the ocean oxidation state rather than an increase in the riverine flux. Increased weathering and riverine flux may have played a role during the maximum glacial retreat, prior to the deposition of the Doushantuo Member II black shales, but that alone would not result in long-term (hundred thousand to million year time scale) increase of oceanic Mo and V reservoir in the postglacial ocean.

doubling the riverine flux.

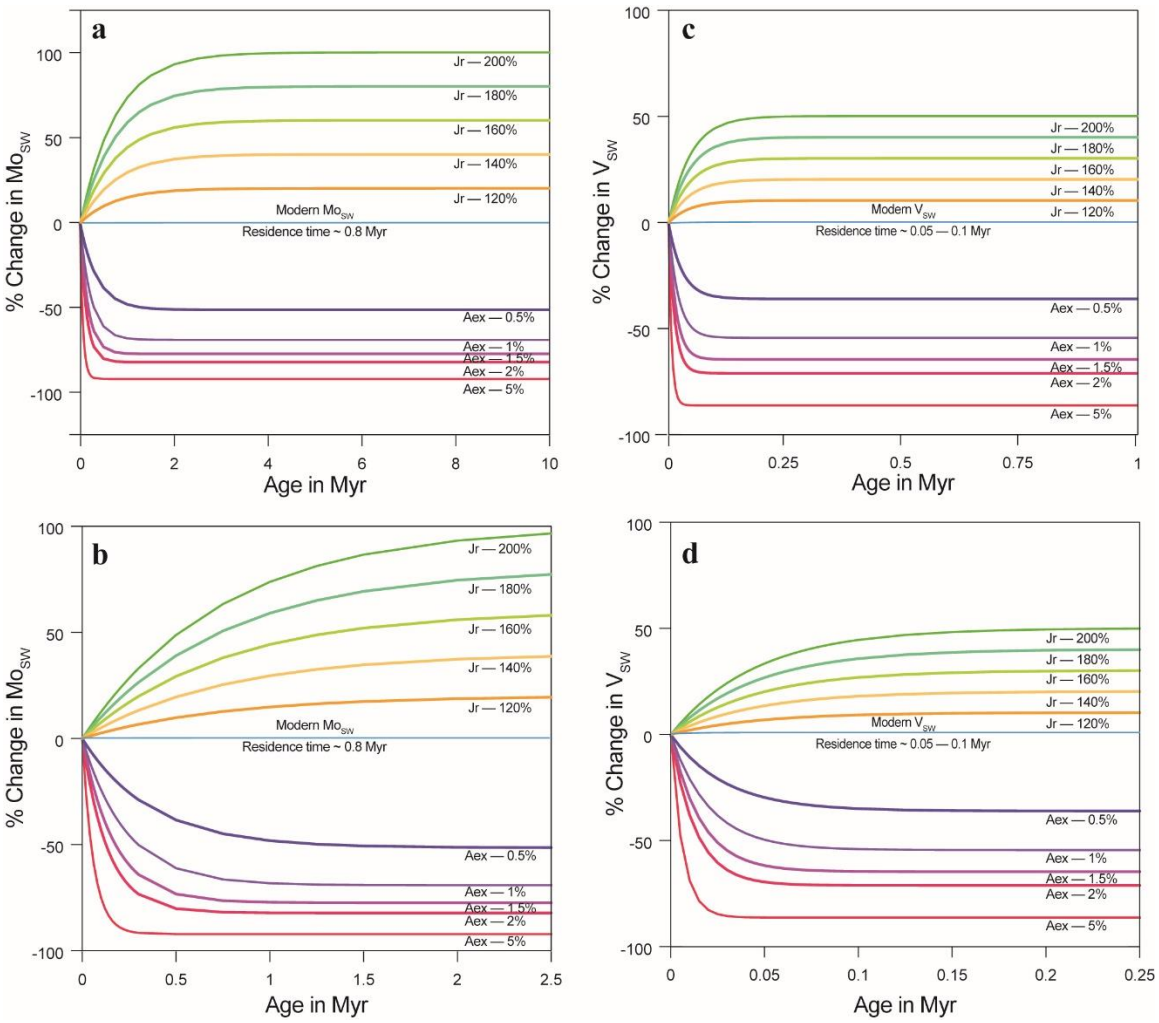

Figure S3 Model results for seawater Mo and V changes through time. a, b, Changes in sweater Mo concentrations in response to increase of riverine flux of Mo (Jr) through enhanced weathering and to increase of anoxic/euxinic environments (Aex) in the ocean. **c, d,** Changes in sweater V concentrations in response to increase of riverine flux of V (Jr) and to increase of anoxic/euxinic environments (Aex). Note that **b** and **d** are the same modeling results of **a** and **c**, respectively, with enlarged time scales. A small percentage increase in anoxic sediments on the continental margin can crash the ocean Mo and V reservoirs within a much shorter period than doubling the riverine flux. Therefore, we interpret that Phanerozoic-like Mo and V enrichments in the lower Doushantuo black shales record a major oxygenation event following the Marinoan glacial retreat.

1.11 Secular trends in sulphur isotopes and Mo, V concentrations

1.11.1 Sulphur isotopes

The lower Doushantuo black shales in the slope and basinal sections have sulphide sulphur isotopes ($\delta^{34}S_{Pyrite}$) down to -35‰ (canyon diablo troilite, CDT). Coeval carbonate associated sulphate sulphur isotopes ($\delta^{34}S_{CAS}$) from the shelf sections, including Xiaofenghe (Xiao et al., 22012), Jiulongwan (McFadden et al., 2008; Li et al., 2010), Zhongling (Li et al., 2010), and Weng'an (Shields et al., 2004) sections, vary from +32‰ to +41‰, with an average of +34‰. Assuming that the $\delta^{34}S_{CAS}$ data from the shelf sections recorded the seawater sulphate sulphur isotope signature, the maximum sulphate-sulphide sulphur isotope offset during the deposition of the lower Doushantuo Member II shales in the deep basinal section would be ≥ 65‰. Such high values are equivalent to maximum fractionations by sulphate reducing bacteria (Sim et al., 2011; Canfield et al., 2005) and the maximum pyrite-coeval sulphate offset observed in the Phanerozoic rock record (Fig. S4) (Algeo and Lyons, 2006; Canfield and Raiswell, 1999; Canfield and Farquhar, 2009). Since increase in the isotopic offset between pyrites and seawater sulphate in the Neoproterozoic has been commonly linked to growth of the marine sulphate reservoir and increase of surface oxidation (Canfield and Raiswell, 1999; Canfield and Farquhar, 2009; Halverson and Hurtgen, 2007), the large sulphur isotope fractionation in the basal Member II shales (Fig. S4) is consistent with a well-oxygenated ocean during deposition of the lower Doushantuo Member II shales. Sulphate-sulphide sulfur isotope offset > 65‰ are thought to indicate at least 1 mM sulphate[65] and thus near Phanerozoic levels of sulphate (Canfield and Raiswell, 1999).

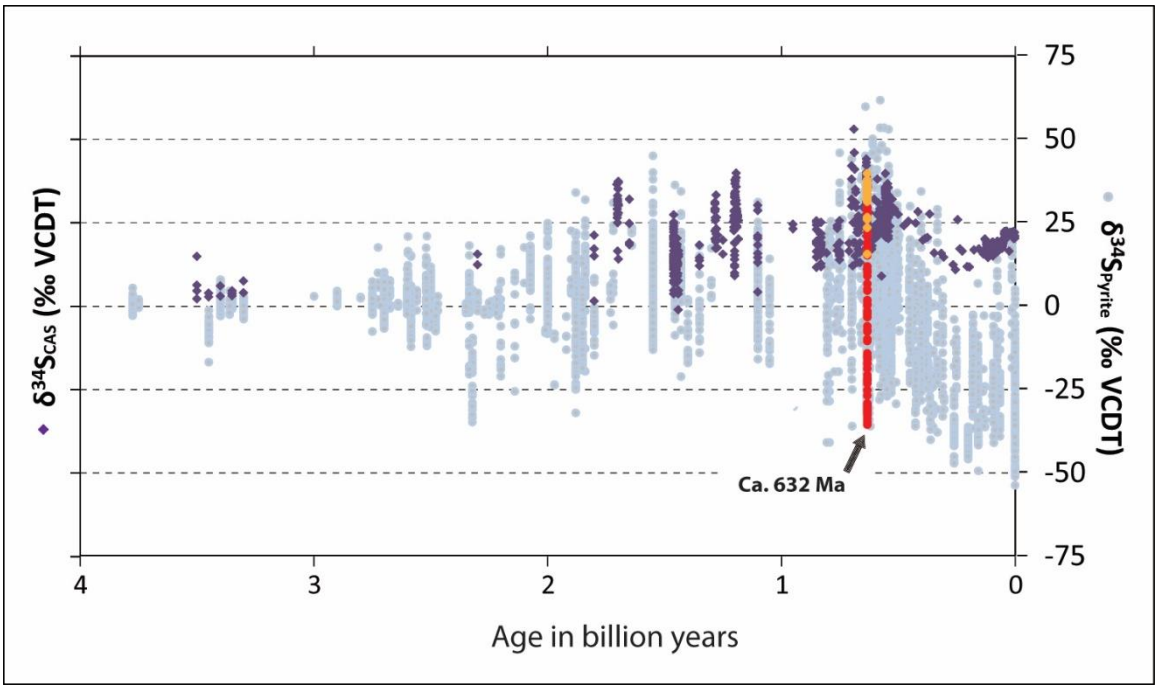

Figure S4 Sulfur isotope composition of sedimentary sulphide ($\delta^{34}S_{Pyrite}$) and carbonate associated sulfate ($\delta^{34}S_{CAS}$) through time. The compilation is modified from Canfield & Farquhar (2009)[65] and Och & Shields (2012)[45], with the lower Doushantuo $\delta^{34}S_{CAS}$–$\delta^{34}S_{Pyrite}$ data added and marked.

1.11.2 Secular Mo, Mo/TOC variations

The secular variations of Mo, Mo/TOC, V, V/TOC through time (Fig. 3 in main text) have been summarized by Scott and others Scott et al., (2008) and Och and Shields-Zhou (2012). We have added additional data that were not included in previous compilations, including new data for this study from the ca. 640 Ma Black River Dolomite (Kendall et al., 2009) (Table S3) and the most recently published data from ca. 663 Ma Datangpo Formation (Li et al., 2012) (see references in Table S2). The unusually high (> 10,000 ppm) Mo and V concentrations from the lower Cambrian metal-enriched (Ni-Mo-PGE) sulphide deposits in south China (compiled in ref. Och and Shields-Zhou,

2012) may be linked to high temperature mineralization rather than seawater derived metal enrichment (Jiang et al., 2007) and therefore, data from this deposit are not included in Figure 3. A complete list of references that were used for the compilation of Mo, Mo/TOC, V, V/TOC trends is provided in Table S2 and new data for this study are included in Table S3. The current compilation (Fig. 3) provides evidence for a significant ocean–atmosphere oxygenation event that may have happened after ca. 640 Ma, closely associated with the glacial retreat of the Marinoan 'Snowball Earth' event.

Supplementary Table S1 Iron speciation, TOC, and trace elemental data from the lower Doushantuo Formation

Taoying section, Guizou Province, South China (Upper Slope)

Sample No.	C_{org}	TIC	$\delta^{34}S_{pyrite}$	Fe_{Mag}	Fe_{Oxide}	Fe_{Carb}	Fe_{Pyrite}	FeHR	FeT	FePy/FeHR	FeHR/FeT	Al	Mo	Mo/TOC	V	V/TOC	U	U/TOC
	(Wt %)	(Wt %)		(Wt %)	(Wt %)	(Wt %)	(Wt %)		(Wt %)			(Wt %)	(ppm)	ppm/wt%	ppm	ppm/wt%	(ppm)	ppm/wt%
Section 1a. 7.3 m is the end of Cap Carbonate																		
TY09-7.6	1.2	0.0	n.d	0.0	0.1	0.0	0.0	0.2	0.8	0.1	0.3	7.4	3.2	2.7	5900	4962	17.9	15.0
TY09-7.9	1.3	0.0	n.d	0.0	0.1	0.0	0.2	0.2	0.7	0.7	0.3	7.7	3.7	3.0	3973	3178	11.3	9.0
TY09-8	1.3	0.0	n.d	0.0	0.1	0.0	0.0	0.2	0.7	0.2	0.2	8.1	1.3	1.0	3950	3080	16.7	13.1
TY09-8.3	1.9	0.0	-3.3	0.0	0.1	0.0	0.0	0.1	0.6	0.1	0.1	8.4	2.8	1.5	2946	1545	16.9	8.9
TY09-8.6	1.5	0.0	4.60	0.0	0.0	0.0	0.0	0.1	0.7	0.2	0.1	7.9	24.8	16.7	285	193	3.8	2.5
TY09-8.8	1.6	0.0	n.d	0.0	0.1	0.0	0.1	0.2	0.6	0.5	0.3	8.7	6.4	4.0	1767	1095	18.4	11.4
TY09-9	2.1	0.0	n.d	0.0	0.0	0.0	0.0	0.1	0.6	0.4	0.2	8.2	4.1	1.9	1451	689	19.1	9.1
TY09-9.4	1.9	0.0	n.d	0.0	0.0	0.0	0.0	0.1	0.6	0.4	0.1	8.6	5.4	2.8	950	489	18.0	9.2
TY09-9.8	1.6	0.0	n.d	0.0	0.1	0.0	0.0	0.1	0.8	0.2	0.2	9.5	2.9	1.8	1516	971	23.7	15.2
TY09-10	1.9	0.0	-5.96	0.0	0.0	0.0	0.0	0.1	0.6	0.2	0.1	8.3	3.1	1.6	835	440	18.7	9.9
TY09-10.2	2.4	0.0	-15.7	0.0	0.0	0.0	0.1	0.1	0.7	1.0	0.2	9.8	29.3	12.3	1178	493	18.5	7.7
TY09-10.4	2.2	0.0	n.d	0.0	0.1	0.0	0.1	0.2	0.6	0.4	0.3	7.7	39.5	18.1	804	369	17.2	7.9
TY09-10.7	1.5	0.0	n.d	0.0	0.0	0.0	0.0	0.1	0.7	0.4	0.2	8.9	11.3	7.3	1853	1196	19.4	12.5
TY09-11	2.1	0.0	-9.9	0.0	0.0	0.0	0.5	0.5	0.4	1.0	1.0	5.5	30.0	14.2	525	249	10.3	4.9
TY09-11.3	2.1	0.0	n.d	0.0	0.1	0.0	0.1	0.2	0.6	0.5	0.3	7.3	11.3	5.3	253	118	8.2	3.8
TY09-11.5	2.4	0.0	n.d	0.0	0.0	0.0	0.1	0.1	0.5	0.7	0.3	7.1	10.6	4.5	247	105	8.0	3.4
TY09-11.8	2.4	0.0	n.d	0.0	0.0	0.0	0.0	0.1	0.5	0.5	0.2	7.2	10.8	4.5	213	88	8.4	3.5
TY09-12	2.2	0.0	n.d	0.0	0.0	0.0	0.0	0.1	0.5	0.2	0.1	7.6	6.2	2.8	294	131	7.7	3.5
Section 1b. 13.0 m is the base of the black shale																		
TY09-13.3	0.4	0.0	n.d	0.0	0.1	0.0	0.7	0.8	1.5	0.9	0.5	8.3	1.4	4.0	1016	2783	7.8	21.4
TY09-13.8	1.3	0.0	-7.6	0.0	0.0	0.0	0.5	0.5	0.8	1.0	0.6	9.0	3.5	2.6	6096	4582	13.1	9.8
TY09-14	2.0	0.0	n.d	0.0	0.1	0.0	0.1	0.2	0.7	0.7	0.3	8.8	14.5	7.2	3040	1499	19.1	9.4
TY09-15.1	1.7	0.0	-26.8	0.0	0.0	0.0	0.4	0.4	1.3	0.9	0.3	19.4	38.2	22.2	2522	1465	33.6	19.5
TY09-15.5	2.5	0.0	n.d	0.0	0.0	0.0	0.4	0.5	0.6	0.9	0.7	7.7	165.3	67.0	669	271	15.7	6.4
TY09-16.3	2.6	0.0	n.d	0.0	0.1	0.0	0.7	0.8	0.7	0.8	1.1	8.8	48.4	18.7	455	176	16.8	6.5
TY09-16.5	3.2	0.0	-31.6	0.0	0.1	0.0	1.4	1.5	2.1	1.0	0.7	8.9	114.4	35.6	424	132	12.5	3.9
TY09-17.5	1.9	0.0	-23.1	0.0	0.4	0.0	0.4	0.8	1.5	0.5	0.6	8.8	13.0	7.0	418	224	5.7	3.0
TY09-18.8	2.6	0.0	-22.3	0.0	0.2	0.0	0.4	0.6	0.8	0.7	0.7	6.7	9.0	3.5	262	101	3.8	1.5
TY09-19.7	2.8	0.0	-22.1	0.0	0.1	0.0	0.4	0.5	0.9	0.8	0.6	7.2	11.5	4.2	313	114	4.7	1.7
TY09-21.3	4.5	0.0	-16.0	0.0	0.1	0.0	0.9	1.0	0.6	0.9	1.0	6.1	12.1	2.7	200	44	6.8	1.5
TY09-22.3	1.0	0.0	0.2	0.0	0.0	0.0	1.5	1.5	1.0	1.0	1.0	5.5	0.3	0.3	185	181	5.4	5.2

Wuhe section, Guizou Province, South China (Lower Slope)

Section 2. 2.3 m is the end of Cap Carbonate

Sample No.	C_{org}	TIC	$\delta^{34}S_{pyrite}$	Fe_{Mag}	Fe_{Oxide}	Fe_{Carb}	Fe_{Pyrite}	FeHR	FeT	FePy/FeHR	FeHR/FeT	Al	Mo	Mo/TOC	V	V/TOC	U	U/TOC
	(Wt %)	(Wt %)		(Wt %)	(Wt %)	(Wt %)	(Wt %)		(Wt %)			(Wt %)	(ppm)	ppm/wt%	ppm	ppm/wt%	(ppm)	ppm/wt%
WH09-2.4	0.7	0.0	n.d	0.0	0.2	0.0	0.2	0.4	2.2	0.4	0.2	10.4	0.6	0.8	4438	6124	13.4	18.4
WH09-2.7	0.6	0.0	-17.2	0.1	0.3	0.0	0.1	0.5	1.7	0.3	0.3	8.7	8.7	14.2	1824	2994	12.3	20.2
WH09-3	0.8	0.2	-32.3	0.0	0.1	0.1	0.6	0.8	1.9	0.7	0.4	8.4	3.8	4.6	584	707	14.0	16.9
WH09-3.2	0.9	0.0	-32.8	0.0	0.0	0.0	1.2	1.3	2.6	1.0	0.5	8.6	38.0	40.5	489	522	13.8	14.7
WH09-3.5	0.8	0.0	-34.6	0.2	0.4	0.0	0.2	0.8	2.1	0.2	0.4	9.4	2.5	3.0	390	485	13.8	17.2
WH09-3.7	1.3	0.0	-33.7	0.1	0.1	0.1	1.7	2.0	3.2	0.9	0.6	9.0	62.3	49.7	333	266	15.8	12.6
WH09-4	0.9	0.1	-32.8	0.0	0.1	0.0	0.7	0.9	2.3	0.9	0.4	8.7	7.8	8.6	324	356	14.0	15.4
WH09-4.3	1.2	0.0	-34.9	0.0	0.0	0.1	1.9	2.1	3.9	0.9	0.5	9.4	172.3	144.9	288	242	12.6	10.6
WH09-4.6	0.8	2.1	-29.1	0.0	0.1	0.7	1.1	2.0	3.2	0.6	0.6	6.6	11.2	14.6	208	272	9.8	12.8
WH09-4.8	1.2	0.2	-30.6	0.0	0.1	0.1	0.6	0.8	2.6	0.7	0.3	8.5	13.5	11.6	241	208	10.0	8.6
WH09-5	0.5	7.5	-26.8	0.4	0.0	2.0	1.3	3.7	5.3	0.3	0.7	3.4	39.5	84.7	171	367	5.5	11.9
WH09-5.4	1.3	1.4	-32.4	0.0	0.0	0.4	1.6	2.0	3.14	0.8	0.6	8.47	41.21	32.0	185	144	5.84	4.5
WH09-5.6	1.1	3.5	-30.5	0.0	0.1	0.9	1.4	2.5	3.96	0.6	0.6	7.03	42.42	37.9	199	178	5.34	4.8
WH09-5.8	0.8	3.1	-29.8	0.0	0.1	0.8	1.5	2.4	3.49	0.6	0.7	6.64	21.92	27.7	213	270	3.87	4.9
WH09-6.0	1.4	0.0	-33.7	0.0	0.0	0.0	2.6	2.6	3.79	1.0	0.7	9.99	29.94	22.0	212	156	4.36	3.2
WH09-6.3	1.4	0.0	-33.5	0.0	0.0	0.0	2.7	2.7	3.84	1.0	0.7	10.13	27.25	19.6	213	153	3.87	2.8
WH09-6.5	1.2	0.0	-32.5	0.0	0.7	0.0	0.0	0.7	2.46	0.0	0.3	9.33	58.11	50.4	184	160	4.25	3.7
WH09-6.8	1.2	0.0	-32.4	0.0	0.0	0.0	1.3	1.4	2.88	1.0	0.5	9.63	37.62	31.5	207	173	5.22	4.4
WH09-7.0	1.2	0.1	-31.1	0.0	0.0	0.1	1.9	2.1	3.43	0.9	0.6	9.15	26.05	22.6	221	192	3.68	3.2
WH09-7.3	1.3	0.5	-30.0	0.0	0.0	0.3	1.5	1.8	2.9	0.8	0.6	8.2	12.6	9.9	174	136	5.1	4.0
WH09-8.6	1.2	0.8	-31.6	0.0	0.0	0.3	2.2	2.5	3.76	0.9	0.7	8.65	23.95	20.5	170	145	2.94	2.5
WH09-9.4	0.8	0.5	-31.7	0.0	0.1	0.2	2.0	2.3	3.4	0.9	0.7	7.8	8.0	10.1	170	216	5.9	7.5
WH09-9.7	1.3	0.2	-32.0	0.0	0.0	0.2	1.9	2.1	3.0	0.9	0.7	7.9	11.5	9.1	134	106	4.2	3.3
WH09-11.6	1.3	0.0	-30.1	0.0	0.0	0.1	1.9	2.0	3.0	1.0	0.7	6.8	11.9	9.5	143	114	3.6	2.8
WH09-13.7	0.6	4.0	-21.0	0.0	0.0	0.7	1.6	2.2	2.5	0.7	0.9	4.2	3.9	6.5	94	156	3.9	6.5

Yuanjia Section, Hunan Province, South China (Basinal)

Section 3. 4.6 m is the end of Cap Carbonate

Sample No.	C_{org}	TIC	$\delta^{34}S_{Pyrite}$	Fe_{Mag}	Fe_{Oxide}	Fe_{Carb}	Fe_{Pyrite}	FeHR	FeT	FePy/FeHR	FeHR/FeT	Al	Mo	Mo/TOC	V	V/TOC	U	U/TOC
	(Wt %)	(Wt %)		(Wt %)	(Wt %)	(Wt %)	(Wt %)		(Wt %)			(Wt %)	(ppm)	ppm/wt%	ppm	ppm/wt%	(ppm)	ppm/wt%
WHH-5.6	1.7	0.0	-14.2	0.0	0.0	0.0	0.4	0.4	0.7	0.9	0.65	9.9	13.4	7.7	6417	3680	9.3	5.3
WHH-5.7	1.5	0.0	-26.7	0.0	0.1	0.0	1.6	1.7	2.4	0.9	0.7	9.6	64.3	43.8	2767	1884	17.9	12.2
WHH-5.9	0.5	-	-	-	-	-	-	-	1.9	-	-	9.4	120.1	255.5	-	-	-	-
WHH-6.3	2.4	0.0	-30.3	0.0	0.1	0.2	1.7	1.9	2.7	0.9	0.7	8.8	135.9	55.6	1193	488	19.7	8.1
WHH-6.4	2.7	0.0	-31.7	0.0	0.1	0.1	2.1	2.3	3.1	0.9	0.7	8.7	148.0	55.3	847	317	20.1	7.5
WHH-6.8	3.0	0.0	-35.5	0.0	0.0	0.2	2.3	2.5	2.9	0.9	0.8	7.6	97.3	32.3	497	165	12.5	4.1
WHH-6.9	2.1	0.0	-25.2	0.0	0.0	0.1	2.8	2.9	4.2	1.0	0.7	8.6	25.2	12.1	370	178	11.0	5.3
WHH-7.2	2.7	0.0	n.d	0.0	0.0	0.1	3.5	3.7	4.2	1.0	0.9	7.1	37.3	13.8	-	-	8.8	3.3
WHH-7.4	3.6	0.0	-30.2	0.0	0.0	0.1	3.5	3.7	4.5	1.0	0.8	7.4	36.7	10.1	336	93	10.1	2.8
WHH-7.6	4.1	0.0	-21.4	0.0	0.1	0.0	0.1	0.2	0.6	0.7	0.3	8.5	10.6	2.6	458	113	8.7	2.1
WHH-9.1	0.6	0.0	-7.0	0.0	0.0	0.0	0.0	0.1	0.6	0.2	0.1	6.2	0.1	0.1	-	-	8.0	13.4
WHH-9.5	0.8	0.0	n.d	0.0	0.1	0.0	0.0	0.1	0.7	0.4	0.2	6.2	0.1	0.1	256	313	8.2	10.1

Supplementary Table S2 Reference list used for the compilation of the secular trends of Mo, Mo/TOC, V, and V/TOC, as used in Figure 3.

Age (Ga)	Formation	Location	Reference/Source
0.000	Black Sea Unit 2		Brumsack, 2006
0.000	Sapropel sediments	Tyrrhenian Basin, western Mediterranean	Gehrke et al., 2009
0.000	Peru Margin sediments	East Pacific	Böning, et al.,2004
0.000	East Pacific Margin sediments	San Clemente, Chile Margin	McManus, et al., 2006
0.000	East Pacific Margin sediments	Washington State, North Pacific	Morford, et al., 2005
0.000	Microlaminated sediments	Cariaco Basin, Venezuela	Lyons et al., 2003
0.000	Anoxic sediments	Framvaren Fjord and Saanich Inlet	Algeo and Lyons, 2006
0.081	Julia Creek Oil Shale, Toolebuc Formation	Queensland, Australia	Hirner & Xu., Chem. 1991
0.086	La Luna Formation	Venezuela	Alberdi-Genolet & Tocco, 1999
0.091	C/T Demerara Rise	Demerara Rise	Brumsack, 2006
0.113	Machiques Member	Venezuela	Alberdi-Genolet & Tocco1999
0.154	Kimmeridge Clay Formation	Yorkshire Coast, UK	Tribovillard et al., 1994
0.180	Whitby Mudstone Formation	Yorkshire Coast, UK	Pearce et al., 2008
0.183	Lower Toarcian Shales	Yorkshire Coast, UK	McArthur, et al., 2008
0.247	Kupferschiefer Shales	Northern Zechstein Basin, Poland	Pašava et al.,2010
0.305	Hushpuckney Shale Member, Coffeyville Fm	Oklahoma, USA	Cruse & Lyons, 2004
0.305	Stark Shale Member, Dennis Limestone	Wabaunsee County, Kansas	Hatch & Leventhal,1997
0.309	Unnamed Shale Member	Osage Co, Oklahoma	Hatch & Leventhal, 1997
0.361	Sunbury Shale	Kentucky, USA	Perkins et al., 2008
0.365	Ohio Shale, Clevland Subunit	Kentucky, USA	Perkins et al., 2008
0.365	Ohio Shale, Clevland Subunit	Kentucky, USA	Dahl, T., et al., 2010
0.378	Marcellus Subgroup	New York, USA	Sageman, et al., 2003
0.388	Appalacian Devonian Shale	Pennsylvania, USA	Leventhal, 1991
0.388	Oatka Creek Formation	Livingston County, New York, USA	Werne et al., 2002
0.392	Oatka Creek formation	New Albany Shale, USA	Gordon, G., et al.,2009
0.440	Rastrites Shale, Birkhill Shale	Scotland and Sweden	Dahl, T., et al., 2010
0.465	Almelud Shale,Albjära, Gislövhammar	Tremadoc, Sweden	Dahl, T., et al., 2010
0.485	Alum Shale,Albjära, Gislövhammar	Tremadoc, Sweden	Dahl, T., et al., 2010
0.500	Alum Shale, Andrarum	Sweeden	Dahl, T., et al., 2010
0.515	Alum Shale	Närke Area, Sweden	Leventhal, 1991
0.526	Niutitang Formation	South China	Leventhal, 1991
0.526	Sugaitebulake	Northern Tarim Basin, China	Yu et al., 2009
0.533	Niutitang Formation, Ganziping	China	Dahl, T., et al., 2010
0.540	Ara Group	Oman	Dahl, T., et al., 2010
0.542	Jiumenchong Fm.	Songtao section,South China	Guo, et al., 2007
0.550	Upper Bhander Shale	Vindhyan Basin, India	Paikaray et al., 2008
0.608	Old Fort Pt Fm.	Outcrop, Western Canada	Kendall et al., 2004
0.620	Doushantuo Fm	Songtao section,South China	Guo, et al., 2007
0.625	Kuibis+Schwarzrand Subgroups, Nama Grp	Nama Group, Namibia	Laskowski & Kröner, 1985
0.640	Black River Dolomite	Forest-1 Core, Australia and Tasmania	Kendall et al., (unpublished data)
0.643	Tindelpina Shale Mbr	Blinman-2 and SCYW1a Core, Australia	Kendall et al., 2006
0.650	Sirbu Shale	Vindhyan Basin, India	Paikaray et al., 2008
0.657	Aralka Fm	Wallara-1 Core, Australia	Kendall et al., 2006
0.663	Datangpo Formation	South China	Li et al., 2010
0.700	Lower Bhander Shale	Vindhyan Basin, India	Paikaray et al., 2008
0.715	Rewa Shale	Vindhyan Basin, India	Paikaray et al., 2008

Age (Ga)	Formation	Location	Reference/Source
0.750	AK-10-53-12	Chuar Group, Grand Canyon, USA	Dahl et al., 2011
0.766	Rabanpalli Formation	India	Nagarajan et al., 2007
0.766	Mineral Fork Formation	Utah, USA	Young., 2002
0.771	Rabanpalli Formation	India	Nagarajan et al., 2007
0.800	Red Pine Shale	Uinta Mountais and Cottonwood Group	Condie et al., 2001
0.940	Bijaygarh Shale	Vindhyan Basin, India	Paikaray et al., 2008
1.388	Olentangy Formation	Kentucky, USA	Perkins et al.,2008
1.400	Velkerri Formation (Urapunga-4)	McArthur Basin, Northern Australia	Kendall et al., 2009
1.400	Velkerri Formation, Roper Group	Roper Group, McArthur Basin	Arnold et al., 2004
1.600	Rampur Shale	Vindhyan Basin, India	Paikaray et al., 2008
1.630	Olive Shale	Vindhyan Basin, India	Paikaray et al., 2008
1.730	Wollogorang Formation (Mount Young 2)	McArthur Basin, Northern Australia	Kendall et al., 2009
1.800	RoveFormation	Canadian Sheild, Canada	Kendall et al., 2011
1.800	RoveFormation	Canadian Sheild, Canada	Cameron & Garrels, 1980
1.800	Arangi Shale	Vindhyan Basin, India	Paikaray et al., 2008
1.900	DMH-23 (Black Shale)	Northeastern Labrador, Canada	Hayashi et al., 1997
1.914	Morar Formation	Gwalior, India	Absar et al.,2009
2.000	Zaonezhskaya Formation	NW Russia	Melezhik et al., 1999
2.050	Zaonezhskaya Fm., Ludikovian Series	Karelia, Russia	Scott et al., (unpublished)
2.150	Silverton Formation	Transvaal Supergroup, South Africa	Wronkiewicz et al., 1990
2.350	Strubenkop Formation	Transvaal Supergroup, South Africa	Wronkiewicz et al., 1990
2.400	Gowganda	Canadian Sheild, Canada	Cameron & Garrels, 1980
2.500	Jeerinah, Marra Mamba and Wittenoom	Hamersley Basin, Australia	Alibert & McCulloch,1993
2.500	Gamohann/Kuruman	Transvaal Basin, South Africa	Beukes et al., 1990
2.500	Mt McRae Shale	ABDP-9 Core, Western Australia	Anbar et al., 2007
2.500	Klein Naute Formation-GKP01	South Africa	Kendall et al., 2010
2.530	Gamhaan Formation	South Africa	Scott et al., (unpublished)
2.620	Jeerinah Formation, Fortescue Group	Australia	Scott et al., (unpublished)
2.700	Sandur Superterrane	Bhimangundi, India	Manikyamba & Kerrich, 2006
2.700	Bothaville Formation	Ventersdorp Supergroup, South Africa	Wronkiewicz et al., 1990
2.700	Whim Creek Group	Western Australia	McLennan, et al., 1983
2.700	Lac des Iles and Beardmore	Canadian Sheild, Canada	Cameron & Garrels, 1980
2.740	Michipicoten and Oba	Canadian Sheild, Canada	Cameron & Garrels, 1980
2.850	North Spirit Lake Greenstone Belt	Northwest Ontario, Canada	Nesbitt et al., 2009
2.900	Mozaan Group, Pongola Supergroup	Pongola Supergroup, S. Africa	Laskowski & Kröner, 1985
2.900	Red Lake	Canadian Sheild, Canada	Cameron & Garrels, 1980
3.000	Buhwa Greenstone Belt	Zimbabwe	Fedo et al., 1996
3.070	North Spirit Lake Greenstone Belt	Northwest Ontario, Canada	Nesbitt et al., 2009
3.250	Fig Tree Group	Swaziland Supergroup, South Africa	Hofmann, 2005
3.400	Geogre Creek Group, Mullagine Area	Western Australia	McLennan et al., 1983

Supplementary Table S3 Data used for the compilation of the secular trends of Mo, Mo/TOC, V, and V/TOC

Age (Ga)	Reference/Source	Formation	Location	Sample	TOC	Mo	V
3.25	Hofmann (2005)	Fig Tree Group	Sw aziland Supergroup,	FS1			26.3
3.25	Hofmann (2005)	Fig Tree Group	Sw aziland Supergroup,	FS3			31.9
3.25	Hofmann (2005)	Fig Tree Group	Sw aziland Supergroup,	FS6			156.3
3.25	Hofmann (2005)	Fig Tree Group	Sw aziland Supergroup,	FS9			116.6
3.25	Hofmann (2005)	Fig Tree Group	Sw aziland Supergroup,	FS10			164.0
3.25	Hofmann (2005)	Fig Tree Group	Sw aziland Supergroup,	FS11			171.3
3.25	Hofmann (2005)	Fig Tree Group	Sw aziland Supergroup,	FS12			187.4
3.25	Hofmann (2005)	Fig Tree Group	Sw aziland Supergroup,	FS13			177.4
2.7	Manikyamba and Kerrich (2006)	Sandur Superterrane	Vibhutigudda, India	C12(V)		0.94	297
2.7	Manikyamba and Kerrich (2006)	Sandur Superterrane	Vibhutigudda, India	C22 (V)		1.37	157
2.7	Manikyamba and Kerrich (2006)	Sandur Superterrane	Vibhutigudda, India	C17 (V)			171
2.7	Manikyamba and Kerrich (2006)	Sandur Superterrane	Vibhutigudda, India	C23 (V)		1.34	110
2.7	Manikyamba and Kerrich (2006)	Sandur Superterrane	Vibhutigudda, India	C13 (V)			220
2.7	Manikyamba and Kerrich (2006)	Sandur Superterrane	Vibhutigudda, India	C20 (V)			261
2.7	Manikyamba and Kerrich (2006)	Sandur Superterrane	Vibhutigudda, India	C14 (V)		1.1	265
2.7	Manikyamba and Kerrich (2006)	Sandur Superterrane	Vibhutigudda, India	C21 (V)		1.12	233
2.7	Manikyamba and Kerrich (2006)	Sandur Superterrane	Vibhutigudda, India	C15 (V)			123
2.7	Manikyamba and Kerrich (2006)	Sandur Superterrane	Vibhutigudda, India	C18 (V)		1.71	216
2.7	Manikyamba and Kerrich (2006)	Sandur Superterrane	Bhimangundi, India	C8 (B)		2.62	313
2.7	Manikyamba and Kerrich (2006)	Sandur Superterrane	Bhimangundi, India	C1 (B)		0.83	256
2.7	Manikyamba and Kerrich (2006)	Sandur Superterrane	Bhimangundi, India	C4 (B)		2.38	270
2.7	Manikyamba and Kerrich (2006)	Sandur Superterrane	Bhimangundi, India	C9 (B)		1.51	215
2.7	Manikyamba and Kerrich (2006)	Sandur Superterrane	Bhimangundi, India	C10 (B)			237
2.7	Manikyamba and Kerrich (2006)	Sandur Superterrane	Bhimangundi, India	C5 (B)		1.63	237
2.7	Manikyamba and Kerrich (2006)	Sandur Superterrane	Bhimangundi, India	C2 (B)		0.67	1.99
2.7	Manikyamba and Kerrich (2006)	Sandur Superterrane	Bhimangundi, India	C3 (B)			1.88
2.7	Manikyamba and Kerrich (2006)	Sandur Superterrane	Bhimangundi, India	C7 (B)		0.53	3.16
2.5	Alibert and McCulloch (1993)	Jeerinah, Marra Mamba and Wittenoom Dolomite	Hamersley Basin, Austr	DDH186 J 146.7m (RH1)		2.5	136
2.5	Alibert and McCulloch (1993)	McRae Shale, Dales Gorge, Whaleback Shale and Joffre	Hamersley Basin, Austr	ND-7 (216.8-217.1 m) McRae Shale		5.5	63
2.5	Alibert and McCulloch (1993)	McRae Shale, Dales Gorge, Whaleback Shale and Joffre	Hamersley Basin, Austr	YAM2 S2		1.7	53
2.5	Alibert and McCulloch (1993)	McRae Shale, Dales Gorge, Whaleback Shale and Joffre	Hamersley Basin, Austr	W2(66-76) S5		2.1	75
2.5	Alibert and McCulloch (1993)	McRae Shale, Dales Gorge, Whaleback Shale and Joffre	Hamersley Basin, Austr	W6(104-112) S6			
2.5	Alibert and McCulloch (1993)	McRae Shale, Dales Gorge, Whaleback Shale and Joffre	Hamersley Basin, Austr	Witt-H51 2(B25.5-32) S6		3.3	
2.5	Alibert and McCulloch (1993)	McRae Shale, Dales Gorge, Whaleback Shale and Joffre	Hamersley Basin, Austr	Witt-H51 8(B17.5-20.5) S6		3.3	
2.5	Alibert and McCulloch (1993)	McRae Shale, Dales Gorge, Whaleback Shale and Joffre	Hamersley Basin, Austr	W8(40-49) S12		2.7	56
2.5	Alibert and McCulloch (1993)	McRae Shale, Dales Gorge, Whaleback Shale and Joffre	Hamersley Basin, Austr	W13(31-46) S13		1.7	73
2.5	Alibert and McCulloch (1993)	McRae Shale, Dales Gorge, Whaleback Shale and Joffre	Hamersley Basin, Austr	N85/79 (213.8-229.9) S14		2.4	41
2.5	Alibert and McCulloch (1993)	McRae Shale, Dales Gorge, Whaleback Shale and Joffre	Hamersley Basin, Austr	W23(128-134) S15		1.6	60
2.5	Alibert and McCulloch (1993)	McRae Shale, Dales Gorge, Whaleback Shale and Joffre	Hamersley Basin, Austr	W27(79-96) S16		0.6	19
2.5	Alibert and McCulloch (1993)	McRae Shale, Dales Gorge, Whaleback Shale and Joffre	Hamersley Basin, Austr	S16 Paraburdoo shale		2.6	61
2.5	Alibert and McCulloch (1993)	McRae Shale, Dales Gorge, Whaleback Shale and Joffre	Hamersley Basin, Austr	S16 Paraburdoo chert-siderite		1.7	5
2.5	Alibert and McCulloch (1993)	McRae Shale, Dales Gorge, Whaleback Shale and Joffre	Hamersley Basin, Austr	W37(28-45) Whaleback shale + chert		2.1	13
2.5	Alibert and McCulloch (1993)	McRae Shale, Dales Gorge, Whaleback Shale and Joffre	Hamersley Basin, Austr	W47(20-33) Joffre shale			68

Age (Ga)	Reference/Source	Formation	Location	Sample	TOC	Mo	V
2.7	Wronkiewicz and Condie (1990)	Bothaville Formation	Ventersdorp Supergrou	Average Bothaville Formation			117
2.35	Wronkiewicz and Condie (1990)	Selati Formation	Transvaal Supergroup,	Average Selati Formation			169
2.35	Wronkiewicz and Condie (1990)	Black Reef Formation	Transvaal Supergroup,	Average Black Reef Formation			205
2.35	Wronkiewicz and Condie (1990)	Timeball Hill Formation	Transvaal Supergroup,	Average Timeball Hill Formation			151
2.35	Wronkiewicz and Condie (1990)	Strubenkop Formation	Transvaal Supergroup,	Average Strubenkop Formation			189
2.15	Wronkiewicz and Condie (1990)	Silverton Formation	Transvaal Supergroup,	Average Silverton Formation			154
1.4	Kendall et al. (2009)	Velkerri Formation (Urapunga-4)	McArthur Basin, Northe	136.98-137.05		112	378
1.4	Kendall et al. (2009)	Velkerri Formation (Urapunga-4)	McArthur Basin, Northe	137.19–137.26		110	442
1.4	Kendall et al. (2009)	Velkerri Formation (Urapunga-4)	McArthur Basin, Northe	137.26–137.33		106	499
1.4	Kendall et al. (2009)	Velkerri Formation (Urapunga-4)	McArthur Basin, Northe	137.46–137.52		119	458
1.4	Kendall et al. (2009)	Velkerri Formation (Urapunga-4)	McArthur Basin, Northe	137.75–137.79		105	408
1.4	Kendall et al. (2009)	Velkerri Formation (Urapunga-4)	McArthur Basin, Northe	137.84–137.89		114	559
1.4	Kendall et al. (2009)	Velkerri Formation (Urapunga-4)	McArthur Basin, Northe	325.71–325.78		8.6	106
1.4	Kendall et al. (2009)	Velkerri Formation (Urapunga-4)	McArthur Basin, Northe	326.20–326.28		8.8	97
1.4	Kendall et al. (2009)	Velkerri Formation (Urapunga-4)	McArthur Basin, Northe	326.42–326.48		6	97
1.4	Kendall et al. (2009)	Velkerri Formation (Urapunga-4)	McArthur Basin, Northe	326.48–326.55		6	86
1.4	Kendall et al. (2009)	Velkerri Formation (Urapunga-4)	McArthur Basin, Northe	326.62–326.69		7.5	106
1.73	Kendall et al. (2009)	Wollogorang Formation (Mount Young 2)	McArthur Basin, Northe	72.27-74.29		58	81
1.73	Kendall et al. (2009)	Wollogorang Formation (Mount Young 2)	McArthur Basin, Northe	74.35–74.38		57	64
1.73	Kendall et al. (2009)	Wollogorang Formation (Mount Young 2)	McArthur Basin, Northe	75.08–75.11		41	70
1.73	Kendall et al. (2009)	Wollogorang Formation (Mount Young 2)	McArthur Basin, Northe	75.48–75.51		57	102
1.73	Kendall et al. (2009)	Wollogorang Formation (Mount Young 2)	McArthur Basin, Northe	75.51–75.53		56	106
1.73	Kendall et al. (2009)	Wollogorang Formation (Mount Young 2)	McArthur Basin, Northe	76.00–76.03		56	133
1.73	Kendall et al. (2009)	Wollogorang Formation (Mount Young 2)	McArthur Basin, Northe	76.03–76.08		52	127
1.73	Kendall et al. (2009)	Wollogorang Formation (Mount Young 2)	McArthur Basin, Northe	76.91-76.96 (dol)		49	119
1.73	Kendall et al. (2009)	Wollogorang Formation (Mount Young 2)	McArthur Basin, Northe	76.91–76.96		56	161
0.771	Nagarajan et al. (2007)	Rabanpalli Formation	India	S53			29.4
0.771	Nagarajan et al. (2007)	Rabanpalli Formation	India	S51A			29.5
0.771	Nagarajan et al. (2007)	Rabanpalli Formation	India	E117			24.8
0.771	Nagarajan et al. (2007)	Rabanpalli Formation	India	S51B			28.9
0.766	Nagarajan et al. (2007)	Rabanpalli Formation	India	S38E			32.8
0.766	Nagarajan et al. (2007)	Rabanpalli Formation	India	S4			46.4
0.766	Nagarajan et al. (2007)	Rabanpalli Formation	India	S23			51.9
0.766	Nagarajan et al. (2007)	Rabanpalli Formation	India	C111			41.9
0.766	Nagarajan et al. (2007)	Rabanpalli Formation	India	E121			64.8
0.766	Nagarajan et al. (2007)	Rabanpalli Formation	India	C122			82.8
0.766	Nagarajan et al. (2007)	Rabanpalli Formation	India	E49			64.3
0.766	Nagarajan et al. (2007)	Rabanpalli Formation	India	C103			52.6
0.766	Nagarajan et al. (2007)	Rabanpalli Formation	India	E189			70.4

Age (Ga)	Reference/Source	Formation	Location	Sample	TOC	Mo	V
0.766	Young (2002)	Mineral Fork Formation	Utah, USA	91-48			102
0.766	Young (2002)	Mineral Fork Formation	Utah, USA	20-25			117
0.766	Young (2002)	Mineral Fork Formation	Utah, USA	91-45			142
0.766	Young (2002)	Mineral Fork Formation	Utah, USA	91-43			112
0.766	Young (2002)	Mineral Fork Formation	Utah, USA	20-23			119
0.766	Young (2002)	Mineral Fork Formation	Utah, USA	91-38			116
0.766	Young (2002)	Mineral Fork Formation	Utah, USA	91-36			85
0.766	Young (2002)	Mineral Fork Formation	Utah, USA	20-22			146
0.766	Young (2002)	Mineral Fork Formation	Utah, USA	91-31			122
0.766	Young (2002)	Mineral Fork Formation	Utah, USA	20-21			129
0.766	Young (2002)	Mineral Fork Formation	Utah, USA	20-16			116
0.766	Young (2002)	Mineral Fork Formation	Utah, USA	91-53			131
0.766	Young (2002)	Mineral Fork Formation	Utah, USA	20-15			92
0.766	Young (2002)	Mineral Fork Formation	Utah, USA	91-52			76
0.766	Young (2002)	Big Cottonw ood Formation	Utah, USA	20-19			104
0.766	Young (2002)	Big Cottonw ood Formation	Utah, USA	20-18			107
2.5	Beukes et al. 1990 & Klein and Beukes (1989)	Gamohann/Kuruman	Transvaal Basin, South	AD5 - 157.70 m	5.328		180
2.5	Beukes et al. 1990 & Klein and Beukes (1989)	Gamohann/Kuruman	Transvaal Basin, South	AD5 - 163.70 m	3.767		150
2.5	Beukes et al. 1990 & Klein and Beukes (1989)	Gamohann/Kuruman	Transvaal Basin, South	AD5 - 176.10 m	2.62		150
2.5	Beukes et al. 1990 & Klein and Beukes (1989)	Gamohann/Kuruman	Transvaal Basin, South	AD5 - 181.50 m	2.727		150
2.5	Beukes et al. 1990 & Klein and Beukes (1989)	Gamohann/Kuruman	Transvaal Basin, South	AD5 - 169.00 m	4.952		150
2.5	Beukes et al. 1990 & Klein and Beukes (1989)	Gamohann/Kuruman	Transvaal Basin, South	AD5 - 188.20 m	6.365		150
2.5	Beukes et al. 1990 & Klein and Beukes (1989)	Gamohann/Kuruman	Transvaal Basin, South	AD5 - 188.30 m	3.841		150
2.5	Beukes et al. 1990 & Klein and Beukes (1989)	Gamohann/Kuruman	Transvaal Basin, South	WB98 - 826.00 m	4.187		150
2.5	Beukes et al. 1990 & Klein and Beukes (1989)	Gamohann/Kuruman	Transvaal Basin, South	WB98 - 853.00	2.794		150
2.5	Beukes et al. 1990 & Klein and Beukes (1989)	Gamohann/Kuruman	Transvaal Basin, South	WB98 - 926.00	2.515		
0.62	Guo et al. (2007)	Doushantuo Fm	Songtao section,Guizho	Son510		26.01	238.91
0.62	Guo et al. (2007)	Doushantuo Fm	Songtao section,Guizho	Son511		29.39	97.97
0.62	Guo et al. (2007)	Doushantuo Fm	Songtao section,Guizho	Son512	13.06	37.78	130.63
0.62	Guo et al. (2007)	Doushantuo Fm	Songtao section,Guizho	Son513	2.71	7.53	223.5
0.62	Guo et al. (2007)	Doushantuo Fm	Songtao section,Guizho	Son514	4.54	45.31	1085.02
0.62	Guo et al. (2007)	Doushantuo Fm	Songtao section,Guizho	Son516		0.44	33.44
0.62	Guo et al. (2007)	Doushantuo Fm	Songtao section,Guizho	Son517		0.56	93.82
0.62	Guo et al. (2007)	Doushantuo Fm	Songtao section,Guizho	Son518		0.11	59.57
0.62	Guo et al. (2007)	Doushantuo Fm	Songtao section,Guizho	Son519		0.19	90.36
0.62	Guo et al. (2007)	Doushantuo Fm	Songtao section,Guizho	Son520		0.49	364.73
0.62	Guo et al. (2007)	Doushantuo Fm	Songtao section,Guizho	Son521		0.26	60.4

Age (Ga)	Reference/Source	Formation	Location	Sample	TOC	Mo	V
0.542	Guo et al. (2007)	Guojiaba Fm.	Shatan section, Sichuar	Sat531	0.23	0.9	64.82
0.542	Guo et al. (2007)	Guojiaba Fm.	Shatan section, Sichuar	Sat530		2.85	77.14
0.542	Guo et al. (2007)	Guojiaba Fm.	Shatan section, Sichuar	Sat529	0.56	1.92	71.52
0.542	Guo et al. (2007)	Guojiaba Fm.	Shatan section, Sichuar	Sat528	0.38	1.89	97.73
0.542	Guo et al. (2007)	Guojiaba Fm.	Shatan section, Sichuar	Sat527		3.85	83.1
0.542	Guo et al. (2007)	Guojiaba Fm.	Shatan section, Sichuar	Sat526		2.36	77.63
0.542	Guo et al. (2007)	Guojiaba Fm.	Shatan section, Sichuar	Sat525	0.65	4.03	87.24
0.542	Guo et al. (2007)	Guojiaba Fm.	Shatan section, Sichuar	Sat524	0.69	5.09	82
0.542	Guo et al. (2007)	Guojiaba Fm.	Shatan section, Sichuar	Sat523	0.81	3.93	74.97
0.542	Guo et al. (2007)	Guojiaba Fm.	Shatan section, Sichuar	Sat522	0.62	5.19	102.05
0.542	Guo et al. (2007)	Guojiaba Fm.	Shatan section, Sichuar	Sat521	0.87	4.55	103.28
0.542	Guo et al. (2007)	Guojiaba Fm.	Shatan section, Sichuar	Sat520	0.77	3.37	95.25
0.542	Guo et al. (2007)	Guojiaba Fm.	Shatan section, Sichuar	Sat519	1.13	5.62	92.45
0.542	Guo et al. (2007)	Guojiaba Fm.	Shatan section, Sichuar	Sat518	1.32	6.77	85.34
0.542	Guo et al. (2007)	Guojiaba Fm.	Shatan section, Sichuar	Sat517	1.63	7.05	107.45
0.542	Guo et al. (2007)	Guojiaba Fm.	Shatan section, Sichuar	Sat516	1.74	18.74	162.23
0.542	Guo et al. (2007)	Guojiaba Fm.	Shatan section, Sichuar	Sat515	1.88	44.19	484.23
0.542	Guo et al. (2007)	Guojiaba Fm.	Shatan section, Sichuar	Sat514		13.4	229.96
0.542	Guo et al. (2007)	Guojiaba Fm.	Shatan section, Sichuar	Sat513	3.17	36.59	424.18
0.542	Guo et al. (2007)	Guojiaba Fm.	Shatan section, Sichuar	Sat512	3.88	35.88	406.25
0.542	Guo et al. (2007)	Guojiaba Fm.	Shatan section, Sichuar	Sat511	3.15	38.6	298
0.542	Guo et al. (2007)	Guojiaba Fm.	Shatan section, Sichuar	Sat510	4.08	70.92	188.49
0.542	Guo et al. (2007)	Guojiaba Fm.	Shatan section, Sichuar	Sat509	3.11	38.96	1198.18
0.542	Guo et al. (2007)	Guojiaba Fm.	Shatan section, Sichuar	Sat508	3.37	29.91	2141.22
0.542	Guo et al. (2007)	Guojiaba Fm.	Shatan section, Sichuar	Sat507	3.69	25.5	2049.58
0.542	Guo et al. (2007)	Guojiaba Fm.	Shatan section, Sichuar	Sat506	4.9	70.2	444.05
0.542	Guo et al. (2007)	Guojiaba Fm.	Shatan section, Sichuar	Sat505	4.18	42.79	424.06
0.542	Guo et al. (2007)	Guojiaba Fm.	Shatan section, Sichuar	Sat504	3.12	12.03	215.05
0.542	Guo et al. (2007)	Guojiaba Fm.	Shatan section, Sichuar	Sat503	2.57	5.44	187.79
0.542	Guo et al. (2007)	Guojiaba Fm.	Shatan section, Sichuar	Sat502	0.85	2.21	164.43
0.542	Guo et al. (2007)	Guojiaba Fm.	Shatan section, Sichuar	Sat501		4.98	148.58
0.542	Guo et al. (2007)	Guojiaba Fm.	Shatan section, Sichuar	Sat500		1.06	43.05
0.542	Guo et al. (2007)	Jiumenchong Fm.	Songtao section,Guizho	Son594		111.94	475.48
0.542	Guo et al. (2007)	Jiumenchong Fm.	Songtao section,Guizho	Son593		295.44	2271.46
0.542	Guo et al. (2007)	Jiumenchong Fm.	Songtao section,Guizho	Son592		216.61	1418.17
0.542	Guo et al. (2007)	Jiumenchong Fm.	Songtao section,Guizho	Son591		90.22	563.96
0.542	Guo et al. (2007)	Jiumenchong Fm.	Songtao section,Guizho	Son590		17.97	581.48
0.542	Guo et al. (2007)	Jiumenchong Fm.	Songtao section,Guizho	Son589		112.44	685.75
0.542	Guo et al. (2007)	Jiumenchong Fm.	Songtao section,Guizho	Son588		247.96	1193.56
0.542	Guo et al. (2007)	Jiumenchong Fm.	Songtao section,Guizho	Son587		143.61	2001.25
0.542	Guo et al. (2007)	Jiumenchong Fm.	Songtao section,Guizho	Son586		20.3	200.77
0.542	Guo et al. (2007)	Jiumenchong Fm.	Songtao section,Guizho	Son585		112.13	394.45
0.542	Guo et al. (2007)	Jiumenchong Fm.	Songtao section,Guizho	Son584		74.99	5602.03
0.542	Guo et al. (2007)	Jiumenchong Fm.	Songtao section,Guizho	Son583		132.73	3850.46
0.542	Guo et al. (2007)	Jiumenchong Fm.	Songtao section,Guizho	Son582	1.94	5.03	229.59
0.542	Guo et al. (2007)	Jiumenchong Fm.	Songtao section,Guizho	Son581	3.25	36.72	3246.95

Age (Ga)	Reference/Source	Formation	Location	Sample	TOC	Mo	V
0.526	Jiang et al. (2006)	Niutitang Formation	South China	GZW27		79	684
0.526	Jiang et al. (2006)	Niutitang Formation	South China	GZW28		26	405
0.526	Jiang et al. (2006)	Niutitang Formation	South China	GZW29		26	372
0.526	Jiang et al. (2006)	Niutitang Formation	South China	GZW30		23	417
0.526	Jiang et al. (2006)	Niutitang Formation	South China	ZN28		173	254
0.526	Jiang et al. (2006)	Niutitang Formation	South China	ZN29		42	538
0.526	Jiang et al. (2006)	Niutitang Formation	South China	ZN30		70	1,234
0.526	Jiang et al. (2006)	Niutitang Formation	South China	ZN31		54	8,232
0.526	Jiang et al. (2006)	Niutitang Formation	South China	ZN32		74	3,168
0.526	Jiang et al. (2006)	Niutitang Formation	South China	ZN33			8,603
0.526	Jiang et al. (2006)	Niutitang Formation	South China	ZN34			11,339
0.526	Jiang et al. (2006)	Niutitang Formation	South China	ZN35			15,652
0.526	Jiang et al. (2006)	Niutitang Formation	South China	ZN35-1			16,515
0.526	Yu et al. (2009)	Xiaoerbulake	Northern Tarim Basin, C	XCM2-1	3.93	12	2039
0.526	Yu et al. (2009)	Xiaoerbulake	Northern Tarim Basin, C	XCM-3	5.34	10	2965
0.526	Yu et al. (2009)	Xiaoerbulake	Northern Tarim Basin, C	XCM-5	9.33	1	1049
0.526	Yu et al. (2009)	Xiaoerbulake	Northern Tarim Basin, C	XCM7-1	7.5	79	12207
0.526	Yu et al. (2009)	Xiaoerbulake	Northern Tarim Basin, C	XCM8-1	3.39	57	3976
0.526	Yu et al. (2009)	Xiaoerbulake	Northern Tarim Basin, C	XCM9-1	5.89	43	2883
0.526	Yu et al. (2009)	Xiaoerbulake	Northern Tarim Basin, C	XCM9-2	6.6	41	1728
0.526	Yu et al. (2009)	Xiaoerbulake	Northern Tarim Basin, C	XCMIO-1	8.56	35	1324
0.526	Yu et al. (2009)	Xiaoerbulake	Northern Tarim Basin, C	XCM10-2	9.8	48	998
0.526	Yu et al. (2009)	Xiaoerbulake	Northern Tarim Basin, C	XCM10-3	7.05	24	1069
0.526	Yu et al. (2009)	Xiaoerbulake	Northern Tarim Basin, C	XCM10-4	5.45	15	290
0.526	Yu et al. (2009)	Xiaoerbulake	Northern Tarim Basin, C	XCM10-5	6.56	6	620
0.526	Yu et al. (2009)	Sugaitebulake	Northern Tarim Basin, C	SCM1-1		7	1668
0.526	Yu et al. (2009)	Sugaitebulake	Northern Tarim Basin, C	SCM2-1		14	1338
0.526	Yu et al. (2009)	Sugaitebulake	Northern Tarim Basin, C	SCM3-1		27	4419
0.526	Yu et al. (2009)	Sugaitebulake	Northern Tarim Basin, C	SCM4-1		55	5394
0.526	Yu et al. (2009)	Sugaitebulake	Northern Tarim Basin, C	SCM4-2		33	2286
0.526	Yu et al. (2009)	Sugaitebulake	Northern Tarim Basin, C	ScM5-1		28	1537
0.526	Yu et al. (2009)	Sugaitebulake	Northern Tarim Basin, C	SCM5-2		25	1217
0.526	Yu et al. (2009)	Sugaitebulake	Northern Tarim Basin, C	SCM5-3		28	874
0.526	Yu et al. (2009)	Sugaitebulake	Northern Tarim Basin, C	SCM5-4		24	789
0.526	Yu et al. (2009)	Sugaitebulake	Northern Tarim Basin, C	SCM5-5		16	686

Age (Ga)	Reference/Source	Formation	Location	Sample	TOC	Mo	V
0.515	Leventhal (1991)	Alum Shale	Närke Area, Sweden	7.9-8.5	15.4	220	510
0.515	Leventhal (1991)	Alum Shale	Närke Area, Sweden	9.2-9.9	17.2	210	470
0.515	Leventhal (1991)	Alum Shale	Närke Area, Sweden	10.5-11.5	16.3	150	450
0.515	Leventhal (1991)	Alum Shale	Närke Area, Sweden	13.0-13.7	14.4	180	430
0.515	Leventhal (1991)	Alum Shale	Närke Area, Sweden	14.1-14.5	15.6	180	380
0.515	Leventhal (1991)	Alum Shale	Närke Area, Sweden	14.5-15.2	17.3	160	460
0.515	Leventhal (1991)	Alum Shale	Sydbillingen, Sweeden	4.2-4.3	19.6	280	710
0.515	Leventhal (1991)	Alum Shale	Sydbillingen, Sweeden	6.0-6.1	11.9	260	695
0.515	Leventhal (1991)	Alum Shale	Sydbillingen, Sweeden	11.1-11.2	10.3	120	510
0.515	Leventhal (1991)	Alum Shale	Sydbillingen, Sweeden	13.0-13.1	9.2	125	730
0.515	Leventhal (1991)	Alum Shale	Skvode, Billingen Area,	E	15.1	235	595
0.515	Leventhal (1991)	Alum Shale	Randtad, Billingen Area,	F	16.9	260	845
0.515	Leventhal (1991)	Alum Shale	Randtad, Billingen Area,	G	20.6	275	845
0.515	Leventhal (1991)	Alum Shale	Jämtland cores Autocht	3	7.2	150	640
0.515	Leventhal (1991)	Alum Shale	Jämtland cores Autocht	30	2.7	47	700
0.515	Leventhal (1991)	Alum Shale	Jämtland cores Allochth	37	12.8	340	2000
0.515	Leventhal (1991)	Alum Shale	Jämtland cores Allochth	45	12.3	280	1700
0.515	Leventhal (1991)	Alum Shale	Jämtland cores Allochth	68	13.6	340	1500
0.515	Leventhal (1991)	Alum Shale	Jämtland cores Allochth	83	11.8	250	3100
0.515	Leventhal (1991)	Alum Shale	Jämtland cores Allochth	253	13.8	350	1800
0.3875	Leventhal (1991)	Chattanooga Shale	Kentucky, USA	KY-4	4	70	500
0.3875	Leventhal (1991)	Ohio Shale	Pennsylvania, USA	PA-3	2	30	200
0.3875	Leventhal (1991)	New Albany Shale	Ohio, USA	OH-4	2.5	20	200
0.3875	Leventhal (1991)	Appalacian Devonian Shale	Tennessee, USA	TN-7	2	30	200
0.3875	Leventhal (1991)	Ohio Shale	New York, USA	NY-x	4	70	300
0.3875	Leventhal (1991)	Chattanooga Shale	Ohio, USA		10	160	160
0.3875	Leventhal (1991)	Appalacian Devonian Shale	West Virginia, USA	WV-7	1	5	300
0.3875	Leventhal (1991)	Appalacian Devonian Shale	Pennsylvania, USA	PA-1	1.5	5	250
0.3875	Leventhal (1991)	Appalacian Devonian Shale	Pennsylvania, USA	PA-2	2	70	500
0.3875	Leventhal (1991)	Appalacian Devonian Shale	Pennsylvania, USA	PA-4	1.2	3	200
1.3876	Perkins et al. (2008)	Olentangy Formation	Kentucky, USA	B2	0.65	10	176
0.365	Perkins et al. (2008)	Ohio Shale, Clevland Subunit	Kentucky, USA	A26	15.8	42	406
0.365	Perkins et al. (2008)	Ohio Shale, Clevland Subunit	Kentucky, USA	A25	18.2	55	840
0.365	Perkins et al. (2008)	Ohio Shale, Clevland Subunit	Kentucky, USA	B13	11.7	26	287
0.365	Perkins et al. (2008)	Ohio Shale, Clevland Subunit	Kentucky, USA	B12	13.3	61	592
0.365	Perkins et al. (2008)	Ohio Shale, Clevland Subunit	Kentucky, USA	B11	7.05	128	386
0.365	Perkins et al. (2008)	Ohio Shale, Clevland Subunit	Kentucky, USA	A24	5.67	53	466
0.365	Perkins et al. (2008)	Ohio Shale, 3 Lick Subunit	Kentucky, USA	B9	0.25	7	266
0.365	Perkins et al. (2008)	Ohio Shale, 3 Lick Subunit	Kentucky, USA	A23	0.5	18	381
0.365	Perkins et al. (2008)	Ohio Shale, 3 Lick Subunit	Kentucky, USA	A22	6	87	425
0.365	Perkins et al. (2008)	Ohio Shale, 3 Lick Subunit	Kentucky, USA	B8	17.4	33	455
0.365	Perkins et al. (2008)	Ohio Shale, 3 Lick Subunit	Kentucky, USA	B7	0.28	8	305
0.365	Perkins et al. (2008)	Ohio Shale, 3 Lick Subunit	Kentucky, USA	B6	0.25	3	165
0.365	Perkins et al. (2008)	Ohio Shale, Huron Subunit	Kentucky, USA	B5	5.9	86	271
0.365	Perkins et al. (2008)	Ohio Shale, Huron Subunit	Kentucky, USA	D2	5.52	76	232
0.365	Perkins et al. (2008)	Ohio Shale, Huron Subunit	Kentucky, USA	D1	0.68	14	67
0.365	Perkins et al. (2008)	Ohio Shale, Huron Subunit	Kentucky, USA	A21	2.8	44	246

Age (Ga)	Reference/Source	Formation	Location	Sample	TOC	Mo	V
0.365	Perkins et al. (2008)	Ohio Shale, Huron Subunit	Kentucky, USA	B22	5.46	93	196
0.365	Perkins et al. (2008)	Ohio Shale, Huron Subunit	Kentucky, USA	B14	9.62	125	151
0.365	Perkins et al. (2008)	Ohio Shale, Huron Subunit	Kentucky, USA	D3	6.66	106	184
0.365	Perkins et al. (2008)	Ohio Shale, Huron Subunit	Kentucky, USA	B16	9.18	160	172
0.365	Perkins et al. (2008)	Ohio Shale, Huron Subunit	Kentucky, USA	B3	11	89	153
0.365	Perkins et al. (2008)	Ohio Shale, Huron Subunit	Kentucky, USA	B15	11.5	78	133
0.361	Perkins et al. (2008)	Borden Formation, Henley Subunit	Kentucky, USA	A16	0.2	3	660
0.361	Perkins et al. (2008)	Sunbury Shale	Kentucky, USA	A15	10.5	310	2630
0.361	Perkins et al. (2008)	Sunbury Shale	Kentucky, USA	A20	6.61	150	2290
0.361	Perkins et al. (2008)	Sunbury Shale	Kentucky, USA	A14	13.7	378	2470
0.361	Perkins et al. (2008)	Sunbury Shale	Kentucky, USA	A13	10.7	395	869
0.361	Perkins et al. (2008)	Sunbury Shale	Kentucky, USA	A12	4.59	212	360
0.361	Perkins et al. (2008)	Sunbury Shale	Kentucky, USA	A11	10.7	287	1570
0.361	Perkins et al. (2008)	Sunbury Shale	Kentucky, USA	A10	11.7	215	1590
0.361	Perkins et al. (2008)	Sunbury Shale	Kentucky, USA	A9	11.3	255	447
0.361	Perkins et al. (2008)	Sunbury Shale	Kentucky, USA	A8	10.2	277	1140
0.361	Perkins et al. (2008)	Sunbury Shale	Kentucky, USA	A7	12.8	264	731
0.361	Perkins et al. (2008)	Sunbury Shale	Kentucky, USA	A6	11.5	159	1910
0.361	Perkins et al. (2008)	Sunbury Shale	Kentucky, USA	B23	15.2	263	2230
0.361	Perkins et al. (2008)	Sunbury Shale	Kentucky, USA	A19	12.8	134	1200
0.361	Perkins et al. (2008)	Sunbury Shale	Kentucky, USA	A5	16.6	221	2250
0.361	Perkins et al. (2008)	Sunbury Shale	Kentucky, USA	A2	9.68	169	1150
0.362	Perkins et al. (2008)	Bedford Shale	Kentucky, USA	A1	0.26	15	747
0.362	Perkins et al. (2008)	Bedford Shale	Kentucky, USA	A17	0.11	5	37
0.362	Perkins et al. (2008)	Bedford Shale	Kentucky, USA	B24	0	3	62
0.362	Perkins et al. (2008)	Bedford Shale	Kentucky, USA	A18	0.16	1	73
0.362	Perkins et al. (2008)	Bedford Shale	Kentucky, USA	A27	0.22	3	238

Age (Ga)	Reference/Source	Formation	Location	Sample	TOC	Mo	V
0.3875	Werne et al. (2002)	Oatka Creek Formation	Livingston County, New	328.17	9.81	28	166
0.3875	Werne et al. (2002)	Oatka Creek Formation	Livingston County, New	328.36	3.24	47	195
0.3875	Werne et al. (2002)	Oatka Creek Formation	Livingston County, New	328.57	5.84	79	225
0.3875	Werne et al. (2002)	Oatka Creek Formation	Livingston County, New	328.92	2.71	5	155
0.3875	Werne et al. (2002)	Oatka Creek Formation	Livingston County, New	329.48	0.8	2	55
0.3875	Werne et al. (2002)	Oatka Creek Formation	Livingston County, New	329.68	0.49	1	12
0.3875	Werne et al. (2002)	Oatka Creek Formation	Livingston County, New	329.89	2.17	2	57
0.3875	Werne et al. (2002)	Oatka Creek Formation	Livingston County, New	330.1	4.11	18	148
0.3875	Werne et al. (2002)	Oatka Creek Formation	Livingston County, New	330.37	4.56	31	172
0.3875	Werne et al. (2002)	Oatka Creek Formation	Livingston County, New	330.94	5.19	68	196
0.3875	Werne et al. (2002)	Oatka Creek Formation	Livingston County, New	332.05	8.21	169	252
0.3875	Werne et al. (2002)	Oatka Creek Formation	Livingston County, New	332.15	3.68	27	183
0.3875	Werne et al. (2002)	Oatka Creek Formation	Livingston County, New	332.72	8.61	236	331
0.3875	Werne et al. (2002)	Oatka Creek Formation	Livingston County, New	333.12	8.68	173	277
0.3875	Werne et al. (2002)	Oatka Creek Formation	Livingston County, New	333.59	14.18	279	382
0.3875	Werne et al. (2002)	Oatka Creek Formation	Livingston County, New	333.85	6.68	93	275
0.3875	Werne et al. (2002)	Oatka Creek Formation	Livingston County, New	334.63	11.19	251	328
0.3875	Werne et al. (2002)	Oatka Creek Formation	Livingston County, New	335.26	9.86	206	337
0.3875	Werne et al. (2002)	Oatka Creek Formation	Livingston County, New	336.27	9.51	192	310
0.3875	Werne et al. (2002)	Oatka Creek Formation	Livingston County, New	336.69	11.17	234	363
0.3875	Werne et al. (2002)	Oatka Creek Formation	Livingston County, New	337.09	17.3	394	421
0.3875	Werne et al. (2002)	Oatka Creek Formation	Livingston County, New	337.2	11.7	229	383
0.3875	Werne et al. (2002)	Oatka Creek Formation	Livingston County, New	337.3	8.4	53	210
0.3875	Werne et al. (2002)	Oatka Creek Formation	Livingston County, New	337.41	2.19	24	204
0.3875	Werne et al. (2002)	Oatka Creek Formation	Livingston County, New	337.5	5.87	16	150
0.3875	Werne et al. (2002)	Oatka Creek Formation	Livingston County, New	337.83	7.18	20	172
0.3875	Werne et al. (2002)	Oatka Creek Formation	Livingston County, New	338.31	4.89	56	192
0.3875	Werne et al. (2002)	Oatka Creek Formation	Livingston County, New	338.53	7.2	14	158
0.3875	Werne et al. (2002)	Oatka Creek Formation	Livingston County, New	338.73	4.81	15	150
0.3875	Werne et al. (2002)	Oatka Creek Formation	Livingston County, New	338.92	7.95	60	265
0.3875	Werne et al. (2002)	Oatka Creek Formation	Livingston County, New	339.11	0.81	3	95
0.3875	Werne et al. (2002)	Oatka Creek Formation	Livingston County, New	339.31	1.19	3	108
0.3875	Werne et al. (2002)	Oatka Creek Formation	Livingston County, New	339.71	3.77	51	280
0.3875	Werne et al. (2002)	Oatka Creek Formation	Livingston County, New	340.09	1.04	11	52
0.3875	Werne et al. (2002)	Oatka Creek Formation	Livingston County, New	340.5	1.95	6	129
0.3875	Werne et al. (2002)	Oatka Creek Formation	Livingston County, New	340.87	2.75	6	198
0.3875	Werne et al. (2002)	Oatka Creek Formation	Livingston County, New	341.09	0.39	1	4
0.3875	Werne et al. (2002)	Oatka Creek Formation	Livingston County, New	341.24	0.26	2	11

Age (Ga)	Reference/Source	Formation	Location	Sample	TOC	Mo	V
0.3775	Sageman et al. (2003)	Marcellus Subgroup	New York, USA		9.81	28	166
0.3775	Sageman et al. (2003)	Marcellus Subgroup	New York, USA		3.24	47	195
0.3775	Sageman et al. (2003)	Marcellus Subgroup	New York, USA		5.84	79	225
0.3775	Sageman et al. (2003)	Marcellus Subgroup	New York, USA		2.71	5	155
0.3775	Sageman et al. (2003)	Marcellus Subgroup	New York, USA		0.8	2	55
0.3775	Sageman et al. (2003)	Marcellus Subgroup	New York, USA		0.49	1	12
0.3775	Sageman et al. (2003)	Marcellus Subgroup	New York, USA		2.17	2	57
0.3775	Sageman et al. (2003)	Marcellus Subgroup	New York, USA		4.11	18	148
0.3775	Sageman et al. (2003)	Marcellus Subgroup	New York, USA		4.56	31	172
0.3775	Sageman et al. (2003)	Marcellus Subgroup	New York, USA		5.19	68	196
0.3775	Sageman et al. (2003)	Marcellus Subgroup	New York, USA		8.21	169	252
0.3775	Sageman et al. (2003)	Marcellus Subgroup	New York, USA		3.68	27	183
0.3775	Sageman et al. (2003)	Marcellus Subgroup	New York, USA		8.61	236	331
0.3775	Sageman et al. (2003)	Marcellus Subgroup	New York, USA		8.68	173	277
0.3775	Sageman et al. (2003)	Marcellus Subgroup	New York, USA		14.18	279	382
0.3775	Sageman et al. (2003)	Marcellus Subgroup	New York, USA		6.68	93	275
0.3775	Sageman et al. (2003)	Marcellus Subgroup	New York, USA		11.19	251	328
0.3775	Sageman et al. (2003)	Marcellus Subgroup	New York, USA		9.86	206	337
0.3775	Sageman et al. (2003)	Marcellus Subgroup	New York, USA		9.51	192	310
0.3775	Sageman et al. (2003)	Marcellus Subgroup	New York, USA		11.17	234	363
0.3775	Sageman et al. (2003)	Marcellus Subgroup	New York, USA		17.3	394	421
0.3775	Sageman et al. (2003)	Marcellus Subgroup	New York, USA		11.7	229	383
0.3775	Sageman et al. (2003)	Marcellus Subgroup	New York, USA		8.4	53	210
0.3775	Sageman et al. (2003)	Marcellus Subgroup	New York, USA		2.19	24	204
0.3775	Sageman et al. (2003)	Marcellus Subgroup	New York, USA		5.87	16	150
0.3775	Sageman et al. (2003)	Marcellus Subgroup	New York, USA		7.18	20	172
0.3775	Sageman et al. (2003)	Marcellus Subgroup	New York, USA		4.89	56	192
0.3775	Sageman et al. (2003)	Marcellus Subgroup	New York, USA		7.2	14	158
0.3775	Sageman et al. (2003)	Marcellus Subgroup	New York, USA		4.81	15	150
0.3775	Sageman et al. (2003)	Marcellus Subgroup	New York, USA		7.95	60	265
0.3775	Sageman et al. (2003)	Marcellus Subgroup	New York, USA		0.81	3	95
0.3775	Sageman et al. (2003)	Marcellus Subgroup	New York, USA		1.19	3	108
0.3775	Sageman et al. (2003)	Marcellus Subgroup	New York, USA		3.77	51	280
0.3775	Sageman et al. (2003)	Marcellus Subgroup	New York, USA		1.04	11	52
0.3775	Sageman et al. (2003)	Marcellus Subgroup	New York, USA		1.95	6	129
0.3775	Sageman et al. (2003)	Marcellus Subgroup	New York, USA		2.75	6	198
0.3775	Sageman et al. (2003)	Marcellus Subgroup	New York, USA		0.39	1	4
0.3775	Sageman et al. (2003)	Marcellus Subgroup	New York, USA		0.26	2	11
0.3775	Sageman et al. (2003)	Marcellus Subgroup	New York, USA				109
0.3775	Sageman et al. (2003)	Marcellus Subgroup	New York, USA		2.21	46	157
0.3775	Sageman et al. (2003)	Marcellus Subgroup	New York, USA		10.13	202	617
0.3775	Sageman et al. (2003)	Marcellus Subgroup	New York, USA		3.37	61	186
0.3775	Sageman et al. (2003)	Marcellus Subgroup	New York, USA		14.74	298	743
0.3775	Sageman et al. (2003)	Marcellus Subgroup	New York, USA		13.02	213	786
0.3775	Sageman et al. (2003)	Marcellus Subgroup	New York, USA		2.25	9	250
0.3775	Sageman et al. (2003)	Marcellus Subgroup	New York, USA				6

Age (Ga)	Reference/Source	Formation	Location	Sample	TOC	Mo	V
0.3775	Sageman et al. (2003)	Geneseo Formation	New York, USA		0.83		129
0.3775	Sageman et al. (2003)	Geneseo Formation	New York, USA		0.88		133
0.3775	Sageman et al. (2003)	Geneseo Formation	New York, USA		0.83		145
0.3775	Sageman et al. (2003)	Geneseo Formation	New York, USA		0.58	1	115
0.3775	Sageman et al. (2003)	Geneseo Formation	New York, USA		1.84	15	183
0.3775	Sageman et al. (2003)	Geneseo Formation	New York, USA		1.05	33	258
0.3775	Sageman et al. (2003)	Geneseo Formation	New York, USA		3.96	23	312
0.3775	Sageman et al. (2003)	Geneseo Formation	New York, USA		4.47	7	100
0.3775	Sageman et al. (2003)	Geneseo Formation	New York, USA		5.79	6	133
0.3775	Sageman et al. (2003)	Geneseo Formation	New York, USA		5.59	16	179
0.3775	Sageman et al. (2003)	Geneseo Formation	New York, USA		4.13	9	169
0.3775	Sageman et al. (2003)	Geneseo Formation	New York, USA		2.83	28	269
0.3775	Sageman et al. (2003)	Geneseo Formation	New York, USA		1.87	18	212
0.3775	Sageman et al. (2003)	Geneseo Formation	New York, USA		3.1	22	154
0.3775	Sageman et al. (2003)	Geneseo Formation	New York, USA		2.61	7	155
0.3775	Sageman et al. (2003)	Geneseo Formation	New York, USA		4.82	3	163
0.3775	Sageman et al. (2003)	Geneseo Formation	New York, USA		4.84	4	166
0.3775	Sageman et al. (2003)	Geneseo Formation	New York, USA		4.49	2	150
0.3775	Sageman et al. (2003)	Geneseo Formation	New York, USA		4.26		155
0.3775	Sageman et al. (2003)	Geneseo Formation	New York, USA		1.67		156
0.3775	Sageman et al. (2003)	Geneseo Formation	New York, USA		0.48		167
0.3775	Sageman et al. (2003)	Geneseo Formation	New York, USA		0.54		161
0.3775	Sageman et al. (2003)	Geneseo Formation	New York, USA		0.36		167
0.3775	Sageman et al. (2003)	Geneseo Formation	New York, USA		0.35	1	170
0.3775	Sageman et al. (2003)	Geneseo Formation	New York, USA		0.31		177
0.3775	Sageman et al. (2003)	Geneseo Formation	New York, USA		0.45		150
0.3775	Sageman et al. (2003)	Middlesex Formation	New York, USA				151
0.3775	Sageman et al. (2003)	Middlesex Formation	New York, USA				158
0.3775	Sageman et al. (2003)	Middlesex Formation	New York, USA		0.24		164
0.3775	Sageman et al. (2003)	Middlesex Formation	New York, USA		1.04	1	184
0.3775	Sageman et al. (2003)	Middlesex Formation	New York, USA		2.62	20	297
0.3775	Sageman et al. (2003)	Middlesex Formation	New York, USA			5	178
0.3775	Sageman et al. (2003)	Middlesex Formation	New York, USA		2.26	2	175
0.3775	Sageman et al. (2003)	Middlesex Formation	New York, USA			17	289
0.3775	Sageman et al. (2003)	Middlesex Formation	New York, USA		2.52	19	268
0.3775	Sageman et al. (2003)	Middlesex Formation	New York, USA			13	180
0.3775	Sageman et al. (2003)	Middlesex Formation	New York, USA		3.66	5	149
0.3775	Sageman et al. (2003)	Middlesex Formation	New York, USA			7	124
0.3775	Sageman et al. (2003)	Middlesex Formation	New York, USA		1.63	15	106
0.3775	Sageman et al. (2003)	Middlesex Formation	New York, USA		0.58	0	129
0.3775	Sageman et al. (2003)	Middlesex Formation	New York, USA			1	117
0.3775	Sageman et al. (2003)	Middlesex Formation	New York, USA		0.36		146
0.3775	Sageman et al. (2003)	Middlesex Formation	New York, USA				136
0.3775	Sageman et al. (2003)	Middlesex Formation	New York, USA				133
0.3775	Sageman et al. (2003)	Middlesex Formation	New York, USA				119

Age (Ga)	Reference/Source	Formation	Location	Sample	TOC	Mo	V
0.3775	Sageman et al. (2003)	Rhinestreet Formation	New York, USA		0.2		195
0.3775	Sageman et al. (2003)	Rhinestreet Formation	New York, USA		0.86		165
0.3775	Sageman et al. (2003)	Rhinestreet Formation	New York, USA		2.14	2	166
0.3775	Sageman et al. (2003)	Rhinestreet Formation	New York, USA		2.07		218
0.3775	Sageman et al. (2003)	Rhinestreet Formation	New York, USA		2.83	5	180
0.3775	Sageman et al. (2003)	Rhinestreet Formation	New York, USA		1.32	4	282
0.3775	Sageman et al. (2003)	Rhinestreet Formation	New York, USA		1.56	8	195
0.3775	Sageman et al. (2003)	Rhinestreet Formation	New York, USA		1.58		165
0.3775	Sageman et al. (2003)	Rhinestreet Formation	New York, USA		1.01		166
0.3775	Sageman et al. (2003)	Rhinestreet Formation	New York, USA		2	12	168
0.3775	Sageman et al. (2003)	Rhinestreet Formation	New York, USA		1.38	30	179
0.3775	Sageman et al. (2003)	Rhinestreet Formation	New York, USA		1.35	15	196
0.3775	Sageman et al. (2003)	Rhinestreet Formation	New York, USA		0.47		175
0.3775	Sageman et al. (2003)	Rhinestreet Formation	New York, USA		1.79	2	191
0.3775	Sageman et al. (2003)	Rhinestreet Formation	New York, USA		0.62		138
0.3775	Sageman et al. (2003)	Rhinestreet Formation	New York, USA		0.93		158
0.3775	Sageman et al. (2003)	Rhinestreet Formation	New York, USA		0.93	1	204
0.3775	Sageman et al. (2003)	Rhinestreet Formation	New York, USA		0.86	2	202
0.3775	Sageman et al. (2003)	Rhinestreet Formation	New York, USA		2.69	9	289
0.3775	Sageman et al. (2003)	Rhinestreet Formation	New York, USA		3.04	24	226
0.3775	Sageman et al. (2003)	Rhinestreet Formation	New York, USA		2.33	1	147
0.3775	Sageman et al. (2003)	Rhinestreet Formation	New York, USA		0.52		133
0.3775	Sageman et al. (2003)	Rhinestreet Formation	New York, USA		0.35		119
0.3775	Sageman et al. (2003)	Rhinestreet Formation	New York, USA		0.4733		127
0.3775	Sageman et al. (2003)	Rhinestreet Formation	New York, USA		0.3495		138
0.3775	Sageman et al. (2003)	Pipe Creek and Hanover Formations	New York, USA		0.56	6	155
0.3775	Sageman et al. (2003)	Pipe Creek and Hanover Formations	New York, USA		2.24	37	110
0.3775	Sageman et al. (2003)	Pipe Creek and Hanover Formations	New York, USA		3.06	30	118
0.3775	Sageman et al. (2003)	Pipe Creek and Hanover Formations	New York, USA		2.63	36	110
0.3775	Sageman et al. (2003)	Pipe Creek and Hanover Formations	New York, USA		2.23	25	128
0.3775	Sageman et al. (2003)	Pipe Creek and Hanover Formations	New York, USA		0.61		147
0.3775	Sageman et al. (2003)	Pipe Creek and Hanover Formations	New York, USA		0.56		150
0.3775	Sageman et al. (2003)	Pipe Creek and Hanover Formations	New York, USA		0.31		138
0.3775	Sageman et al. (2003)	Pipe Creek and Hanover Formations	New York, USA		0.96	6	110
0.3775	Sageman et al. (2003)	Pipe Creek and Hanover Formations	New York, USA		0.25		156
0.3775	Sageman et al. (2003)	Pipe Creek and Hanover Formations	New York, USA		0.58		161
0.3775	Sageman et al. (2003)	Pipe Creek and Hanover Formations	New York, USA		0.26		106
0.3775	Sageman et al. (2003)	Pipe Creek and Hanover Formations	New York, USA		0.22		115
0.3775	Sageman et al. (2003)	Pipe Creek and Hanover Formations	New York, USA		3.22	5	115
0.3775	Sageman et al. (2003)	Pipe Creek and Hanover Formations	New York, USA		2.55	3	103
0.3775	Sageman et al. (2003)	Pipe Creek and Hanover Formations	New York, USA		3.65	9	114
0.3775	Sageman et al. (2003)	Pipe Creek and Hanover Formations	New York, USA		3	3	150
0.3775	Sageman et al. (2003)	Pipe Creek and Hanover Formations	New York, USA		2.63	13	128
0.3775	Sageman et al. (2003)	Pipe Creek and Hanover Formations	New York, USA		3.25	8	117

Age (Ga)	Reference/Source	Formation	Location	Sample	TOC	Mo	V
0.3775	Sageman et al. (2003)	Pipe Creek and Hanover Formations	New York, USA		2.94	18	119
0.3775	Sageman et al. (2003)	Pipe Creek and Hanover Formations	New York, USA		2.56	29	126
0.3775	Sageman et al. (2003)	Pipe Creek and Hanover Formations	New York, USA		1.86	24	132
0.3775	Sageman et al. (2003)	Pipe Creek and Hanover Formations	New York, USA		0.13		88
0.3775	Sageman et al. (2003)	Pipe Creek and Hanover Formations	New York, USA		0.14		186
0.3775	Sageman et al. (2003)	Pipe Creek and Hanover Formations	New York, USA		0.37		105
0.3775	Sageman et al. (2003)	Pipe Creek and Hanover Formations	New York, USA		0.06		83
0.3775	Sageman et al. (2003)	Pipe Creek and Hanover Formations	New York, USA		0.1		128
0.3775	Sageman et al. (2003)	Pipe Creek and Hanover Formations	New York, USA		0.47		96
0.3775	Sageman et al. (2003)	Pipe Creek and Hanover Formations	New York, USA		1.86	16	113
0.3775	Sageman et al. (2003)	Pipe Creek and Hanover Formations	New York, USA		0.5		121
0.3775	Sageman et al. (2003)	Pipe Creek and Hanover Formations	New York, USA		0.63		122
0.3775	Sageman et al. (2003)	Pipe Creek and Hanover Formations	New York, USA		0.22		123
0.3775	Sageman et al. (2003)	Pipe Creek and Hanover Formations	New York, USA		0.43	2	140
0.3775	Sageman et al. (2003)	Pipe Creek and Hanover Formations	New York, USA		1.86		128
0.3775	Sageman et al. (2003)	Pipe Creek and Hanover Formations	New York, USA		0.49		146
0.3775	Sageman et al. (2003)	Pipe Creek and Hanover Formations	New York, USA		4.16	3	118
0.3775	Sageman et al. (2003)	Pipe Creek and Hanover Formations	New York, USA		3.61	5	122
0.3775	Sageman et al. (2003)	Pipe Creek and Hanover Formations	New York, USA		3.35	2	121
0.3775	Sageman et al. (2003)	Pipe Creek and Hanover Formations	New York, USA		4.41	1	109
0.3775	Sageman et al. (2003)	Pipe Creek and Hanover Formations	New York, USA		5.4		120
0.3775	Sageman et al. (2003)	Pipe Creek and Hanover Formations	New York, USA		3.96	2	125
0.3775	Sageman et al. (2003)	Pipe Creek and Hanover Formations	New York, USA		4.01	2	119
0.3775	Sageman et al. (2003)	Pipe Creek and Hanover Formations	New York, USA		0.44		55
0.3775	Sageman et al. (2003)	Pipe Creek and Hanover Formations	New York, USA		2.29		136
0.3775	Sageman et al. (2003)	Pipe Creek and Hanover Formations	New York, USA		2.6	15	143
0.3775	Sageman et al. (2003)	Pipe Creek and Hanover Formations	New York, USA		0.78		74
0.3775	Sageman et al. (2003)	Pipe Creek and Hanover Formations	New York, USA		0.49		191

Age (Ga)	Reference/Source	Formation	Location	Sample	TOC	Mo	V
0.309	Hatch and Leventhal (1997)	Excello Shale Member	Marion Co, Iowa	CP41-1 *	4		1690
0.309	Hatch and Leventhal (1997)	Oakley Shale Member	Marion Co, Iowa	CP41-17	24.8		1790
0.309	Hatch and Leventhal (1997)	Excello Shale Member	Monroe Co, Iowa	CP53-4A *	1.4		218
0.309	Hatch and Leventhal (1997)	Excello Shale Member	Monroe Co, Iowa	CP53-4B *	3.8		2230
0.309	Hatch and Leventhal (1997)	Anna Shale Member	Appanoose Co, Iowa	CP22-6D	16.4		465
0.309	Hatch and Leventhal (1997)	Little Osage Shale Member	Appanoose Co, Iowa	CP22-11	18.7		1180
0.309	Hatch and Leventhal (1997)	Excello Shale Member	Appanoose Co, Iowa	CP22-14 *	4.3		1390
0.309	Hatch and Leventhal (1997)	Oakley Shale Member	Appanoose Co, Iowa	CP22-22C	4.8		460
0.309	Hatch and Leventhal (1997)	Oakley Shale Member	Appanoose Co, Iowa	CP22-22E	25.1		2330
0.309	Hatch and Leventhal (1997)	Little Osage Shale Member	Wayne Co, Iowa	CP78-4A	18.7		670
0.309	Hatch and Leventhal (1997)	Little Osage Shale Member	Wayne Co, Iowa	CP78-4B	27.6		1020
0.309	Hatch and Leventhal (1997)	Excello Shale Member	Wayne Co, Iowa	CP78-13A *	3.6		
0.309	Hatch and Leventhal (1997)	Excello Shale Member	Wayne Co, Iowa	CP78-13B*	6.5		620
0.309	Hatch and Leventhal (1997)	Excello Shale Member	Wayne Co, Iowa	CP78-13C*	5.6		
0.309	Hatch and Leventhal (1997)	Anna Shale Member	Putnam Co, Missouri	ANNA	26.3		690
0.309	Hatch and Leventhal (1997)	Excello Shale Member	Randolph Co, Missouri	BM5-2	13.9		350
0.309	Hatch and Leventhal (1997)	Unnamed Shale Member	Randolph Co, Missouri	BM2-5	21.2		690
0.309	Hatch and Leventhal (1997)	Excello Shale Member	Randolph Co, Missouri	SS-1	13.7		500
0.309	Hatch and Leventhal (1997)	Excello Shale Member	Randolph Co, Missouri	SS-9 *	0.4		
0.309	Hatch and Leventhal (1997)	Excello Shale Member	Randolph Co, Missouri	SS-10 *	1.5		300
0.309	Hatch and Leventhal (1997)	Excello Shale Member	Randolph Co, Missouri	SS- 11	16		1500
0.309	Hatch and Leventhal (1997)	Little Osage Shale Member	Chariton Co, Missouri	BM14-2	23.1		800
0.309	Hatch and Leventhal (1997)	Little Osage Shale Member	Chariton Co, Missouri	BM14-3	15		140
0.309	Hatch and Leventhal (1997)	Little Osage Shale Member	Johnson Co, Missouri	MC 105-2 *	9.6		1700
0.309	Hatch and Leventhal (1997)	Excello Shale Member	Johnson Co, Missouri	MC105-6 *	3.8		500
0.309	Hatch and Leventhal (1997)	Excello Shale Member	Johnson Co, Missouri	MC86-2 *	9.2		640
0.309	Hatch and Leventhal (1997)	Anna Shale Member	Bates Co, Missouri	MC121-2	19.7		520
0.309	Hatch and Leventhal (1997)	Anna Shale Member	Bates Co, Missouri	MC 121-3	9.9		100
0.309	Hatch and Leventhal (1997)	Excello Shale Member	Leavenworth Co, Kansa	EDS1A-9 *	1.1		370
0.309	Hatch and Leventhal (1997)	Excello Shale Member	Leavenworth Co, Kansa	EDS1A-8 *	0.9		530
0.309	Hatch and Leventhal (1997)	Excello Shale Member	Leavenworth Co, Kansa	EDS1A-7 *	2.4		530
0.309	Hatch and Leventhal (1997)	Excello Shale Member	Leavenworth Co, Kansa	EDS 1A-6 *	1.6		370
0.309	Hatch and Leventhal (1997)	Excello Shale Member	Leavenworth Co, Kansa	EDS 1A-5 *	3.1		800
0.309	Hatch and Leventhal (1997)	Excello Shale Member	Greenwood Co, Kansas	871-12	18.9		
0.309	Hatch and Leventhal (1997)	Excello Shale Member	Greenwood Co, Kansas	349-3	21.6		
0.309	Hatch and Leventhal (1997)	Unnamed Shale Member	Greenwood Co, Kansas	349-46	14.9		
0.309	Hatch and Leventhal (1997)	Anna Shale Member	Craig Co, Oklahoma	1535u-5	9.5		266
0.309	Hatch and Leventhal (1997)	Little Osage Shale Member	Craig Co, Oklahoma	1535u-25	11		508
0.309	Hatch and Leventhal (1997)	Excello Shale Member	Craig Co, Oklahoma	1535-7	14.8		865
0.309	Hatch and Leventhal (1997)	Unnamed Shale Member	Craig Co, Oklahoma	1535-23	7.2		202
0.309	Hatch and Leventhal (1997)	Unnamed Shale Member	Craig Co, Oklahoma	1535-25	14.6		344
0.309	Hatch and Leventhal (1997)	Excello Shale Member	Osage Co, Oklahoma	1044-32	9.9		449
0.309	Hatch and Leventhal (1997)	Unnamed Shale Member	Osage Co, Oklahoma	1044-46	5.5		147
0.309	Hatch and Leventhal (1997)	Unnamed Shale Member	Osage Co, Oklahoma	1044-47	15.2		333

Age (Ga)	Reference/Source	Formation	Location	Sample	TOC	Mo	V
0.305	Cruse and Lyons (2004)	Hushpuckney Shale Member, Coffeyville Formation	Oklahoma, USA	289.3-14GR	0.81		132
0.305	Cruse and Lyons (2004)	Hushpuckney Shale Member, Coffeyville Formation	Oklahoma, USA	289.3-10GR	0.91		148
0.305	Cruse and Lyons (2004)	Hushpuckney Shale Member, Coffeyville Formation	Oklahoma, USA	289.3-9GR	0.9		154
0.305	Cruse and Lyons (2004)	Hushpuckney Shale Member, Coffeyville Formation	Oklahoma, USA	289.3-8GR	0.88		140
0.305	Cruse and Lyons (2004)	Hushpuckney Shale Member, Coffeyville Formation	Oklahoma, USA	289.3-7GR	0.98		152
0.305	Cruse and Lyons (2004)	Hushpuckney Shale Member, Coffeyville Formation	Oklahoma, USA	289.3-6GR	0.94		159
0.305	Cruse and Lyons (2004)	Hushpuckney Shale Member, Coffeyville Formation	Oklahoma, USA	289.3-5GR	0.94		156
0.305	Cruse and Lyons (2004)	Hushpuckney Shale Member, Coffeyville Formation	Oklahoma, USA	289.3-4GR	1.03	25	154
0.305	Cruse and Lyons (2004)	Hushpuckney Shale Member, Coffeyville Formation	Oklahoma, USA	298.3-3GR	1.16	32	145
0.305	Cruse and Lyons (2004)	Hushpuckney Shale Member, Coffeyville Formation	Oklahoma, USA	289.3-2GR	1.16	14	174
0.305	Cruse and Lyons (2004)	Hushpuckney Shale Member, Coffeyville Formation	Oklahoma, USA	289.3-1GR	1.76	9	223
0.305	Cruse and Lyons (2004)	Hushpuckney Shale Member, Coffeyville Formation	Oklahoma, USA	289.3-1B	6.65	6	398
0.305	Cruse and Lyons (2004)	Hushpuckney Shale Member, Coffeyville Formation	Oklahoma, USA	289.3-2B	10.28	13	588
0.305	Cruse and Lyons (2004)	Hushpuckney Shale Member, Coffeyville Formation	Oklahoma, USA	289.3-3B	10.39	16	663
0.305	Cruse and Lyons (2004)	Hushpuckney Shale Member, Coffeyville Formation	Oklahoma, USA	289.3-4B	9.35	34	449
0.305	Cruse and Lyons (2004)	Hushpuckney Shale Member, Coffeyville Formation	Oklahoma, USA	289.3-5B	11.95		752
0.305	Cruse and Lyons (2004)	Hushpuckney Shale Member, Coffeyville Formation	Oklahoma, USA	289.3-6B	11.7		728
0.305	Cruse and Lyons (2004)	Hushpuckney Shale Member, Coffeyville Formation	Oklahoma, USA	289.3-7B	12.25	15	719
0.305	Cruse and Lyons (2004)	Hushpuckney Shale Member, Coffeyville Formation	Oklahoma, USA	289.3-8B	10.04		649
0.305	Cruse and Lyons (2004)	Hushpuckney Shale Member, Coffeyville Formation	Oklahoma, USA	289.3-9B	10.68	31	700
0.305	Cruse and Lyons (2004)	Hushpuckney Shale Member, Coffeyville Formation	Oklahoma, USA	289.3-12B	13.71		767
0.305	Cruse and Lyons (2004)	Hushpuckney Shale Member, Coffeyville Formation	Oklahoma, USA	289.3-13B	7.42	80	834
0.305	Cruse and Lyons (2004)	Hushpuckney Shale Member, Coffeyville Formation	Oklahoma, USA	289.3-15B	8.95	33	1.05
0.305	Cruse and Lyons (2004)	Hushpuckney Shale Member, Coffeyville Formation	Oklahoma, USA	294.0-19B	9.43	142	1.9
0.305	Cruse and Lyons (2004)	Hushpuckney Shale Member, Coffeyville Formation	Oklahoma, USA	294.0-17B	10.45		990
0.305	Cruse and Lyons (2004)	Hushpuckney Shale Member, Coffeyville Formation	Oklahoma, USA	294.0-16B	5.92		602
0.305	Cruse and Lyons (2004)	Hushpuckney Shale Member, Coffeyville Formation	Oklahoma, USA	294.0-15B	5.18		248
0.305	Cruse and Lyons (2004)	Hushpuckney Shale Member, Coffeyville Formation	Oklahoma, USA	294.0-14B		10	239
0.305	Cruse and Lyons (2004)	Hushpuckney Shale Member, Coffeyville Formation	Oklahoma, USA	294.0-13B	4.64		207
0.305	Cruse and Lyons (2004)	Hushpuckney Shale Member, Coffeyville Formation	Oklahoma, USA	294.0-12B	6.17		190
0.305	Cruse and Lyons (2004)	Hushpuckney Shale Member, Coffeyville Formation	Oklahoma, USA	294.0-9B	5.43		246
0.305	Cruse and Lyons (2004)	Hushpuckney Shale Member, Coffeyville Formation	Oklahoma, USA	294.0-1GT	6.08		274
0.305	Cruse and Lyons (2004)	Hushpuckney Shale Member, Coffeyville Formation	Oklahoma, USA	294.0-2GT	5.51	51	270
0.305	Cruse and Lyons (2004)	Hushpuckney Shale Member, Coffeyville Formation	Oklahoma, USA	294.0-3GT	4.77		220
0.305	Cruse and Lyons (2004)	Hushpuckney Shale Member, Coffeyville Formation	Oklahoma, USA	294.0-4GT	3	14	191
0.305	Cruse and Lyons (2004)	Hushpuckney Shale Member, Coffeyville Formation	Oklahoma, USA	294.0-5GT	1.97		154
0.305	Cruse and Lyons (2004)	Hushpuckney Shale Member, Coffeyville Formation	Oklahoma, USA	294.0-6GT	1.96	7	131
0.305	Cruse and Lyons (2004)	Hushpuckney Shale Member, Coffeyville Formation	Oklahoma, USA	294.0-7GT	2.2	5	126
0.305	Cruse and Lyons (2004)	Hushpuckney Shale Member, Coffeyville Formation	Oklahoma, USA	294.0-8GT	2.3	5	134
0.305	Cruse and Lyons (2004)	Hushpuckney Shale Member, Coffeyville Formation	Oklahoma, USA	294.0-9GT	2.37	3	110
0.305	Cruse and Lyons (2004)	Hushpuckney Shale Member, Coffeyville Formation	Oklahoma, USA	294.0-10GT	2.65	4	103
0.305	Cruse and Lyons (2004)	Hushpuckney Shale Member, Coffeyville Formation	Oklahoma, USA	294.0-11GT	2.97	2	118
0.305	Cruse and Lyons (2004)	Hushpuckney Shale Member, Coffeyville Formation	Oklahoma, USA	294.0-12GT	2.02	2	106
0.305	Cruse and Lyons (2004)	Hushpuckney Shale Member, Coffeyville Formation	Oklahoma, USA	294.0-13GT			117
0.305	Cruse and Lyons (2004)	Hushpuckney Shale Member, Coffeyville Formation	Oklahoma, USA	294.0-14GT			121
0.305	Cruse and Lyons (2004)	Hushpuckney Shale Member, Coffeyville Formation	Oklahoma, USA	294.0-15GT		9	133

Age (Ga)	Reference/Source	Formation	Location	Sample	TOC	Mo	V
0.305	Cruse and Lyons (2004)	Hushpuckney Shale Member, Coffeyville Formation	Iowa, USA	1036.7-6GR		47	67
0.305	Cruse and Lyons (2004)	Hushpuckney Shale Member, Coffeyville Formation	Iowa, USA	1036.7-5GR			120
0.305	Cruse and Lyons (2004)	Hushpuckney Shale Member, Coffeyville Formation	Iowa, USA	1036.7-4GR			125
0.305	Cruse and Lyons (2004)	Hushpuckney Shale Member, Coffeyville Formation	Iowa, USA	1036.7-3GR		58	127
0.305	Cruse and Lyons (2004)	Hushpuckney Shale Member, Coffeyville Formation	Iowa, USA	1036.7-2GR		39	133
0.305	Cruse and Lyons (2004)	Hushpuckney Shale Member, Coffeyville Formation	Iowa, USA	1036.7-1GR			190
0.305	Cruse and Lyons (2004)	Hushpuckney Shale Member, Coffeyville Formation	Iowa, USA	1036.7-1BR		52	345
0.305	Cruse and Lyons (2004)	Hushpuckney Shale Member, Coffeyville Formation	Iowa, USA	1036.7-2BR		71	619
0.305	Cruse and Lyons (2004)	Hushpuckney Shale Member, Coffeyville Formation	Iowa, USA	1036.7-3BR			407
0.305	Cruse and Lyons (2004)	Hushpuckney Shale Member, Coffeyville Formation	Iowa, USA	1036.7-4BR		90	864
0.305	Cruse and Lyons (2004)	Hushpuckney Shale Member, Coffeyville Formation	Iowa, USA	1036.7-5BR			1796
0.305	Cruse and Lyons (2004)	Hushpuckney Shale Member, Coffeyville Formation	Iowa, USA	1036.7-6BR			2.53
0.305	Cruse and Lyons (2004)	Hushpuckney Shale Member, Coffeyville Formation	Iowa, USA	1036.7-7BR		372	2.91
0.305	Cruse and Lyons (2004)	Hushpuckney Shale Member, Coffeyville Formation	Iowa, USA	1036.7-8BR			2.04
0.305	Cruse and Lyons (2004)	Hushpuckney Shale Member, Coffeyville Formation	Iowa, USA	1036.7-9BR		306	2.45
0.305	Cruse and Lyons (2004)	Hushpuckney Shale Member, Coffeyville Formation	Iowa, USA	1039.2-10BT			589
0.305	Cruse and Lyons (2004)	Hushpuckney Shale Member, Coffeyville Formation	Iowa, USA	1039.2-9BT			1
0.305	Cruse and Lyons (2004)	Hushpuckney Shale Member, Coffeyville Formation	Iowa, USA	1039.2-8BT			1.68
0.305	Cruse and Lyons (2004)	Hushpuckney Shale Member, Coffeyville Formation	Iowa, USA	1039.2-7BT		206	1.42
0.305	Cruse and Lyons (2004)	Hushpuckney Shale Member, Coffeyville Formation	Iowa, USA	1039.2-6BT			2.22
0.305	Cruse and Lyons (2004)	Hushpuckney Shale Member, Coffeyville Formation	Iowa, USA	1039.2-5BT			2.17
0.305	Cruse and Lyons (2004)	Hushpuckney Shale Member, Coffeyville Formation	Iowa, USA	1039.2-4BT		428	2.75
0.305	Cruse and Lyons (2004)	Hushpuckney Shale Member, Coffeyville Formation	Iowa, USA	1039.2-3BT			2.7
0.305	Cruse and Lyons (2004)	Hushpuckney Shale Member, Coffeyville Formation	Iowa, USA	1039.2-2BT		364	2.35
0.305	Cruse and Lyons (2004)	Hushpuckney Shale Member, Coffeyville Formation	Iowa, USA	1039.2-1BT			759
0.305	Cruse and Lyons (2004)	Hushpuckney Shale Member, Coffeyville Formation	Iowa, USA	1039.2-1GT			91
0.305	Cruse and Lyons (2004)	Hushpuckney Shale Member, Coffeyville Formation	Iowa, USA	1039.2-2GT			24
0.305	Cruse and Lyons (2004)	Hushpuckney Shale Member, Coffeyville Formation	Iowa, USA	1039.2-3GT			5
0.305	Cruse and Lyons (2004)	Hushpuckney Shale Member, Coffeyville Formation	Iowa, USA	1039.2-4GT			10

Age (Ga)	Reference/Source	Formation	Location	Sample	TOC	Mo	V
0.305	Hatch and Leventhal (1992)	Stark Shale Member, Dennis Limestone	Wabaunsee County, Ka	S-1	21.7	320	2600
0.305	Hatch and Leventhal (1992)	Stark Shale Member, Dennis Limestone	Wabaunsee County, Ka	*S-2-2*	24.4	29	3500
0.305	Hatch and Leventhal (1992)	Stark Shale Member, Dennis Limestone	Wabaunsee County, Ka	*S-2-1*	29.5	25	3900
0.305	Hatch and Leventhal (1992)	Stark Shale Member, Dennis Limestone	Wabaunsee County, Ka	*S-3-2*	2.1	67	200
0.305	Hatch and Leventhal (1992)	Stark Shale Member, Dennis Limestone	Wabaunsee County, Ka	*S-3-1*	2.4	150	190
0.305	Hatch and Leventhal (1992)	Stark Shale Member, Dennis Limestone	Wabaunsee County, Ka	*S-4-3*	7.5	93	760
0.305	Hatch and Leventhal (1992)	Stark Shale Member, Dennis Limestone	Wabaunsee County, Ka	*S-4-2*	10.8	15	1200
0.305	Hatch and Leventhal (1992)	Stark Shale Member, Dennis Limestone	Wabaunsee County, Ka	*S-4-I*	21.4	67	3600
0.305	Hatch and Leventhal (1992)	Stark Shale Member, Dennis Limestone	Wabaunsee County, Ka	S-5	14.4	91	620
0.305	Hatch and Leventhal (1992)	Stark Shale Member, Dennis Limestone	Wabaunsee County, Ka	*S-6-2*	19.2	30	3200
0.305	Hatch and Leventhal (1992)	Stark Shale Member, Dennis Limestone	Wabaunsee County, Ka	*S-6-1*	11.7	6	2000
0.305	Hatch and Leventhal (1992)	Stark Shale Member, Dennis Limestone	Wabaunsee County, Ka	S- 7	2.2	180	110
0.305	Hatch and Leventhal (1992)	Stark Shale Member, Dennis Limestone	Wabaunsee County, Ka	*S-8-2*	17.9	170	370
0.305	Hatch and Leventhal (1992)	Stark Shale Member, Dennis Limestone	Wabaunsee County, Ka	*S-8-1*	23.4	440	490
0.305	Hatch and Leventhal (1992)	Stark Shale Member, Dennis Limestone	Wabaunsee County, Ka	*S-9-2*	0.5	520	42
0.305	Hatch and Leventhal (1992)	Stark Shale Member, Dennis Limestone	Wabaunsee County, Ka	*S-9-1*	0.9	670	64
0.305	Hatch and Leventhal (1992)	Stark Shale Member, Dennis Limestone	Wabaunsee County, Ka	*S-10*	17.9	760	1600
0.305	Hatch and Leventhal (1992)	Stark Shale Member, Dennis Limestone	Wabaunsee County, Ka	*S-11*	13.5	820	1100
0.305	Hatch and Leventhal (1992)	Stark Shale Member, Dennis Limestone	Wabaunsee County, Ka	*S-12-2*	12	850	2300
0.305	Hatch and Leventhal (1992)	Stark Shale Member, Dennis Limestone	Wabaunsee County, Ka	*S-12-1*	23.6	630	3500
0.305	Hatch and Leventhal (1992)	Stark Shale Member, Dennis Limestone	Wabaunsee County, Ka	*S-13*	1.6	13	150
0.247	Pasava et al. (2010)	Kupferschiefer Shales	Northern Zechstein Bas	13a	6.31	30	200
0.247	Pasava et al. (2010)	Kupferschiefer Shales	Northern Zechstein Bas	12b	1.52	20	130
0.247	Pasava et al. (2010)	Kupferschiefer Shales	Northern Zechstein Bas	11a	2.4	60	200
0.247	Pasava et al. (2010)	Kupferschiefer Shales	Northern Zechstein Bas	9b	4.94	110	360
0.247	Pasava et al. (2010)	Kupferschiefer Shales	Northern Zechstein Bas	5a	9.41	260	380
0.247	Pasava et al. (2010)	Kupferschiefer Shales	Northern Zechstein Bas	3b	10.32	340	520
0.08105	Hirner and Xu (1991)	Julia Creek Oil Shale, Toolebuc Formation	Queensland, Australia	bulk			1650
0.08105	Hirner and Xu (1991)	Julia Creek Oil Shale, Toolebuc Formation	Queensland, Australia	bulk			2000
0.08105	Hirner and Xu (1991)	Julia Creek Oil Shale, Toolebuc Formation	Queensland, Australia	bulk			
0.08105	Hirner and Xu (1991)	Julia Creek Oil Shale, Toolebuc Formation	Queensland, Australia	bulk		175	1690
0.08105	Hirner and Xu (1991)	Julia Creek Oil Shale, Toolebuc Formation	Queensland, Australia	chloroform extract		270	104
0.08105	Hirner and Xu (1991)	Julia Creek Oil Shale, Toolebuc Formation	Queensland, Australia	Dichloromethane extract		295	4210
0.08105	Hirner and Xu (1991)	Julia Creek Oil Shale, Toolebuc Formation	Queensland, Australia	Humic+culvic acids		221	2079
0.08105	Hirner and Xu (1991)	Julia Creek Oil Shale, Toolebuc Formation	Queensland, Australia	HCl/HF demin			1677
0.08105	Hirner and Xu (1991)	Julia Creek Oil Shale, Toolebuc Formation	Queensland, Australia	HCl/HF demin			1580
0.08105	Hirner and Xu (1991)	Julia Creek Oil Shale, Toolebuc Formation	Queensland, Australia	Kiba demin			105

Age (Ga)	Reference/Source	Formation	Location	Sample	TOC	Mo	V
0.0004535	Gehrke et al. (2009)	Sapropel sediments	Tyrrhenian Basin, w est	974C 6H5 core	4.09	38.5	
0.0004535	Gehrke et al. (2009)	Sapropel sediments	Tyrrhenian Basin, w est	974C 6H5 core	4.27	48.8	
0.0004535	Gehrke et al. (2009)	Sapropel sediments	Tyrrhenian Basin, w est	974C 6H5 core	4.52	37.3	
0.0004535	Gehrke et al. (2009)	Sapropel sediments	Tyrrhenian Basin, w est	974C 6H5 core	4.28	84	
0.0004535	Gehrke et al. (2009)	Sapropel sediments	Tyrrhenian Basin, w est	974C 6H5 core	0.22	5.56	
0.0004535	Gehrke et al. (2009)	Sapropel sediments	Tyrrhenian Basin, w est	974C 6H5 core	0.24	3.32	
0.0004535	Gehrke et al. (2009)	Sapropel sediments	Tyrrhenian Basin, w est	974C 6H5 core	0.2	6.06	
0.0004535	Gehrke et al. (2009)	Sapropel sediments	Tyrrhenian Basin, w est	974C 6H5 core	0.27	4.87	
0.0004535	Gehrke et al. (2009)	Sapropel sediments	Tyrrhenian Basin, w est	974C 6H5 core	0.24	5.94	
0.0004535	Gehrke et al. (2009)	Sapropel sediments	Tyrrhenian Basin, w est	974C 6H5 core	0.95	5.92	
0.0004535	Gehrke et al. (2009)	Sapropel sediments	Tyrrhenian Basin, w est	974C 6H5 core	1.23	9.27	
0.0004535	Gehrke et al. (2009)	Sapropel sediments	Tyrrhenian Basin, w est	974C 6H5 core	1.16	4.34	
0.0004535	Gehrke et al. (2009)	Sapropel sediments	Tyrrhenian Basin, w est	974C 6H5 core	1.38	2.72	
0.0004535	Gehrke et al. (2009)	Sapropel sediments	Tyrrhenian Basin, w est	974C 6H5 core	1.44	2.73	
0.0004535	Gehrke et al. (2009)	Sapropel sediments	Tyrrhenian Basin, w est	974C 6H5 core	1.22	2.31	
0.0004535	Gehrke et al. (2009)	Sapropel sediments	Tyrrhenian Basin, w est	974C 6H5 core	0.27	0.5	
0.0004535	Gehrke et al. (2009)	Sapropel sediments	Tyrrhenian Basin, w est	974C 6H5 core	0.29	0.63	
0.0004535	Gehrke et al. (2009)	Sapropel sediments	Tyrrhenian Basin, w est	974C 6H5 core	0.29	0.33	
0.0004535	Gehrke et al. (2009)	Sapropel sediments	Tyrrhenian Basin, w est	974C 6H5 core	0.23	0.53	
0.0004535	Gehrke et al. (2009)	Sapropel sediments	Tyrrhenian Basin, w est	974C 6H5 core	0.26	1.54	
3.4	McLennan et al. (1983)	George Creek Group, Pilgangoora Area	Western Australia	Pg1			154
3.4	McLennan et al. (1983)	George Creek Group, Pilgangoora Area	Western Australia	Pg2			125
3.4	McLennan et al. (1983)	George Creek Group, Pilgangoora Area	Western Australia	Pg3			153
3.4	McLennan et al. (1983)	George Creek Group, Pilgangoora Area	Western Australia	Pg4			168
3.4	McLennan et al. (1983)	George Creek Group, Pilgangoora Area	Western Australia	Pg5			167
3.4	McLennan et al. (1983)	George Creek Group, Pilgangoora Area	Western Australia	Pg6			169
3.4	McLennan et al. (1983)	George Creek Group, Pilgangoora Area	Western Australia	Pg7			128
3.4	McLennan et al. (1983)	Geogre Creek Group, Mullagine Area	Western Australia	MC			294
3.4	McLennan et al. (1983)	Geogre Creek Group, Mullagine Area	Western Australia	80-05			95
3.4	McLennan et al. (1983)	Geogre Creek Group, Mullagine Area	Western Australia	80-06			224
2.7	McLennan et al. (1983)	Whim Creek Group	Western Australia	WC1			209
2.7	McLennan et al. (1983)	Whim Creek Group	Western Australia	WC3			118
2.9	Laskow ski and Kroner (1985)	Nsuze Group, Pongola Supergroup	Pongola Supergroup, S.	WR			179
2.9	Laskow ski and Kroner (1985)	Mozaan Group, Pongola Supergroup	Pongola Supergroup, S.	WR			166
2.9	Laskow ski and Kroner (1985)	Mozaan Group, Pongola Supergroup	Pongola Supergroup, S.	CMF			159
0.625	Laskow ski and Kroner (1985)	Kuibis+Schw arzrand Subgroups, Nama Group	Nama Group, Namibia	WR			129
0.625	Laskow ski and Kroner (1985)	Kuibis+Schw arzrand Subgroups, Nama Group	Nama Group, Namibia	CMF			136
0.625	Laskow ski and Kroner (1985)	Schw arzrand+Fish River Subgroups, Nama Group	Nama Group, Namibia	WR			94
0.625	Laskow ski and Kroner (1985)	Schw arzrand+Fish River Subgroups, Nama Group	Nama Group, Namibia	CMF			127

Age (Ga)	Reference/Source	Formation	Location	Sample	TOC	Mo	V
3	Fedo et al. (1996)	Buhwa Greenstone Belt	Zimbabwe	ZB 2			112
3	Fedo et al. (1996)	Buhwa Greenstone Belt	Zimbabwe	ZB 6			96
3	Fedo et al. (1996)	Buhwa Greenstone Belt	Zimbabwe	ZB 12A			248
3	Fedo et al. (1996)	Buhwa Greenstone Belt	Zimbabwe	ZB 12B			298
3	Fedo et al. (1996)	Buhwa Greenstone Belt	Zimbabwe	ZB 14			255
3	Fedo et al. (1996)	Buhwa Greenstone Belt	Zimbabwe	ZB 21			40
3	Fedo et al. (1996)	Buhwa Greenstone Belt	Zimbabwe	ZB 42			155
3	Fedo et al. (1996)	Buhwa Greenstone Belt	Zimbabwe	ZB 121			138
3	Fedo et al. (1996)	Buhwa Greenstone Belt	Zimbabwe	ZB 146			56
3	Fedo et al. (1996)	Buhwa Greenstone Belt	Zimbabwe	ZB 195			35
3	Fedo et al. (1996)	Buhwa Greenstone Belt	Zimbabwe	ZB 208			136
3	Fedo et al. (1996)	Buhwa Greenstone Belt	Zimbabwe	ZB 212			113
3	Fedo et al. (1996)	Buhwa Greenstone Belt	Zimbabwe	ZB 218			119
3	Fedo et al. (1996)	Buhwa Greenstone Belt	Zimbabwe	ZB 220			117
3	Fedo et al. (1996)	Buhwa Greenstone Belt	Zimbabwe	ZB 222			144
3	Fedo et al. (1996)	Buhwa Greenstone Belt	Zimbabwe	ZB 223			132
3	Fedo et al. (1996)	Buhwa Greenstone Belt	Zimbabwe	ZB224			120
3	Fedo et al. (1996)	Buhwa Greenstone Belt	Zimbabwe	ZB 226			130
3	Fedo et al. (1996)	Buhwa Greenstone Belt	Zimbabwe	ZB 229			90
3	Fedo et al. (1996)	Buhwa Greenstone Belt	Zimbabwe	ZB 234			142
3.07	Nesbitt et al. (2009)	North Spirit Lake Greenstone Belt	Northwest Ontario, Can	1-7			171
3.07	Nesbitt et al. (2009)	North Spirit Lake Greenstone Belt	Northwest Ontario, Can	1-8			96
3.07	Nesbitt et al. (2009)	North Spirit Lake Greenstone Belt	Northwest Ontario, Can	2-15			26
2.85	Nesbitt et al. (2009)	North Spirit Lake Greenstone Belt	Northwest Ontario, Can	3-1			143
2.85	Nesbitt et al. (2009)	North Spirit Lake Greenstone Belt	Northwest Ontario, Can	3-2			76
2.85	Nesbitt et al. (2009)	North Spirit Lake Greenstone Belt	Northwest Ontario, Can	3-3			50
2.85	Nesbitt et al. (2009)	North Spirit Lake Greenstone Belt	Northwest Ontario, Can	3-4			57
2.85	Nesbitt et al. (2009)	North Spirit Lake Greenstone Belt	Northwest Ontario, Can	3-5			169
2.85	Nesbitt et al. (2009)	North Spirit Lake Greenstone Belt	Northwest Ontario, Can	3-8			66
2.85	Nesbitt et al. (2009)	North Spirit Lake Greenstone Belt	Northwest Ontario, Can	3-9			155
2.85	Nesbitt et al. (2009)	North Spirit Lake Greenstone Belt	Northwest Ontario, Can	3-10			150
2.85	Nesbitt et al. (2009)	North Spirit Lake Greenstone Belt	Northwest Ontario, Can	3-11			129
2.85	Nesbitt et al. (2009)	North Spirit Lake Greenstone Belt	Northwest Ontario, Can	3-12			44
2.85	Nesbitt et al. (2009)	North Spirit Lake Greenstone Belt	Northwest Ontario, Can	3-13			26
2.85	Nesbitt et al. (2009)	North Spirit Lake Greenstone Belt	Northwest Ontario, Can	3-14			154
2.85	Nesbitt et al. (2009)	North Spirit Lake Greenstone Belt	Northwest Ontario, Can	3-15			75
2.85	Nesbitt et al. (2009)	North Spirit Lake Greenstone Belt	Northwest Ontario, Can	3-16			142
2.85	Nesbitt et al. (2009)	North Spirit Lake Greenstone Belt	Northwest Ontario, Can	3-17			140
2.85	Nesbitt et al. (2009)	North Spirit Lake Greenstone Belt	Northwest Ontario, Can	3-18			74
2.85	Nesbitt et al. (2009)	North Spirit Lake Greenstone Belt	Northwest Ontario, Can	3-19			154
2.85	Nesbitt et al. (2009)	North Spirit Lake Greenstone Belt	Northwest Ontario, Can	3-21			72

Age (Ga)	Reference/Source	Formation	Location	Sample	TOC	Mo	V
2.9	Cameron and Garrels (1980)	Red Lake	Canadian Sheild, Canad	1		2	150
2.9	Cameron and Garrels (1980)	Atikokan	Canadian Sheild, Canad	2		5	130
2.7	Cameron and Garrels (1980)	Lac des Iles and Beardmore	Canadian Sheild, Canad	3		3.5	150
2.74	Cameron and Garrels (1980)	Michipicoten and Oba	Canadian Sheild, Canad	4		4	75
2.74	Cameron and Garrels (1980)	Timmins	Canadian Sheild, Canad	5		2	110
2.4	Cameron and Garrels (1980)	Gowganda	Canadian Sheild, Canad	11		1	210
1.8	Cameron and Garrels (1980)	Rove	Canadian Sheild, Canad	13		6	170
1.8	Cameron and Garrels (1980)	Albanel	Canadian Sheild, Canad	14		2	89
0.657	Kendall et al., (2006)	Aralka Fm	Wallara-1 Core, Australi	BK-04-WALLARA-1A		4.81	192
0.657	Kendall et al., (2006)	Aralka Fm	Wallara-1 Core, Australi	BK-04-WALLARA-1B		4.66	186.6
0.657	Kendall et al., (2006)	Aralka Fm	Wallara-1 Core, Australi	BK-04-WALLARA-2A		5.08	174.6
0.657	Kendall et al., (2006)	Aralka Fm	Wallara-1 Core, Australi	BK-04-WALLARA-2B		5.03	174.5
0.657	Kendall et al., (2006)	Aralka Fm	Wallara-1 Core, Australi	BK-04-WALLARA-3		4.85	144.5
0.657	Kendall et al., (2006)	Aralka Fm	Wallara-1 Core, Australi	BK-04-WALLARA-4A		4.21	113.6
0.657	Kendall et al., (2006)	Aralka Fm	Wallara-1 Core, Australi	BK-04-WALLARA-4B		4.96	158
0.657	Kendall et al., (2006)	Aralka Fm	Wallara-1 Core, Australi	BK-04-WALLARA-5A		4.03	109.3
0.643	Kendall et al., (2006)	Tindelpina Shale Mbr	Blinman-2 and SCYW1a	BK-04-BLINMAN-1		2.67	180.9
0.643	Kendall et al., (2006)	Tindelpina Shale Mbr	Blinman-2 and SCYW1a	BK-04-BLINMAN-3		2.63	179.8
0.643	Kendall et al., (2006)	Tindelpina Shale Mbr	Blinman-2 and SCYW1a	BK-04-BLINMAN-4		2.36	166.7
0.643	Kendall et al., (2006)	Tindelpina Shale Mbr	Blinman-2 and SCYW1a	BK-04-BLINMAN-5		2.2	177.8
0.643	Kendall et al., (2006)	Tindelpina Shale Mbr	Blinman-2 and SCYW1a	BK-04-BLINMAN-6		2.06	179.4
0.643	Kendall et al., (2006)	Tindelpina Shale Mbr	Blinman-2 and SCYW1a	BK-04-BLINMAN-7		2.93	188.8
0.643	Kendall et al., (2006)	Tindelpina Shale Mbr	Blinman-2 and SCYW1a	BK-04-BLINMAN-9		3.09	189.5
0.643	Kendall et al., (2006)	Tindelpina Shale Mbr	Blinman-2 and SCYW1a	BK-04-BLINMAN-10		2.83	187.9
0.643	Kendall et al., (2006)	Tindelpina Shale Mbr	Blinman-2 and SCYW1a	BK-04-BLINMAN-11		2.86	187.7
0.643	Kendall et al., (2006)	Tindelpina Shale Mbr	Blinman-2 and SCYW1a	BK-04-SCYW1a-3-4		4.11	194.7
0.643	Kendall et al., (2006)	Tindelpina Shale Mbr	Blinman-2 and SCYW1a	BK-04-SCYW1a-5		3.22	201.7
0.643	Kendall et al., (2006)	Tindelpina Shale Mbr	Blinman-2 and SCYW1a	BK-04-SCYW1a-6-7		4.32	182.9
0.608	Kendall et al., (2004)	Old Fort Pt Fm.	Outcrop, Western Cana	BK-01-014B		4.86	144.6
0.608	Kendall et al., (2004)	Old Fort Pt Fm.	Outcrop, Western Cana	BK-01-015A		7.8	151.6
0.608	Kendall et al., (2004)	Old Fort Pt Fm.	Outcrop, Western Cana	BK-01-015B		6.37	138
0.608	Kendall et al., (2004)	Old Fort Pt Fm.	Outcrop, Western Cana	BK-01-015C		7.85	148.4
0.608	Kendall et al., (2004)	Old Fort Pt Fm.	Outcrop, Western Cana	BK-01-015D		6.52	114

Age (Ga)	Reference/Source	Formation	Location	Sample	TOC	Mo	V
2.5	Anbar et al., (2007)	Mt McRae Shale	ABDP-9 Core, Western	127.25	6.9	10.4	110.8
2.5	Anbar et al., (2007)	Mt McRae Shale	ABDP-9 Core, Western	128.17	6.5	13.3	111.7
2.5	Anbar et al., (2007)	Mt McRae Shale	ABDP-9 Core, Western	129.01	6.1	9.2	127.6
2.5	Anbar et al., (2007)	Mt McRae Shale	ABDP-9 Core, Western	130.06		13.0	102.9
2.5	Anbar et al., (2007)	Mt McRae Shale	ABDP-9 Core, Western	130.71	5.5	7.3	75.0
2.5	Anbar et al., (2007)	Mt McRae Shale	ABDP-9 Core, Western	135.58	7.2	8.3	52.6
2.5	Anbar et al., (2007)	Mt McRae Shale	ABDP-9 Core, Western	136.15	8.2	15.2	58.1
2.5	Anbar et al., (2007)	Mt McRae Shale	ABDP-9 Core, Western	136.67	7.7	17.3	58.4
2.5	Anbar et al., (2007)	Mt McRae Shale	ABDP-9 Core, Western	136.94	9.0	17.5	65.0
2.5	Anbar et al., (2007)	Mt McRae Shale	ABDP-9 Core, Western	137.31		23.5	69.8
2.5	Anbar et al., (2007)	Mt McRae Shale	ABDP-9 Core, Western	137.68	9.4	11.9	62.1
2.5	Anbar et al., (2007)	Mt McRae Shale	ABDP-9 Core, Western	137.96	10.8	19.1	64.5
2.5	Anbar et al., (2007)	Mt McRae Shale	ABDP-9 Core, Western	138.38	10.9	19.0	77.3
2.5	Anbar et al., (2007)	Mt McRae Shale	ABDP-9 Core, Western	138.74		16.8	70.0
2.5	Anbar et al., (2007)	Mt McRae Shale	ABDP-9 Core, Western	139.01	11.0	19.0	70.5
2.5	Anbar et al., (2007)	Mt McRae Shale	ABDP-9 Core, Western	139.65	9.9	20.7	86.1
2.5	Anbar et al., (2007)	Mt McRae Shale	ABDP-9 Core, Western	139.97	12.1	25.0	93.8
2.5	Anbar et al., (2007)	Mt McRae Shale	ABDP-9 Core, Western	140.25	12.4	22.6	98.0
2.5	Anbar et al., (2007)	Mt McRae Shale	ABDP-9 Core, Western	140.5	15.3	29.1	109.9
2.5	Anbar et al., (2007)	Mt McRae Shale	ABDP-9 Core, Western	140.95	16.1	30.5	86.7
2.5	Anbar et al., (2007)	Mt McRae Shale	ABDP-9 Core, Western	141.17	12.6	20.4	87.5
2.5	Anbar et al., (2007)	Mt McRae Shale	ABDP-9 Core, Western	141.47	13.0	21.9	101.3
2.5	Anbar et al., (2007)	Mt McRae Shale	ABDP-9 Core, Western	141.72		18.6	94.9
2.5	Anbar et al., (2007)	Mt McRae Shale	ABDP-9 Core, Western	142.08	11.6	19.1	98.0
2.5	Anbar et al., (2007)	Mt McRae Shale	ABDP-9 Core, Western	142.6		13.5	60.1
2.5	Anbar et al., (2007)	Mt McRae Shale	ABDP-9 Core, Western	143.45	13.1	41.4	102.9
2.5	Anbar et al., (2007)	Mt McRae Shale	ABDP-9 Core, Western	144.36	8.7	33.7	81.3
2.5	Anbar et al., (2007)	Mt McRae Shale	ABDP-9 Core, Western	145.61	13.4	40.1	101.3
2.5	Anbar et al., (2007)	Mt McRae Shale	ABDP-9 Core, Western	146.45	15.2	40.3	115.8
2.5	Anbar et al., (2007)	Mt McRae Shale	ABDP-9 Core, Western	148.27	10.4	20.2	94.1
2.5	Anbar et al., (2007)	Mt McRae Shale	ABDP-9 Core, Western	149.3	12.1	37.1	85.8
2.5	Anbar et al., (2007)	Mt McRae Shale	ABDP-9 Core, Western	150.24	7.7	16.5	90.9
2.5	Anbar et al., (2007)	Mt McRae Shale	ABDP-9 Core, Western	188.01	4.0	4.6	63.3
0.64	Kendall et al., (unpublished)	Black River Dolomite	Forest-1 Core, Australia	RC06-FOR01-A - 835.84-835.87 m	5.1	13.9	194.2
0.64	Kendall et al., (unpublished)	Black River Dolomite	Forest-1 Core, Australia	RC06-FOR01-B - 835.77-835.79 m	5.6	14.1	196.9
0.64	Kendall et al., (unpublished)	Black River Dolomite	Forest-1 Core, Australia	RC06-FOR01-C - 835.70-835.72 m	5.3	13.9	203.6
0.64	Kendall et al., (unpublished)	Black River Dolomite	Forest-1 Core, Australia	RC06-FOR01-D - 835.65-835.68 m	5.6	12.4	195.0
0.64	Kendall et al., (unpublished)	Black River Dolomite	Forest-1 Core, Australia	RC06-FOR01-E - 835.58-835.62 m	5.3	12.0	195.6
0.64	Kendall et al., (unpublished)	Black River Dolomite	Forest-1 Core, Australia	RC06-FOR02-B - 828.11-828.15 m	6.5	29.2	320.6
0.64	Kendall et al., (unpublished)	Black River Dolomite	Forest-1 Core, Australia	RC06-FOR02-D - 828.23-828.27 m	6.6	28.9	326.6
0.64	Kendall et al., (unpublished)	Black River Dolomite	Forest-1 Core, Australia	RC06-FOR02-G - 828.37-828.40 m	6.5	32.9	367.3
0.64	Kendall et al., (unpublished)	Black River Dolomite	Forest-1 Core, Australia	RC06-FOR02-H - 828.48-828.50 m	6.4	30.2	344.7
0.64	Kendall et al., (unpublished)	Black River Dolomite	Forest-1 Core, Australia	RC06-FOR02-I - 828.55 - 828.58 m	6.8	28.8	349.2
1.4	Arnold et al., (2004)	Velkerri Formation, Roper Group	Roper Group, McArthur	156.1 m	8	33	
1.4	Arnold et al., (2004)	Velkerri Formation, Roper Group	Roper Group, McArthur	173.0 m	3.9	24	
1.4	Arnold et al., (2004)	Velkerri Formation, Roper Group	Roper Group, McArthur	204.1 m	5.4	14	
1.4	Arnold et al., (2004)	Velkerri Formation, Roper Group	Roper Group, McArthur	214.1 m	4.7	30	
1.4	Arnold et al., (2004)	Velkerri Formation, Roper Group	Roper Group, McArthur	363.0 m	2.7	11	

Age (Ga)	Reference/Source	Formation	Location	Sample	TOC	Mo	V
0.8	Condie et al., (2001)	Red Pine Shale	Uinta Mountais and Cott	Utah, USA			84
0.8	Condie et al., (2001)	Red Pine Shale	Uinta Mountais and Cott	Utah, USA			177
0.8	Condie et al., (2001)	Red Pine Shale	Uinta Mountais and Cott	Utah, USA			177
0.8	Condie et al., (2001)	Red Pine Shale	Uinta Mountais and Cott	Utah, USA			102
0.8	Condie et al., (2001)	Red Pine Shale	Uinta Mountais and Cott	Utah, USA			119
0.8	Condie et al., (2001)	Red Pine Shale	Uinta Mountais and Cott	Utah, USA			113
0.8	Condie et al., (2001)	Hades Peak Formation	Uinta Mountais and Cott	Utah, USA			90
0.8	Condie et al., (2001)	Hades Peak Formation	Uinta Mountais and Cott	Utah, USA			83
0.8	Condie et al., (2001)	Hades Peak Formation	Uinta Mountais and Cott	Utah, USA			75
0.8	Condie et al., (2001)	Mt Watson Formation	Uinta Mountais and Cott	Utah, USA			57
0.8	Condie et al., (2001)	Mt Watson Formation	Uinta Mountais and Cott	Utah, USA			78
0.8	Condie et al., (2001)	Mt Watson Formation	Uinta Mountais and Cott	Utah, USA			92
0.8	Condie et al., (2001)	Red Castle Formation	Uinta Mountais and Cott	Utah, USA			91
0.8	Condie et al., (2001)	Red Castle Formation	Uinta Mountais and Cott	Utah, USA			108
0.8	Condie et al., (2001)	Moosehorn Lake Formation	Uinta Mountais and Cott	Utah, USA			93
0.8	Condie et al., (2001)	Moosehorn Lake Formation	Uinta Mountais and Cott	Utah, USA			95
0.8	Condie et al., (2001)	Moosehorn Lake Formation	Uinta Mountais and Cott	Utah, USA			98
0.8	Condie et al., (2001)	Big Cottonw ood Group	Uinta Mountais and Cott	Utah, USA			137
0.8	Condie et al., (2001)	Big Cottonw ood Group	Uinta Mountais and Cott	Utah, USA			125
0.8	Condie et al., (2001)	Big Cottonw ood Group	Uinta Mountais and Cott	Utah, USA			108
1.9	Hayashi et al., (1997)	DMH-13 (Black Shale)	Labrador, Canada				165
1.9	Hayashi et al., (1997)	DMH-13 (Black Shale)	Labrador, Canada			2	247
1.9	Hayashi et al., (1997)	DMH-13 (Black Shale)	Labrador, Canada			2	214
1.9	Hayashi et al., (1997)	DMH-13 (Black Shale)	Labrador, Canada				209
1.9	Hayashi et al., (1997)	DMH-14 (Black Shale)	Labrador, Canada				240
1.9	Hayashi et al., (1997)	DMH-14 (Black Shale)	Labrador, Canada			2	315
1.9	Hayashi et al., (1997)	DMH-14 (Black Shale)	Labrador, Canada				269
1.9	Hayashi et al., (1997)	DMH-15 (Black Shale)	Labrador, Canada				295
1.9	Hayashi et al., (1997)	DMH-15 (Black Shale)	Labrador, Canada			3	274
1.9	Hayashi et al., (1997)	DMH-15 (Black Shale)	Labrador, Canada			3	262
1.9	Hayashi et al., (1997)	DMH-15 (Black Shale)	Labrador, Canada				300
1.9	Hayashi et al., (1997)	DMH-16 (Black Shale)	Labrador, Canada				383
1.9	Hayashi et al., (1997)	DMH-16 (Black Shale)	Labrador, Canada			5	294
1.9	Hayashi et al., (1997)	DMH-16 (Black Shale)	Labrador, Canada			4	326
1.9	Hayashi et al., (1997)	DMH-16 (Black Shale)	Labrador, Canada				325
1.9	Hayashi et al., (1997)	DMH-23 (Black Shale)	Labrador, Canada				219
1.9	Hayashi et al., (1997)	DMH-23 (Black Shale)	Labrador, Canada			5	296
1.9	Hayashi et al., (1997)	DMH-23 (Black Shale)	Labrador, Canada			4	252
1.9	Hayashi et al., (1997)	DMH-23 (Black Shale)	Labrador, Canada			4	232
0.75	Dahl et al., (2011)	Chuar Group, Grand Canyon	SMC	AK-10-60-35	10.3	2.7	
0.75	Dahl et al., (2011)	Chuar Group, Grand Canyon	SMC	AK-10-60-33	6.8	3.4	
0.75	Dahl et al., (2011)	Chuar Group, Grand Canyon	SMC	AK-10-60-29	5.3	0.7	
0.75	Dahl et al., (2011)	Chuar Group, Grand Canyon	SMC	AK-10-60-28	5.2	5.2	

Age (Ga)	Reference/Source	Formation	Location	Sample	TOC	Mo	V
0.75	Dahl et al., (2011)	Chuar Group, Grand Canyon	SMC	AK-10-60-35	10.3	2.7	
0.75	Dahl et al., (2011)	Chuar Group, Grand Canyon	SMC	AK-10-60-33	6.8	3.4	
0.75	Dahl et al., (2011)	Chuar Group, Grand Canyon	SMC	AK-10-60-29	5.3	0.7	
0.75	Dahl et al., (2011)	Chuar Group, Grand Canyon	SMC	AK-10-60-28	5.2	5.2	
2	Melezhik et al., (1999)	Zaonezhskaya Formation		Chert	2	41	59
2	Melezhik et al., (1999)	Zaonezhskaya Formation		Breccia of shungite rocks II	37.7	7	117
2	Melezhik et al., (1999)	Zaonezhskaya Formation		Breccia of shungite rocks II	35.5	10	127
2	Melezhik et al., (1999)	Zaonezhskaya Formation		Shungite rock III	31.4	12	154
2	Melezhik et al., (1999)	Zaonezhskaya Formation		Black dolostone	n.d.	49	416
2	Melezhik et al., (1999)	Zaonezhskaya Formation		Black limestone	n.d.	38	483
2	Melezhik et al., (1999)	Zaonezhskaya Formation		Black dolostone	1	7	46
2	Melezhik et al., (1999)	Zaonezhskaya Formation		Black dolostone	1.4	8	78
2	Melezhik et al., (1999)	Zaonezhskaya Formation		Siltstone	0.9		227
2	Melezhik et al., (1999)	Zaonezhskaya Formation		Sooty shungite rock III	25.2	40	589
2	Melezhik et al., (1999)	Zaonezhskaya Formation		Sooty shungite rock II	45.5	86	593
0.55	Paikaray et al., (2008)	Upper Bhander Shale	Vindhyan Basin, India				122
0.55	Paikaray et al., (2008)	Upper Bhander Shale	Vindhyan Basin, India				78
0.55	Paikaray et al., (2008)	Upper Bhander Shale	Vindhyan Basin, India				105
0.55	Paikaray et al., (2008)	Upper Bhander Shale	Vindhyan Basin, India				147
0.55	Paikaray et al., (2008)	Upper Bhander Shale	Vindhyan Basin, India				153
0.55	Paikaray et al., (2008)	Upper Bhander Shale	Vindhyan Basin, India				148
0.65	Paikaray et al., (2008)	Sirbu Shale	Vindhyan Basin, India				105
0.65	Paikaray et al., (2008)	Sirbu Shale	Vindhyan Basin, India				88
0.65	Paikaray et al., (2008)	Sirbu Shale	Vindhyan Basin, India				83
0.65	Paikaray et al., (2008)	Sirbu Shale	Vindhyan Basin, India				88
0.65	Paikaray et al., (2008)	Sirbu Shale	Vindhyan Basin, India				127
0.65	Paikaray et al., (2008)	Sirbu Shale	Vindhyan Basin, India				132
0.65	Paikaray et al., (2008)	Sirbu Shale	Vindhyan Basin, India				120
0.65	Paikaray et al., (2008)	Sirbu Shale	Vindhyan Basin, India				94
0.65	Paikaray et al., (2008)	Sirbu Shale	Vindhyan Basin, India				80
0.65	Paikaray et al., (2008)	Sirbu Shale	Vindhyan Basin, India				81
0.7	Paikaray et al., (2008)	Low er Bhander Shale	Vindhyan Basin, India				137
0.7	Paikaray et al., (2008)	Low er Bhander Shale	Vindhyan Basin, India				125
0.7	Paikaray et al., (2008)	Low er Bhander Shale	Vindhyan Basin, India				137
0.7	Paikaray et al., (2008)	Low er Bhander Shale	Vindhyan Basin, India				129
0.7	Paikaray et al., (2008)	Low er Bhander Shale	Vindhyan Basin, India				156
0.7	Paikaray et al., (2008)	Low er Bhander Shale	Vindhyan Basin, India				115
0.7	Paikaray et al., (2008)	Low er Bhander Shale	Vindhyan Basin, India				151
0.7	Paikaray et al., (2008)	Low er Bhander Shale	Vindhyan Basin, India				80
0.7	Paikaray et al., (2008)	Low er Bhander Shale	Vindhyan Basin, India				110
0.715	Paikaray et al., (2008)	Rew a Shale	Vindhyan Basin, India				106
0.715	Paikaray et al., (2008)	Rew a Shale	Vindhyan Basin, India				92
0.715	Paikaray et al., (2008)	Rew a Shale	Vindhyan Basin, India				100
0.715	Paikaray et al., (2008)	Rew a Shale	Vindhyan Basin, India				120
0.715	Paikaray et al., (2008)	Rew a Shale	Vindhyan Basin, India				90

Age (Ga)	Reference/Source	Formation	Location	Sample	TOC	Mo	V
0.94	Paikaray et al., (2008)	Bijaygarh Shale	Vindhyan Basin, India		2.85		157
0.94	Paikaray et al., (2008)	Bijaygarh Shale	Vindhyan Basin, India		2.85		236
0.94	Paikaray et al., (2008)	Bijaygarh Shale	Vindhyan Basin, India		2.85		166
0.94	Paikaray et al., (2008)	Bijaygarh Shale	Vindhyan Basin, India		2.85		139
0.94	Paikaray et al., (2008)	Bijaygarh Shale	Vindhyan Basin, India		2.85		76
0.94	Paikaray et al., (2008)	Bijaygarh Shale	Vindhyan Basin, India		2.85		99
0.94	Paikaray et al., (2008)	Bijaygarh Shale	Vindhyan Basin, India		2.85		151
0.94	Paikaray et al., (2008)	Bijaygarh Shale	Vindhyan Basin, India		2.85		85
0.94	Paikaray et al., (2008)	Bijaygarh Shale	Vindhyan Basin, India		2.85		96
0.94	Paikaray et al., (2008)	Bijaygarh Shale	Vindhyan Basin, India		2.85		152
1.6	Paikaray et al., (2008)	Rampur Shale	Vindhyan Basin, India		1.02		98
1.6	Paikaray et al., (2008)	Rampur Shale	Vindhyan Basin, India		1.02		98
1.6	Paikaray et al., (2008)	Rampur Shale	Vindhyan Basin, India		1.02		100
1.6	Paikaray et al., (2008)	Rampur Shale	Vindhyan Basin, India		1.02		105
1.6	Paikaray et al., (2008)	Rampur Shale	Vindhyan Basin, India		1.02		83
1.6	Paikaray et al., (2008)	Rampur Shale	Vindhyan Basin, India		1.02		15
1.6	Paikaray et al., (2008)	Rampur Shale	Vindhyan Basin, India		1.02		90
1.6	Paikaray et al., (2008)	Rampur Shale	Vindhyan Basin, India		1.02		90
1.6	Paikaray et al., (2008)	Rampur Shale	Vindhyan Basin, India		1.02		111
1.6	Paikaray et al., (2008)	Rampur Shale	Vindhyan Basin, India		1.02		97
1.6	Paikaray et al., (2008)	Rampur Shale	Vindhyan Basin, India		1.02		81
1.6	Paikaray et al., (2008)	Rampur Shale	Vindhyan Basin, India		1.02		100
1.6	Paikaray et al., (2008)	Rampur Shale	Vindhyan Basin, India		1.02		88
1.6	Paikaray et al., (2008)	Rampur Shale	Vindhyan Basin, India		1.02		92
1.6	Paikaray et al., (2008)	Rampur Shale	Vindhyan Basin, India		1.02		92
1.63	Paikaray et al., (2008)	Olive Shale	Vindhyan Basin, India				103
1.63	Paikaray et al., (2008)	Olive Shale	Vindhyan Basin, India				122
1.63	Paikaray et al., (2008)	Olive Shale	Vindhyan Basin, India				112
1.63	Paikaray et al., (2008)	Olive Shale	Vindhyan Basin, India				82
1.63	Paikaray et al., (2008)	Olive Shale	Vindhyan Basin, India				116
1.63	Paikaray et al., (2008)	Olive Shale	Vindhyan Basin, India				128
1.63	Paikaray et al., (2008)	Olive Shale	Vindhyan Basin, India				145
1.63	Paikaray et al., (2008)	Olive Shale	Vindhyan Basin, India				157
1.63	Paikaray et al., (2008)	Olive Shale	Vindhyan Basin, India				236
1.63	Paikaray et al., (2008)	Olive Shale	Vindhyan Basin, India				128
1.63	Paikaray et al., (2008)	Olive Shale	Vindhyan Basin, India				120
1.63	Paikaray et al., (2008)	Olive Shale	Vindhyan Basin, India				126
1.63	Paikaray et al., (2008)	Olive Shale	Vindhyan Basin, India				121
1.63	Paikaray et al., (2008)	Olive Shale	Vindhyan Basin, India				144
1.63	Paikaray et al., (2008)	Olive Shale	Vindhyan Basin, India				181
1.8	Paikaray et al., (2008)	Arangi Shale	Vindhyan Basin, India		2.78		96
1.8	Paikaray et al., (2008)	Arangi Shale	Vindhyan Basin, India		2.78		98
1.8	Paikaray et al., (2008)	Arangi Shale	Vindhyan Basin, India		2.78		105
1.8	Paikaray et al., (2008)	Arangi Shale	Vindhyan Basin, India		2.78		131
1.8	Paikaray et al., (2008)	Arangi Shale	Vindhyan Basin, India		2.78		112

Age (Ga)	Reference/Source	Formation	Location	Sample	TOC	Mo	V
2.05	Scott et al., (unpublished)	Zaonezhskaya Fm., Ludikovian Series	Karelia, Russia	C-5190	7.40		563.49
2.05	Scott et al., (unpublished)	Zaonezhskaya Fm., Ludikovian Series	Karelia, Russia	C-5190	5.20		194.06
2.05	Scott et al., (unpublished)	Zaonezhskaya Fm., Ludikovian Series	Karelia, Russia	C-5190	9.30		128.18
2.05	Scott et al., (unpublished)	Zaonezhskaya Fm., Ludikovian Series	Karelia, Russia	C-5190	6.80		923.88
2.05	Scott et al., (unpublished)	Zaonezhskaya Fm., Ludikovian Series	Karelia, Russia	C-5190	10.10		333.92
2.05	Scott et al., (unpublished)	Zaonezhskaya Fm., Ludikovian Series	Karelia, Russia	C34	10.20		1953.51
2.05	Scott et al., (unpublished)	Zaonezhskaya Fm., Ludikovian Series	Karelia, Russia	C34	0.40		69.90
2.05	Scott et al., (unpublished)	Zaonezhskaya Fm., Ludikovian Series	Karelia, Russia	C34	1.80		1295.63
2.1	Scott et al., (unpublished)	Sengoma Argillite Formation, Pretoria Series		106.5		0.40	88.12
2.1	Scott et al., (unpublished)	Sengoma Argillite Formation, Pretoria Series		120.5		0.21	102.09
2.1	Scott et al., (unpublished)	Sengoma Argillite Formation, Pretoria Series		154.7		1.15	98.37
2.1	Scott et al., (unpublished)	Sengoma Argillite Formation, Pretoria Series		156.78		1.52	99.27
2.1	Scott et al., (unpublished)	Sengoma Argillite Formation, Pretoria Series		171.5	10	1.57	87.71
2.1	Scott et al., (unpublished)	Sengoma Argillite Formation, Pretoria Series		173.67		3.50	137.16
2.1	Scott et al., (unpublished)	Sengoma Argillite Formation, Pretoria Series		181.25		1.40	90.32
2.1	Scott et al., (unpublished)	Sengoma Argillite Formation, Pretoria Series		186.57	11	48.87	1197.66
2.1	Scott et al., (unpublished)	Sengoma Argillite Formation, Pretoria Series		200.7	13.3	10.02	128.21
2.1	Scott et al., (unpublished)	Sengoma Argillite Formation, Pretoria Series		202.5	15.5	6.75	159.10
2.1	Scott et al., (unpublished)	Sengoma Argillite Formation, Pretoria Series		205.25	14.2	26.34	159.82
2.1	Scott et al., (unpublished)	Sengoma Argillite Formation, Pretoria Series		209	15.9	7.35	133.25
2.1	Scott et al., (unpublished)	Sengoma Argillite Formation, Pretoria Series		212.7	16	7.99	112.12
2.1	Scott et al., (unpublished)	Sengoma Argillite Formation, Pretoria Series		216.8		0.63	104.96
2.1	Scott et al., (unpublished)	Sengoma Argillite Formation, Pretoria Series		219		0.54	109.84
2.1	Scott et al., (unpublished)	Sengoma Argillite Formation, Pretoria Series		238.2		1.27	108.23
2.1	Scott et al., (unpublished)	Sengoma Argillite Formation, Pretoria Series		286.6		1.67	114.91
2.62	Scott et al., (unpublished)	Jeerinah Formation, Fortescue Group		FVG-1 707.95	10.4		110.13
2.62	Scott et al., (unpublished)	Jeerinah Formation, Fortescue Group		FVG-1752.65	6		97.79
2.62	Scott et al., (unpublished)	Jeerinah Formation, Fortescue Group		FVG-1765.8	9.9		53.42
2.62	Scott et al., (unpublished)	Jeerinah Formation, Fortescue Group		FVG-1774	4.4		73.36
2.62	Scott et al., (unpublished)	Jeerinah Formation, Fortescue Group		FVG-1794.1	4.7		95.28
2.53	Scott et al., (unpublished)	Jeerinah Formation, Fortescue Group		WB-98469.89			76.08
2.53	Scott et al., (unpublished)	Jeerinah Formation, Fortescue Group		WB-98474.1	4.8		129.00
2.53	Scott et al., (unpublished)	Jeerinah Formation, Fortescue Group		WB-98477.5	3.9		77.34
2.53	Scott et al., (unpublished)	Jeerinah Formation, Fortescue Group		WB-98507.39	3		21.01
2.53	Scott et al., (unpublished)	Jeerinah Formation, Fortescue Group		WB-98509.1			13.81
2.53	Scott et al., (unpublished)	Jeerinah Formation, Fortescue Group		WB-98512.95	2.9		63.62

Age (Ga)	Reference/Source	Formation	Location	Sample	TOC	Mo	V
0.1125	Alberdi-Genolet and Tocco (1999)	Machiques Member	Venezuela	MA-24	6.1	95	152
0.1125	Alberdi-Genolet and Tocco (1999)	Machiques Member	Venezuela	MA-26	5.7	186	318
0.1125	Alberdi-Genolet and Tocco (1999)	Machiques Member	Venezuela	MA-31			
0.1125	Alberdi-Genolet and Tocco (1999)	Machiques Member	Venezuela	MA-32	10	828	1135
0.1125	Alberdi-Genolet and Tocco (1999)	Machiques Member	Venezuela	MA-39	3.8	240	459
0.1125	Alberdi-Genolet and Tocco (1999)	Machiques Member	Venezuela	MA-42	2.6	47	469
0.1125	Alberdi-Genolet and Tocco (1999)	Machiques Member	Venezuela	MA-46	0.5		21
0.1125	Alberdi-Genolet and Tocco (1999)	Machiques Member	Venezuela	MA-48	0.6		5.5
0.1125	Alberdi-Genolet and Tocco (1999)	Machiques Member	Venezuela	MA-61	0.7	1	151
0.1125	Alberdi-Genolet and Tocco (1999)	Machiques Member	Venezuela	MA-53	2.8		
0.1125	Alberdi-Genolet and Tocco (1999)	Machiques Member	Venezuela	MA-65	5.4	136	892
0.1125	Alberdi-Genolet and Tocco (1999)	Machiques Member	Venezuela	MA-68	3.6	72	300
0.086	Alberdi-Genolet and Tocco (1999)	Machiques Member	Venezuela	MA-72	4.2	224	930
0.086	Alberdi-Genolet and Tocco (1999)	Machiques Member	Venezuela	MA-79	2.9	194	1496
0.086	Alberdi-Genolet and Tocco (1999)	La Luna Formation	Venezuela	LU-98	3.8	73	281
0.086	Alberdi-Genolet and Tocco (1999)	La Luna Formation	Venezuela	LU-100	1.5	19	48
0.086	Alberdi-Genolet and Tocco (1999)	La Luna Formation	Venezuela	LU-106	5.2	82	958
0.086	Alberdi-Genolet and Tocco (1999)	La Luna Formation	Venezuela	LU-108	5.3	218	1765
0.086	Alberdi-Genolet and Tocco (1999)	La Luna Formation	Venezuela	LU-115	5	89	1525
0.086	Alberdi-Genolet and Tocco (1999)	La Luna Formation	Venezuela	LU-119	6.5	177	2112
0.086	Alberdi-Genolet and Tocco (1999)	La Luna Formation	Venezuela	LU-121	4.5	126	4065
0.086	Alberdi-Genolet and Tocco (1999)	La Luna Formation	Venezuela	LU-125	3.4	45	1497
0.086	Alberdi-Genolet and Tocco (1999)	La Luna Formation	Venezuela	LU-128	1.3	44	232
0.086	Alberdi-Genolet and Tocco (1999)	La Luna Formation	Venezuela	LU-138	3.6	42	683
0.086	Alberdi-Genolet and Tocco (1999)	La Luna Formation	Venezuela	LU-141	5.1	126	1401
0.086	Alberdi-Genolet and Tocco (1999)	La Luna Formation	Venezuela	LU-145	5.4	30	462
0.086	Alberdi-Genolet and Tocco (1999)	La Luna Formation	Venezuela	LU-147	7.2	62	1389
0.086	Alberdi-Genolet and Tocco (1999)	La Luna Formation	Venezuela	LU-151	5.6	192	1433
0.086	Alberdi-Genolet and Tocco (1999)	La Luna Formation	Venezuela	LU-153	3.1	56	1085
0.086	Alberdi-Genolet and Tocco (1999)	La Luna Formation	Venezuela	9989	6.3	103	1108
0.086	Alberdi-Genolet and Tocco (1999)	La Luna Formation	Venezuela	10019	7.5	127	1982
0.086	Alberdi-Genolet and Tocco (1999)	La Luna Formation	Venezuela	10049	5.3	83	1110
0.086	Alberdi-Genolet and Tocco (1999)	La Luna Formation	Venezuela	10100		1	310
0.086	Alberdi-Genolet and Tocco (1999)	La Luna Formation	Venezuela	10128		42	3899
0.086	Alberdi-Genolet and Tocco (1999)	La Luna Formation	Venezuela	10221	2.53	39	1179
0.091	Brumsack (2006)	C/T Demerara Rise	Demerara Rise	C/T Demerara Rise	10.4	80	1066
0.091	Brumsack (2006)	C/T mean	Mean	C/T mean	8.07	316	1016
0.091	Brumsack (2006)	C/T Gubbio	Gubbio Section	C/T Gubbio	8.92	27	613
0	Brumsack (2006)	Peru margin			8	42	152
0	Brumsack (2006)	Namibian mud lens			5	40	138
0	Brumsack (2006)	Gulf of California			4	12	101
0	Brumsack (2006)	Mediterranean sapropels > 2% TOC			7	105	518
0	Brumsack (2006)	Black Sea Unit 1			5	51	100
0	Brumsack (2006)	Black Sea Unit 2			17	117	196

Age (Ga)	Reference/Source	Formation	Location	Sample	TOC	Mo	V
1.914	Absar et al., (2009)	Morar Formation	Gwalior, India	TUN-1b			56
1.914	Absar et al., (2009)	Morar Formation	Gwalior, India	JSX-2b			45
1.914	Absar et al., (2009)	Morar Formation	Gwalior, India	JSX-3b			97
1.914	Absar et al., (2009)	Morar Formation	Gwalior, India	BDE-1b			36
1.914	Absar et al., (2009)	Morar Formation	Gwalior, India	SDL-2c			44
2.5	Kendall, B. et al. (2010)	Klein Naute Formation-GKP01	South Africa	238.57	2.5	3.4	
2.50	Kendall, B. et al. (2010)	Klein Naute Formation-GKP01	South Africa	239.53	2.4	5.1	
2.50	Kendall, B. et al. (2010)	Klein Naute Formation-GKP01	South Africa	240.50	1.6	5.9	
2.50	Kendall, B. et al. (2010)	Klein Naute Formation-GKP01	South Africa	241.27	2.0	4.7	
2.50	Kendall, B. et al. (2010)	Klein Naute Formation-GKP01	South Africa	242.70	3.3	6.8	
2.50	Kendall, B. et al. (2010)	Klein Naute Formation-GKP01	South Africa	243.55	3.2	5.5	
2.50	Kendall, B. et al. (2010)	Klein Naute Formation-GKP01	South Africa	244.45	4.0	6.0	
2.50	Kendall, B. et al. (2010)	Klein Naute Formation-GKP01	South Africa	245.51	3.0	5.2	
2.50	Kendall, B. et al. (2010)	Klein Naute Formation-GKP01	South Africa	246.45	3.3	5.1	
2.50	Kendall, B. et al. (2010)	Klein Naute Formation-GKP01	South Africa	249.68	3.4	6.4	
2.50	Kendall, B. et al. (2010)	Klein Naute Formation-GKP01	South Africa	250.45	4.1	1.5	
2.50	Kendall, B. et al. (2010)	Klein Naute Formation-GKP01	South Africa	253.35	2.7	0.9	
2.50	Kendall, B. et al. (2010)	Klein Naute Formation-GKP01	South Africa	260.07	2.7	2.9	
2.50	Kendall, B. et al. (2010)	Klein Naute Formation-GKP01	South Africa	261.00	2.3	1.8	
2.50	Kendall, B. et al. (2010)	Klein Naute Formation-GKP01	South Africa	261.95	2.6	2.1	
2.50	Kendall, B. et al. (2010)	Klein Naute Formation-GKP01	South Africa	262.30	1.8	1.7	
2.50	Kendall, B. et al. (2010)	Klein Naute Formation-GKP01	South Africa	263.85	2.3	2.8	
2.50	Kendall, B. et al. (2010)	Klein Naute Formation-GKP01	South Africa	265.55	2.7	1.6	
2.50	Kendall, B. et al. (2010)	Klein Naute Formation-GKP01	South Africa	266.40	2.6	2.0	
2.50	Kendall, B. et al. (2010)	Klein Naute Formation-GKP01	South Africa	267.40	3.1	1.4	
2.50	Kendall, B. et al. (2010)	Klein Naute Formation-GKP01	South Africa	268.93	2.5	1.7	
2.50	Kendall, B. et al. (2010)	Klein Naute Formation-GKP01	South Africa	269.25	1.6	3.4	
2.50	Kendall, B. et al. (2010)	Klein Naute Formation-GKP01	South Africa	273.00	1.8	1.4	
2.50	Kendall, B. et al. (2010)	Klein Naute Formation-GKP01	South Africa	273.95	2.4	1.4	
2.50	Kendall, B. et al. (2010)	Klein Naute Formation-GKP01	South Africa	274.50	2.2	1.5	
2.50	Kendall, B. et al. (2010)	Klein Naute Formation-GKP01	South Africa	275.50	2.1	2.6	
2.50	Kendall, B. et al. (2010)	Klein Naute Formation-GKP01	South Africa	276.10	2.6	2.8	
2.50	Kendall, B. et al. (2010)	Klein Naute Formation-GKP01	South Africa	276.65	2.3	2.3	
2.50	Kendall, B. et al. (2010)	Klein Naute Formation-GKP01	South Africa	277.15		2.1	
2.50	Kendall, B. et al. (2010)	Klein Naute Formation-GKP01	South Africa	277.75	2.1	7.0	
2.50	Kendall, B. et al. (2010)	Klein Naute Formation-GKP01	South Africa	278.60	2.4	2.5	
2.50	Kendall, B. et al. (2010)	Klein Naute Formation-GKP01	South Africa	279.35	2.5	2.1	
2.50	Kendall, B. et al. (2010)	Klein Naute Formation-GKP01	South Africa	280.27	1.6	2.3	
2.50	Kendall, B. et al. (2010)	Klein Naute Formation-GKP01	South Africa	281.59	1.8	1.4	
2.50	Kendall, B. et al. (2010)	Klein Naute Formation-GKP01	South Africa	283.65	2.5	3.6	
2.50	Kendall, B. et al. (2010)	Klein Naute Formation-GKP01	South Africa	284.25	1.6	2.7	
2.50	Kendall, B. et al. (2010)	Klein Naute Formation-GKP01	South Africa	286.65	2.4	3.3	
2.50	Kendall, B. et al. (2010)	Klein Naute Formation-GKP01	South Africa	290.57	1.5	1.6	
2.50	Kendall, B. et al. (2010)	Klein Naute Formation-GKP01	South Africa	291.55	2.0	2.4	

Age (Ga)	Reference/Source	Formation	Location	Sample	TOC	Mo	V
2.50	Kendall, B. et al. (2010)	Klein Naute Formation-GKP01	South Africa	292.47	2.1	1.9	
2.50	Kendall, B. et al. (2010)	Klein Naute Formation-GKP01	South Africa	293.38	2.6	2.2	
2.50	Kendall, B. et al. (2010)	Klein Naute Formation-GKP01	South Africa	297.85	3.7	5.8	
2.50	Kendall, B. et al. (2010)	Klein Naute Formation-GKP01	South Africa	299.40	3.4	5.5	
2.50	Kendall, B. et al. (2010)	Klein Naute Formation-GKP01	South Africa	300.42	2.0	5.3	
2.50	Kendall, B. et al. (2010)	Klein Naute Formation-GKP01	South Africa	301.47	2.3	5.1	
2.50	Kendall, B. et al. (2010)	Klein Naute Formation-GKP01	South Africa	302.50	2.9	4.5	
2.50	Kendall, B. et al. (2010)	Klein Naute Formation-GKP01	South Africa	303.50	2.8	2.9	
2.50	Kendall, B. et al. (2010)	Klein Naute Formation-GKP01	South Africa	304.08	2.0	3.9	
2.50	Kendall, B. et al. (2010)	Klein Naute Formation-GKP01	South Africa	305.34	2.4	5.5	
2.50	Kendall, B. et al. (2010)	Klein Naute Formation-GKP01	South Africa	306.28	3.9	6.3	
2.50	Kendall, B. et al. (2010)	Klein Naute Formation-GKP01	South Africa	307.62	3.8	3.9	
2.50	Kendall, B. et al. (2010)	Klein Naute Formation-GKP01	South Africa	308.40	3.8	1.7	
2.50	Kendall, B. et al. (2010)	Klein Naute Formation-GKP01	South Africa	309.45	4.7	5.6	
2.50	Kendall, B. et al. (2010)	Klein Naute Formation-GKP01	South Africa	310.45	4.8	4.8	
2.50	Kendall, B. et al. (2010)	Klein Naute Formation-GKP01	South Africa	311.48	4.4	4.5	
2.50	Kendall, B. et al. (2010)	Klein Naute Formation-GKP01	South Africa	312.73	8.8	8.6	
2.50	Kendall, B. et al. (2010)	Klein Naute Formation-GKP01	South Africa	314.10	2.4	2.5	
2.50	Kendall, B. et al. (2010)	Klein Naute Formation-GKP01	South Africa	315.85	5.8	6.8	
2.50	Kendall, B. et al. (2010)	Klein Naute Formation-GKP01	South Africa	316.35	3.9	5.1	
2.50	Kendall, B. et al. (2010)	Klein Naute Formation-GKP01	South Africa	317.55	3.3	3.8	
2.50	Kendall, B. et al. (2010)	Klein Naute Formation-GKP01	South Africa	318.72	6.3	7.6	
2.50	Kendall, B. et al. (2010)	Klein Naute Formation-GKP01	South Africa	319.75	5.1	5.1	
2.50	Kendall, B. et al. (2010)	Klein Naute Formation-GKP01	South Africa	321.65	3.6	2.2	
2.50	Kendall, B. et al. (2010)	Klein Naute Formation-GKP01	South Africa	322.23	4.5	1.7	
2.50	Kendall, B. et al. (2010)	Klein Naute Formation-GKP01	South Africa	323.07	2.0	1.2	
2.50	Kendall, B. et al. (2010)	Klein Naute Formation-GKP01	South Africa	324.36	4.2	2.0	
2.50	Kendall, B. et al. (2010)	Klein Naute Formation-GKP01	South Africa	325.40	1.6	0.5	
2.50	Kendall, B. et al. (2010)	Klein Naute Formation-GKP01	South Africa	326.85	2.5	0.4	
2.50	Kendall, B. et al. (2010)	Klein Naute Formation-GKP01	South Africa	328.50	3.1	0.7	
2.50	Kendall, B. et al. (2010)	Klein Naute Formation-GKP01	South Africa	330.00	1.7	0.5	
2.50	Kendall, B. et al. (2010)	Nauga Formation-GKP01	South Africa	483.60	3.6	1.4	
2.50	Kendall, B. et al. (2010)	Nauga Formation-GKP01	South Africa	484.38	3.2	0.5	
2.50	Kendall, B. et al. (2010)	Nauga Formation-GKP01	South Africa	484.92	3.0	1.5	
2.50	Kendall, B. et al. (2010)	Nauga Formation-GKP01	South Africa	486.07	3.0	2.6	
2.50	Kendall, B. et al. (2010)	Nauga Formation-GKP01	South Africa	486.76	2.8	1.0	
2.50	Kendall, B. et al. (2010)	Nauga Formation-GKP01	South Africa	487.68	1.7	0.9	
2.50	Kendall, B. et al. (2010)	Nauga Formation-GKP01	South Africa	490.18	3.1	1.1	
2.50	Kendall, B. et al. (2010)	Nauga Formation-GKP01	South Africa	491.89	2.5	1.0	
2.50	Kendall, B. et al. (2010)	Nauga Formation-GKP01	South Africa	493.33	3.0	0.9	
2.50	Kendall, B. et al. (2010)	Nauga Formation-GKP01	South Africa	494.51	3.2	0.9	
2.50	Kendall, B. et al. (2010)	Nauga Formation-GKP01	South Africa	495.75	3.6	1.4	
2.50	Kendall, B. et al. (2010)	Nauga Formation-GKP01	South Africa	637.14	1.8	1.1	
2.50	Kendall, B. et al. (2010)	Nauga Formation-GKP01	South Africa	637.72	1.5	1.1	
2.50	Kendall, B. et al. (2010)	Nauga Formation-GKP01	South Africa	638.15	1.8	1.2	
2.50	Kendall, B. et al. (2010)	Nauga Formation-GKP01	South Africa	638.56	1.7	1.2	
2.50	Kendall, B. et al. (2010)	Nauga Formation-GKP01	South Africa	639.35	1.5	1.5	
2.50	Kendall, B. et al. (2010)	Nauga Formation-GKP01	South Africa	639.83	1.4	0.9	

Age (Ga)	Reference/Source	Formation	Location	Sample	TOC	Mo	V
2.50	Kendall, B. et al. (2010)	Klein Naute Fm-GKF01	South Africa	234.20	1.9	6.1	
2.50	Kendall, B. et al. (2010)	Klein Naute Fm-GKF01	South Africa	235.19	1.4	4.8	
2.50	Kendall, B. et al. (2010)	Klein Naute Fm-GKF01	South Africa	236.03	0.7	4.3	
2.50	Kendall, B. et al. (2010)	Klein Naute Fm-GKF01	South Africa	241.94	3.9	13.3	
2.50	Kendall, B. et al. (2010)	Klein Naute Fm-GKF01	South Africa	263.74	2.4	3.6	
2.50	Kendall, B. et al. (2010)	Klein Naute Fm-GKF01	South Africa	264.43	4.2	6.5	
2.50	Kendall, B. et al. (2010)	Klein Naute Fm-GKF01	South Africa	264.92	3.7	5.5	
2.50	Kendall, B. et al. (2010)	Klein Naute Fm-GKF01	South Africa	265.67	1.9	6.2	
2.50	Kendall, B. et al. (2010)	Klein Naute Fm-GKF01	South Africa	266.60	3.3	9.4	
2.50	Kendall, B. et al. (2010)	Klein Naute Fm-GKF01	South Africa	267.46	3.0	2.4	
2.50	Kendall, B. et al. (2010)	Klein Naute Fm-GKF01	South Africa	267.93	6.1	9.4	
2.50	Kendall, B. et al. (2010)	Klein Naute Fm-GKF01	South Africa	268.75	5.6	8.6	
2.50	Kendall, B. et al. (2010)	Klein Naute Fm-GKF01	South Africa	269.58	6.4	11.7	
2.50	Kendall, B. et al. (2010)	Klein Naute Fm-GKF01	South Africa	271.90	12.7	18.9	
2.50	Kendall, B. et al. (2010)	Klein Naute Fm-GKF01	South Africa	272.71	9.8	21.8	
2.50	Kendall, B. et al. (2010)	Klein Naute Fm-GKF01	South Africa	273.57	9.2	16.4	
2.50	Kendall, B. et al. (2010)	Klein Naute Fm-GKF01	South Africa	274.23	10.5	19.0	
2.50	Kendall, B. et al. (2010)	Klein Naute Fm-GKF01	South Africa	275.45	5.1	7.1	
2.50	Kendall, B. et al. (2010)	Klein Naute Fm-GKF01	South Africa	277.55	4.5	4.4	
2.50	Kendall, B. et al. (2010)	Klein Naute Fm-GKF01	South Africa	278.47	3.8	4.8	
2.50	Kendall, B. et al. (2010)	Klein Naute Fm-GKF01	South Africa	279.40	3.9	1.3	
2.50	Kendall, B. et al. (2010)	Klein Naute Fm-GKF01	South Africa	280.02	5.0	6.9	
2.50	Kendall, B. et al. (2010)	Klein Naute Fm-GKF01	South Africa	281.35	3.5	2.3	
2.50	Kendall, B. et al. (2010)	Klein Naute Fm-GKF01	South Africa	282.47	1.8	0.6	
2.50	Kendall, B. et al. (2010)	Klein Naute Fm-GKF01	South Africa	283.50	4.1	2.1	
2.50	Kendall, B. et al. (2010)	Klein Naute Fm-GKF01	South Africa	284.68	3.8	2.1	
2.50	Kendall, B. et al. (2010)	Klein Naute Fm-GKF01	South Africa	285.30	3.6	1.4	
2.50	Kendall, B. et al. (2010)	Klein Naute Fm-GKF01	South Africa	286.81	6.6	5.6	
2.50	Kendall, B. et al. (2010)	Klein Naute Fm-GKF01	South Africa	288.10	12.5	15.2	
2.50	Kendall, B. et al. (2010)	Klein Naute Fm-GKF01	South Africa	289.05	3.1	4.0	
2.50	Kendall, B. et al. (2010)	Nauga Formation-GKF01	South Africa	439.64	3.4	1.6	
2.50	Kendall, B. et al. (2010)	Nauga Formation-GKF01	South Africa	440.30	3.8	2.1	
2.50	Kendall, B. et al. (2010)	Nauga Formation-GKF01	South Africa	441.67	4.0	2.3	
2.50	Kendall, B. et al. (2010)	Nauga Formation-GKF01	South Africa	442.49	3.8	2.7	
2.50	Kendall, B. et al. (2010)	Nauga Formation-GKF01	South Africa	443.51	3.6	2.5	
2.50	Kendall, B. et al. (2010)	Nauga Formation-GKF01	South Africa	444.70	3.5	2.6	
2.50	Kendall, B. et al. (2010)	Nauga Formation-GKF01	South Africa	445.88	3.7	2.2	
2.50	Kendall, B. et al. (2010)	Nauga Formation-GKF01	South Africa	446.51	3.8	2.4	
2.50	Kendall, B. et al. (2010)	Nauga Formation-GKF01	South Africa	447.19	4.0	2.4	
2.50	Kendall, B. et al. (2010)	Nauga Formation-GKF01	South Africa	448.16	4.7	2.3	
2.50	Kendall, B. et al. (2010)	Nauga Formation-GKF01	South Africa	448.68	3.7	2.4	
2.50	Kendall, B. et al. (2010)	Nauga Formation-GKF01	South Africa	449.13	3.5	2.4	
2.50	Kendall, B. et al. (2010)	Nauga Formation-GKF01	South Africa	450.40		1.5	
2.50	Kendall, B. et al. (2010)	Nauga Formation-GKF01	South Africa	451.38	2.9	1.5	
2.50	Kendall, B. et al. (2010)	Nauga Formation-GKF01	South Africa	452.15	2.6	1.5	
2.50	Kendall, B. et al. (2010)	Nauga Formation-GKF01	South Africa	452.90	2.9	1.9	

Age (Ga)	Reference/Source	Formation	Location	Sample	TOC	Mo	V
2.50	Kendall, B. et al. (2010)	Nauga Formation-GKF01	South Africa	453.80	2.7	1.5	
2.50	Kendall, B. et al. (2010)	Nauga Formation-GKF01	South Africa	454.71	2.8	1.5	
2.50	Kendall, B. et al. (2010)	Nauga Formation-GKF01	South Africa	616.11	2.1	0.9	
2.50	Kendall, B. et al. (2010)	Nauga Formation-GKF01	South Africa	617.00	2.8	1.2	
2.50	Kendall, B. et al. (2010)	Nauga Formation-GKF01	South Africa	618.00	2.6	1.1	
2.50	Kendall, B. et al. (2010)	Nauga Formation-GKF01	South Africa	618.86	2.4	0.9	
2.50	Kendall, B. et al. (2010)	Nauga Formation-GKF01	South Africa	619.81	2.1	0.9	
2.50	Kendall, B. et al. (2010)	Nauga Formation-GKF01	South Africa	620.27	1.7	0.8	
2.50	Kendall, B. et al. (2010)	Nauga Formation-GKF01	South Africa	620.88	1.3	0.7	
2.50	Kendall, B. et al. (2010)	Nauga Formation-GKF01	South Africa	621.88	1.2	0.7	
2.50	Kendall, B. et al. (2010)	Nauga Formation-GKF01	South Africa	623.07	1.2	0.7	
2.50	Kendall, B. et al. (2010)	Nauga Formation-GKF01	South Africa	625.18	1.7	0.9	
2.50	Kendall, B. et al. (2010)	Nauga Formation-GKF01	South Africa	625.90	1.6	0.8	
2.50	Kendall, B. et al. (2010)	Nauga Formation-GKF01	South Africa	626.54	1.9	0.5	
2.50	Kendall, B. et al. (2010)	Nauga Formation-GKF01	South Africa	627.00	2.7	1.1	
2.50	Kendall, B. et al. (2010)	Nauga Formation-GKF01	South Africa	829.35	2.7	0.2	
2.50	Kendall, B. et al. (2010)	Nauga Formation-GKF01	South Africa	830.46	1.8	0.9	
2.50	Kendall, B. et al. (2010)	Nauga Formation-GKF01	South Africa	831.24	2.2	1.3	
2.50	Kendall, B. et al. (2010)	Nauga Formation-GKF01	South Africa	831.58	1.7	0.9	
2.50	Kendall, B. et al. (2010)	Nauga Formation-GKF01	South Africa	832.36	2.0	1.4	
2.50	Kendall, B. et al. (2010)	Nauga Formation-GKF01	South Africa	833.84	2.0	0.8	
2.50	Kendall, B. et al. (2010)	Nauga Formation-GKF01	South Africa	835.10	2.0	1.1	
2.50	Kendall, B. et al. (2010)	Nauga Formation-GKF01	South Africa	836.30	1.9	0.7	
2.50	Kendall, B. et al. (2010)	Nauga Formation-GKF01	South Africa	836.94	1.8	1.1	
2.50	Kendall, B. et al. (2010)	Nauga Formation-GKF01	South Africa	837.70	1.4	0.8	
0	Böning, P. et al., (2004)	Peru margin	South America	126MC	2.0	22	156
0	Böning, P. et al., (2004)	Peru margin	South America	2MC	6.4	40	174
0	Böning, P. et al., (2004)	Peru margin	South America	5MC	7.0	66	184
0	Böning, P. et al., (2004)	Peru margin	South America	29MC	7.9	51	155
0	Böning, P. et al., (2004)	Peru margin	South America	120MC	9.8	74	250
0	Böning, P. et al., (2004)	Peru margin	South America	45MC	20.7	96	166
0	Böning, P. et al., (2004)	Peru margin	South America	104MC	16.8	96	281
0	Böning, P. et al., (2004)	Peru margin	South America	71MC	19.5	40	178
0	Böning, P. et al., (2004)	Peru margin	South America	18MC	20.6	117	419
0	Böning, P. et al., (2004)	Peru margin	South America	8MC	14.4	53	210
0	Böning, P. et al., (2004)	Peru margin	South America	1MC	21.3	39	458
0	Böning, P. et al., (2004)	Peru margin	South America	122MC	20.6	57	377
0	Böning, P. et al., (2004)	Peru margin	South America	35MC	6.2	27	87

Age (Ga)	Reference/Source	Formation	Location	Sample	TOC	Mo	V
0.18	Pearce et al., (2009)	Whitby Mudstone Formation	Yorkshire Coast, UK	Tfa 01-30 - 19.87 m	3.5	15.8	
0.18	Pearce et al., (2009)	Whitby Mudstone Formation	Yorkshire Coast, UK	Tfa 01-29 - 19.37 m	3.1	43.0	
0.18	Pearce et al., (2009)	Whitby Mudstone Formation	Yorkshire Coast, UK	Tfa 01-27 - 18.37 m	3.3	33.6	
0.18	Pearce et al., (2009)	Whitby Mudstone Formation	Yorkshire Coast, UK	Tfa 01-25 - 17.38 m	3.1	23.1	
0.18	Pearce et al., (2009)	Whitby Mudstone Formation	Yorkshire Coast, UK	Tfa 01-21 - 15.38 m	3.4	30.5	
0.18	Pearce et al., (2009)	Whitby Mudstone Formation	Yorkshire Coast, UK	Tfa 01-18 - 13.88 m	2.3	15.8	
0.18	Pearce et al., (2009)	Whitby Mudstone Formation	Yorkshire Coast, UK	Tfa 01-16 - 12.88 m	3.5	22.5	
0.18	Pearce et al., (2009)	Whitby Mudstone Formation	Yorkshire Coast, UK	Tfa 01-15 - 11.88 m	3.8	39.3	
0.18	Pearce et al., (2009)	Whitby Mudstone Formation	Yorkshire Coast, UK	Tfa 01-04 - 10.20 m	3.9	26.1	
0.18	Pearce et al., (2009)	Whitby Mudstone Formation	Yorkshire Coast, UK	Tfa 00-85 - 8.65 m	4.3	34.7	
0.18	Pearce et al., (2009)	Whitby Mudstone Formation	Yorkshire Coast, UK	Tfa 00-32 - 7.44 m	4.7	15.9	
0.18	Pearce et al., (2009)	Whitby Mudstone Formation	Yorkshire Coast, UK	Tex 00-81 - 6.15 m	3.8	9.5	
0.18	Pearce et al., (2009)	Whitby Mudstone Formation	Yorkshire Coast, UK	Tex 97-46 - 5.42 m	5.6	4.1	
0.18	Pearce et al., (2009)	Whitby Mudstone Formation	Yorkshire Coast, UK	Tex 00-22 - 4.68 m	6.0	7.6	
0.18	Pearce et al., (2009)	Whitby Mudstone Formation	Yorkshire Coast, UK	Tex 00-24 - 4.50 m	6.9	4.9	
0.181	Pearce et al., (2009)	Whitby Mudstone Formation	Yorkshire Coast, UK	Tex 00-25 - 4.30 m	6.6	6.3	
0.181	Pearce et al., (2009)	Whitby Mudstone Formation	Yorkshire Coast, UK	Tex 06-38 - 4.01 m	8.9	6.4	
0.181	Pearce et al., (2009)	Whitby Mudstone Formation	Yorkshire Coast, UK	Tex 06-28 - 3.86 m	14.7	7.5	
0.181	Pearce et al., (2009)	Whitby Mudstone Formation	Yorkshire Coast, UK	Tex 97-39 - 3.53 m	9.4	14.4	
0.181	Pearce et al., (2009)	Whitby Mudstone Formation	Yorkshire Coast, UK	Tex 97-27 - 3.31 m	10.2	15.6	
0.181	Pearce et al., (2009)	Whitby Mudstone Formation	Yorkshire Coast, UK	Tex 06-16 - 3.08 m	9.9	11.2	
0.181	Pearce et al., (2009)	Whitby Mudstone Formation	Yorkshire Coast, UK	Tex 06-08 - 2.95 m	8.6	7.6	
0.181	Pearce et al., (2009)	Whitby Mudstone Formation	Yorkshire Coast, UK	Tex 06-06 - 2.92 m	12.1	6.2	
0.181	Pearce et al., (2009)	Whitby Mudstone Formation	Yorkshire Coast, UK	Tex 06-01 - 2.81 m	8.8	7.8	
0.181	Pearce et al., (2009)	Whitby Mudstone Formation	Yorkshire Coast, UK	Tex 00-74 - 2.68 m	7.8	7.5	
0.181	Pearce et al., (2009)	Whitby Mudstone Formation	Yorkshire Coast, UK	Tex 00-73 - 2.18 m	9.1	5.5	
0.181	Pearce et al., (2009)	Whitby Mudstone Formation	Yorkshire Coast, UK	Tex 00-16 - 2.08 m	9.2	7.2	
0.181	Pearce et al., (2009)	Whitby Mudstone Formation	Yorkshire Coast, UK	Tex 01-02 - 1.80 m	9.9	7.1	
0.181	Pearce et al., (2009)	Whitby Mudstone Formation	Yorkshire Coast, UK	Tex 00-72 - 1.59 m	8.7	6.0	
0.181	Pearce et al., (2009)	Whitby Mudstone Formation	Yorkshire Coast, UK	Tex 97-09 - 1.38 m	9.0	6.0	
0.181	Pearce et al., (2009)	Whitby Mudstone Formation	Yorkshire Coast, UK	Tex 97-08 - 1.38 m	9.0	5.8	
0.181	Pearce et al., (2009)	Whitby Mudstone Formation	Yorkshire Coast, UK	TC05-A01 - 1.21 m	4.9	6.4	
0.181	Pearce et al., (2009)	Whitby Mudstone Formation	Yorkshire Coast, UK	Tex 00-14 - 1.16 m	5.1	6.8	
0.181	Pearce et al., (2009)	Whitby Mudstone Formation	Yorkshire Coast, UK	Tex 00-71 - 1.14 m	6.6	3.8	
0.181	Pearce et al., (2009)	Whitby Mudstone Formation	Yorkshire Coast, UK	TC05-A02 - 1.09 m	6.2	3.6	
0.181	Pearce et al., (2009)	Whitby Mudstone Formation	Yorkshire Coast, UK	TC05-A03 - 0.89 m	7.2	3.7	
0.181	Pearce et al., (2009)	Whitby Mudstone Formation	Yorkshire Coast, UK	Tex 00-13 - 0.67 m	6.9	3.8	
0.181	Pearce et al., (2009)	Whitby Mudstone Formation	Yorkshire Coast, UK	Tex 97-28 - 0.42 m	7.8	6.1	
0.181	Pearce et al., (2009)	Whitby Mudstone Formation	Yorkshire Coast, UK	Tex 97-32 - 0.15 m	8.8	7.3	
0.181	Pearce et al., (2009)	Whitby Mudstone Formation	Yorkshire Coast, UK	TC05-B01 - 0.06 m	3.5	8.0	
0.181	Pearce et al., (2009)	Whitby Mudstone Formation	Yorkshire Coast, UK	TC05-B02 - 0.04 m	3.6	6.8	
0.181	Pearce et al., (2009)	Whitby Mudstone Formation	Yorkshire Coast, UK	TC05-B03 - –0.01 m	4.8	4.0	
0.181	Pearce et al., (2009)	Whitby Mudstone Formation	Yorkshire Coast, UK	TC05-B04 - –0.16 m	5.4	4.4	
0.181	Pearce et al., (2009)	Whitby Mudstone Formation	Yorkshire Coast, UK	Tse 97-36 - –0.25 m	6.7	4.1	
0.181	Pearce et al., (2009)	Whitby Mudstone Formation	Yorkshire Coast, UK	TC05-C01 - –0.36 m	4.5	4.3	
0.182	Pearce et al., (2009)	Whitby Mudstone Formation	Yorkshire Coast, UK	Tse 00-68 - –0.46 m	4.2	6.7	
0.182	Pearce et al., (2009)	Whitby Mudstone Formation	Yorkshire Coast, UK	TC05-C02 - –0.63 m	4.4	5.9	
0.182	Pearce et al., (2009)	Whitby Mudstone Formation	Yorkshire Coast, UK	Tse 00-15 - –0.65 m	5.7	3.3	

Age (Ga)	Reference/Source	Formation	Location	Sample	TOC	Mo	V
0.182	Pearce et al., (2009)	Whitby Mudstone Formation	Yorkshire Coast, UK	TC05-C03 - –0.68 m	4.1	4.9	
0.182	Pearce et al., (2009)	Whitby Mudstone Formation	Yorkshire Coast, UK	TC05-C04 - –0.73 m	4.0	4.0	
0.183	McArthur et al., (2008)	Alum Shale Member	Yorkshire Coast, UK	67.66	1.2	2.7	
0.183	McArthur et al., (2008)	Alum Shale Member	Yorkshire Coast, UK	63.17	2.1	1	
0.183	McArthur et al., (2008)	Alum Shale Member	Yorkshire Coast, UK	57.47	2.7	5	
0.183	McArthur et al., (2008)	Alum Shale Member	Yorkshire Coast, UK	56.2	2	1	
0.183	McArthur et al., (2008)	Alum Shale Member	Yorkshire Coast, UK	55.34	2.3	3.2	
0.183	McArthur et al., (2008)	Alum Shale Member	Yorkshire Coast, UK	53.64	2.4	2.4	
0.183	McArthur et al., (2008)	Alum Shale Member	Yorkshire Coast, UK	51.87	2.1	2.5	
0.183	McArthur et al., (2008)	Alum Shale Member	Yorkshire Coast, UK	51.67	2.2	3.1	
0.183	McArthur et al., (2008)	Alum Shale Member	Yorkshire Coast, UK	51.52	1.8	3.3	
0.183	McArthur et al., (2008)	Alum Shale Member	Yorkshire Coast, UK	51.37	1.9	2.1	
0.183	McArthur et al., (2008)	Alum Shale Member	Yorkshire Coast, UK	50.5	2.8	8.6	
0.183	McArthur et al., (2008)	Alum Shale Member	Yorkshire Coast, UK	50.36	2.5	6.9	
0.183	McArthur et al., (2008)	Alum Shale Member	Yorkshire Coast, UK	49.63	2.4	7.2	
0.183	McArthur et al., (2008)	Alum Shale Member	Yorkshire Coast, UK	49.29	2.4	5.1	
0.183	McArthur et al., (2008)	Alum Shale Member	Yorkshire Coast, UK	49.19	2.5	6	
0.183	McArthur et al., (2008)	Alum Shale Member	Yorkshire Coast, UK	48.64	3.2	15.9	
0.183	McArthur et al., (2008)	Alum Shale Member	Yorkshire Coast, UK	47.02	2.6	4.4	
0.183	McArthur et al., (2008)	Alum Shale Member	Yorkshire Coast, UK	44.66	3.9	18.4	
0.183	McArthur et al., (2008)	Mulgrave Shale Member	Yorkshire Coast, UK	43.9	2.6	8.3	
0.183	McArthur et al., (2008)	Mulgrave Shale Member	Yorkshire Coast, UK	43.53	2.7	7.4	
0.183	McArthur et al., (2008)	Mulgrave Shale Member	Yorkshire Coast, UK	43.46	2.6	5.6	
0.183	McArthur et al., (2008)	Mulgrave Shale Member	Yorkshire Coast, UK	42.77	2.1	3.7	
0.183	McArthur et al., (2008)	Mulgrave Shale Member	Yorkshire Coast, UK	42.49	2.4	3.5	
0.183	McArthur et al., (2008)	Mulgrave Shale Member	Yorkshire Coast, UK	35.04	3.4	17.4	
0.183	McArthur et al., (2008)	Mulgrave Shale Member	Yorkshire Coast, UK	35	3.6	15	
0.183	McArthur et al., (2008)	Mulgrave Shale Member	Yorkshire Coast, UK	34.48	3.2	12.1	
0.183	McArthur et al., (2008)	Mulgrave Shale Member	Yorkshire Coast, UK	34.28	2.8	13.7	
0.183	McArthur et al., (2008)	Mulgrave Shale Member	Yorkshire Coast, UK	34.21	3	17.5	
0.183	McArthur et al., (2008)	Mulgrave Shale Member	Yorkshire Coast, UK	34.01	3.2	23.5	
0.183	McArthur et al., (2008)	Mulgrave Shale Member	Yorkshire Coast, UK	33.97	3.3	16.5	
0.183	McArthur et al., (2008)	Mulgrave Shale Member	Yorkshire Coast, UK	33.71	3.2	23	
0.183	McArthur et al., (2008)	Mulgrave Shale Member	Yorkshire Coast, UK	33.1	3.5	20.8	
0.183	McArthur et al., (2008)	Mulgrave Shale Member	Yorkshire Coast, UK	32.45	3.1	24.7	
0.183	McArthur et al., (2008)	Mulgrave Shale Member	Yorkshire Coast, UK	32.37	3.4	15.5	
0.183	McArthur et al., (2008)	Mulgrave Shale Member	Yorkshire Coast, UK	31.97	3.6	45	
0.183	McArthur et al., (2008)	Mulgrave Shale Member	Yorkshire Coast, UK	31.22	3	21.1	
0.183	McArthur et al., (2008)	Mulgrave Shale Member	Yorkshire Coast, UK	30.3	3.4	26.3	
0.183	McArthur et al., (2008)	Mulgrave Shale Member	Yorkshire Coast, UK	30.27	3.1	19.7	
0.183	McArthur et al., (2008)	Mulgrave Shale Member	Yorkshire Coast, UK	29.3	3.5	26.6	
0.183	McArthur et al., (2008)	Mulgrave Shale Member	Yorkshire Coast, UK	29.2	2.7	18.7	
0.183	McArthur et al., (2008)	Mulgrave Shale Member	Yorkshire Coast, UK	27.4	3.4	21.5	
0.183	McArthur et al., (2008)	Mulgrave Shale Member	Yorkshire Coast, UK	27.32	3.6	21.6	
0.183	McArthur et al., (2008)	Mulgrave Shale Member	Yorkshire Coast, UK	26.37	2.6	14	
0.183	McArthur et al., (2008)	Mulgrave Shale Member	Yorkshire Coast, UK	25.68	3.7	22.8	
0.183	McArthur et al., (2008)	Mulgrave Shale Member	Yorkshire Coast, UK	25.57	3.5	19.4	

Age (Ga)	Reference/Source	Formation	Location	Sample	TOC	Mo	V
0.183	McArthur et al., (2008)	Mulgrave Shale Member	Yorkshire Coast, UK	24.02	4.3	23.1	
0.183	McArthur et al., (2008)	Mulgrave Shale Member	Yorkshire Coast, UK	23.8	3	23.2	
0.183	McArthur et al., (2008)	Mulgrave Shale Member	Yorkshire Coast, UK	23.25	3.5	29	
0.183	McArthur et al., (2008)	Mulgrave Shale Member	Yorkshire Coast, UK	22.95	3.8	23.8	
0.183	McArthur et al., (2008)	Mulgrave Shale Member	Yorkshire Coast, UK	22.9	4.6	36.3	
0.183	McArthur et al., (2008)	Mulgrave Shale Member	Yorkshire Coast, UK	22.3	3.7	23.6	
0.183	McArthur et al., (2008)	Mulgrave Shale Member	Yorkshire Coast, UK	21.73	4.6	7.8	
0.183	McArthur et al., (2008)	Mulgrave Shale Member	Yorkshire Coast, UK	21.33	3.7	11.8	
0.183	McArthur et al., (2008)	Mulgrave Shale Member	Yorkshire Coast, UK	20.5	5.8	5.4	
0.183	McArthur et al., (2008)	Mulgrave Shale Member	Yorkshire Coast, UK	19.77	5	4.3	
0.183	McArthur et al., (2008)	Mulgrave Shale Member	Yorkshire Coast, UK	19.24	5.3	5.4	
0.183	McArthur et al., (2008)	Mulgrave Shale Member	Yorkshire Coast, UK	17.41	18.2	10.5	
0.183	McArthur et al., (2008)	Mulgrave Shale Member	Yorkshire Coast, UK	16.49	10.1	5.1	
0.183	McArthur et al., (2008)	Mulgrave Shale Member	Yorkshire Coast, UK	16.36	9.8	5.6	
0.183	McArthur et al., (2008)	Mulgrave Shale Member	Yorkshire Coast, UK	15.95	7.8	6.5	
0.183	McArthur et al., (2008)	Mulgrave Shale Member	Yorkshire Coast, UK	14.75	6.2	3.2	
0.183	McArthur et al., (2008)	Mulgrave Shale Member	Yorkshire Coast, UK	14.39	5.9	4.9	
0.183	McArthur et al., (2008)	Mulgrave Shale Member	Yorkshire Coast, UK	14.22	5.7	7.8	
0.183	McArthur et al., (2008)	Grey Shale Member	Yorkshire Coast, UK	13.88	3.7	4.7	
0.183	McArthur et al., (2008)	Grey Shale Member	Yorkshire Coast, UK	13.67	6.3	3.6	
0.183	McArthur et al., (2008)	Grey Shale Member	Yorkshire Coast, UK	13.22	5	5.5	
0.183	McArthur et al., (2008)	Grey Shale Member	Yorkshire Coast, UK	12.52	4.6	3.1	
0.183	McArthur et al., (2008)	Grey Shale Member	Yorkshire Coast, UK	11.78	4.7	5.1	
0.183	McArthur et al., (2008)	Grey Shale Member	Yorkshire Coast, UK	9.86	2	1.2	
0.183	McArthur et al., (2008)	Grey Shale Member	Yorkshire Coast, UK	8.55	1.6	1.7	
0.183	McArthur et al., (2008)	Grey Shale Member	Yorkshire Coast, UK	8.24	3.7	21.1	
0.183	McArthur et al., (2008)	Grey Shale Member	Yorkshire Coast, UK	5.11	2.1	4.1	
0.183	McArthur et al., (2008)	Grey Shale Member	Yorkshire Coast, UK	1.89	1.1	2.3	
0.183	McArthur et al., (2008)	Grey Shale Member	Yorkshire Coast, UK	1.25	1.9	1.4	
0.183	McArthur et al., (2008)	Grey Shale Member	Yorkshire Coast, UK	1.19	3	4.1	
0.183	McArthur et al., (2008)	Grey Shale Member	Yorkshire Coast, UK	0.86	1.5	2.4	
0.183	McArthur et al., (2008)	Grey Shale Member	Yorkshire Coast, UK	0.2	1.3	5.6	
0.183	McArthur et al., (2008)	Grey Shale Member	Yorkshire Coast, UK	0.15	2.6	13.9	
0.154	Tribovillard, et al., (1994)	Kimmeridge Clay Formation - Lower Layer	Yorkshire Coast, UK	128.2	2.7		161
0.154	Tribovillard, et al., (1994)	Kimmeridge Clay Formation - Lower Layer	Yorkshire Coast, UK	128.4	3.0	7	139
0.154	Tribovillard, et al., (1994)	Kimmeridge Clay Formation - Lower Layer	Yorkshire Coast, UK	126.5	4.0		184
0.154	Tribovillard, et al., (1994)	Kimmeridge Clay Formation - Lower Layer	Yorkshire Coast, UK	120.5	3.6	6	113
0.154	Tribovillard, et al., (1994)	Kimmeridge Clay Formation - Lower Layer	Yorkshire Coast, UK	126.6	5.2	17	263
0.154	Tribovillard, et al., (1994)	Kimmeridge Clay Formation - Lower Layer	Yorkshire Coast, UK	128.6	6.1	13	135
0.154	Tribovillard, et al., (1994)	Kimmeridge Clay Formation - Lower Layer	Yorkshire Coast, UK	128.6	4.6	12	196
0.154	Tribovillard, et al., (1994)	Kimmeridge Clay Formation - Lower Layer	Yorkshire Coast, UK	128.7	6.4	14	148
0.154	Tribovillard, et al., (1994)	Kimmeridge Clay Formation - Lower Layer	Yorkshire Coast, UK	128.7	7.6		187
0.154	Tribovillard, et al., (1994)	Kimmeridge Clay Formation - Lower Layer	Yorkshire Coast, UK	126.7	7.7	38	139
0.154	Tribovillard, et al., (1994)	Kimmeridge Clay Formation - Lower Layer	Yorkshire Coast, UK	128.3	7.5		169
0.154	Tribovillard, et al., (1994)	Kimmeridge Clay Formation - Lower Layer	Yorkshire Coast, UK	128.8	8.8		149
0.154	Tribovillard, et al., (1994)	Kimmeridge Clay Formation - Lower Layer	Yorkshire Coast, UK	126.8	9.5		144
0.154	Tribovillard, et al., (1994)	Kimmeridge Clay Formation - Lower Layer	Yorkshire Coast, UK	126.8	8.0		162
0.154	Tribovillard, et al., (1994)	Kimmeridge Clay Formation - Lower Layer	Yorkshire Coast, UK	128.8	5.3		171

Age (Ga)	Reference/Source	Formation	Location	Sample	TOC	Mo	V
0.154	Tribovillard, et al., (1994)	Kimmeridge Clay Formation - Lower Layer	Yorkshire Coast, UK	126.8	8.6		177
0.154	Tribovillard, et al., (1994)	Kimmeridge Clay Formation - Lower Layer	Yorkshire Coast, UK	126.8	5.8		168
0.154	Tribovillard, et al., (1994)	Kimmeridge Clay Formation - Lower Layer	Yorkshire Coast, UK	128.8	6.5		188
0.154	Tribovillard, et al., (1994)	Kimmeridge Clay Formation - Lower Layer	Yorkshire Coast, UK	128.9	6.9		170
0.154	Tribovillard, et al., (1994)	Kimmeridge Clay Formation - Lower Layer	Yorkshire Coast, UK	128.9	7.0		185
0.154	Tribovillard, et al., (1994)	Kimmeridge Clay Formation - Lower Layer	Yorkshire Coast, UK	129.0	4.8	15	143
0.154	Tribovillard, et al., (1994)	Kimmeridge Clay Formation - Lower Layer	Yorkshire Coast, UK	129.1	1.5	4	186
0.154	Tribovillard, et al., (1994)	Kimmeridge Clay Formation - Lower Layer	Yorkshire Coast, UK	129.2	1.8		132
0.154	Tribovillard, et al., (1994)	Kimmeridge Clay Formation - Upper Layer	Yorkshire Coast, UK	121.6	4.4	8	437
0.154	Tribovillard, et al., (1994)	Kimmeridge Clay Formation - Upper Layer	Yorkshire Coast, UK	121.5	8.1	40	420
0.154	Tribovillard, et al., (1994)	Kimmeridge Clay Formation - Upper Layer	Yorkshire Coast, UK	121.5	12.3	160	402
0.154	Tribovillard, et al., (1994)	Kimmeridge Clay Formation - Upper Layer	Yorkshire Coast, UK	121.4	20.0	220	328
0.154	Tribovillard, et al., (1994)	Kimmeridge Clay Formation - Upper Layer	Yorkshire Coast, UK	121.4	28.9	200	242
0.154	Tribovillard, et al., (1994)	Kimmeridge Clay Formation - Upper Layer	Yorkshire Coast, UK	121.4	31.4	200	223
0.154	Tribovillard, et al., (1994)	Kimmeridge Clay Formation - Upper Layer	Yorkshire Coast, UK	121.4	17.5	130	418
0.154	Tribovillard, et al., (1994)	Kimmeridge Clay Formation - Upper Layer	Yorkshire Coast, UK	121.4	13.7	140	375
0.154	Tribovillard, et al., (1994)	Kimmeridge Clay Formation - Upper Layer	Yorkshire Coast, UK	121.3	13.8	120	410
0.154	Tribovillard, et al., (1994)	Kimmeridge Clay Formation - Upper Layer	Yorkshire Coast, UK	121.3	9.2	160	396
0.154	Tribovillard, et al., (1994)	Kimmeridge Clay Formation - Upper Layer	Yorkshire Coast, UK	121.3	15.6	110	362
0.154	Tribovillard, et al., (1994)	Kimmeridge Clay Formation - Upper Layer	Yorkshire Coast, UK	121.2	11.5	60	389
0.154	Tribovillard, et al., (1994)	Kimmeridge Clay Formation - Upper Layer	Yorkshire Coast, UK	121.2	7.7	30	409
0.154	Tribovillard, et al., (1994)	Kimmeridge Clay Formation - Upper Layer	Yorkshire Coast, UK	121.1	9.1	60	394
0.154	Tribovillard, et al., (1994)	Kimmeridge Clay Formation - Upper Layer	Yorkshire Coast, UK	121.0	14.2	200	359
0.154	Tribovillard, et al., (1994)	Kimmeridge Clay Formation - Upper Layer	Yorkshire Coast, UK	121.0	5.4	70	327
0.392	Gordon et al., (2009)	Oatka Creek Formation	New York, USA	329.48	0.8	2	
0.392	Gordon et al., (2009)	Oatka Creek Formation	New York, USA	333.12	8.7	173	
0.392	Gordon et al., (2009)	Oatka Creek Formation	New York, USA	334.63	11.2	251	
0.392	Gordon et al., (2009)	Oatka Creek Formation	New York, USA	335.87	9.5	192	
0.392	Gordon et al., (2009)	Oatka Creek Formation	New York, USA	336.69	17.3	394	
0.392	Gordon et al., (2009)	Oatka Creek Formation	New York, USA	338.53	4.8	15	
0.392	Gordon et al., (2009)	Oatka Creek Formation	New York, USA	341.09	0.4	1	
0.365	Dahl et al., (2010)	Clegg Creek	New Albany, USA	Clegg 873-B8+22	12.3	219.9	
0.365	Dahl et al., (2010)	Clegg Creek	New Albany, USA	Clegg 873-B10+69	9.4	157.5	
0.367	Dahl et al., (2010)	Chattanooga Shale	New Albany, USA	Chattanoga K8/7/94-22	13.6	118.0	
0.367	Dahl et al., (2010)	Chattanooga Shale	New Albany, USA	Chattanoga K8/7/94-23	14.7	127.7	
0.440	Dahl et al., (2010)	Birkhill Shale, Dobs Linn outcrop,	Scotland	DL6 - 13.30 m	1.44	17.5	
0.440	Dahl et al., (2010)	Rastrites Shale, Billegrav-1 core	Sweden	BG-4 - 26.55 m	1.99	17.5	
0.440	Dahl et al., (2010)	Rastrites Shale, Lönstorp-1 core	Sweden	Lön97154 - 64.90 m		16.9	
0.440	Dahl et al., (2010)	Rastrites Shale, Lönstorp-1 core	Sweden	Lön79002 - 72.40 m		6.8	
0.465	Dahl et al., (2010)	Almelund Shale, Albjära-1 core	Sweden	Alb79013 - 50.10 m	2.1	6.1	
0.465	Dahl et al., (2010)	Almelund Shale, Albjära-1 core	Sweden	Alb79016 - 94.90 m	1.9	5.4	
0.485	Dahl et al., (2010)	Alum Shale Formation, Albjära-1 core	Sweden	Alb97160 - 139.03 m	4.6	32.6	
0.485	Dahl et al., (2010)	Alum Shale Formation, Gislövhammar-2 core	Sweden	Gis89934 - 24.03 m	7.3	57.0	
0.485	Dahl et al., (2010)	Alum Shale Formation, Gislövhammar-2 core	Sweden	Gis89933 - 26.00 m	8.7	118.6	
0.485	Dahl et al., (2010)	Alum Shale Formation, Gislövhammar-2 core	Sweden	Gis89931 - 28.00 m	7.3	104.3	

Age (Ga)	Reference/Source	Formation	Location	Sample	TOC	Mo	V
0.500	Dahl et al., (2010)	Alum Shale Formation, Andrarum-3 core	Sweeden	Alum0760 - 7.60 m	12.4	125.4	
0.500	Dahl et al., (2010)	Alum Shale Formation, Andrarum-3 core	Sweeden	Alum1128 - 11.28 m	9.1	64.7	
0.500	Dahl et al., (2010)	Alum Shale Formation, Andrarum-3 core	Sweeden	Alum1178 - 11.78 m	7.1	44.5	
0.500	Dahl et al., (2010)	Alum Shale Formation, Andrarum-3 core	Sweeden	Alum1200 - 12.00 m	9.1	53.4	
0.500	Dahl et al., (2010)	Alum Shale Formation, Andrarum-3 core	Sweeden	Alum1300 - 13.00 m	9.1	41.0	
0.500	Dahl et al., (2010)	Alum Shale Formation, Andrarum-3 core	Sweeden	Alum1370 -13.70 m	7.5	48.2	
0.533	Dahl et al., (2010)	Niutitang Formation, Ganziping	China	Ganziping - ZG-3 - –0.70 m	11.9	209	
0.532	Dahl et al., (2010)	Niutitang Formation, Ganziping	China	Ganziping - ZG-7 - 1.50 m	11	115	
0.532	Dahl et al., (2010)	Niutitang Formation, Ganziping	China	Ganziping - ZG-11 - 1.80 m	9.4	102	
0.532	Dahl et al., (2010)	Niutitang Formation, Ganziping	China	Ganziping - ZG-17 - 4.50 m	7.2	293	
0.531	Dahl et al., (2010)	Niutitang Formation, Ganziping	China	Ganziping - ZG-26 - 46.50 m	1.7	54	
0.531	Dahl et al., (2010)	Niutitang Formation, Ganziping	China	Ganziping - ZG-29 - 61.30 m	4.8	35	
0.532	Dahl et al., (2010)	Niutitang Formation, Yuanling	China	Yuanling - L-60 - 0.00 m	7.4	22	
0.530	Dahl et al., (2010)	Niutitang Formation, Yuanling	China	Yuanling - L-66 - 6.00 m	9.6	12	
0.540	Dahl et al., (2010)	Ara Group, MMNW Core	Oman	MMNW-7 - 2860 m		132.3	
0.540	Dahl et al., (2010)	Ara Group, MMNW Core	Oman	MMNW-7 - 2840 m	2.9	36.3	
0.540	Dahl et al., (2010)	Ara Group, MMNW Core	Oman	MMNW-7 - 2670 m	2.63	57.7	
0.540	Dahl et al., (2010)	Ara Group, MMNW Core	Oman	MMNW-7 - 2640 m		17	
0.540	Dahl et al., (2010)	Ara Group, MMNW Core	Oman	MMNW-7 - 2535 m	11.58	76.2	
0.540	Dahl et al., (2010)	Ara Group, MMNW Core	Oman	ALNR-1 - 4484 m	4.42	45.7	
0.540	Dahl et al., (2010)	Ara Group, MMNW Core	Oman	ALNR-1 - 4330 m	1.53	23.6	
0.540	Dahl et al., (2010)	Ara Group, MMNW Core	Oman	ALNR-1 - 4282 m	2.37	24.4	
0.540	Dahl et al., (2010)	Ara Group, ALNR-1 Core	Oman	ALNR-1 - 4136 m	3.85	20.5	
0.540	Dahl et al., (2010)	Ara Group, ALNR-1 Core	Oman	ALNR-1 - 4096 m	3.07	16.4	
0.663	Li, C. et al., (2012)	Datangpo Formation, Minle Section	South China	ML-16	0.1	1.4	
0.663	Li, C. et al., (2012)	Datangpo Formation, Minle Section	South China	ML-15	0.1	0.9	
0.663	Li, C. et al., (2012)	Datangpo Formation, Minle Section	South China	ML-10	3.9	3.8	
0.663	Li, C. et al., (2012)	Datangpo Formation, Minle Section	South China	ML-09	3.6	5	
0.663	Li, C. et al., (2012)	Datangpo Formation, Minle Section	South China	ML-08	3.1	8.6	
0.663	Li, C. et al., (2012)	Datangpo Formation, Minle Section	South China	ML-07	2.1	10.2	
0.663	Li, C. et al., (2012)	Datangpo Formation, Minle Section	South China	ML-06	1.9	3.6	
0.663	Li, C. et al., (2012)	Datangpo Formation, Minle Section	South China	ML-05	2	14	
0.663	Li, C. et al., (2012)	Datangpo Formation, Minle Section	South China	ML-04	2.4	15	
0.663	Li, C. et al., (2012)	Datangpo Formation, Minle Section	South China	ML-03	1.6	7	
0.663	Li, C. et al., (2012)	Datangpo Formation, Minle Section	South China	ML-02	1.7	9	
0.663	Li, C. et al., (2012)	Datangpo Formation, Minle Section	South China	ML-01	1.9	39	
0.663	Li, C. et al., (2012)	Datangpo Formation, Yangjiaping Section	South China	SH-06	0.1	0.6	
0.663	Li, C. et al., (2012)	Datangpo Formation, Yangjiaping Section	South China	SH-02	0.4	1.6	
0.663	Li, C. et al., (2012)	Datangpo Formation, Yangjiaping Section	South China	SH-05	3.8	31.9	
1.8	Kendall, B. et al. (2011)	Rove Formation, 89-MC-1 Core	Canada	R40 - 352.5 m	2.22	32	
1.8	Kendall, B. et al. (2011)	Rove Formation, 89-MC-1 Core	Canada	R39 - 344.0 m	1.7	20	
1.8	Kendall, B. et al. (2011)	Rove Formation, 89-MC-1 Core	Canada	R38 - 342.5 m	0.48	10.5	
1.8	Kendall, B. et al. (2011)	Rove Formation, 89-MC-1 Core	Canada	R35 - 325.0 m	1.7	24	
1.8	Kendall, B. et al. (2011)	Rove Formation, 89-MC-1 Core	Canada	R34 - 323.0 m	1.75	20	
1.8	Kendall, B. et al. (2011)	Rove Formation, 89-MC-1 Core	Canada	R33 - 317.0 m	3.14	32	
1.8	Kendall, B. et al. (2011)	Rove Formation, 89-MC-1 Core	Canada	R32 - 315.0 m	3.22	35	
1.8	Kendall, B. et al. (2011)	Rove Formation, 89-MC-1 Core	Canada	R31 - 314.0 m	3.93	42	
1.8	Kendall, B. et al. (2011)	Rove Formation, 89-MC-1 Core	Canada	R30 - 310.5 m	2.7	24	
1.8	Kendall, B. et al. (2011)	Rove Formation, 89-MC-1 Core	Canada	R29 - 310.0 m	2.8	29	

Supplementary Table S3B Additional new data used for the compilation of the secular trends of Mo, Mo/TOC, V, and V/TOC

Age (Ga)	Formation	Location	Samples	TOC	Fe_{HR}/Fe_T	Fe_{PY}/Fe_{HR}	DOP	Mo	V
0.64	Black River Dolomite	Forest-1 Core, Australia and Tasmania	RC06-FOR01-A - 835.84-835.87 m	5.1	1.03	0.94		13.9	194
0.64	Black River Dolomite	Forest-1 Core, Australia and Tasmania	RC06-FOR01-B - 835.77-835.79 m	5.6	0.99	0.95		14.1	197
0.64	Black River Dolomite	Forest-1 Core, Australia and Tasmania	RC06-FOR01-C - 835.70-835.72 m	5.3	1.11	0.96		13.9	204
0.64	Black River Dolomite	Forest-1 Core, Australia and Tasmania	RC06-FOR01-D - 835.65-835.68 m	5.6	0.98	0.95		12.4	195
0.64	Black River Dolomite	Forest-1 Core, Australia and Tasmania	RC06-FOR01-E - 835.58-835.62 m	5.3	1.02	0.95		12.0	196
0.64	Black River Dolomite	Forest-1 Core, Australia and Tasmania	RC06-FOR02-B - 828.11-828.15 m	6.5	0.79	0.93		29.2	321
0.64	Black River Dolomite	Forest-1 Core, Australia and Tasmania	RC06-FOR02-D - 828.23-828.27 m	6.6	0.80	0.93		28.9	327
0.64	Black River Dolomite	Forest-1 Core, Australia and Tasmania	RC06-FOR02-G - 828.37-828.40 m	6.5	0.80	0.93		32.9	367
0.64	Black River Dolomite	Forest-1 Core, Australia and Tasmania	RC06-FOR02-H - 828.48-828.50 m	6.4	0.90	0.93		30.2	345
0.64	Black River Dolomite	Forest-1 Core, Australia and Tasmania	RC06-FOR02-I - 828.55 - 828.58 m	6.8	0.81	0.90		28.8	349
2.05	Zaonezhskaya Fm., Ludikovian Series	Karelia, Russia	C-5190-83	9.3			0.5	7	128
2.05	Zaonezhskaya Fm., Ludikovian Series	Karelia, Russia	C34-64.8	10.2			0.9	74	1954
2.05	Zaonezhskaya Fm., Ludikovian Series	Karelia, Russia	C34-90.7	0.4			0.9	4	70
2.05	Zaonezhskaya Fm., Ludikovian Series	Karelia, Russia	C34-96.5	1.8			0.8	28	1296
2.1	Sengoma Argillite Formation, Pretoria Series	Lobatse, Botswana	171.5	10			0.8	1.6	88
2.1	Sengoma Argillite Formation, Pretoria Series	Lobatse, Botswana	186.57	11			0.7	48.9	1198
2.1	Sengoma Argillite Formation, Pretoria Series	Lobatse, Botswana	200.7	13.3			0.9	10.0	128
2.1	Sengoma Argillite Formation, Pretoria Series	Lobatse, Botswana	202.5	15.5			0.9	6.8	159
2.1	Sengoma Argillite Formation, Pretoria Series	Lobatse, Botswana	205.25	14.2			0.9	26.3	160
2.1	Sengoma Argillite Formation, Pretoria Series	Lobatse, Botswana	209	15.9			0.8	7.4	133
2.1	Sengoma Argillite Formation, Pretoria Series	Lobatse, Botswana	212.7	16			0.7	8.0	112
2.53	Gamhaan Formation	South Africa	WB-98507.39	3			0.5	2.9	21
2.62	Jeerinah Formation, Fortescue Group	WA, Australia	FVG-1 707.95	10.4			0.9	5	110
2.62	Jeerinah Formation, Fortescue Group	WA, Australia	FVG-1752.65	6			0.8	2	98
2.62	Jeerinah Formation, Fortescue Group	WA, Australia	FVG-1765.8	9.9			0.7	2	53
2.62	Jeerinah Formation, Fortescue Group	WA, Australia	FVG-1774	4.4			0.9	3	73
2.62	Jeerinah Formation, Fortescue Group	WA, Australia	FVG-1794.1	4.7			0.7	4	95

APPENDIX B: CHAPTER 3

1. Data Repository

1.1 Depositional ages of the stratigraphic units in the Wuhe section, Guizhou Province, South China

The Wuhe section (GPS coordinates: 26°45'93.6"N, 108°25'0.5"E) in Guizhou Province, South China is paleogeographically located in the lower slope of the Ediacaran Yangtze platform (Jiang et al., 2011). Well-exposed strata in this locality include the Doushantuo (120 m), Dengying (12 m), Liuchapo (40 m) Formations and a few meters of the basal Niutitang Formation. The Doushantuo Formation can be divided into four distinct members (Member I–IV) that are roughly correlatable with those in the Yangtze Gorges area (Jiang et al., 2011). The base of the Doushantuo Formation consists of a 2.3-m-thick cap carbonate (Member I) that overlies the glacial diamictite of the Nantuo Formation and serves as a marker for regional stratigraphic correlation (Jiang et al., 2006). The top of the Doushantuo Formation is characterized by 3.5- to 5-m-thick, organic-rich black shales with sparse fist-sized phosphatic-pyrite nodules (Member IV). This black shale interval is also a distinctive marker across the Ediacaran Yangtze platform that is correlatable with the Member IV black shales in the Yangtze Gorges area (Jiang et al., 2011), the top of which has been dated at 551.1 ± 0.7 Ma (Condon et al., 2005). The majority of the Doushantuo Formation consists of laminated black shales with subordinate micritic or microcrystalline dolostone and a few layers of olistostrome dolostone breccias. In the middle of the Doushantuo Formation, a thick (2.5 m) carbonate breccia layer may record a regional stratigraphic discontinuity that has been tentatively correlated across the Yangtze platform (Jiang et al., 2007, 2011). This interval also marks the Member II and III boundary (Fig. 2 in main text).

The 12-m-thick Dengying Formation in this section is composed of micritic-microcrystalline dolostone with lenticular chert beds or nodules. This unit is most likely time-equivalent to the lowermost portion (Hamajing Member) of the Dengying Formation in the Yangtze Gorges area (Jiang et al., 2007, 2011; Zhou and Xiao, 2007). The overlying Liuchapo Formation consists of 40-m-thick black cherts with thin black shale interbeds, which is in turn overlain by phosphatic organic-rich black shale of the Niutitang Formation, which is also locally named as the Jiumenchong Formation in some literature. Only a few meters of the basal Niutitang Formation are continuously exposed in this section. The base of the Nititang Formation contains sponge spicules in the sampling locality and has trilobites in correlative shallow-water sections, and thus it is certainly of Cambrian age.

Based on the distinctive marker beds and regional stratigraphic correlation with those in the Yangtze Gorges area, the base and top of the Doushantuo Formation is reasonably assigned as ca. 635 Ma and ca. 551 Ma, respectively. Regional stratigraphic analyses would also correlate the Member II-Member III transition with the regional stratigraphic discontinuity in shallow-water facies (Jiang et al., 2007, 2011). If this regional discontinuity recorded a sea-level fall event, it might be time-equivalent with the Gaskiers glaciation at ca. 580 Ma. This age is also roughly consistent with the age estimate based on a simple scaling with known radiometric ages (Condon et al., 2005) and thickness, assuming that no substantial gaps of missing time. The Liuchapo-Niutitang boundary is traditionally considered as the Ediacaran-Cambrian (E-C) boundary, but a recent U-Pb age of 522.7 ± 4.9 Ma (Wang et al., 2012) from the base of the Niutitang

Formation in an adjacent section in Taoying suggested that the E-C boundary may be located within the Liuchapo Formation.

1.2 Sampling

Samples were collected at an average spacing of 20-50 cm (depending on the availability of black shales) along the eastern side of the Qingshui River in a dry season when part of river channel was exposed, leaving fresh and clean outcrops. Large samples (0.5-1 kg) were collected from the field and cut into slabs in labs before powdering. Only the center part of samples without macroscopic pyrites was used for chemical analyses.

1.3 Analytical methods

Major and trace elemental abundances, iron speciation, and total organic carbon (TOC) were mostly analyzed at the Biogeochemistry lab at the University of California, Riverside (UCR). A portion of the samples were analyzed at the W. M. Keck Foundation Laboratory for Environmental Biogeochemistry, Arizona State University (ASU). Sample preparation and analyses follow the previously published methods (Poulton and Canfield, 2005; Scott et al., 2008; Li et al., 2010; Kendall et al., 2010).

Powdered sample splits were ashed for 8-10 hours at 550°C and dissolved completely by HF-HNO3-HCL acid digestion. Trace and major element concentrations were determined on a TheroFinnigan X-Series (ASU) and Agilent 7500E (UCR) quadrupole ICP-MS (inductively coupled plasma mass spectrometry). Accuracy and precision were monitored with duplicate samples and the US Geological Survey Devonian black shale standard SDO-1, and reproducibility in individual runs was better than 95% for the presented elements.

Biogeochemically highly reactive iron (Fe_{HR}) is defined as pyrite iron (Fe_{PY}) plus other iron phases that are potentially reactive with hydrogen sulphide on diagenetic time scales: carbonate-associated iron (Fe_{Carb}), ferric oxides (Fe_{Ox}), and magnetite (Fe_{Mag}). Hence highly reactive iron $Fe_{HR} = Fe_{PY} + Fe_{Carb} + Fe_{Ox} + Fe_{Mag}$ (Poultom and Canfield, 2005). Fe_{PY} was calculated (assuming a stoichiometry of FeS_2) from the weight percentage of sulphur extracted during a 2 hour hot chromous chloride distillation followed by iodometric titration. Other iron species including Fe_{Carb}, Fe_{Ox}, and Fe_{Mag} were extracted sequentially using sodium acetate solution (for Fe_{Carb}), dithionite solution (for Fe_{Ox}), and ammonium oxalate (Fe_{Mag}).

The sequential extracts were analyzed with an Agilent 7500ce ICP-MS. Total iron concentrations (Fe_T) were determined by HF-HNO_3-HCl acid digestion followed by ICP-MS analysis. Reproducibility of iron measurements, monitored by duplicate analyses within and between sample batches, was better than 94%. Total organic carbon (TOC) contents were determined by taking the difference between carbonate carbon liberated by 4M HCl and total carbon released by combustion at 1,400°C, both of which were measured with an Eltra C/S determinator at UCR (Scott et al., 2008; Sahoo et al., 2012).

Pyrite sulfur was extracted for isotope measurements using chromous chloride distillation and reprecipitation as Ag_2S. Suphur isotope measurements were made with a ThermoFinnigan Delta V continuous-flow stable-isotope-ratio mass spectrometer at UCR. Sulphur isotope data are reported as per mil (‰) deviations from the isotope composition of Vienna Cañon Diablo Troilite (VCDT). Reproducibility was better than 0.2% on the basis of single-run and long-term standard monitoring.

Table DR1: Geochemical data from the Wuhe section.

Sample No.	Strat. Height (m)	Lithology	TIC (Wt %)	C_{org} (Wt %)	S_{PY} (Wt %)	C_{Org}/S_{PY}	$\delta^{34}S_{PY}$ (‰)	Fe_{Mag} (Wt %)	Fe_{Oxide} (Wt %)	Fe_{Carb} (Wt %)	Fe_{PY} (Wt %)	Fe_{HR} (Wt %)	Fe_{T} (Wt %)	Fe_{HR}/Fe_{T}	Fe_{PY}/Fe_{HR}	DOP
WH09-2.4	2.4	Black Shale	0.0	0.7	0.2	4.1		0.0	0.2	0.0	0.2	0.4	2.2	0.17	0.41	0.17
WH09-2.7	2.7	Black Shale	0.0	0.6	0.2	3.6	-17.2	0.1	0.3	0.0	0.1	0.5	1.7	0.29	0.29	
WH09-3	3.0	Black Shale	0.2	0.8	0.6	1.3	-32.3	0.0	0.1	0.1	0.6	0.8	1.9	0.39	0.73	
WH09-3.2	3.2	Black Shale	0.0	0.9	1.4	0.7	-32.8	0.0	0.0	0.0	1.2	1.3	2.6	0.49	0.97	0.68
WH09-3.5	3.5	Black Shale	0.0	0.8	0.2	3.8	-34.6	0.2	0.4	0.0	0.2	0.8	2.1	0.40	0.23	
WH09-3.7	3.7	Black Shale	0.0	1.3	2.0	0.6	-33.7	0.1	0.1	0.1	1.7	2.0	3.2	0.63	0.87	
WH09-4	4.0	Black Shale	0.1	0.9	0.9	1.1	-32.8	0.0	0.1	0.0	0.7	0.9	2.3	0.38	0.85	
WH09-4.3	4.3	Black Shale	0.0	1.2	2.2	0.5	-34.9	0.0	0.0	0.1	1.9	2.1	3.9	0.54	0.91	
WH09-4.6	4.6	Black Shale	2.1	0.8	1.3	0.6	-29.1	0.0	0.1	0.7	1.1	2.0	3.2	0.62	0.57	
WH09-4.8	4.8	Black Shale	0.2	1.2	0.7	1.8	-30.6	0.0	0.1	0.1	0.6	0.8	2.6	0.30	0.72	
WH09-5.0	5.0	Calcareous Black Shale	7.5	0.5	1.5	0.3	-26.8	0.4	0.0	2.0	1.3	3.7	5.3	0.70	0.34	0.25
WH09-5.4	5.4	Black Shale	1.4	1.3	1.8	0.7	-32.4	0.0	0.0	0.4	1.6	2.0	3.1	0.64	0.79	
WH09-5.6	5.6	Calcareous Black Shale	3.5	1.1	1.7	0.7	-30.5	0.0	0.1	0.9	1.4	2.5	4.0	0.63	0.58	
WH09-5.8	5.8	Calcareous Black Shale	3.1	0.8	1.8	0.4	-29.8	0.0	0.1	0.8	1.5	2.4	3.5	0.69	0.64	
WH09-6.0	6.0	Black Shale	0.0	1.4	3.0	0.5	-33.7	0.0	0.0	0.0	2.6	2.6	3.8	0.69	1.00	
WH09-6.3	6.3	Black Shale	0.0	1.4	3.1	0.5	-33.5	0.0	0.0	0.0	2.7	2.7	3.8	0.70	0.99	
WH09-6.5	6.5	Black Shale	0.0	1.2	0.0	30.2	-32.5	0.0	0.7	0.0	0.0	0.7	2.5	0.29	0.05	
WH09-6.8	6.8	Black Shale	0.0	1.2	1.5	0.8	-32.4	0.0	0.0	0.0	1.3	1.4	2.9	0.48	0.97	
WH09-7.0	7.0	Black Shale	0.1	1.2	2.2	0.5	-31.1	0.0	0.0	0.1	1.9	2.1	3.4	0.62	0.91	
WH09-7.3	7.3	Black Shale	0.5	1.3	1.7	0.7	-30.0	0.0	0.0	0.3	1.5	1.8	2.9	0.62	0.83	0.31
WH09-8.6	8.6	Black Shale	0.8	1.2	2.5	0.5	-31.6	0.0	0.0	0.3	2.2	2.5	3.8	0.67	0.87	
WH09-9.4	9.4	Black Shale	0.5	0.8	2.3	0.3	-31.7	0.0	0.1	0.2	2.0	2.3	3.4	0.68	0.86	
WH09-9.7	9.7	Black Shale	0.2	1.3	2.2	0.6	-32.0	0.0	0.0	0.2	1.9	2.1	3.0	0.71	0.91	0.73
WH09-11.6	11.6	Black Shale	0.0	1.3	2.2	0.6	-30.1	0.0	0.0	0.1	1.9	2.0	3.0	0.67	0.95	0.75
WH09-13.7	13.7	Calcareous Black Shale	4.0	0.6	1.8	0.3	-21.0	0.0	0.0	0.7	1.6	2.2	2.5	0.91	0.70	0.60
WH09-21.5	21.5	Black Shale	0.2	0.9	1.9	0.5	-17.6	0.0	0.1	0.1	1.7	1.9	3.0	0.64	0.87	0.63
WH09-24.1	24.1	Black Shale	0.3	1.0	2.8	0.4	-10.6	0.0	0.0	0.2	2.5	2.6	3.7	0.71	0.93	0.71
WH09-26.0	26.0	Black Shale	0.3	1.9	2.8	0.7	0.3	0.0	0.0	0.2	2.4	2.6	3.3	0.81	0.93	0.80
WH09-29.0	29.0	Black Shale	0.2	1.6	3.1	0.5	-3.6	0.0	0.0	0.1	2.7	2.8	3.7	0.76	0.95	0.84
WH09-32.4	32.4	Black Shale	2.0	1.3	2.8	0.5	3.0	0.0	0.0	0.1	2.4	2.5	2.9	0.88	0.95	0.88
WH09-35.1	35.1	Black Shale	0.7	2.2	2.5	0.9	3.8	0.0	0.0	0.1	2.2	2.3	2.6	0.88	0.97	0.90
WH09-38.5	38.5	Calcareous Black Shale	3.3	1.4	2.6	0.5	4.5	0.0	0.0	0.1	2.3	2.4	3.9	0.62	0.95	0.88
WH09-41.1	41.1	Black Shale	0.7	2.5	3.6	0.7	3.5	0.0	0.0	0.1	3.1	3.2	3.6	0.88	0.97	0.91
WH09-44.3	44.3	Calcareous Black Shale	7.1	1.7	1.7	1.0	5.5	0.0	0.0	0.2	1.4	1.7	1.9	0.90	0.86	0.77
WH09-47.5	47.5	Black Shale	0.7	5.7	3.2	1.8	5.7	0.0	0.0	0.2	2.8	2.9	2.4	1.00	0.95	0.92
WH09-50.1	50.1	Calcareous Black Shale	3.4	3.6	2.6	1.4	1.8	0.0	0.0	0.2	2.3	2.4	2.6	0.94	0.94	0.89
WH09-53.4	53.4	Black Shale	0.8	3.3	3.3	1.0	-0.2	0.0	0.0	0.1	2.9	3.0	3.6	0.82	0.97	0.92
WH09-54.9	54.9	Black Shale	1.4	1.6	4.0	0.4	-4.4	0.0	0.0	0.1	3.5	3.6	3.1	1.00	0.96	
WH09-56.3	56.3	Black Shale	1.7	0.9	4.5	0.2	0.6	0.0	0.0	0.1	3.9	4.0	2.8	1.00	0.97	
WH09-57.3	57.3	Black Shale	0.8	0.7	1.7	0.4	5.7	0.0	0.0	0.0	1.5	1.5	2.4	0.61	0.98	0.87
WH09-60.7	60.7	Calcareous Black Shale	6.4	1.8	0.9	1.9	-11.0	0.0	0.1	0.2	0.8	1.1	1.3	0.79	0.77	
WH09-61.1	61.1	Calcareous Black Shale	10.3	0.3	0.5	0.6	5.3	0.0	0.2	0.3	0.4	1.0	1.2	0.85	0.41	
WH09-62.4	62.4	Calcareous Black Shale	9.1	0.3	0.1	1.9	-10.5	0.0	0.2	0.5	0.1	0.9	1.0	0.88	0.14	
WH09-63.1	63.1	Calcareous Black Shale	3.6	0.7	1.0	0.7	-8.8	0.1	0.0	0.2	0.9	1.1	1.4	0.77	0.81	
WH09-63.7	63.7	Black Shale	0.0	2.1	0.6	3.8	-21.5	0.1	0.0	0.0	0.5	0.6	1.6	0.38	0.79	
WH09-63.9	63.9	Black Shale	0.2	1.0	0.6	1.8	-17.4	0.1	0.1	0.1	0.5	0.7	1.0	0.68	0.71	
WH09-64.5	64.5	Black Shale	0.2	2.1	2.0	1.1	-15.4	0.0	0.0	0.0	1.7	1.8	2.5	0.70	0.99	0.86
WH09-65.5	65.5	Black Shale	0.9	0.6	0.9	0.7	-7.9	0.0	0.0	0.1	0.8	0.9	1.5	0.61	0.81	
WH09-66.3	66.3	Black Shale	0.0	1.6	0.1	14.1	-13.4	0.2	0.8	0.0	0.1	1.1	1.9	0.56	0.09	0.07
WH09-66.8	66.8	Black Shale	0.0	2.1	0.5	4.4	-17.8	0.4	0.5	0.0	0.4	1.4	2.4	0.58	0.30	
WH09-67.1	67.1	Black Shale	0.0	2.7	0.0	93.9	-16.5	0.2	0.9	0.0	0.0	1.2	2.3	0.49	0.02	0.02
WH09-67.4	67.4	Black Shale	0.0	2.2	0.0	88.2	-16.2	0.5	0.7	0.0	0.0	1.3	2.4	0.54	0.02	
WH09-81.9	81.9	Black Shale	0.4	1.0	2.3	0.4	-10.7	0.0	0.0	0.2	2.0	2.2	4.0	0.56	0.90	0.62
WH09-82.8	82.8	Black Shale	0.6	0.6	2.4	0.3	-7.6	0.0	0.0	0.3	2.1	2.4	2.8	0.84	0.88	0.71
WH09-83.7	83.7	Black Shale	0.3	1.5	2.8	0.5	-3.1	0.0	0.0	0.2	2.4	2.6	5.0	0.52	0.93	0.76
WH09-84.5	84.5	Black Shale	1.0	1.2	2.8	0.4	-3.5	0.0	0.0	0.3	2.4	2.7	2.8	0.98	0.89	0.77
WH09-85.7	85.7	Black Shale	0.7	3.1	3.7	0.8	4.8	0.0	0.0	0.1	3.2	3.4	4.1	0.82	0.96	0.92
WH09-86.6	86.6	Black Shale	1.0	1.3	3.0	0.4	-2.4	0.0	0.0	0.2	2.6	2.9	3.4	0.85	0.91	
WH09-87.1	87.1	Calcareous Black Shale	4.3	1.2	2.1	0.6	-1.7	0.0	0.0	0.3	1.8	2.1	2.4	0.89	0.85	0.79
WH09-88.3	88.3	Black Shale	0.0	3.6	2.7	1.3	1.9	0.3	0.5	0.2	2.3	3.3	3.8	0.88	0.70	
WH09-89.2	89.2	Black Shale	0.7	3.5	4.1	0.9	6.7	0.0	0.0	0.1	3.6	3.7	4.2	0.88	0.97	0.91
WH09-90.7	90.7	Black Shale	1.1	1.6	2.9	0.5	-0.1	0.0	0.0	0.1	2.5	2.6	3.0	0.86	0.97	0.89
WH09-91.5	91.5	Black Shale	1.1	2.0	2.8	0.7	1.5	0.0	0.0	0.1	2.5	2.6	3.1	0.81	0.97	0.91
WH09-93.0	93.0	Black Shale	0.2	2.7	2.7	1.0	4.0	0.1	0.0	0.0	2.3	2.4	3.1	0.77	0.95	0.85
WH09-94.0	94.0	Calcareous Black Shale	9.6	3.4	0.8	4.4	4.0	0.0	0.0	0.3	0.7	0.9	1.2	0.76	0.71	0.51
WH09-95.6	95.6	Black Shale	0.4	3.4	4.1	0.8	4.4	0.0	0.0	0.1	3.6	3.7	4.4	0.83	0.97	0.92
WH09-96.3	96.3	Black Shale	0.5	2.0	3.7	0.5	5.3	0.0	0.0	0.1	3.2	3.3	3.9	0.85	0.97	0.92
WH09-97.9	97.9	Black Shale	0.7	2.7	3.7	0.7	7.0	0.0	0.0	0.1	3.2	3.3	3.5	0.94	0.97	0.92
WH09-99.6	99.6	Black Shale	1.1	2.9	1.9	1.5	5.7	0.0	0.0	0.1	1.7	1.8	2.2	0.81	0.96	0.85
WH09-100.4	100.4	Black Shale	0.1	2.9	1.8	1.7	1.9	0.0	0.0	0.0	1.5	1.6	2.2	0.72	0.96	0.84
WH09-101.2	101.2	Calcareous Black Shale	7.6	0.9	1.5	0.6	2.6	0.0	0.0	0.2	1.3	1.5	1.7	0.89	0.87	0.79
WH09-102.4	102.4	Black Shale	0.7	5.9	3.2	1.9	3.0	0.0	0.0	0.1	2.7	2.8	3.0	0.93	0.97	0.92
WH09-103.3	103.3	Calcareous Black Shale	3.5	5.4	1.6	3.4	3.0	0.0	0.0	0.2	1.4	1.6	1.8	0.88	0.87	
WH09-104.1	104.1	Black Shale	0.9	4.8	3.0	1.6	6.1	0.0	0.0	0.1	2.6	2.7	3.4	0.79	0.96	0.90
WH09-105.3	105.3	Black Shale	1.0	5.0	2.4	2.1	2.5	0.1	0.1	0.1	2.1	2.3	3.2	0.72	0.90	0.84

Al (Wt %)	Fe/Al	Mo (ppm)	Mo/TOC (ppm/Wt%)	V (ppm)	V/TOC (ppm/Wt%)	U (ppm)	U/TOC (ppm/Wt%)	Re (ppb)	Re/TOC (ppb/Wt%)	Cr (ppm)	Ti (Wt %)	Cr/Ti (ppm/ppm)	Age (Ma)
10	0.21	1	0.8	4438	6124	13.4	18.4	547	754	201	0.4	0.0449	Early Ediacaran (635-580)
9	0.20	9	14.2	1824	2994	12.3	20.2	229	376				Early Ediacaran (635-580)
8	0.23	4	4.6	584	707	14.0	16.9	732	887	56	0.4	0.0145	Early Ediacaran (635-580)
9	0.30	38	40.5	489	522	13.8	14.7	703	750	63	0.3	0.0198	Early Ediacaran (635-580)
9	0.22	2	3.0	390	485	13.8	17.2	5	6	53	0.4	0.0139	Early Ediacaran (635-580)
9	0.35	62	49.7	333	266	15.8	12.6	24	19	57	0.4	0.0151	Early Ediacaran (635-580)
9	0.26	8	8.6	324	356	14.0	15.4	64	70	57	0.4	0.0149	Early Ediacaran (635-580)
9	0.41	172	144.9	288	242	12.6	10.6	26	22	59	0.4	0.0149	Early Ediacaran (635-580)
7	0.48	11	14.6	208	272	9.8	12.8	13	17	49	0.3	0.0153	Early Ediacaran (635-580)
9	0.31	13	11.6	241	208	10.0	8.6	15	13	58	0.4	0.0156	Early Ediacaran (635-580)
3	1.53	40	84.7	171	367	5.5	11.9	22	48	25	0.1	0.0203	Early Ediacaran (635-580)
8	0.37	41	32.0	185	144	6.4	5.0	38	29		0.3		Early Ediacaran (635-580)
7	0.56	42	37.9	199	178	5.9	5.3	31	28		0.3		Early Ediacaran (635-580)
7	0.53	22	27.7	213	270	4.3	5.4	37	47		0.3		Early Ediacaran (635-580)
10	0.38	30	22.0	212	156	4.8	3.5	23	17		0.4		Early Ediacaran (635-580)
10	0.38	27	19.6	213	153	4.3	3.1	41	30		0.4		Early Ediacaran (635-580)
9	0.26	58	50.4	184	160	4.7	4.1	24	21		0.4		Early Ediacaran (635-580)
10	0.30	38	31.5	207	173	5.8	4.8	25	21		0.4		Early Ediacaran (635-580)
9	0.37	26	22.6	221	192	4.1	3.5	36	32		0.4		Early Ediacaran (635-580)
8	0.35	13	9.9	174	136	5.7	4.4	30	24	55	0.4	0.0136	Early Ediacaran (635-580)
9	0.43	24	20.5	170	145	3.2	2.8	16	14		0.4		Early Ediacaran (635-580)
8	0.44	8	10.1	170	216	5.9	7.5	18	23	50	0.4	0.0135	Early Ediacaran (635-580)
8	0.37	12	9.1	134	106	4.2	3.3	10	8	49	0.3	0.0164	Early Ediacaran (635-580)
7	0.44	12	9.5	143	114	3.6	2.8	8	6	44	0.3	0.0168	Early Ediacaran (635-580)
4	0.59	4	6.5	94	156	3.9	6.5	4	7	38	0.2	0.0163	Early Ediacaran (635-580)
6	0.50	1	0.9	79	85	1.7	1.8	9	10	69	0.4	0.0179	Early Ediacaran (635-580)
6	0.66	1	1.3	81	79	2.0	1.9	10	9	74	0.4	0.0171	Early Ediacaran (635-580)
6	0.54	1	0.7	77	41	2.6	1.4	8	4	69	0.4	0.0191	Early Ediacaran (635-580)
6	0.58	1	0.9	81	50	1.7	1.1	6	4	70	0.4	0.0187	Early Ediacaran (635-580)
4	0.76	1	0.9	50	37	1.5	1.1	6	4	44	0.2	0.0181	Early Ediacaran (635-580)
4	0.69	1	0.5	49	23	1.5	0.7	5	2	43	0.2	0.0200	Early Ediacaran (635-580)
6	0.61	3	1.8	109	77	5.7	4.0	8	6	82	0.4	0.0227	Early Ediacaran (635-580)
5	0.74	2	0.9	99	40	3.8	1.5	13	5	88	0.4	0.0215	Early Ediacaran (635-580)
2	0.79	2	1.2	86	52	2.9	1.7	10	6	59	0.2	0.0390	Early Ediacaran (635-580)
4	0.65	7	1.2	113	20	13.1	2.3	46	8	86	0.3	0.0275	Early Ediacaran (635-580)
3	0.75	4	1.0	77	21	5.6	1.6	18	5	54	0.2	0.0230	Early Ediacaran (635-580)
5	0.67	4	1.1	112	34	5.6	1.7	27	8	74	0.3	0.0240	Early Ediacaran (635-580)
5	0.65	2	1.4	101	63	6.7	4.2	6	4	52	0.3	0.0158	Early Ediacaran (635-580)
4	0.65	1	1.0	89	98	4.8	5.3	28	30	34	0.3	0.0108	Early Ediacaran (635-580)
6	0.39	1	1.0	90	134	4.0	5.9	3	4	58	0.4	0.0149	Early Ediacaran (635-580)
3	0.46	7	3.7	108	61	12.1	6.8	23	13		0.1		Middle Ediacaran (580-550)
2	0.56	5	17.3	68	236	7.7	26.7	32	112		0.1		Middle Ediacaran (580-550)
2	0.59	2	7.4	85	312	0.2	0.8	11	40		0.1		Middle Ediacaran (580-550)
4	0.39	2	3.3	250	340	8.3	11.3	1235	1679		0.2		Middle Ediacaran (580-550)
6	0.26	14	6.8	28842	13523	10.2	4.8	883	414		0.3		Middle Ediacaran (580-550)
4	0.27	9	8.5	15271	14723	2.5	2.5		0		0.2		Middle Ediacaran (580-550)
8	0.32	15	7.0	3570	1690	17.1	8.1	1322	626	230	0.4	0.0555	Middle Ediacaran (580-550)
8	0.19	3	5.0	3563	6107	10.4	17.8	172	295		0.5		Middle Ediacaran (580-550)
7	0.28	11	6.4	30167	18318	8.6	5.2	42	25	1422	0.3	0.4167	Middle Ediacaran (580-550)
9	0.28	14	6.7	6370	3065	9.9	4.8	1640	789		0.5		Middle Ediacaran (580-550)
9	0.27	9	3.4	6946	2547	8.8	3.2	646	237	552	0.4	0.1362	Middle Ediacaran (580-550)
8	0.28	6	2.6	5665	2617	9.1	4.2	358	165		0.5		Middle Ediacaran (580-550)
7	0.56	1	0.9	75	73	1.7	1.7	6	6	70	0.4	0.0176	Middle Ediacaran (580-550)
6	0.50	1	1.1	67	110	1.3	2.1	5	8	53	0.3	0.0151	Middle Ediacaran (580-550)
8	0.59	2	1.2	116	77	3.0	2.0	12	8	101	0.5	0.0184	Middle Ediacaran (580-550)
5	0.57	1	0.8	66	56	1.6	1.4	7	6	55	0.3	0.0156	Middle Ediacaran (580-550)
8	0.52	4	1.2	82	27	7.5	2.4	17	5	79	0.3	0.0237	Middle Ediacaran (580-550)
6	0.54	2	1.9	71	55	0.4	0.3	30	23		0.5		Middle Ediacaran (580-550)
3	0.72	1	1.1	46	39	1.8	1.5	7	6	41	0.2	0.0191	Middle Ediacaran (580-550)
7	0.57	5	1.3	107	30	8.1	2.3	27	8		0.5		Middle Ediacaran (580-550)
7	0.57	3	0.8	103	29	5.3	1.5	16	4	82	0.4	0.0223	Middle Ediacaran (580-550)
5	0.64	2	1.2	63	40	4.3	2.8	12	7	56	0.3	0.0184	Middle Ediacaran (580-550)
4	0.71	1	0.7	58	30	1.5	0.8	9	5	52	0.3	0.0180	Middle Ediacaran (580-550)
4	0.71	1	0.5	63	23	1.6	0.6	7	3	54	0.3	0.0201	Middle Ediacaran (580-550)
2	0.82	1	0.3	32	9	1.7	0.5	7	2	25	0.1	0.0231	Middle Ediacaran (580-550)
5	0.94	3	1.0	89	26	3.4	1.0	17	5	75	0.3	0.0223	Middle Ediacaran (580-550)
5	0.76	2	0.9	74	36	2.3	1.2	11	6	64	**0.3**	0.0200	Middle Ediacaran (580-550)
6	0.60	2	0.8	92	34	2.3	0.9	11	4	76	0.4	0.0191	Middle Ediacaran (580-550)
3	0.71	1	0.3	44	15	1.2	0.4	6	2	47	0.2	0.0252	Middle Ediacaran (580-550)
4	0.62	1	0.4	57	20	1.5	0.5	7	2	56	0.2	0.0270	Middle Ediacaran (580-550)
2	0.85	3	2.8	111	119	5.2	5.5	22	23	63	0.1	0.0503	Middle Ediacaran (580-550)
4	0.79	7	1.2	106	18	10.2	1.7	43	7	71	0.2	0.0296	Middle Ediacaran (580-550)
3	0.60	6	1.2	83	15	4.4	0.8	57	11		0.2		Middle Ediacaran (580-550)
4	0.79	6	1.2	100	21	8.2	1.7	42	9	87	0.3	0.0297	Middle Ediacaran (580-550)
5	0.70	5	1.1	105	21	7.9	1.6	34	7	73	0.3	0.0277	Middle Ediacaran (580-550)

Stratigraphic Unit	Sample No.	Strat. Height (m)	Lithology	TIC (Wt %)	C_{org} (Wt %)	S_{PY} (Wt %)	C_{Org}/S_{PY}	$\delta^{34}S_{PY}$ (‰)	Fe_{Mag} (Wt %)	Fe_{Oxide} (Wt %)	Fe_{Carb} (Wt %)	Fe_{PY} (Wt %)	Fe_{HR} (Wt %)	Fe_T (Wt %)	Fe_{HR}/Fe_T	Fe_{PY}/Fe_{HR}	DOP
Doushantuo Fm. Member IV	WH09-114.5	114.5	Black Shale	1.4	1.1	0.8	1.5	-7.3	0.0	0.0	0.0	0.7	0.7	1.0	0.70	0.98	0.76
Doushantuo Fm. Member IV	WH09-115.3	115.3	Black Shale	0.7	3.8	1.6	2.4	-23.3	0.0	0.0	0.1	1.4	1.5	2.5	0.60	0.95	0.78
Doushantuo Fm. Member IV	WH09-115.5	115.5	Black Shale	0.8	1.5	1.9	0.8	-15.1	0.1	0.0	0.1	1.6	1.8	2.5	0.74	0.90	
Doushantuo Fm. Member IV	WH09-115.9	115.9	Black Shale	0.6	2.9	1.8	1.6	-23.2	0.1	0.0	0.1	1.6	1.7	2.4	0.72	0.90	
Doushantuo Fm. Member IV	WH09-116.3	116.3	Black Shale	1.5	1.9	1.2	1.6	-21.6	0.0	0.0	0.2	1.0	1.2	1.9	0.65	0.84	
Doushantuo Fm. Member IV	WH09-116.8	116.8	Black Shale	0.6	5.0	1.3	3.8	-21.5	0.1	0.0	0.1	1.2	1.3	1.8	0.73	0.88	
Doushantuo Fm. Member IV	WH09-117.4	117.4	Black Shale	1.3	5.2	2.8	1.9	-15.9	0.1	0.0	0.1	2.4	2.7	3.2	0.83	0.92	
Doushantuo Fm. Member IV	WH09-117.8	117.8	Black Shale	0.8	8.5	2.5	3.5	-14.2	0.0	0.0	0.1	2.1	2.3	3.4	0.67	0.94	0.87
Doushantuo Fm. Member IV	WH09-118.3	118.3	Black Shale	0.8	9.3	2.3	4.1	-15.0	0.0	0.0	0.2	2.0	2.2	2.6	0.84	0.90	
Doushantuo Fm. Member IV	WH09-118.9	118.9	Calcareous Black Shale	4.0	7.0	1.2	5.6	-11.7	0.0	0.0	0.2	1.1	1.2	1.3	0.92	0.87	0.79
Doushantuo Fm. Member IV	WH09-119.5	119.5	Calcareous Black Shale	3.2	7.1	1.2	5.7	-12.7	0.0	0.0	0.2	1.1	1.3	1.5	0.88	0.85	
Doushantuo Fm. Member IV	WH09-120.0	120.0	Calcareous Black Shale	4.7	4.1	0.6	7.3	-9.9	0.0	0.0	0.1	0.5	0.6	0.8	0.67	0.86	0.76
Liuchapo Formation	WH09-131.5	131.5	Black Shale-Chert	0.0	0.1	0.3	0.4	-0.1	0.0	0.0	0.0	0.2	0.3	0.4	0.76	0.78	
Liuchapo Formation	WH09-132.6	132.6	Black Shale-Chert	0.0	0.1	0.1	0.5	13.1	0.0	0.0	0.0	0.1	0.1	0.2	0.67	0.62	
Liuchapo Formation	WH09-133.5	133.5	Black Shale-Chert	0.1	0.2	0.1	1.6	22.5	0.0	0.0	0.0	0.1	0.2	0.2	0.81	0.63	
Liuchapo Formation	WH09-135.0	135.0	Black Shale-Chert	0.1	0.1	0.2	0.7	3.8	0.0	0.0	0.0	0.2	0.3	0.4	0.61	0.73	
Liuchapo Formation	WH09-136.7	136.7	Black Shale-Chert	0.1	0.1	0.2	0.3	-6.7	0.0	0.0	0.0	0.2	0.3	0.5	0.48	0.75	
Liuchapo Formation	WH09-137.8	137.8	Black Shale-Chert	0.0	0.3	0.5	0.6	-3.1	0.0	0.0	0.0	0.5	0.5	0.7	0.75	0.88	
Liuchapo Formation	WH09-138.5	138.5	Black Shale-Chert	0.1	0.7	0.2	3.7	-6.9	0.0	0.0	0.0	0.2	0.2	0.4	0.61	0.72	
Liuchapo Formation	WH09-139.5	139.5	Black Shale-Chert	0.9	0.4	0.2	2.2	4.9	0.0	0.0	0.1	0.1	0.3	0.4	0.61	0.54	
Liuchapo Formation	WH09-140.6	140.6	Black Shale-Chert	0.9	0.6	0.4	1.4	5.2	0.0	0.0	0.0	0.4	0.5	0.8	0.57	0.80	
Liuchapo Formation	WH09-141.2	141.2	Black Shale-Chert	0.7	1.5	0.7	2.3	4.6	0.1	0.1	0.0	0.6	0.7	0.9	0.81	0.78	
Liuchapo Formation	WH09-142.1	142.1	Black Shale-Chert	1.8	4.3	0.2	23.0	6.7	0.1	0.4	0.1	0.2	0.8	0.9	0.81	0.21	
Liuchapo Formation	WH09-143.2	143.2	Black Shale-Chert	1.0	3.7	0.1	45.1	6.3	0.1	0.5	0.1	0.1	0.8	1.0	0.74	0.09	
Liuchapo Formation	WH09-144.1	144.1	Black Shale-Chert	1.0	3.9	0.1	47.1	3.8	0.1	0.4	0.0	0.1	0.6	0.7	0.77	0.13	
Liuchapo Formation	WH09-144.8	144.8	Black Shale-Chert	0.1	2.6	0.1	38.2	5.7	0.0	0.0	0.0	0.1	0.1	0.1	1.00	0.52	
Liuchapo Formation	WH09-145.4	145.4	Black Shale-Chert	0.3	3.8	0.1	31.0	7.4	0.1	0.2	0.0	0.1	0.4	0.5	0.83	0.25	
Liuchapo Formation	WH09-146.3	146.3	Black Shale-Chert	5.6	3.3	0.4	9.1	6.1	0.1	0.1	0.1	0.3	0.6	0.6	0.90	0.56	
Liuchapo Formation	WH09-147.5	147.5	Black Shale-Chert	0.2	5.2	0.1	64.0	7.5	0.1	0.0	0.0	0.1	0.2	0.2	0.91	0.39	
Liuchapo Formation	WH09-148.4	148.4	Black Shale-Chert	0.6	0.3	0.1	4.0	13.3	0.0	0.0	0.0	0.1	0.2	0.1	1.00	0.46	
Liuchapo Formation	WH09-149.7	149.7	Black Shale-Chert	0.3	0.1	0.2	0.7	2.1	0.0	0.0	0.0	0.1	0.2	0.3	0.74	0.70	
Liuchapo Formation	WH09-150.6	150.6	Black Shale-Chert	0.0	2.5	0.2	12.9	3.3	0.0	0.0	0.0	0.2	0.2	0.2	1.00	0.72	
Niutitang Formation	WH09-151.6	151.6	Calcareous Black Shale	5.1	28.1	0.7	39.1	-3.5	0.1	0.4	0.1	0.6	1.2	1.3	0.94	0.51	
Niutitang Formation	WH09-152.3	152.3	Black Shale	0.2	1.8	0.1	21.4	-7.4	0.0	0.0	0.0	0.1	0.1	0.1	1.00	0.59	
Niutitang Formation	WH09-153.5	153.5	Black Shale	1.6	3.6	0.1	26.4	1.1	0.1	0.2	0.1	0.1	0.5	0.5	0.95	0.25	
Niutitang Formation	WH09-154.2	154.2	Black Shale	0.1	1.9	0.1	15.3	7.1	0.0	0.0	0.0	0.1	0.2	0.2	1.00	0.57	
Niutitang Formation	WH09-155.1	155.1	Black Shale	0.1	5.4	0.1	36.4	3.1	0.1	0.1	0.0	0.1	0.3	0.4	0.87	0.42	

Al (Wt %)	Fe/Al	Mo (ppm)	Mo/TOC (ppm/Wt%)	V (ppm)	V/TOC (ppm/Wt%)	U (ppm)	U/TOC (ppm/Wt%)	Re (ppb)	Re/TOC (ppb/Wt%)	Cr (ppm)	Ti (Wt %)	Cr/Ti (ppm/ppm)	Age (Ma)
3	0.35	2	1.3	92	81	3.0	2.6	15	13	59	0.1	0.0432	Late Ediacaran (550-542)
7	0.35	68	18.1	2956	785	18.4	4.9	1063	282	508	0.3	0.1476	Late Ediacaran (550-542)
7	0.33	76	52.2	966	666	13.6	9.4	74	51		0.4		Late Ediacaran (550-542)
8	0.30	126	43.5	1693	584	13.9	4.8	432	149		0.5		Late Ediacaran (550-542)
7	0.27	66	33.9	1089	564	11.1	5.8	21	11		0.4		Late Ediacaran (550-542)
6	0.32	79	15.8	773	154	8.8	1.8	184	37		0.3		Late Ediacaran (550-542)
5	0.61	95	18.1	278	53	20.4	3.9	51	10		0.3		Late Ediacaran (550-542)
5	0.66	61	7.2	126	15	20.2	2.4	15	2	64	0.3	0.0243	Late Ediacaran (550-542)
4	0.73	34	3.7	138	15	13.7	1.5	8	1	69	0.2	0.0388	Late Ediacaran (550-542)
2	0.68	35	5.1	100	14	31.5	4.5	12	2	28	0.1	0.0239	Late Ediacaran (550-542)
2	0.61	33	4.7	177	25	19.4	2.7	42	6	54	0.1	0.0452	Late Ediacaran (550-542)
2	0.37	22	5.5	396	97	18.5	4.5	66	16	72	0.1	0.0586	Late Ediacaran (550-542)
1	0.32	0.83	7.2	44	384	1.1	9.7	5	42	37	0.0	0.0740	Late Ediacaran (550-542)
1	0.20	0.52	10.1	19	363	0.5	9.5	11	211	42	0.0	0.1147	Late Ediacaran (550-542)
1	0.20	0.68	3.9	11	62	0.9	4.8	10	56	33	0.0	0.1046	Late Ediacaran (550-542)
2	0.21	0.53	3.5	22	150	1.0	6.5	88	586	44	0.1	0.0555	Late Ediacaran (550-542)
4	0.15	0.38	5.6	35	510	1.5	21.8	6	95	44	0.1	0.0367	Late Ediacaran (550-542)
4	0.18	0.47	1.5	43	134	0.0	0.1	5	16	43	0.1	0.0448	Late Ediacaran (550-542)
3	0.14	0.89	1.4	22	34	0.9	1.4	7	10	36	0.1	0.0421	Late Ediacaran (550-542)
2	0.18	0.49	1.3	38	100	0.7	1.9	5	14	51	0.1	0.0533	Late Ediacaran (550-542)
3	0.25	0.51	0.9	72	122	0.9	1.4	12	21	95	0.1	0.0670	Late Ediacaran (550-542)
3	0.31	0.49	0.3	75	50	1.9	1.3	7	5	93	0.1	0.0666	Late Ediacaran (550-542)
2	0.42	2.80	0.6	831	191	11.4	2.6	16	4	303	0.1	0.2771	Late Ediacaran (550-542)
2	0.53	0.94	0.2	212	57	4.6	1.2	25	7	174	0.1	0.1919	Late Ediacaran (550-542)
2	0.35	0.45	0.2	268	68	5.5	1.4	96	25	219	0.1	0.2132	Late Ediacaran (550-542)
0	0.40	0.87	0.2	167	65	3.0	1.2	33	13	95	0.0	0.6842	Late Ediacaran (550-542)
2	0.31	0.52	0.2	199	52	3.0	0.8	19	5	126	0.1	0.1755	Late Ediacaran (550-542)
1	0.65	0.53	0.1	248	75	6.5	2.0	15	5	99	0.0	0.2286	Late Ediacaran (550-542)
1	0.29	0.36	1.1	238	46	2.7	0.5	37	7	99	0.0	0.3149	Late Ediacaran (550-542)
0	0.32	0.38	3.3	24	74	0.9	2.8	20	62	18	0.0	0.3720	Late Ediacaran (550-542)
1	0.49	0.95	0.4	24	212	0.1	1.3	40	348	29	0.0	0.1195	Late Ediacaran (550-542)
0	0.83	0.46	0.2	323	127	7.3	2.9	45	18	342	0.0	3.3008	Late Ediacaran (550-542)
2	0.76	239	8.5	145	5	258.9	9.2	20	1	36	0.1	0.0421	Early Cambrian (542-525)
0	0.56	11	5.8	612	333	3.4	1.9	136	74	39	0.0	0.6775	Early Cambrian (542-525)
2	0.32	0.76	0.2	196	55	4.0	1.1	41	11	138	0.1	0.1808	Early Cambrian (542-525)
0	0.42	0.67	0.4	104	56	2.1	1.1	68	37	71	0.0	0.3441	Early Cambrian (542-525)
1	0.29	0.83	0.2	401	75	7.7	1.4	10	2	248	0.1	0.3873	Early Cambrian (542-525)

Index

TIC = Total inorganic carbon	Fe_{HR}/Fe_T = ratio of highly reactive iron to total iron
C_{org} = Total organic carbon	Fe_{PY}/Fe_{HR} = ratio of pyrite iron to highly reactive iron
TOC = Total organic carbon	DOP = Degree of pyritization
S_{PY} = Sulfur Pyrite	Fe/Al = ratio of Iron to aluminium
S_T = Sulfur Total	Mo = Molybdenum
Fe_{Mag} = Iron magnetite	Mo/TOC = ratio of Mo to total organic carbon
Fe_{Oxide} = Iron oxide	V = Vanadium
Fe_{Carb} = Iron carbonate	V/TOC = ratio of V to total organic carbon
Fe_{PY} = Iron pyrite	U = Uranium
Fe_{HR} = Iron highly reactive	U/TOC = ratio of U to total organic carbon
Fe_T = Iron total	ppm = parts per million
Al = Aluminium	wt% = weight percentage

Table DR2: Summary of redox-sensitive trace element data of the Ediacaran-Early Cambrian (ca. 635–520 Ma) euxinic shales

Stratigraphic Unit	Sample No.	Strat. Height (m)	Lithology	TOC (Wt %)	S_{PY} (Wt %)	TOC/ S_{PY}	FeHR/ FeT	FePY/ FeHR	DOP	Mo (ppm)	Mo/TOC (ppm/Wt%)	V (ppm)	V/TOC (ppm/Wt%)	U (ppm)	U/TOC (ppm/Wt%)	Re (ppb)	Re/TOC (ppb/Wt%)	Cr (ppm)	Ti (Wt %)	Cr/Ti (ppm/ppm) x 1000	Age Estimates (Ma)
This Study, Wuhe section, Guizou Province, South China (2.4 to 13.7 m is from Sahoo et al., 2012)																					
Doushantuo Fm. Member II	WH09-2.4	2.4	Black Shale	0.7	0.2	4.1	0.2	0.4	0.2	1	0.8	4438	6124	13.4	18.4	547	754	201	0.45	44.9	635.1
Doushantuo Fm. Member II	WH09-2.7	2.7	Black Shale	0.6	0.2	3.6	0.3	0.3		9	14.2	1824	2994	12.3	20.2	229	376				634.9
Doushantuo Fm. Member II	WH09-3	3.0	Black Shale	0.8	0.6	1.3	0.4	0.7		4	4.6	584	707	14.0	16.9	732	887	56	0.39	14.5	634.7
Doushantuo Fm. Member II	WH09-3.2	3.2	Black Shale	0.9	1.4	0.7	0.5	1.0	0.7	38	40.5	489	522	13.8	14.7	703	750	63	0.32	19.8	634.5
Doushantuo Fm. Member II	WH09-3.5	3.5	Black Shale	0.8	0.2	3.8	0.4	0.2		2	3.0	390	485	13.8	17.2	5	6	53	0.38	13.9	634.3
Doushantuo Fm. Member II	WH09-3.7	3.7	Black Shale	1.3	2.0	0.6	0.6	0.9		62	49.7	333	266	15.8	12.6	24	19	57	0.37	15.1	634.1
Doushantuo Fm. Member II	WH09-4	4.0	Black Shale	0.9	0.9	1.1	0.4	0.9		8	8.6	324	356	14.0	15.4	64	70	57	0.39	14.9	633.9
Doushantuo Fm. Member II	WH09-4.3	4.3	Black Shale	1.2	2.2	0.5	0.5	0.9		172	144.9	288	242	12.6	10.6	26	22	59	0.40	14.9	633.7
Doushantuo Fm. Member II	WH09-4.6	4.6	Black Shale	0.8	1.3	0.6	0.6	0.6		11	14.6	208	272	9.8	12.8	13	17	49	0.32	15.3	633.5
Doushantuo Fm. Member II	WH09-4.8	4.8	Black Shale	1.2	0.7	1.8	0.3	0.7		13	11.6	241	208	10.0	8.6	15	13	58	0.37	15.6	633.3
Doushantuo Fm. Member II	WH09-5.0	5.0	Calcareous Black Shale	0.5	1.5	0.3	0.7	0.3	0.3	40	84.7	171	367	5.5	11.9	22	48	25	0.12	20.3	633.2
Doushantuo Fm. Member II	WH09-5.4	5.4	Black Shale	1.3	1.8	0.7	0.6	0.8		41	32.0	185	144	6.4	5.0	38	29		0.35		632.9
Doushantuo Fm. Member II	WH09-5.6	5.6	Calcareous Black Shale	1.1	1.7	0.7	0.6	0.6		42	37.9	199	178	5.9	5.3	31	28		0.30		632.8
Doushantuo Fm. Member II	WH09-5.8	5.8	Calcareous Black Shale	0.8	1.8	0.4	0.7	0.6		22	27.7	213	270	4.3	5.4	37	47		0.29		632.6
Doushantuo Fm. Member II	WH09-6.0	6.0	Black Shale	1.4	3.0	0.5	0.7	1.0		30	22.0	212	156	4.8	3.5	23	17		0.43		632.5
Doushantuo Fm. Member II	WH09-6.3	6.3	Black Shale	1.4	3.1	0.5	0.7	1.0		27	19.6	213	153	4.3	3.1	41	30		0.42		632.2
Doushantuo Fm. Member II	WH09-6.5	6.5	Black Shale	1.2	0.0	30.2	0.3	0.0		58	50.4	184	160	4.7	4.1	24	21		0.41		632.1
Doushantuo Fm. Member II	WH09-6.8	6.8	Black Shale	1.2	1.5	0.8	0.5	1.0		38	31.5	207	173	5.8	4.8	25	21		0.44		631.9
Doushantuo Fm. Member II	WH09-7.0	7.0	Black Shale	1.2	2.2	0.5	0.6	0.9		26	22.6	221	192	4.1	3.5	36	32		0.42		631.7
Doushantuo Fm. Member II	WH09-7.3	7.3	Black Shale	1.3	1.7	0.7	0.6	0.8	0.3	13	9.9	174	136	5.7	4.4	30	24	55	0.40	13.6	631.5
Doushantuo Fm. Member II	WH09-8.6	8.6	Black Shale	1.2	2.5	0.5	0.7	0.9		24	20.5	170	145	3.2	2.8	16	14		0.40		630.5
Doushantuo Fm. Member II	WH09-9.4	9.4	Black Shale	0.8	2.3	0.3	0.7	0.9		8	10.1	170	216	5.9	7.5	18	23	50	0.37	13.5	630.0
Doushantuo Fm. Member II	WH09-9.7	9.7	Black Shale	1.3	2.2	0.6	0.7	0.9	0.7	12	9.1	134	106	4.2	3.3	10	8	49	0.30	16.4	629.7
Doushantuo Fm. Member II	WH09-11.6	11.6	Black Shale	1.3	2.2	0.6	0.7	1.0	0.7	12	9.5	143	114	3.6	2.8	8	6	44	0.26	16.8	628.3
Doushantuo Fm. Member II	WH09-13.7	13.7	Calcareous Black Shale	0.6	1.8	0.3	0.9	0.7	0.6	4	6.5	94	156	3.9	6.5	4	7	38	0.23	16.3	626.8
Doushantuo Fm. Member II	WH09-21.5	21.5	Black Shale	0.9	1.9	0.5	0.6	0.9	0.6	1	0.9	79	85	1.7	1.8	9	10	69	0.39	17.9	621.1
Doushantuo Fm. Member II	WH09-24.1	24.1	Black Shale	1.0	2.8	0.4	0.7	0.9	0.7	1	1.3	81	79	2.0	1.9	10	9	74	0.43	17.1	619.2
Doushantuo Fm. Member II	WH09-26.0	26.0	Black Shale	1.9	2.8	0.7	0.8	0.9	0.8	1	0.7	77	41	2.6	1.4	8	4	69	0.36	19.1	617.8
Doushantuo Fm. Member II	WH09-29.0	29.0	Black Shale	1.6	3.1	0.5	0.8	1.0	0.8	1	0.9	81	50	1.7	1.1	6	4	70	0.38	18.7	615.6
Doushantuo Fm. Member II	WH09-32.4	32.4	Black Shale	1.3	2.8	0.5	0.9	1.0	0.9	1	0.9	50	37	1.5	1.1	6	4	44	0.24	18.1	613.1
Doushantuo Fm. Member II	WH09-35.1	35.1	Black Shale	2.2	2.5	0.9	0.9	1.0	0.9	1	0.5	49	23	1.5	0.7	5	2	43	0.21	20.0	611.1
Doushantuo Fm. Member II	WH09-38.5	38.5	Calcareous Black Shale	1.4	2.6	0.5	0.6	1.0	0.9	3	1.8	109	77	5.7	4.0	8	6	82	0.36	22.7	606.8
Doushantuo Fm. Member II	WH09-41.1	41.1	Black Shale	2.5	3.6	0.7	0.9	1.0	0.9	2	0.9	99	40	3.8	1.5	13	5	88	0.41	21.5	603.6
Doushantuo Fm. Member II	WH09-44.3	44.3	Calcareous Black Shale	1.7	1.7	1.0	0.9	0.9	0.8	2	1.2	86	52	2.9	1.7	10	6	59	0.15	39.0	599.6
Doushantuo Fm. Member II	WH09-47.5	47.5	Black Shale	5.7	3.2	1.8	1.0	0.9	0.9	7	1.2	113	20	13.1	2.3	46	8	86	0.31	27.5	595.5
Doushantuo Fm. Member II	WH09-50.1	50.1	Calcareous Black Shale	3.6	2.6	1.4	0.9	0.9	0.9	4	1.0	77	21	5.6	1.6	18	5	54	0.23	23.0	592.3
Doushantuo Fm. Member II	WH09-53.4	53.4	Black Shale	3.3	3.3	1.0	0.8	1.0	0.9	4	1.1	112	34	5.6	1.7	27	8	74	0.31	24.0	588.2
Doushantuo Fm. Member II	WH09-54.9	54.9	Black Shale	1.6	4.0	0.4	1.0	1.0		2	1.4	101	63	6.7	4.2	6	4	52	0.33	15.8	586.3
Doushantuo Fm. Member II	WH09-56.3	56.3	Black Shale	0.9	4.5	0.2	1.0	1.0		1	1.0	89	98	4.8	5.3	28	30	34	0.31	10.8	584.5
Doushantuo Fm. Member II	WH09-57.3	57.3	Black Shale	0.7	1.7	0.4	0.6	1.0	0.9	1	1.0	90	134	4.0	5.9	3	4	58	0.39	14.9	583.3

Stratigraphic Unit	Sample No.	Strat. Height (m)	Lithology	TOC (Wt %)	S_{PY} (Wt %)	TOC/ S_{PY}	FeHR/ FeT	FePY/ FeHR	DOP	Mo (ppm)	Mo/TOC (ppm/Wt%)	V (ppm)	V/TOC (ppm/Wt%)	U (ppm)	U/TOC (ppm/Wt%)	Re (ppb)	Re/TOC (ppb/Wt%)	Cr (ppm)	Ti (Wt %)	Cr/Ti (ppm/ppm) x 1000	Age Estimates (Ma)
Doushantuo Fm. Member III	WH09-60.7	60.7	Calcareous Black Shale	1.8	0.9	1.9	0.8	0.8		7	3.7	108	61	12.1	6.8	23	13		0.13		579.0
Doushantuo Fm. Member III	WH09-61.1	61.1	Calcareous Black Shale	0.3	0.5	0.6	0.9	0.4		5	17.3	68	236	7.7	26.7	32	112		0.10		578.7
Doushantuo Fm. Member III	WH09-62.4	62.4	Calcareous Black Shale	0.3	0.1	1.9	0.9	0.1		2	7.4	85	312	0.2	0.8	11	40		0.10		577.9
Doushantuo Fm. Member III	WH09-63.1	63.1	Calcareous Black Shale	0.7	1.0	0.7	0.8	0.8		2	3.3	250	340	8.3	11.3	1235	1679		0.20		577.4
Doushantuo Fm. Member III	WH09-63.7	63.7	Black Shale	2.1	0.6	3.8	0.4	0.8		14	6.8	28842	13523	10.2	4.8	883	414		0.31		577.0
Doushantuo Fm. Member III	WH09-63.9	63.9	Black Shale	1.0	0.6	1.8	0.7	0.7		9	8.5	15271	14723	2.5	2.5		0		0.18		576.9
Doushantuo Fm. Member III	WH09-64.5	64.5	Black Shale	2.1	2.0	1.1	0.7	1.0	0.9	15	7.0	3570	1690	17.1	8.1	1322	626	230	0.41	55.5	576.4
Doushantuo Fm. Member III	WH09-65.5	65.5	Black Shale	0.6	0.9	0.7	0.6	0.8		3	5.0	3563	6107	10.4	17.8	172	295		0.46		575.8
Doushantuo Fm. Member III	WH09-66.3	66.3	Black Shale	1.6	0.1	14.1	0.6	0.1	0.1	11	6.4	30167	18318	8.6	5.2	42	25	1422	0.34	416.7	575.2
Doushantuo Fm. Member III	WH09-66.8	66.8	Black Shale	2.1	0.5	4.4	0.6	0.3		14	6.7	6370	3065	9.9	4.8	1640	789		0.49		574.9
Doushantuo Fm. Member III	WH09-67.1	67.1	Black Shale	2.7	0.0	93.9	0.5	0.0	0.0	9	3.4	6946	2547	8.8	3.2	646	237	552	0.41	136.2	574.7
Doushantuo Fm. Member III	WH09-67.4	67.4	Black Shale	2.2	0.0	88.2	0.5	0.0		6	2.6	5665	2617	9.1	4.2	358	165		0.48		574.5
Doushantuo Fm. Member III	WH09-81.9	81.9	Black Shale	1.0	2.3	0.4	0.6	0.9	0.6	1	0.9	75	73	1.7	1.7	6	6	70	0.40	17.6	569.5
Doushantuo Fm. Member III	WH09-82.8	82.8	Black Shale	0.6	2.4	0.3	0.8	0.9	0.7	1	1.1	67	110	1.3	2.1	5	8	53	0.35	15.1	569.2
Doushantuo Fm. Member III	WH09-83.7	83.7	Black Shale	1.5	2.8	0.5	0.5	0.9	0.8	2	1.2	116	77	3.0	2.0	12	8	101	0.55	18.4	568.9
Doushantuo Fm. Member III	WH09-84.5	84.5	Black Shale	1.2	2.8	0.4	1.0	0.9	0.8	1	0.8	66	56	1.6	1.4	7	6	55	0.35	15.6	568.6
Doushantuo Fm. Member III	WH09-85.7	85.7	Black Shale	3.1	3.7	0.8	0.8	1.0	0.9	4	1.2	82	27	7.5	2.4	17	5	79	0.33	23.7	568.2
Doushantuo Fm. Member III	WH09-86.6	86.6	Black Shale	1.3	3.0	0.4	0.8	0.9		2	1.9	71	55	0.4	0.3	30	23		0.46		567.9
Doushantuo Fm. Member III	WH09-87.1	87.1	Calcareous Black Shale	1.2	2.1	0.6	0.9	0.9	0.8	1	1.1	46	39	1.8	1.5	7	6	41	0.21	19.1	567.7
Doushantuo Fm. Member III	WH09-88.3	88.3	Black Shale	3.6	2.7	1.3	0.9	0.7		5	1.3	107	30	8.1	2.3	27	8		0.47		567.3
Doushantuo Fm. Member III	WH09-89.2	89.2	Black Shale	3.5	4.1	0.9	0.9	1.0	0.9	3	0.8	103	29	5.3	1.5	16	4	82	0.37	22.3	567.0
Doushantuo Fm. Member III	WH09-90.7	90.7	Black Shale	1.6	2.9	0.5	0.9	1.0	0.9	2	1.2	63	40	4.3	2.8	12	7	56	0.30	18.4	566.5
Doushantuo Fm. Member III	WH09-91.5	91.5	Black Shale	2.0	2.8	0.7	0.8	1.0	0.9	1	0.7	58	30	1.5	0.8	9	5	52	0.29	18.0	566.2
Doushantuo Fm. Member III	WH09-93.0	93.0	Black Shale	2.7	2.7	1.0	0.8	1.0	0.8	1	0.5	63	23	1.6	0.6	7	3	54	0.27	20.1	565.7
Doushantuo Fm. Member III	WH09-94.0	94.0	Calcareous Black Shale	3.4	0.8	4.4	0.8	0.7	0.5	1	0.3	32	9	1.7	0.5	7	2	25	0.11	23.1	565.3
Doushantuo Fm. Member III	WH09-95.6	95.6	Black Shale	3.4	4.1	0.8	0.8	1.0	0.9	3	1.0	89	26	3.4	1.0	17	5	75	0.34	22.3	564.8
Doushantuo Fm. Member III	WH09-96.3	96.3	Black Shale	2.0	3.7	0.5	0.8	1.0	0.9	2	0.9	74	36	2.3	1.2	11	6	64	0.32	20.0	564.5
Doushantuo Fm. Member III	WH09-97.9	97.9	Black Shale	2.7	3.7	0.7	0.9	1.0	0.9	2	0.8	92	34	2.3	0.9	11	4	76	0.40	19.1	564.0
Doushantuo Fm. Member III	WH09-99.6	99.6	Black Shale	2.9	1.9	1.5	0.8	1.0	0.8	1	0.3	44	15	1.2	0.4	6	2	47	0.19	25.2	563.4
Doushantuo Fm. Member III	WH09-100.4	100.4	Black Shale	2.9	1.8	1.7	0.7	1.0	0.8	1	0.4	57	20	1.5	0.5	7	2	56	0.21	27.0	563.1
Doushantuo Fm. Member III	WH09-101.2	101.2	Calcareous Black Shale	0.9	1.5	0.6	0.9	0.9	0.8	3	2.8	111	119	5.2	5.5	22	23	63	0.12	50.3	562.9
Doushantuo Fm. Member III	WH09-102.4	102.4	Black Shale	5.9	3.2	1.9	0.9	1.0	0.9	7	1.2	106	18	10.2	1.7	43	7	71	0.24	29.6	562.5
Doushantuo Fm. Member III	WH09-103.3	103.3	Calcareous Black Shale	5.4	1.6	3.4	0.9	0.9		6	1.2	83	15	4.4	0.8	57	11		0.23		562.1
Doushantuo Fm. Member III	WH09-104.1	104.1	Black Shale	4.8	3.0	1.6	0.8	1.0	0.9	6	1.2	100	21	8.2	1.7	42	9	87	0.29	29.7	561.9
Doushantuo Fm. Member III	WH09-105.3	105.3	Black Shale	5.0	2.4	2.1	0.7	0.9	0.8	5	1.1	105	21	7.9	1.6	34	7	73	0.26	27.7	561.5
Doushantuo Fm. Member III	WH09-106.4	106.4	Black Shale	4.3	2.6	1.7	0.7	1.0	0.9	3	0.7	98	23	4.3	1.0	17	4	70	0.36	19.7	561.1
Doushantuo Fm. Member III	WH09-107.4	107.4	Black Shale	2.9	3.3	0.9	0.8	1.0	0.9	4	1.3	93	32	5.5	1.9	26	9	67	0.11	60.7	560.7
Doushantuo Fm. Member III	WH09-108.3	108.3	Black Shale	0.5	1.7	0.3	0.8	0.9		2	4.5	64	123	1.3	2.5	31	59		0.37		560.4
Doushantuo Fm. Member III	WH09-110.7	110.7	Calcareous Black Shale	0.6	1.0	0.7	1.0	0.8	0.7	19	30.2	45	70	5.5	8.5	4	6	54	0.07	78.4	559.6
Doushantuo Fm. Member IV	WH09-114.5	114.5	Black Shale	1.1	0.8	1.5	0.7	1.0	0.8	2	1.3	92	81	3.0	2.6	15	13	59	0.14	43.2	558.3
Doushantuo Fm. Member IV	WH09-115.3	115.3	Black Shale	3.8	1.6	2.4	0.6	0.9	0.8	68	18.1	2956	785	18.4	4.9	1063	282	508	0.34	147.6	557.3
Doushantuo Fm. Member IV	WH09-115.5	115.5	Black Shale	1.5	1.9	0.8	0.7	0.9		76	52.2	966	666	13.6	9.4	74	51		0.44		557.0
Doushantuo Fm. Member IV	WH09-115.9	115.9	Black Shale	2.9	1.8	1.6	0.7	0.9		126	43.5	1693	584	13.9	4.8	432	149		0.47		556.5
Doushantuo Fm. Member IV	WH09-116.3	116.3	Black Shale	1.9	1.2	1.6	0.6	0.8		66	33.9	1089	564	11.1	5.8	21	11		0.43		555.9
Doushantuo Fm. Member IV	WH09-116.8	116.8	Black Shale	5.0	1.3	3.8	0.7	0.9		79	15.8	773	154	8.8	1.8	184	37		0.31		555.3
Doushantuo Fm. Member IV	WH09-117.4	117.4	Black Shale	5.2	2.8	1.9	0.8	0.9		95	18.1	278	53	20.4	3.9	51	10		0.31		554.5
Doushantuo Fm. Member IV	WH09-117.8	117.8	Black Shale	8.5	2.5	3.5	0.7	0.9	0.9	61	7.2	126	15	20.2	2.4	15	2	64	0.27	24.3	553.9
Doushantuo Fm. Member IV	WH09-118.3	118.3	Black Shale	9.3	2.3	4.1	0.8	0.9		34	3.7	138	15	13.7	1.5	8	1	69	0.18	38.8	553.3
Doushantuo Fm. Member IV	WH09-118.9	118.9	Calcareous Black Shale	7.0	1.2	5.6	0.9	0.9	0.8	35	5.1	100	14	31.5	4.5	12	2	28	0.12	23.9	552.5
Doushantuo Fm. Member IV	WH09-119.5	119.5	Calcareous Black Shale	7.1	1.2	5.7	0.9	0.8		33	4.7	177	25	19.4	2.7	42	6	54	0.12	45.2	551.7
Doushantuo Fm. Member IV	WH09-120.0	120.0	Calcareous Black Shale	4.1	0.6	7.3	0.7	0.9	0.8	22	5.5	396	97	18.5	4.5	66	16	72	0.12	58.6	551.0

Stratigraphic Unit	Sample No.	Strat. Height (m)	Lithology	TOC (Wt %)	S_{PY} (Wt %)	TOC/ S_{PY}	FeHR/ FeT	FePY/ FeHR	DOP	Mo (ppm)	Mo/TOC (ppm/Wt%)	V (ppm)	V/TOC (ppm/Wt%)	U (ppm)	U/TOC (ppm/Wt%)	Re (ppb)	Re/TOC (ppb/Wt%)	Cr (ppm)	Ti (Wt %)	Cr/Ti (ppm/ppm) x 1000	Age Estimates (Ma)
Liuchapo Formation	WH09-131.5	131.5	Black Shale-Chert	0.1	0.3	0.4	0.8	0.8		0.83	7.2	44	384	1.1	9.7	5	42	37	0.05	74.0	545.0
Liuchapo Formation	WH09-132.6	132.6	Black Shale-Chert	0.1	0.1	0.5	0.7	0.6		0.52	10.1	19	363	0.5	9.5	11	211	42	0.04	114.7	544.7
Liuchapo Formation	WH09-133.5	133.5	Black Shale-Chert	0.2	0.1	1.6	0.8	0.6		0.68	3.9	11	62	0.9	4.8	10	56	33	0.03	104.6	544.4
Liuchapo Formation	WH09-135.0	135.0	Black Shale-Chert	0.1	0.2	0.7	0.6	0.7		0.53	3.5	22	150	1.0	6.5	88	586	44	0.08	55.5	544.0
Liuchapo Formation	WH09-136.7	136.7	Black Shale-Chert	0.1	0.2	0.3	0.5	0.7		0.38	5.6	35	510	1.5	21.8	6	95	44	0.12	36.7	543.5
Liuchapo Formation	WH09-137.8	137.8	Black Shale-Chert	0.3	0.5	0.6	0.7	0.9		0.47	1.5	43	134	0.0	0.1	5	16	43	0.10	44.8	543.2
Liuchapo Formation	WH09-138.5	138.5	Black Shale-Chert	0.7	0.2	3.7	0.6	0.7		0.89	1.4	22	34	0.9	1.4	7	10	36	0.08	42.1	543.0
Liuchapo Formation	WH09-139.5	139.5	Black Shale-Chert	0.4	0.2	2.2	0.6	0.5		0.49	1.3	38	100	0.7	1.9	5	14	51	0.09	53.3	542.7
Liuchapo Formation	WH09-140.6	140.6	Black Shale-Chert	0.6	0.4	1.4	0.6	0.8		0.51	0.9	72	122	0.9	1.4	12	21	95	0.14	67.0	542.4
Liuchapo Formation	WH09-141.2	141.2	Black Shale-Chert	1.5	0.7	2.3	0.8	0.8		0.49	0.3	75	50	1.9	1.3	7	5	93	0.14	66.6	542.3
Liuchapo Formation	WH09-142.1	142.1	Black Shale-Chert	4.3	0.2	23.0	0.8	0.2		2.80	0.6	831	191	11.4	2.6	16	4	303	0.11	277.1	542.0
Liuchapo Formation	WH09-143.2	143.2	Black Shale-Chert	3.7	0.1	45.1	0.7	0.1		0.94	0.2	212	57	4.6	1.2	25	7	174	0.09	191.9	539.7
Liuchapo Formation	WH09-144.1	144.1	Black Shale-Chert	3.9	0.1	47.1	0.8	0.1		0.45	0.2	268	68	5.5	1.4	96	25	219	0.10	213.2	537.8
Liuchapo Formation	WH09-144.8	144.8	Black Shale-Chert	2.6	0.1	38.2	1.0	0.5		0.87	0.2	167	65	3.0	1.2	33	13	95	0.01	684.2	536.3
Liuchapo Formation	WH09-145.4	145.4	Black Shale-Chert	3.8	0.1	31.0	0.8	0.2		0.52	0.2	199	52	3.0	0.8	19	5	126	0.07	175.5	535.1
Liuchapo Formation	WH09-146.3	146.3	Black Shale-Chert	3.3	0.4	9.1	0.9	0.6		0.53	0.1	248	75	6.5	2.0	15	5	99	0.04	228.6	533.2
Liuchapo Formation	WH09-147.5	147.5	Black Shale-Chert	5.2	0.1	64.0	0.9	0.4		0.36	1.1	238	46	2.7	0.5	37	7	99	0.03	314.9	530.6
Liuchapo Formation	WH09-148.4	148.4	Black Shale-Chert	0.3	0.1	4.0	1.0	0.5		0.38	3.3	24	74	0.9	2.8	20	62	18	0.00	372.0	528.7
Liuchapo Formation	WH09-149.7	149.7	Black Shale-Chert	0.1	0.2	0.7	0.7	0.7		0.95	0.4	24	212	0.1	1.3	40	348	29	0.02	119.5	526.0
Liuchapo Formation	WH09-150.6	150.6	Black Shale-Chert	2.5	0.2	12.9	1.0	0.7		0.46	0.2	323	127	7.3	2.9	45	18	342	0.01	3300.8	524.1
Niutitang Formation	WH09-151.6	151.6	Calcareous Black Shale	28.1	0.7	39.1	0.9	0.5		239	8.5	145	5	258.9	9.2	20	1	36	0.09	42.1	522.0
Niutitang Formation	WH09-152.3	152.3	Black Shale	1.8	0.1	21.4	1.0	0.6		11	5.8	612	333	3.4	1.9	136	74	39	0.01	677.5	520.5
Niutitang Formation	WH09-153.5	153.5	Black Shale	3.6	0.1	26.4	1.0	0.2		0.76	0.2	196	55	4.0	1.1	41	11	138	0.08	180.8	518.0
Niutitang Formation	WH09-154.2	154.2	Black Shale	1.9	0.1	15.3	1.0	0.6		0.67	0.4	104	56	2.1	1.1	68	37	71	0.02	344.1	516.5
Niutitang Formation	WH09-155.1	155.1	Black Shale	5.4	0.1	36.4	0.9	0.4		0.83	0.2	401	75	7.7	1.4	10	2	248	0.06	387.3	514.6
Yuanjia Section, Hunan Province, South China (Sahoo et al., 2012)																					
Doushantuo Fm. Member II	WHH-5.6	5.6	Black Shale	1.7	1.7	0.4	0.6	0.9		4	2	6417	3680	10	6	1819	1043		0.59		634.9
Doushantuo Fm. Member II	WHH-5.7	5.7	Black Shale	1.5	1.5	1.9	0.7	0.9		1	1	2767	1884	18	12	26	18	171.4	0.54	31.6	634.7
Doushantuo Fm. Member II	WHH-5.9	5.9	Black Shale	1.6	1.6						0										634.5
Doushantuo Fm. Member II	WHH-6.3	6.3	Black Shale	2.4	2.4	2.0	0.7	0.9		1	1	1193	488	20	8	405	165	86.42	0.51	16.8	633.2
Doushantuo Fm. Member II	WHH-6.4	6.4	Black Shale	2.7	2.7	2.4	0.7	0.9		1	0	847	317	20	7	140	52	85.83	0.50	17.1	632.6
Doushantuo Fm. Member II	WHH-6.8	6.8	Black Shale	3.0	3.0	2.6	0.8	0.9		1	0	497	165	13	4	28	9	72.5	0.43	16.7	632.5
Doushantuo Fm. Member II	WHH-6.9	6.9	Black Shale	2.1	2.1	3.2	0.7	1.0		1	0	370	178	11	5			85.98	0.55	15.7	632.1
Doushantuo Fm. Member II	WHH-6.95	6.95	Black Shale					1.0								238					630.5
Doushantuo Fm. Member II	WHH-7.2	7.2	Black Shale	2.7	2.7	4.0	0.9	1.0		1	0			9	3	25	9	62.48	0.40	15.8	629.7
Doushantuo Fm. Member II	WHH-7.4	7.4	Black Shale	3.6	3.6	4.1	0.8	1.0		1	0	336	93	10	3	38	11	65.63	0.42	15.6	628.3
Doushantuo Fm. Member II	WHH-7.6	7.6	Black Shale	4.1	4.1	0.1	0.3	0.7		32	8	458	113	9	2	86	21	86.98	0.55	15.9	626.0
Doushantuo Fm. Member II	WHH-9.1	9.1	Black Shale	0.6	0.6	0.0	0.1	0.2		40	67.1			8	13	75	126	48.23	0.38	12.7	619.2
Doushantuo Fm. Member II	WHH-9.5	9.5	Black Shale	0.8	0.8	0.1	0.2	0.4		15	18.9	256	313	8	10	52	64	51.78	0.40	13.0	618.0

Taoying section, Guizou Province, South China (Sahoo et al., 2012)

Section a. 7.3 m is the end of the Cap Carbonate

Stratigraphic Unit	Sample No.	Strat. Height (m)	Lithology	TOC (Wt %)	S_{PY} (Wt %)	TOC/ S_{PY}	FeHR/ FeT	FePY/ FeHR	DOP	Mo (ppm)	Mo/TOC (ppm/Wt%)	V (ppm)	V/TOC (ppm/Wt%)	U (ppm)	U/TOC (ppm/Wt%)	Re (ppb)	Re/TOC (ppb/Wt%)	Cr (ppm)	Ti (Wt %)	Cr/Ti (ppm/ppm) x 1000	Age Estimates (Ma)
Doushantuo Fm. Member II	TY09-7.6	7.6	Black Shale	1.2	0.0	36.9	0.3	0.1		3	3	5900	4962	17.89	15.05	1224	1030	242	0.40	59.8	634.0
Doushantuo Fm. Member II	TY09-7.9	7.9	Black Shale	1.3	0.2	6.9	0.3	0.7	0.4	4	3	3973	3178	11.31	9.04	2764	2211	135	0.38	35.6	632.7
Doushantuo Fm. Member II	TY09-8.0	8.0	Black Shale	1.3	0.0	29.4	0.2	0.2		1	1	3950	3080	16.74	13.06	2452	1912	129	0.43	30.2	632.3
Doushantuo Fm. Member II	TY09-8.3	8.3	Black Shale	1.9	0.0	277.8	0.1	0.1		3	1	2946	1545	16.89	8.86	25	13	114	0.44	26.0	631.1
Doushantuo Fm. Member II	TY09-8.6	8.6	Black Shale	1.5	0.0	73.2	0.1	0.2		25	17	285	193	3.77	2.55	1794	1212				629.9
Doushantuo Fm. Member II	TY09-8.8	8.8	Black Shale	1.6	0.1	18.1	0.3	0.5		6	4	1767	1095	18.43	11.42	2576	1596	84	0.45	18.7	629.1
Doushantuo Fm. Member II	TY09-9.0	9.0	Black Shale	2.1	0.0	48.1	0.2	0.4		4	2	1451	689	19.06	9.06	28	13	75	0.45	16.5	628.3
Doushantuo Fm. Member II	TY09-9.4	9.4	Black Shale	1.9	0.0	55.0	0.1	0.4		5	3	950	489	17.98	9.25	1565	805	68	0.47	14.3	626.6
Doushantuo Fm. Member II	TY09-9.8	9.8	Black Shale	1.6	0.0	48.0	0.2	0.2		3	2	1516	971	23.69	15.17	855	548	89	0.51	17.7	625.0
Doushantuo Fm. Member II	TY09-10.0	10.0	Black Shale	1.9	0.0	100.3	0.1	0.2		3	2	835	440	18.69	9.86	612	323	67	0.47	14.3	624.2
Doushantuo Fm. Member II	TY09-10.2	10.2	Black Shale	2.4	0.1	17.8	0.2	1.0	0.5	29	12	1178	493	18.51	7.74	3068	1283	79	0.45	17.6	623.4
Doushantuo Fm. Member II	TY09-10.4	10.4	Black Shale	2.2	0.1	24.2	0.3	0.4		39	18	804	369	17.17	7.89	1775	815	59	0.46	12.9	622.5
Doushantuo Fm. Member II	TY09-10.7	10.7	Black Shale	1.5	0.0	32.7	0.2	0.4		11	7	1853	1196	19.37	12.51	26	16	88	0.47	18.7	621.3
Doushantuo Fm. Member II	TY09-11.0	11.0	Black Shale	2.1	0.5	4.1	1.0	1.0	0.8	30	14	525	249	10.29	4.88	1827	866	48	0.30	16.1	620.1
Doushantuo Fm. Member II	TY09-11.3	11.3	Black Shale	2.1	0.1	21.6	0.3	0.5		11	5	253	118	8.17	3.81	36	17	61	0.45	13.8	618.9
Doushantuo Fm. Member II	TY09-11.5	11.5	Black Shale	2.4	0.1	21.3	0.3	0.7		11	5	247	105	8.04	3.41	86	37	52	0.47	11.1	618.0
Doushantuo Fm. Member II	TY09-11.8	11.8	Black Shale	2.4	0.1	43.9	0.2	0.5		11	4	213	88	8.44	3.49	17	7	54	0.48	11.3	616.8
Doushantuo Fm. Member II	TY09-12.0	12.0	Black Shale	2.2	0.0	128.4	0.1	0.2		6	3	294	131	7.75	3.45	149	66	61	0.46	13.2	616.0
Section b. 13.0 m is the base of the black shale																					
Doushantuo Fm. Member II	TY09-13.3	13.3	Black Shale	0.4	0.8		0.5	0.9		1	4	1016	2783	7.82	21.41	39	106	270	0.45	60.2	634.0
Doushantuo Fm. Member II	TY09-13.8	13.8	Black Shale	1.3	0.6	2.4	0.6	1.0	0.8	3	3	6096	4582	13.08	9.83	1440	1083	212	0.36	58.3	634.7
Doushantuo Fm. Member II	TY09-14.0	14.0	Black Shale	2.0	0.2	12.3	0.3	0.7		15	7	3040	1499	19.06	9.40	165	81	130	0.44	29.4	633.0
Doushantuo Fm. Member II	TY09-15.1	15.1	Black Shale	1.7	0.4	4.0	0.3	0.9	0.7	38	22	2522	1465	33.61	19.52	2702	1569	133	0.58	22.9	632.0
Doushantuo Fm. Member II	TY09-15.5	15.5	Black Shale	2.5	0.5	5.2	0.7	0.9		165	67	669	271	15.71	6.37	905	367	62	0.43	14.6	632.3
Doushantuo Fm. Member II	TY09-16.3	16.3	Black Shale	2.6	0.7	3.4	1.0	0.8		48	19	455	176	16.82	6.51	162	63	60	0.45	13.2	629.8
Doushantuo Fm. Member II	TY09-16.5	16.5	Black Shale	3.2	1.6	2.0	0.7	1.0	0.9	114	36	424	132	12.49	3.89	93	29	81	0.49	16.6	629.0
Doushantuo Fm. Member II	TY09-17.5	17.5	Black Shale	1.9	0.5	4.1	0.6	0.5	0.5	13	7	418	224	5.67	3.03	77	41	94	0.54	17.2	628.0
Doushantuo Fm. Member II	TY09-18.8	18.8	Black Shale	2.6	0.5	5.6	0.7	0.7	0.5	9	3	262	101	3.77	1.46	55	21	63	0.38	16.4	626.0
Doushantuo Fm. Member II	TY09-19.7	19.7	Black Shale	2.8	0.5	5.7	0.6	0.8	0.6	11	4	313	114	4.67	1.69	33	12	73	0.45	16.2	622.0
Doushantuo Fm. Member II	TY09-21.3	21.3	Black Shale	4.5	1.0	4.3	1.0	0.9	0.8	12	3	200	44	6.83	1.51	32	7	48	0.30	15.9	619.2
Doushantuo Fm. Member II	TY09-22.3	22.3	Black Shale	1.0	1.7	0.6	1.0	1.0	0.9	0	0.3	185	181	5.37	5.24	4	4	83	0.30	27.4	617.8

Shatan section, Sichuan Province, South China (Guo et al., 2007)

Stratigraphic Unit	Sample No.	Strat. Height (m)	Lithology	TOC (Wt %)	S_{PY} (Wt %)	TOC/ S_{PY}	FeHR/ FeT	FePY/ FeHR	DOP	Mo (ppm)	Mo/TOC (ppm/Wt%)	V (ppm)	V/TOC (ppm/Wt%)	U (ppm)	U/TOC (ppm/Wt%)	Re (ppb)	Re/TOC (ppb/Wt%)	Cr (ppm)	Ti (Wt %)	Cr/Ti (ppm/ppm) x 1000	Age Estimates (Ma)
Guojiaba Formation	Sat531	154.1	Black shale	0.23	0.25	0.92				0.9	3.9	65	282	2.3	10.1			56	0.30	18.4	520.8
Guojiaba Formation	Sat530	131.5	Black shale		0.23	0.00				2.9		77		3.5				64	0.36	17.8	522.5
Guojiaba Formation	Sat529	124.5	Black shale	0.56	0.13	4.31				1.9	3.4	72	128	2.9	5.2			61	0.34	18.2	523.0
Guojiaba Formation	Sat528	118.5	Black shale	0.38	0.39	0.97				1.9	5.0	98	257	3.2	8.4			84	0.42	19.9	523.5
Guojiaba Formation	Sat527	113.5	Black shale		0.24	0.00				3.9		83		3.0				70	0.41	17.2	523.9
Guojiaba Formation	Sat526	109	Black shale							2.4		78		3.3				69	0.38	18.1	524.2
Guojiaba Formation	Sat525	102.4	Black shale	0.65	0.43	1.51				4.0	6.2	87	134	3.8	5.9			74	0.38	19.3	524.7
Guojiaba Formation	Sat524	99.4	Black shale	0.69	1.2	0.58				5.1	7.4	82	119	3.8	5.5			66	0.37	18.2	525.0
Guojiaba Formation	Sat523	93.5	Black shale	0.81	0.44	1.84				3.9	4.9	75	93	4.1	5.0			66	0.34	19.1	525.4
Guojiaba Formation	Sat522	90	Black shale	0.62	0.51	1.22				5.2	8.4	102	165	4.6	7.4			85	0.42	20.1	525.7
Guojiaba Formation	Sat521	86.1	Black shale	0.87	0.39	2.23				4.6	5.2	103	119	4.5	5.2			82	0.45	18.3	526.0
Guojiaba Formation	Sat520	80.8	Black shale	0.77	0.41	1.88				3.4	4.4	95	124	4.0	5.2			78	0.41	18.7	526.4
Guojiaba Formation	Sat519	76.5	Black shale	1.13	1.31	0.86				5.6	5.0	92	82	5.7	5.0			82	0.42	19.7	526.7
Guojiaba Formation	Sat518	70.7	Black shale	1.32	0.69	1.91				6.8	5.1	85	65	6.4	4.9			71	0.41	17.2	527.1
Guojiaba Formation	Sat517	67.1	Black shale	1.63	0.81	2.01				7.1	4.3	107	66	6.4	3.9			87	0.44	19.8	527.4
Guojiaba Formation	Sat516	61.5	Black shale	1.74	1.27	1.37				18.7	10.8	162	93	10.9	6.3			96	0.44	21.8	527.8
Guojiaba Formation	Sat515	56.3	Black shale	1.88	1.43	1.31				44.2	23.5	484	258	21.3	11.3			114	0.51	22.4	528.2
Guojiaba Formation	Sat514	53.5	Black shale							13.4		230		13.3				27	0.12	21.8	528.4
Guojiaba Formation	Sat513	50.9	Black shale	3.17	0.22	14.41				36.6	11.5	424	134	19.5	6.1			91	0.43	21.1	528.6
Guojiaba Formation	Sat512	46.4	Black shale	3.88	0.63	6.16				35.9	9.2	406	105	18.4	4.7			92	0.41	22.5	529.0
Guojiaba Formation	Sat511	42.4	Black shale	3.15	1.3	2.42				38.6	12.3	298	95	20.4	6.5			86	0.35	24.7	529.3
Guojiaba Formation	Sat510	38.4	Black shale	4.08	0.91	4.48				70.9	17.4	188	46	44.6	10.9			87	0.34	25.5	529.6
Guojiaba Formation	Sat509	36.4	Black shale	3.11	1.6	1.94				39.0	12.5	1198	385	22.8	7.3			104	0.37	28.0	529.7
Guojiaba Formation	Sat508	34	Black shale	3.37	0.68	4.96				29.9	8.9	2141	635	17.3	5.1			128	0.36	35.5	529.9
Guojiaba Formation	Sat507	32	Black shale	3.69	1.51	2.44				25.5	6.9	2050	555	16.1	4.4			164	0.38	43.1	530.1
Guojiaba Formation	Sat506	30	Black shale	4.9	0.75	6.53				70.2	14.3	444	91	23.4	4.8			101	0.43	23.4	530.2
Guojiaba Formation	Sat505	28.7	Black shale	4.18	0.94	4.45				42.8	10.2	424	101	29.9	7.2			103	0.40	25.9	530.3
Guojiaba Formation	Sat504	27.6	Black shale	3.12	1.3	2.40				12.0	3.9	215	69	12.3	3.9			103	0.41	25.4	530.4
Guojiaba Formation	Sat503	26.8	Black shale	2.57	0.97	2.65				5.4	2.1	188	73	8.7	3.4			109	0.40	26.8	530.5
Guojiaba Formation	Sat502	25.8	Black shale	0.85	0.5	1.70				2.2	2.6	164	193	8.1	9.5			104	0.43	24.0	530.5
Guojiaba Formation	Sat501	25.25	Black shale							5.0		149		5.6				103	0.44	23.2	530.6
Guojiaba Formation	Sat500	25.05	Black shale							1.1		43		9.3				13	0.03	42.4	530.6

Shongtao section, Sichuan Province, South China (Guo et al., 2007)																				
Stratigraphic Unit	**Sample No.**	**Strat. Height (m)**	**Lithology**	**TOC (Wt %)**	**S_{PY} (Wt %)**	**TOC/ S_{PY}**	**FeHR/ FeT**	**FePY/ FeHR**	**DOP**	**Mo (ppm)**	**Mo/TOC (ppm/Wt%)**	**V (ppm)**	**V/TOC (ppm/Wt%)**	**U (ppm)**	**U/TOC (ppm/Wt%)**	**Re (ppb)**	**Re/TOC (ppb/Wt%)**	**Cr (ppm)**	**Ti (Wt %)**	**Cr/Ti (ppm/ppm) x 1000**	**Age Estimates (Ma)**
Jiumenchong Formation	Son594	58.45	Black shale		1.12					111.9		475		39.4				84	0.39	21.4	529.4
Jiumenchong Formation	Son593	57.45	Black shale		3.03					295.4		2271		44.6				93	0.36	26.1	529.6
Jiumenchong Formation	Son592	55.85	Black shale		3.67					216.6		1418		76.5				100	0.37	26.6	529.8
Jiumenchong Formation	Son591	54.35	Black shale		3.98					90.2		564		48.1				74	0.32	23.2	530.0
Jiumenchong Formation	Son590	51.45	Carbonate		1.11					18.0		581		10.7				43	0.10	41.2	530.5
Jiumenchong Formation	Son589	50.3	Black shale		3.93					112.4		686		59.6				71	0.29	24.1	530.7
Jiumenchong Formation	Son588	49.6	Black shale		4.86					248.0		1194		98.5				140	0.29	48.6	530.8
Jiumenchong Formation	Son587	48.6	Black shale		3.7					143.6		2001		45.9				109	0.26	41.3	530.9
Jiumenchong Formation	Son586	47.95	Black shale		0.38					20.3		201		16.8				7	0.02	38.7	531.0
Jiumenchong Formation	Son585	47.75	Black shale		4					112.1		394		65.7				59	0.21	27.7	531.0
Jiumenchong Formation	Son584	46	Black shale		2.88					75.0		5602		42.9				441	0.30	146.0	531.3
Jiumenchong Formation	Son583	45	Black shale		3.36					132.7		3850		48.2				175	0.29	59.7	531.5
Jiumenchong Formation	Son582	44.35	Black shale	1.94	0.62	3.13				5.0	2.6	230	118	18.4	9.5			49	0.01	406.0	531.6
Jiumenchong Formation	Son581	44.15	Black shale	3.25	3.2	1.02				36.7	11.3	3247	999	48.6	14.9			1877	0.23	831.3	531.6
Liuchapo Formation	Son500	44.05	Chert	0.8	0.11	7.27				13.4	16.8	578	722	11.5	14.4			77	0.01	916.3	542.0
Liuchapo Formation	Son501	43.87	Chert	0.26	1.85	0.14				34.7	133.3	1394	5362	51.8	199.2			9	0.10	9.3	541.9
Liuchapo Formation	Son502	43.52	Chert	2.32	0.1	23.20				11.3	4.9	275	118	6.9	3.0			60	0.01	1121.2	542.2
Liuchapo Formation	Son503	42.97	Chert	1.09	12.5	0.09				9.8	9.0	111	101	7.6	7.0			50	0.01	696.8	542.5
Liuchapo Formation	Son505	38	Chert	1.25						3.3	2.6	163	131	3.0	2.4			48	0.00	998.3	544.7
Liuchapo Formation	Son506	32	Chert	4.6						3.1	0.7	248	54	4.9	1.1			74	0.01	729.4	547.3
Liuchapo Formation	Son507	28	Chert	0.6	18.05	0.03				0.7	1.1	44	73	2.0	3.3			25	0.04	60.6	549.1
Liuchapo Formation	Son508	26	Chert	0.31	0.44	0.70				1.7	5.4	7	24	0.7	2.4			4	0.01	57.9	550.0
Silikou Section, South China (Chang et al., 2010, 2012)																					
Laobao Formation	SLK-12	12	Black Shale-Chert				0.61		0.09	5.38		15.53		2.06							549
Laobao Formation	SLK-16	16	Black Shale-Chert				0.55		0.1	8.45		70.62		5.73							549
Laobao Formation	SLK-40	40	Black Shale-Chert				0.65		0.33	2.97		36.09		1.75							548
Laobao Formation	SLK-43	43	Black Shale-Chert				0.56		0.35	3.05		28.59		0.89							548
Laobao Formation	SLK-51	51	Black Shale-Chert				0.64		0.27	3.69		49.99		1.18							547
Laobao Formation	SLK-57	57	Black Shale-Chert				0.43		0.32	2.96		27.61		0.78							547
Laobao Formation	SLK-74	74	Black Shale-Chert				0.58		0.06	2.26		46.63		1.55							546
Laobao Formation	SLK-78	78	Black Shale-Chert				0.37		0.32	2.92		46.31		1.18							546
Laobao Formation	SLK-82	82	Black Shale-Chert				0.7		0.37	3.09		25.04		0.8							546
Laobao Formation	SLK-83	83	Black Shale-Chert				0.38		0.01	2.5		85.98		1.21							546
Laobao Formation	SLK-90	90	Black Shale-Chert				0.5		0.17	2.5		39.51		0.92							545
Laobao Formation	SLK-103	103	Black Shale-Chert				0.83		0.54	3.04		65.44		1.3							545
Laobao Formation	SLK-107	107	Black Shale-Chert				0.53		0.49	3.03		54.74		1.1							544
Laobao Formation	SLK-117	117	Black Shale-Chert				0.27		0.01	2.53		52.5		1.22							544

Jiulongwan Section, Yangtze Geroges, South China (Li et al., 2010)

Stratigraphic Unit	Sample No.	Strat. Height (m)	Lithology	TOC (Wt %)	S_{PY} (Wt %)	TOC/ S_{PY}	FeHR/ FeT	FePY/ FeHR	DOP	Mo (ppm)	Mo/TOC (ppm/Wt%)	V (ppm)	V/TOC (ppm/Wt%)	U (ppm)	U/TOC (ppm/Wt%)	Re (ppb)	Re/TOC (ppb/Wt%)	Cr (ppm)	Ti (Wt %)	Cr/Ti (ppm/ppm) x 1000	Age Estimates (Ma)
Doushantuo Fm. Member IV	HN-23	154	Shale/Carbonate	15.1	2.2	6.8	0.7	0.8		180.7	12										552
Doushantuo Fm. Member IV	HN-21	152	Shale/Carbonate	5.2	1.2	4.4	0.4	0.9		136	26.3										553
Doushantuo Fm. Member IV	HN-18	149	Shale/Carbonate	6.4	1.1	5.8	0.5	0.9		111.4	17.3										555
Doushantuo Fm. Member IV	HN-15	146	Shale/Carbonate	5	1.6	3.1	0.5	0.9		161.3	32.6										558
Doushantuo Fm. Member IV	HN-13	144	Shale/Carbonate	4.8	1.2	4.1	0.4	0.9		71.8	15.1										559
Doushantuo Fm. Member IV	HN-09	144	Shale/Carbonate	4.6	2.2	2.1	0.8	0.9		113.9	24.6										559
Doushantuo Fm. Member IV	HN-12	143	Shale/Carbonate	5.1	2.4	2.1	0.8	0.9		125.1	24.5										560
Doushantuo Fm. Member IV	HN-11	142.2	Shale/Carbonate	2	2.4	0.8	0.7	0.9		121.7	61.5										560
Doushantuo Fm. Member III	HN-08	141.5	Shale/Carbonate	0.2	0.3	0.6	0.7	0.7		0.6	3.3										561
Doushantuo Fm. Member III	HN-10	140.9	Shale/Carbonate	0.3	0.4	0.6	0.8	0.7		2.8	10.2										561
Doushantuo Fm. Member II	JS-68O	79	Shale/Carbonate	0.7	0.8	0.9	0.5	0.7		0.5	0.7										608
Doushantuo Fm. Member II	JS-68I	79	Shale/Carbonate	0.8	0.7	1.1	0.5	0.7		0.5	0.6										608
Doushantuo Fm. Member II	JS-60	70	Shale/Carbonate	1.6	0.8	2.1	0.5	0.8		0.9	0.5										614
Doushantuo Fm. Member II	JS-56	64	Shale/Carbonate	0.6	1.2	0.6	0.5	0.8		0.5	0.8										616
Doushantuo Fm. Member II	JS-48	56	Shale/Carbonate	1	0.6	1.7	0.4	0.7		0.3	0.3										619
Doushantuo Fm. Member II	JS-42	49	Shale/Carbonate	0.9	0.9	0.9	0.5	0.7		0.8	0.9										621
Doushantuo Fm. Member II	JS-24	19.7	Shale/Carbonate	2.9	1.3	2.3	0.5	0.8		1.6	0.6										632
Doushantuo Fm. Member II	JS-21	16	Shale/Carbonate	1.8	1.1	1.7	0.6	0.8		1.1	0.6										633
Doushantuo Fm. Member II	JS-18	8	Shale/Carbonate	1.2	1.4	0.9	0.6	0.8		1.3	1.1										634
Doushantuo Fm. Member II	JS-17	6	Shale/Carbonate	0.5	1.8	0.3	0.8	0.8		1.7	3.3										635
Doushantuo Fm. Member II	JS-15*	5.3	Shale/Carbonate	0.1	0.9	0.1	0.5	0.8		0	0										635
Doushantuo Fm. Member II	JS-14*	0.1	Shale/Carbonate	0.5	3.9	0.1	1	0.8		3.9	7.8										636

Zhongling Section, Yangtze Geroges, South China (Li et al., 2010)

Doushantuo Fm. Member IV	SH-42	286	Shale/Carbonate	0.1	0.9	0.1	0.8	1		0.4	4.2										552
Doushantuo Fm. Member IV	SH-79	284.5	Black Shale	0.6	0.2	4.2	1	0.8		0.1	0.1										552
Doushantuo Fm. Member IV	SH-44	282	Shale/Carbonate	0	0.1	0.1	1	0.7		0.1											553
Doushantuo Fm. Member III	SH-73	124	Black Shale	0.1	0.1	0.8	1	0.7		0.3	2.9										601
Doushantuo Fm. Member II	SH-26	29	Shale/Carbonate	0.7	1.5	0.4	0.7	0.7		4.7	7.1										627
Doushantuo Fm. Member II	SH-24	27	Shale/Carbonate	3.8	2.9	1.3	0.8	0.7		9.6	2.5										628
Doushantuo Fm. Member II	SH-23	19.5	Black Shale	2.9	2.3	1.3	0.7	0.8		12.7	4.3										630
Doushantuo Fm. Member II	SH-18	14.5	Black Shale	2	3.3	0.6	0.8	0.9		12.4	6.1										631
Doushantuo Fm. Member II	SH-13	7.5	Shale/Carbonate	0.1	2	0.1	0.9	0.7		0.7	5.2										633

Goz Creek Section, Wernecke Mountains, NW Canada (Johnston et al., 2013)

Stratigraphic Unit	Sample No.	Strat. Height (m)	Lithology	TOC (Wt %)	S_{PY} (Wt %)	TOC/ S_{PY}	FeHR/ FeT	FePY/ FeHR	DOP	Mo (ppm)	Mo/TOC (ppm/Wt%)	V (ppm)	V/TOC (ppm/Wt%)	U (ppm)	U/TOC (ppm/Wt%)	Re (ppb)	Re/TOC (ppb/Wt%)	Cr (ppm)	Ti (Wt %)	Cr/Ti (ppm/ppm) x 1000	Age Estimates (Ma)
Sheepbed Fm.	F849	20	Siliciclastics (Shale)	0.12			0.78	0.02		0.0	0.1	121	1008					68	0.36	18.9	631.9
Sheepbed Fm.	F849	22	Siliciclastics (Shale)	0.21			0.77	0.04		0.0	0.1	114	543					53	0.34	15.8	631.6
Sheepbed Fm.	F849	26	Siliciclastics (Shale)	0.27			0.74	0.09		3.0	11.1	124	459					48	0.30	16.0	631.0
Sheepbed Fm.	F849	29.3	Siliciclastics (Shale)	0.45			0.66	0.09		2.0	4.4	142	316					65	0.36	18.1	630.5
Sheepbed Fm.	F849	30.2	Siliciclastics (Shale)				0.52	0.02		2.0		131						55	0.38	14.3	630.4
Sheepbed Fm.	F849	40	Siliciclastics (Shale)	0.61			0.55	0.09		1.0	1.6	124	203					64	0.32	19.8	628.9
Sheepbed Fm.	F849	46	Siliciclastics (Shale)	0.19			0.44	0.12		0.0	0.1	101	532					43	0.31	13.8	628.0
Sheepbed Fm.	F849	50	Siliciclastics (Shale)	0.2			0.51	0.07		0.0	0.1	144	720					77	0.41	18.9	627.4
Sheepbed Fm.	F849	54	Siliciclastics (Shale)	0.6			0.46	0.05		0.0	0.0	118	197					66	0.34	19.3	626.8
Sheepbed Fm.	F849	60	Siliciclastics (Shale)	0.29			0.57	0.06		1.0	3.5	107	369					50	0.36	13.9	625.9
Sheepbed Fm.	F849	66	Siliciclastics (Shale)	0.49			0.38	0.02		0.0	0.0	85	173					40	0.20	20.2	625.0
Sheepbed Fm.	F849	72	Siliciclastics (Shale)				0.47	0.15		2.0		107						63	0.38	16.7	624.1
Sheepbed Fm.	F849	85	Siliciclastics (Shale)	0.52			0.43	0.11		2.0	3.9	99	190					59	0.38	15.4	622.2
Sheepbed Fm.	F849	87	Siliciclastics (Shale)	0.6			0.49	0.04		1.0	1.7	101	168					53	0.29	18.4	621.9
Sheepbed Fm.	F849	93	Siliciclastics (Shale)				0.39	0.08		0.0		64						34	0.16	21.8	621.0
Sheepbed Fm.	F849	99	Siliciclastics (Shale)	1.15			0.67	0.15		2.0	1.7	94	82					49	0.34	14.6	620.1
Sheepbed Fm.	F849	103	Siliciclastics (Shale)				0.41	0.09		2.0		85						49	0.36	13.6	619.5
Sheepbed Fm.	F849	107	Siliciclastics (Shale)				0.49	0.06		2.0		102						67	0.21	31.9	618.9
Sheepbed Fm.	F849	113	Siliciclastics (Shale)				0.38	0.07		2.0		92						55	0.30	18.4	618.0
Sheepbed Fm.	F849	125	Siliciclastics (Shale)	0.79			0.49	0.14		2.0	2.5	119	151					58	0.36	16.1	616.2
Sheepbed Fm.	F849	133	Siliciclastics (Shale)				0.45	0.06		1.0		97						62	0.40	15.7	615.0
Sheepbed Fm.	F849	143	Siliciclastics (Shale)	0.5			0.41	0.08		1.0	2.0	138	276					77	0.36	21.4	613.6
Sheepbed Fm.	F849	145	Siliciclastics (Shale)	0.64			0.38	0.08		2.0	3.1	136	213					67	0.32	20.7	613.3
Sheepbed Fm.	F849	147	Siliciclastics (Shale)	0.77			0.46	0.02		1.0	1.3	132	171					76	0.39	19.5	613.0
Sheepbed Fm.	F849	155	Siliciclastics (Shale)	0.43			0.47	0.14		2.0	4.7	141	328					73	0.41	17.9	611.8
Sheepbed Fm.	F849	157	Siliciclastics (Shale)	0.53			0.47	0.05		3.0	5.7	187	353					73	0.29	25.4	611.5
Sheepbed Fm.	F849	161	Siliciclastics (Shale)				0.50	0.00		0.0		128						68	0.38	18.0	610.9
Sheepbed Fm.	F849	165	Siliciclastics (Shale)				0.53	0.05		2.0		142						67	0.31	21.5	610.3
Sheepbed Fm.	F849	176	Siliciclastics (Shale)				0.62	0.01		3.0		144						61	0.53	11.6	608.6
Sheepbed Fm.	F849	184	Siliciclastics (Shale)	0.46			0.47	0.09		1.0	2.2	175	380					80	0.34	23.8	607.4
Sheepbed Fm.	F849	188.5	Siliciclastics (Shale)				0.48	0.06		2.0		170						78	0.47	16.7	606.8
Sheepbed Fm.	F849	191	Siliciclastics (Shale)	0.59			0.41	0.05		1.0	1.7	110	186					61	0.23	26.1	606.4
Sheepbed Fm.	F849	195	Siliciclastics (Shale)				0.73	0.06		2.0		162						76	0.46	16.7	605.8
Sheepbed Fm.	F849	197	Siliciclastics (Shale)	0.62			0.45	0.02		2.0	3.2	162	261					75	0.38	19.9	605.5
Sheepbed Fm.	F849	199	Siliciclastics (Shale)	0.28			0.39	0.00		1.0	3.6	130	464					68	0.32	21.0	605.2
Sheepbed Fm.	F849	201	Siliciclastics (Shale)	0.84			0.41	0.02		1.0	1.2	159	189					69	0.43	16.0	604.9
Sheepbed Fm.	F849	208.5	Siliciclastics (Shale)				0.38	0.03		0.0		110						70	0.38	18.5	603.8
Sheepbed Fm.	F849	221	Siliciclastics (Shale)	0.55			0.42	0.11		1.0	1.8	125	227					71	0.46	15.4	601.9
Sheepbed Fm.	F849	223	Siliciclastics (Shale)	0.4			0.43	0.02		0.0	0.0	105	263					70	0.33	21.2	601.6
Sheepbed Fm.	F849	225	Siliciclastics (Shale)				0.91	0.02		0.0		117						78	0.48	16.3	601.3
Sheepbed Fm.	F849	227	Siliciclastics (Shale)	0.79			0.41	0.03		0.0	0.0	125	158					79	0.40	20.0	601.0
Sheepbed Fm.	F849	229	Siliciclastics (Shale)	0.5			0.38	0.04		0.0	0.0	94	188					69	0.41	16.9	600.7
Sheepbed Fm.	F849	234	Siliciclastics (Shale)	0.11			0.40	0.07		1.0	9.1	108	982					72	0.42	17.2	600.0
Sheepbed Fm.	F849	236	Siliciclastics (Shale)	0.25			0.44	0.02		1.0	4.0	106	424					62	0.40	15.7	599.7
Sheepbed Fm.	F849	240	Siliciclastics (Shale)				0.55	0.01		0.0		91						65	0.34	19.4	599.1
Sheepbed Fm.	F849	244	Siliciclastics (Shale)	0.12			0.41	0.01		0.0	0.1	84	700					67	0.34	19.6	598.5

Stratigraphic Unit	Sample No.	Strat. Height (m)	Lithology	TOC (Wt %)	S_{PY} (Wt %)	TOC/ S_{PY}	FeHR/ FeT	FePY/ FeHR	DOP	Mo (ppm)	Mo/TOC (ppm/Wt%)	V (ppm)	V/TOC (ppm/Wt%)	U (ppm)	U/TOC (ppm/Wt%)	Re (ppb)	Re/TOC (ppb/Wt%)	Cr (ppm)	Ti (Wt %)	Cr/Ti (ppm/ppm) x 1000	Age Estimates (Ma)
Sheepbed Fm.	F849	253	Siliciclastics (Shale)				0.48	0.04		2.0		112						75	0.30	25.0	597.2
Sheepbed Fm.	F849	254	Siliciclastics (Shale)	0.17			0.40	0.02		0.0	0.1	88	518					73	0.36	20.3	597.0
Sheepbed Fm.	F849	258	Siliciclastics (Shale)				0.51	0.03		0.0		93						77	0.46	16.7	596.4
Sheepbed Fm.	F849	264	Siliciclastics (Shale)	0.15			0.42	0.01		0.0	0.1	110	733					75	0.42	17.9	595.5
Sheepbed Fm.	F849	266	Siliciclastics (Shale)				0.63	0.02		0.0		99						69	0.50	13.7	595.2
Sheepbed Fm.	F849	270	Siliciclastics (Shale)				0.44	0.01		0.0		110						72	0.43	16.7	594.6
Sheepbed Fm.	F849	274	Siliciclastics (Shale)				0.45	0.02		0.0		102						81	0.43	18.8	594.0
Sheepbed Fm.	F849	276	Siliciclastics (Shale)	0.15			0.40	0.00		0.0	0.1	101	673					77	0.40	19.5	593.7
Sheepbed Fm.	F849	302	Siliciclastics (Shale)	0.15			0.48	0.00		0.0	0.1	98	653					78	0.50	15.5	589.8
Sheepbed Fm.	F849	320	Siliciclastics (Shale)	0.21			0.45	0.00		0.0	0.1	97	462					74	0.36	20.6	587.2
Sheepbed Fm.	F849	346	Siliciclastics (Shale)				0.37	0.03		0.0		97						74	0.50	14.7	583.3
Sheepbed Fm.	F849	360	Siliciclastics (Shale)	0.35			0.48	0.01		0.0	0.0	10	29					11	0.06	18.4	581.2
Sheepbed Fm.	F849	364	Siliciclastics (Shale)	0.15			0.46	0.07		0.0	0.1	130	867					79	0.58	13.7	580.6
Sheepbed Fm.	F849	366	Siliciclastics (Shale)	0.07			0.77	0.10		0.0	0.1	60	857					48	0.34	14.3	580.3
Sheepbed Fm.	F849	368	Siliciclastics (Shale)	0.19			0.64	0.08		0.0	0.1	92	484					73	0.39	18.7	580.0
Blue Flow er Fm.	F850	262	Siliciclastics (Shale)	0.21			0.46	0.00		0.0	0.1	5	24					4	0.06	6.7	567.9
Blue Flow er Fm.	F850	263.5	Siliciclastics (Shale)	0.26			0.36	0.00		0.0	0.0	70	269					23	0.29	7.9	567.7
Blue Flow er Fm.	F850	266	Siliciclastics (Shale)	0.15			0.44	0.00		0.0	0.1	93	620					66	0.27	24.5	567.5
Blue Flow er Fm.	F850	272.5	Siliciclastics (Shale)	0.97			0.52	0.12		0.0	0.0	75	77					65	0.29	22.6	566.9
Blue Flow er Fm.	F850	273	Siliciclastics (Shale)	0.04			0.56	0.07		0.0	0.3	78	1950					60	0.30	20.0	566.8
Blue Flow er Fm.	F850	276	Siliciclastics (Shale)	0.23			0.42	0.03		0.0	0.0	49	213					43	0.29	14.9	566.5
Blue Flow er Fm.	F850	282	Siliciclastics (Shale)	0.14			0.73	0.05		0.0	0.1	65	464					42	0.22	19.5	566.0
Blue Flow er Fm.	F850	311	Siliciclastics (Shale)	0.07			0.54	0.08		0.0	0.1	30	429					30	0.16	19.2	563.2
Blue Flow er Fm.	F850	312	Siliciclastics (Shale)	0.08			0.60	0.02		0.0	0.1	29	363					30	0.17	17.9	563.1
Blue Flow er Fm.	F850	332.5	Siliciclastics (Shale)	0.14			0.36	0.00		0.0	0.1	78	557					34	0.43	7.9	561.2
Blue Flow er Fm.	F850	335	Siliciclastics (Shale)	0.15			0.86	0.02		0.0	0.1	53	353					30		0.0	560.9
Blue Flow er Fm.	F850	337	Siliciclastics (Shale)	0.11			0.71	0.07		0.0	0.1	23	209					18	0.15	12.0	560.7
Blue Flow er Fm.	F850	344.8	Siliciclastics (Shale)	0.08			0.38	0.00		0.0	0.1	104	1300					63	0.31	20.6	560.0
Risky Fm.	F850	388	Siliciclastics (Shale)	0.12			0.39	0.02		0.0	0.1	103	858					64	0.47	13.7	555.9
Risky Fm.	F850	391	Siliciclastics (Shale)	0.22			0.60	0.07		0.0	0.1	73	332					41	0.23	17.5	555.6
Risky Fm.	F850	393.5	Siliciclastics (Shale)	0.13			0.60	0.01		0.0	0.1	96	738					46	0.30	15.3	555.4
Risky Fm.	F850	395	Siliciclastics (Shale)	0.09			0.59	0.02		0.0	0.1	103	1144					58	0.37	15.6	555.2
Xiaoerbulake Sectin, Lower Cambrian, Tarim Basin, North China (Yu et al., 2009)																					
Yuertushi Fm.	XCM2-1		Shale	3.93						12	3	2039	519	37.1	9.44	9.69	2.47	1163	1.45	80.2	540
Yuertushi Fm.	XCM-3		Shale	5.34						10	2	2965	555	27	5.06	10.45	1.96	1057	0.82	129.7	540
Yuertushi Fm.	XCM-5		Shale	9.33						1	0	1049	112	74.4	7.97	2.43	0.26	308	0.10	324.2	540
Yuertushi Fm.	XCM7-1		Shale	7.5						79	11	12207	1628	194.9	25.99	30.32	4.04	1471	3.23	45.5	540
Yuertushi Fm.	XCM8-1		Shale	3.39						57	17	3976	1173	71.8	21.18	20.65	6.09	646	1.11	58.2	540
Yuertushi Fm.	XCM9-1		Shale	5.89						43	7	2883	489	65.9	11.19	14.67	2.49	609	1.24	49.1	540
Yuertushi Fm.	XCM9-2		Shale	6.6						41	6	1728	262	70.6	10.70	10.87	1.65	411	0.79	52.3	540
Yuertushi Fm.	XCM10-1		Shale	8.56						35	4	1324	155	69.2	8.08	9.75	1.14	265	1.23	21.5	540
Yuertushi Fm.	XCM10-2		Shale	9.8						48	5	998	102	52	5.31	15.54	1.59	187	0.84	22.2	540
Yuertushi Fm.	XCM10-3		Shale	7.05						24	3	1069	152	32.8	4.65	10.67	1.51	252	0.61	41.1	540
Yuertushi Fm.	XCM10-4		Shale	5.45						15	3	290	53	25.6	4.70	8.76	1.61	119	0.70	17.1	540
Yuertushi Fm.	XCM10-5		Shale	6.56						6	1	620	95	21.1	3.22	5.54	0.84	218	0.74	29.4	540

APPENDIX C: CHAPTER 4

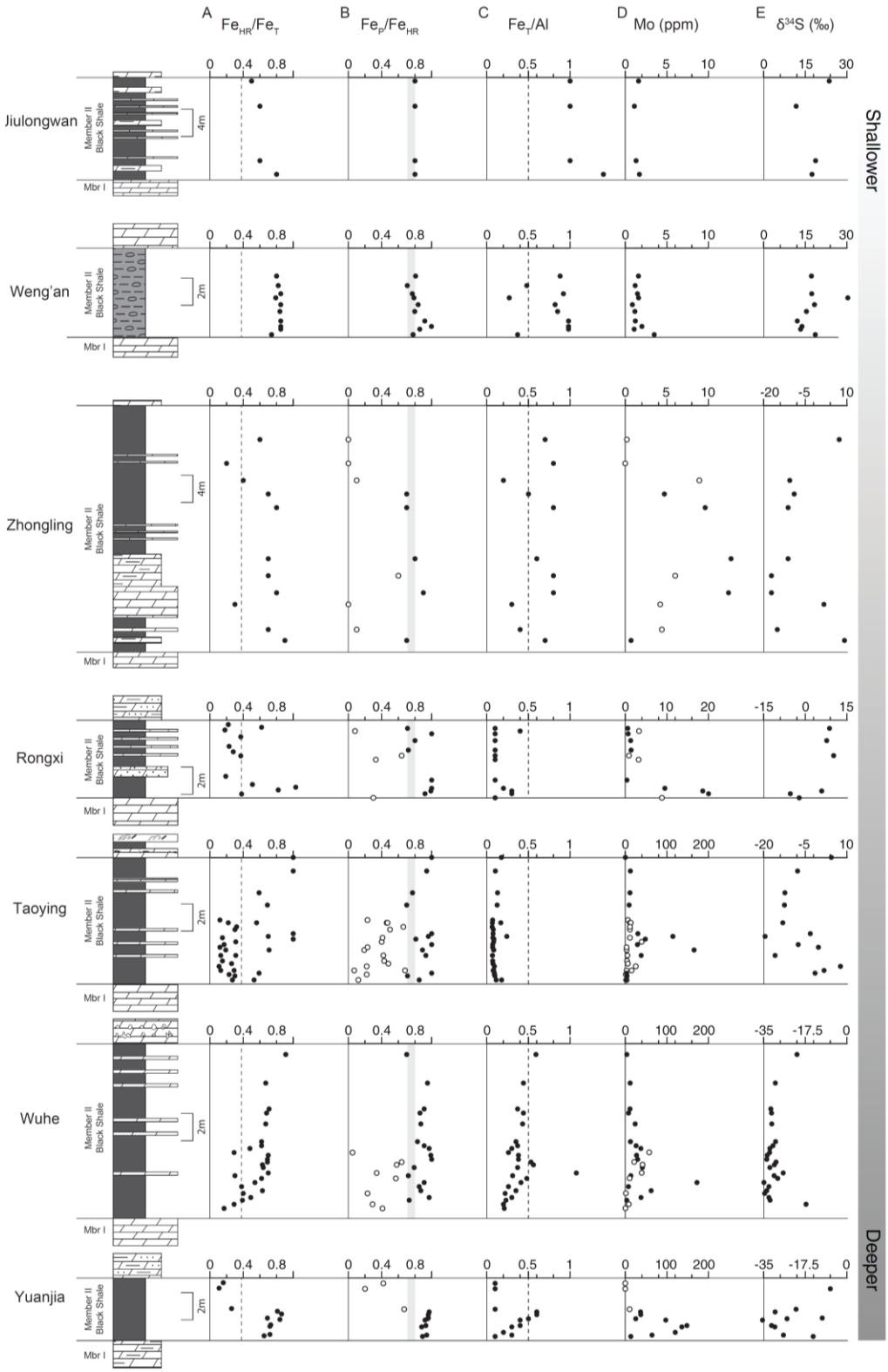

Figure S1 Iron speciation, Mo abundances and pyrite sulfur isotopes (δ^{34}Spyrite) of the Doushantuo Member II black shales (**A**) Highly reactive iron over total iron (Fe_{HR}/Fe_T). Fe_{HR}/Fe_T > 0.38 (dashed line) indicates anoxic conditions. Majority of the shale samples are anoxic, except for some oxic shales in the shelf-margin (Rongxi) and upper slope (Taoying) sections. (**B**) The ratio of pyrite over highly reactive iron (Fe_{PY}/Fe_{HR}). Samples with Fe_{HR}/Fe_T > 0.38 and Fe_{HR}/Fe_T > 0.7 (gray line) indicate deposition from euxinic environments (filled circles). Open circles represent samples with Fe_{HR}/Fe_T < 0.38, which may suggest oxic depositional conditions. (**C**) Total iron (Fe_T) and aluminum (Al) ratios (Fe_T/Al) of Member II black shales. Dashed line marks the average crustal Fe_T/Al ratio of ~0.5 (or average shale Fe_T/Al ratio from shales deposited from oxic environments (**D**) Mo concentrations (ppm) of Member II black shales. Data of the Jiulongwan and Zhongling sections are from Li et al. (2010). Note near crustal Mo values from shelf sections (Jiulongwan, Weng'an, and Zhongling). (**E**) Pyrite sulfur isotopes ($\delta^{34}S_p$) from Member II black shales. Note that higher $\delta^{34}S_p$ values are observed from the inner shelf settings (Jiulongwan and Weng'an).

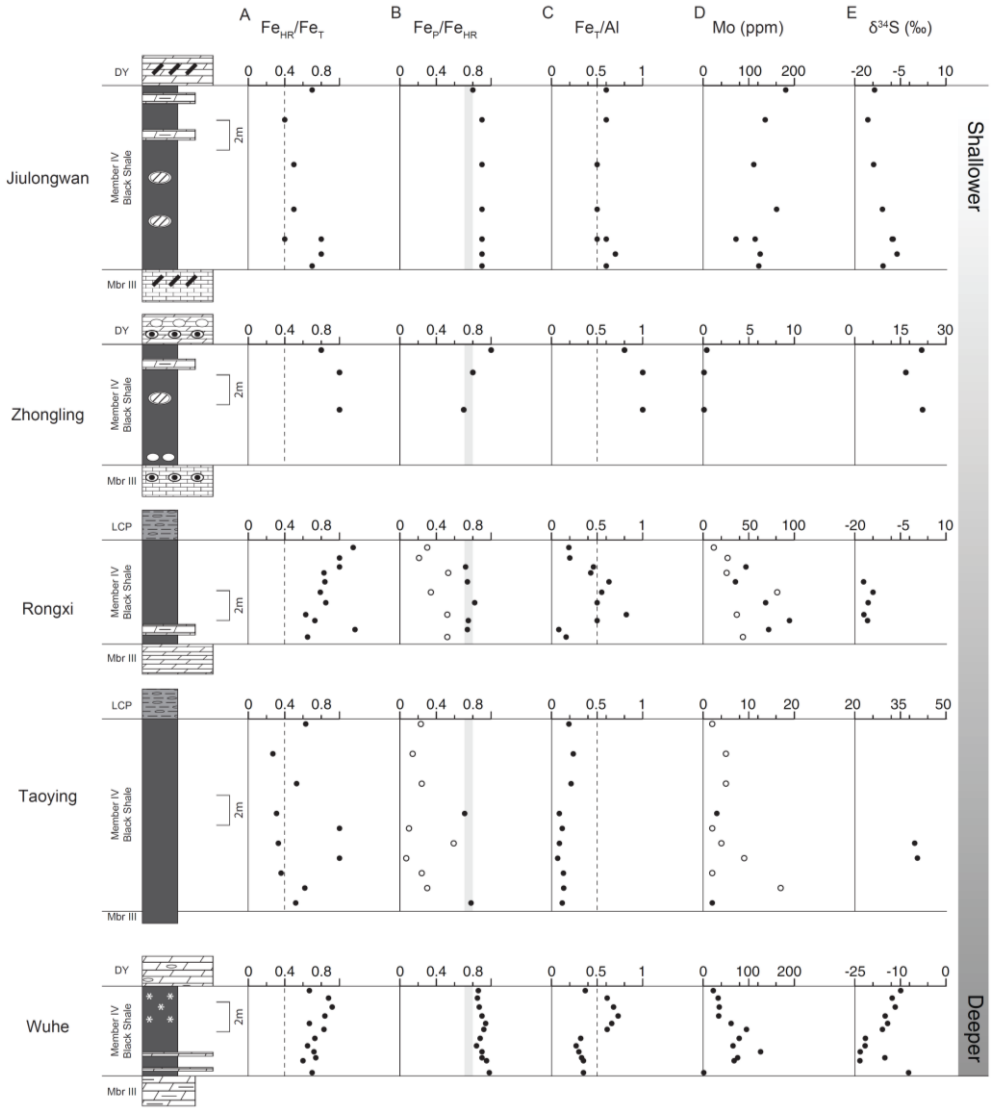

Figure S2 Iron speciation, Mo abundances and pyrite sulfur isotopes (δ^{34}Spyrite) of the Doushantuo Member IV black shales. (**A**) Highly reactive iron over total iron (Fe_{HR}/Fe_T). Fe_{HR}/Fe_T > 0.38 (dashed line) indicates anoxic conditions. Majority of the shale samples are anoxic, except for some oxic shales in the upper slope (Taoying) section. (**B**) The ratio of pyrite over highly reactive iron (Fe_P/Fe_{HR}). Samples with Fe_{HR}/Fe_T > 0.38 and Fe_{HR}/Fe_T > 0.7 (gray line) indicate deposition from euxinic environments (filled circles). Open circles represent samples with Fe_{HR}/Fe_T < 0.38, which may suggest oxic depositional conditions. (**C**) Total iron (Fe_T) and aluminum (Al) ratios (Fe_T/Al) of Member IV black shales. Dashed line marks the average crustal Fe_T/Al ratio of ~0.5 (or average shale Fe_T/Al ratio from shales deposited from oxic environments (**D**) Mo concentrations (ppm) of Member IV black shales. Data of the Jiulongwan and Zhongling sections are from Li et al. (2010). Note near crustal Mo values from the outer shelf section at Zhongling and low Mo values at Taoying (upper slope). (**E**) Pyrite sulfur isotopes ($\delta^{34}S_p$) from Member II black shales. Note that higher $\delta^{34}S_p$ values are observed from Zhongling and Taoying sections.

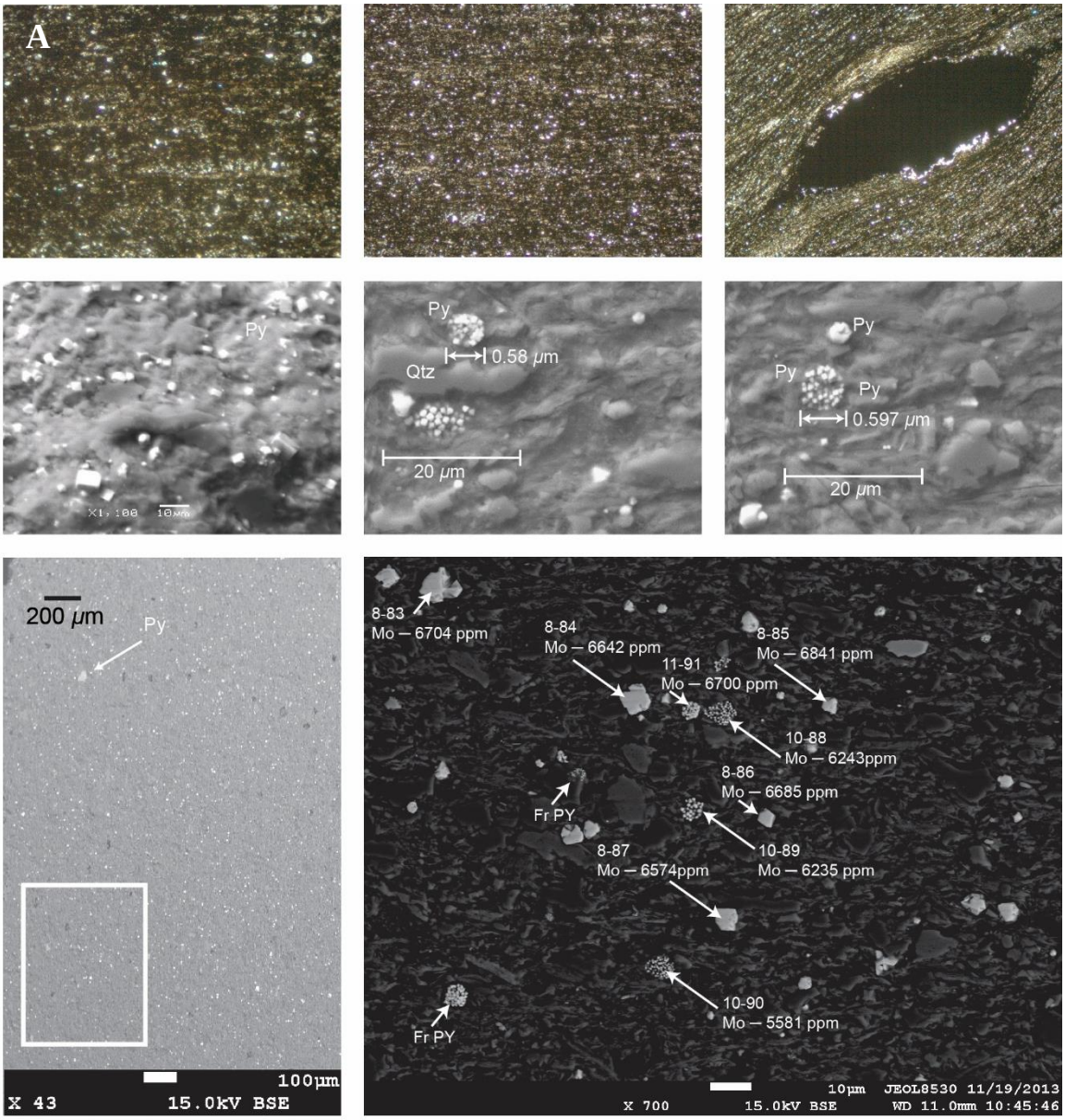
A
Py
Py
Qtz
0.58 μm
20 μm
Py
Py
Py
0.597 μm
20 μm
200 μm
Py
100μm
X 43
15.0kV BSE
8-83
Mo – 6704 ppm
8-84
Mo – 6642 ppm
8-85
Mo – 6841 ppm
11-91
Mo – 6700 ppm
10-88
Mo – 6243ppm
8-86
Mo – 6685 ppm
Fr PY
8-87
Mo – 6574ppm
10-89
Mo – 6235 ppm
10-90
Mo – 5581 ppm
Fr PY
10μm JEOL8530 11/19/2013
X 700 15.0kV BSE WD 11.0mm 10:45:46

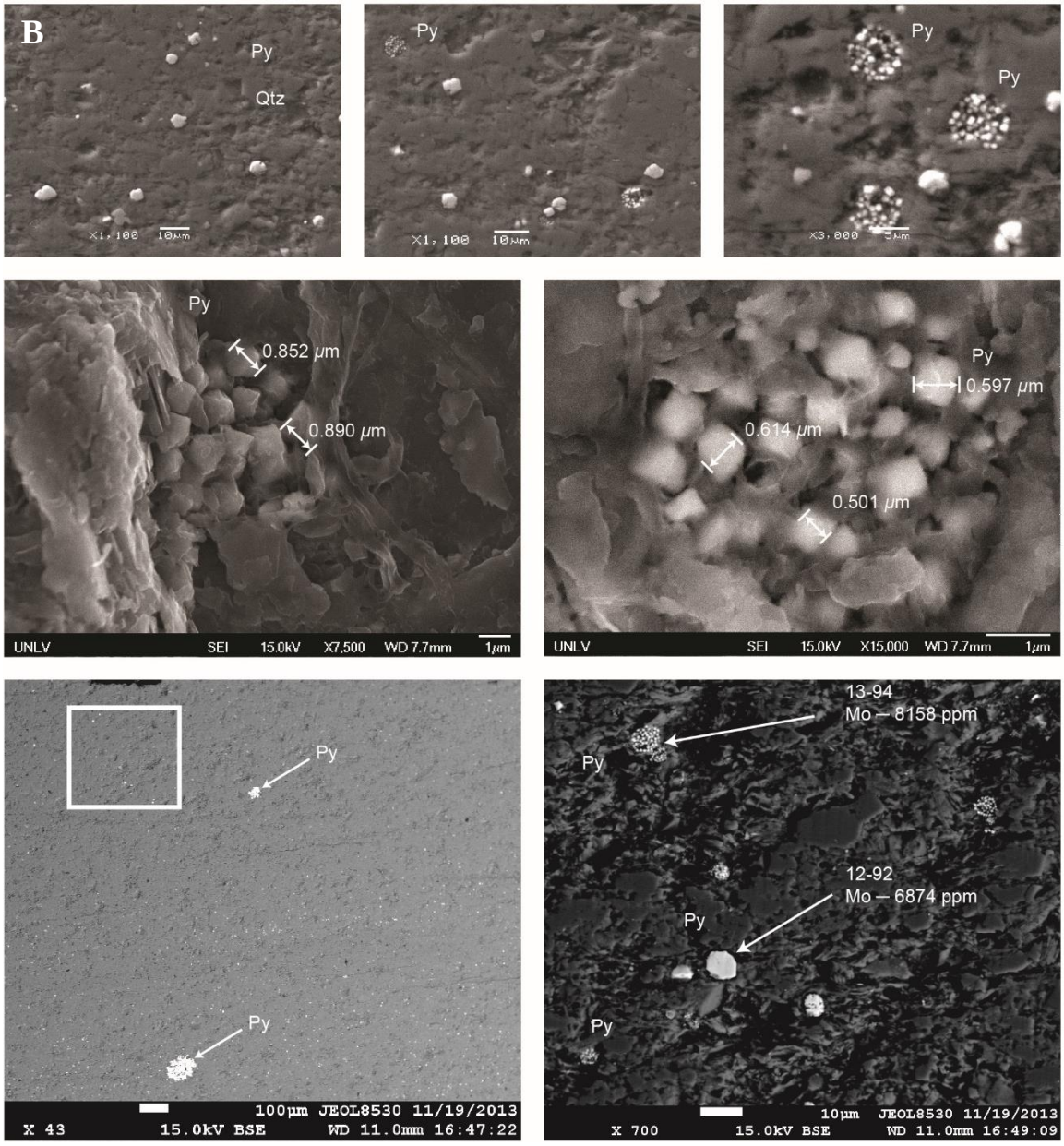

Figure S3 Backscattered electron (BSE) images of framboids from Member II. For this probe study, we selected two samples from Member II; WH09-4.3 (~172 ppm of Mo) and WHH-6.4 (~148 ppm of Mo). The purpose was to test if the high RSE (in this case, Mo) was primarily driven by Mo enrichment in pyrite framboids. (**A**) Sample WH09-4.3 from the lower slope Wuhe section. Up to 6000 ppm of Mo in pyrite framboids indicates a close association of Mo with sulfides. (**B**) Sample WHH-6.4 from the basinal section at Yuanjia. Again, high Mo concentrations (> 6000 ppm) in pyrite framboids suggest strong affinity of Mo with sulfide. In both samples, the shale matrix have reasonable Mo enrichments, however the uptake capability for Mo is much higher in the framboids than whole rock matrix (See Table 2).

Table 1 Geochemical data from the early Ediacaran and late Ediacaran black shales (ca. ~632 and ~551 Ma).

Member II, Wang'an section, Guizou Province, South China—Inner Shelf (This Study)

	Sample No.	Strat. Height (m)	Lithology	TIC (Wt %)	C_{org} (Wt %)	DOP	C_{Org}/S_{PY}	$\delta^{34}S_{PY}$ (‰)	Fe_{Mag} (Wt %)	Fe_{Oxide} (Wt %)	Fe_{Carb} (Wt %)	Fe_{PY} (Wt %)	Fe_{HR} (Wt %)	Fe_T (Wt %)	Fe_{HR}/Fe_T	Fe_{PY}/Fe_{HR}
Doushantuo Fm. Member II	WA09-3-6	9.9	Phosphatic Shale	6.61	0.20	0.82	0.18	18.62	0.00	0.00	0.12	0.99	1.11	1.5	0.89	0.74
	WA09-3-10	10.3	Phosphatic Shale	0.60	0.19	0.91	0.17	13.33	0.00	0.00	0.00	1.01	1.01	1.2	1.00	0.82
	WA09-3-12	10.5	Phosphatic Shale	0.97	0.13	0.92	0.07	13.82	0.00	0.01	0.00	1.57	1.57	1.6	1.00	0.96
	WA09-3-15	10.9	Phosphatic Shale	0.99	0.12	0.90	0.11	12.14	0.00	0.00	0.00	1.02	1.02	1.2	1.00	0.88
	WA09-3-19	11.6	Phosphatic Shale	1.28	0.26	0.92	0.15	15.45	0.00	0.00	0.01	1.50	1.52	2.0	0.99	0.76
	WA09-3-22	12.1	Phosphatic Shale	1.26	0.25	0.91	0.16	18.28	0.00	0.00	0.00	1.39	1.39	1.7	1.00	0.80
	WA09-3-26	12.6	Phosphatic Shale	1.39	0.51	0.87	0.29	30.27	0.00	0.02	0.08	1.54	1.64	2.2	0.94	0.75
	WA09-3-29	12.9	Phosphatic Shale	0.94	0.29	0.90	0.19	17.32	0.00	0.00	0.01	1.35	1.35	1.8	1.00	0.73
	WA09-3-33	13.5	Phosphatic Shale	1.35	0.35	0.85	0.27		0.00	0.03	0.00	1.14	1.17	1.7	0.97	0.67
	WA09-3-37	14.2	Phosphatic Shale	1.24	0.29	0.87	0.17	17.20	0.00	0.08	0.00	1.49	1.57	2.0	0.95	0.77
			Average	1.7	0.26	0.89	0.17	17.38	0.00	0.01	0.02	1.30	1.34	1.71	0.97	0.79
			STDEV	1.8	0.11	0.0	0.1	5.3	0.0	0.0	0.0	0.2	0.2	0.3	0.0	0.1

S_{PY} (Wt %)	Al (Wt %)	Fe/Al	Al_2O_3	TiO_2	Mo (ppm)	Mo/TOC (ppm/Wt%)	V (ppm)	V/TOC (ppm/Wt%)	U (ppm)	U/TOC (ppm/Wt%)	Re (ppb)	Re/TOC (ppb/Wt%)	Cr (ppm)	Ti (Wt %)	Cr/Ti (ppm/ppm)
1.14	4.0	0.4	7.57	0.29	3.48	17.2	64	315	7.13	35.1	2.96	14.6	31	0.18	0.0179
1.16	0.9	1.3	1.79	0.07	1.07	5.5	29	149	22.28	114.6	4.83	24.8	8	0.04	0.0182
1.80	0.7	2.3	1.35	0.07	2.00	14.9	19	140	13.33	98.8	2.42	18.0	8	0.04	0.0197
1.17	0.5	2.2	1.01	0.09	1.21	9.9	19	156	17.78	144.7	1.26	10.2	7	0.05	0.0142
1.73	2.3	0.9	4.42	0.27	1.16	4.5	35	135	10.10	38.9	1.72	6.6	28	0.16	0.0173
1.60	2.1	0.8	3.99	0.25	0.86	3.5	33	132	10.69	43.0	1.25	5.0	25	0.15	0.0165
1.77	8.3	0.3	15.62	0.79	1.60	3.1	94	184	6.17	12.0	0.82	1.6	78	0.47	0.0165
1.54	2.0	0.9	3.81	0.38	1.47	5.1	50	175	10.77	37.6	0.41	1.4	39	0.23	0.0169
1.31	3.6	0.5	6.86	0.50	1.19	3.4	63	181	8.85	25.2	1.64	4.7	49	0.30	0.0163
1.71	2.3	0.9	4.37	0.29	1.59	5.5	43	149	10.55	36.4	1.30	4.5	34	0.17	0.0201
1.49	2.69	1.04	5.08	0.30	1.56	7.24	44.95	171.42	11.76	58.63	1.86	9.15	30.83	0.18	0.02
0.27	2.3	0.7	4.3	0.2	0.7	5.0	23.6	54.0	4.9	44.2	1.3	7.7	21.8	0.1	0.0

Member II, Rongxi section, Hunan Province, South China—Shelf Margin (This Study)

	Sample No.	Strat. Height (m)	Lithology	TIC (Wt %)	C_{org} (Wt %)	DOP	C_{Org}/S_{PY}	$\delta^{34}S_{PY}$ (‰)	Fe_{Mag} (Wt %)	Fe_{Oxide} (Wt %)	Fe_{Carb} (Wt %)	Fe_{PY} (Wt %)	Fe_{HR} (Wt %)	Fe_T (Wt %)	Fe_{HR}/Fe_T	Fe_{PY}/Fe_{HR}
Doushantuo Fm. Member II	RX09-4.5	4.5	Black Shale	0	3.18	0.24	27.76	-2.164	0.00	0.18	0.05	0.10	0.33	0.9	0.30	0.38
	RX09-4.8	4.8	Black Shale	0	2.96	0.85	2.12	-5.374	0.00	0.00	0.11	1.21	1.32	1.6	0.92	0.82
	RX09-5.0	5.0	Black Shale	0	2.79	0.89	1.27	5.853	0.00	0.00	0.03	1.90	1.93	1.9	0.99	1.00
	RX09-5.2	5.2	Black Shale	0	0.85	0.85	1.43		0.00	0.00	0.00	0.52	0.52	1.0	1.00	0.51
	RX09-5.8	5.8	Black Shale	0	1.46	0.56	11.87		0.00	0.00	0.00	0.11	0.11	0.6	1.00	0.19
	RX09-7.3	7.3	Black Shale	0	2.99	0.25	24.76		0.00	0.21	0.00	0.11	0.32	0.9	0.33	0.37
	RX09-7.6	7.6	Black Shale	0	2.33	0.38	19.95	10.2	0.00	0.06	0.00	0.10	0.16	0.6	0.64	0.28
	RX09-8.0	8.0	Black Shale	0	2.93	0.40	25.09		0.00	0.04	0.00	0.10	0.14	0.6	0.72	0.23
	RX09-8.7	8.7	Black Shale	0	0.94	0.57	3.50	7.73	0.00	0.06	0.00	0.23	0.29	0.8	0.80	0.37
	RX09-9.2	9.2	Black Shale	0	2.82	0.52	23.09		0.00	0.00	0.00	0.11	0.11	0.6	1.00	0.18
	RX09-9.6	9.6	Black Shale	0	2.50	0.40	19.93	8.7	0.00	0.05	0.00	0.11	0.15	0.7	0.71	0.22
			Average	0	2.34	0.54	14.62	4.16	0.00	0.05	0.02	0.42	0.49	0.92	0.76	0.41
			STDEV	0	0.85	0.2	10.7	6.4	0.0	0.1	0.0	0.6	0.6	0.4	0.26	0.27

S_{PY} (Wt %)	Al (Wt %)	Fe/Al	Al_2O_3	TiO_2	Mo (ppm)	Mo/TOC (ppm/Wt%)	V (ppm)	V/TOC (ppm/Wt%)	U (ppm)	U/TOC (ppm/Wt%)	Re (ppb)	Re/TOC (ppb/Wt%)	Cr (ppm)	Ti (Wt %)	Cr/Ti (ppm/ppm)
0.11	7.2	0.1	13.62	0.73	8.77	2.8	491	155	6.83	2.2	13.91	4.4	77	0.44	0.0176
1.39	4.8	0.3	9.05	0.40	20.04	6.8	275	93	3.86	1.3	2.50	0.8	47	0.24	0.0195
2.19	5.4	0.3	10.21	0.39	18.63	6.7	232	83	4.21	1.5	5.94	2.1	43	0.23	0.0186
0.59	6.7	0.2	12.73	0.60	9.54	11.2	339	398	5.54	6.5	0.84	1.0	64	0.36	0.0178
0.12	6.4	0.1	12.15	0.74	0.40	0.3	415	285	2.61	1.8	37.64	25.8	74	0.45	0.0166
0.12	6.3	0.1	11.92	0.58	3.16	1.1	234	78	2.87	1.0	27.49	9.2	61	0.35	0.0177
0.12	5.6	0.1	10.52	0.43	0.92	0.4	206	88	2.38	1.0	40.98	17.6	47	0.26	0.0184
0.12	5.8	0.1	11.01	0.59	1.36	0.5	243	83	2.72	0.9	22.62	7.7	59	0.35	0.0168
0.27	5.9	0.1	11.20	0.56	1.31	1.4	169	180	2.51	2.7	4.16	4.4	54	0.33	0.0160
0.12	7.4	0.1	13.96	0.65	0.74	0.3	274	97	3.64	1.3	53.95	19.1	68	0.39	0.0175
0.13	7.7	0.1	14.62	0.64	0.62	0.2	239	95	4.28	1.7	51.28	20.5	70	0.38	0.0182
0.48	6.30	0.15	11.91	0.57	5.95	2.87	283.33	148.72	3.77	1.99	23.76	10.25	60.41	0.34	0.02
0.69	0.9	0.1	1.7	0.1	7.4	3.7	95.7	103.7	1.4	1.6	19.9	8.9	11.5	0.1	0.0

Member II, Taoying section, Guizou Province, South China—Upper Slope (Sahoo et al., 2012)

	Sample No.	Strat. Height (m)	Lithology	TIC (Wt %)	C_{org} (Wt %)	DOP	C_{Org}/S_{PY}	$\delta^{34}S_{PY}$ (‰)	Fe_{Mag} (Wt %)	Fe_{Oxide} (Wt %)	Fe_{Carb} (Wt %)	Fe_{PY} (Wt %)	Fe_{HR} (Wt %)	Fe_T (Wt %)	Fe_{HR}/Fe_T	Fe_{PY}/Fe_{HR}
Doushantuo Fm. Member II	TY09-7.6	7.6	Black Shale	0	1.19		36.9		0.0	0.1	0.0	0.0	0.2	0.8	0.27	0.12
	TY09-7.9	7.9	Black Shale	0	1.25	0.44	6.9		0.0	0.1	0.0	0.2	0.2	0.7	0.30	0.71
	TY09-8.0	8.0	Black Shale	0	1.28		29.4		0.0	0.1	0.0	0.0	0.2	0.7	0.23	0.22
	TY09-8.3	8.3	Black Shale	0	1.91		277.8	-3.3	0.0	0.1	0.0	0.0	0.1	0.6	0.13	0.07
	TY09-8.6	8.6	Black Shale	0	1.48		73.2	4.6	0.0	0.0	0.0	0.0	0.1	0.7	0.11	0.22
	TY09-8.8	8.8	Black Shale	0	1.61		18.1		0.0	0.1	0.0	0.1	0.2	0.6	0.26	0.48
	TY09-9.0	9.0	Black Shale	0	2.10		48.1		0.0	0.0	0.0	0.0	0.1	0.6	0.15	0.43
	TY09-9.4	9.4	Black Shale	0	1.94		55.0		0.0	0.0	0.0	0.0	0.1	0.6	0.13	0.42
	TY09-9.8	9.8	Black Shale	0	1.56		48.0		0.0	0.1	0.0	0.0	0.1	0.8	0.19	0.19
	TY09-10.0	10.0	Black Shale	0	1.90		100.3	-6.0	0.0	0.0	0.0	0.0	0.1	0.6	0.12	0.23
	TY09-10.2	10.2	Black Shale	0	2.39	0.50	17.8	-15.7	0.0	0.0	0.0	0.1	0.1	0.7	0.17	1.00
	TY09-10.4	10.4	Black Shale	0	2.18		24.2		0.0	0.1	0.0	0.1	0.2	0.6	0.31	0.40
	TY09-10.7	10.7	Black Shale	0	1.55		32.7		0.0	0.0	0.0	0.0	0.1	0.7	0.15	0.41
	TY09-11.0	11.0	Black Shale	0	2.11	0.83	4.1	-9.9	0.0	0.0	0.0	0.5	0.5	0.4	1.00	1.00
	TY09-11.3	11.3	Black Shale	0	2.14		21.6		0.0	0.1	0.0	0.1	0.2	0.6	0.30	0.50
	TY09-11.5	11.5	Black Shale	0	2.36		21.3		0.0	0.0	0.0	0.1	0.1	0.5	0.32	0.66
	TY09-11.8	11.8	Black Shale	0	2.42		43.9		0.0	0.0	0.0	0.0	0.1	0.5	0.22	0.46
	TY09-12.0	12.0	Black Shale	0	2.24		128.4		0.0	0.0	0.0	0.0	0.1	0.5	0.12	0.23
Section b. 13.0 m is the base of the black shale																
Doushantuo Fm. Member II	TY09-13.3	13.3	Black Shale	0	0.37		0.5		0.0	0.1	0.0	0.7	0.8	1.5	0.53	0.85
	TY09-13.8	13.8	Black Shale	0	1.33	0.77	2.4	-7.6	0.0	0.0	0.0	0.5	0.5	0.8	0.59	1.00
	TY09-14.0	14.0	Black Shale	0	2.03		12.3		0.0	0.1	0.0	0.1	0.2	0.7	0.29	0.68
	TY09-15.1	15.1	Black Shale	0	1.72	0.73	4.0	-26.8	0.0	0.0	0.0	0.4	0.4	1.3	0.31	0.93
	TY09-15.5	15.5	Black Shale	0	2.47		5.2		0.0	0.0	0.0	0.4	0.5	0.6	0.71	0.89
	TY09-16.3	16.3	Black Shale	0	2.58		3.4		0.0	0.1	0.0	0.7	0.8	0.7	1.00	0.81
	TY09-16.5	16.5	Black Shale	0	3.21	0.86	2.0	-31.6	0.0	0.1	0.0	1.4	1.5	2.1	0.70	0.96
	TY09-17.5	17.5	Black Shale	0	1.87	0.47	4.1	-23.1	0.0	0.4	0.0	0.4	0.8	1.5	0.56	0.47
	TY09-18.8	18.8	Black Shale	0	2.58	0.53	5.6	-22.3	0.0	0.2	0.0	0.4	0.6	0.8	0.69	0.70
	TY09-19.7	19.7	Black Shale	0	2.76	0.62	5.7	-22.1	0.0	0.1	0.0	0.4	0.5	0.9	0.59	0.77
	TY09-21.3	21.3	Black Shale	0	4.52	0.81	4.3	-16.0	0.0	0.1	0.0	0.9	1.0	0.6	1.00	0.94
	TY09-22.3	22.3	Black Shale	0	1.03	0.92	0.6	0.2	0.0	0.0	0.0	1.5	1.5	1.0	1.00	1.00
			Average	0	2.00	0.68	34.59	-13.81	0.01	0.08	0.00	0.30	0.39	0.80	0.42	0.59
			STDEV	0	0.76	0.2	55.3	11.1	0.0	0.1	0.0	0.4	0.4	0.4	0.30	0.30

S_{PY} (Wt %)	Al (Wt %)	Fe/Al	Al_2O_3	TiO_2	Mo (ppm)	Mo/TOC (ppm/Wt%)	V (ppm)	V/TOC (ppm/Wt%)	U (ppm)	U/TOC (ppm/Wt%)	Re (ppb)	Re/TOC (ppb/Wt%)	Cr (ppm)	Ti (Wt %)	Cr/Ti (ppm/ppm)
0.03	7.4	0.1	14.07	0.68	3	2.7	5900	4962	17.89	15.05	1224	1030	242	0.40	0.0598
0.18	7.7	0.1	14.51	0.63	4	3.0	3973	3178	11.31	9.04	2764	2211	135	0.38	0.0356
0.04	8.1	0.1	15.35	0.71	1	1.0	3950	3080	16.74	13.06	2452	1912	129	0.43	0.0302
0.01	8.4	0.1	15.87	0.73	3	1.5	2946	1545	16.89	8.86	25	13	114	0.44	0.0260
0.02	7.9	0.1	14.91		25	16.7	285	193	3.77	2.55	1794	1212			
0.09	8.7	0.1	16.35	0.74	6	4.0	1767	1095	18.43	11.42	2576	1596	84	0.45	0.0187
0.04	8.2	0.1	15.43	0.75	4	1.9	1451	689	19.06	9.06	28	13	75	0.45	0.0165
0.04	8.6	0.1	16.19	0.79	5	2.8	950	489	17.98	9.25	1565	805	68	0.47	0.0143
0.03	9.5	0.1	17.88	0.84	3	1.8	1516	971	23.69	15.17	855	548	89	0.51	0.0177
0.02	8.3	0.1	15.61	0.78	3	1.6	835	440	18.69	9.86	612	323	67	0.47	0.0143
0.13	9.8	0.1	18.58	0.75	29	12.3	1178	493	18.51	7.74	3068	1283	79	0.45	0.0176
0.09	7.7	0.1	14.53	0.76	39	18.1	804	369	17.17	7.89	1775	815	59	0.46	0.0129
0.05	8.9	0.1	16.82	0.79	11	7.3	1853	1196	19.37	12.51	26	16	88	0.47	0.0187
0.52	5.5	0.1	10.46	0.49	30	14.2	525	249	10.29	4.88	1827	866	48	0.30	0.0161
0.10	7.3	0.1	13.86	0.74	11	5.3	253	118	8.17	3.81	36	17	61	0.45	0.0138
0.11	7.1	0.1	13.44	0.78	11	4.5	247	105	8.04	3.41	86	37	52	0.47	0.0111
0.06	7.2	0.1	13.55	0.80	11	4.5	213	88	8.44	3.49	17	7	54	0.48	0.0113
0.02	7.6	0.1	14.30	0.77	6	2.8	294	131	7.75	3.45	149	66	61	0.46	0.0132
0.77	8.3	0.2	15.70	0.75	1	4.0	1016	2783	7.82	21.41	39	106	270	0.45	0.0602
0.55	9.0	0.1	16.99	0.61	3	2.6	6096	4582	13.08	9.83	1440	1083	212	0.36	0.0583
0.17	8.8	0.1	16.56	0.74	15	7.2	3040	1499	19.06	9.40	165	81	130	0.44	0.0294
0.43	19.4	0.1		0.97	38	22.2	2522	1465	33.61	19.52	2702	1569	133	0.58	0.0229
0.47	7.7	0.1	14.57	0.71	165	67.0	669	271	15.71	6.37	905	367	62	0.43	0.0146
0.75	8.8	0.1	16.70	0.75	48	18.7	455	176	16.82	6.51	162	63	60	0.45	0.0132
1.64	8.9	0.2	16.73	0.81	114	35.6	424	132	12.49	3.89	93	29	81	0.49	0.0166
0.45	8.8	0.2	16.62	0.91	13	7.0	418	224	5.67	3.03	77	41	94	0.54	0.0172
0.46	6.7	0.1	12.64	0.64	9	3.5	262	101	3.77	1.46	55	21	63	0.38	0.0164
0.48	7.2	0.1	13.52	0.75	11	4.2	313	114	4.67	1.69	33	12	73	0.45	0.0162
1.05	6.1	0.1	11.47	0.50	12	2.7	200	44	6.83	1.51	32	7	48	0.30	0.0159
1.69	5.5	0.2	10.46	0.51	0	0.3	185	181	5.37	5.24	4	4	83	0.30	0.0274
0.35	8.30	0.10	14.95	0.73	21.28	9.36	1485	1032.10	13.57	8.01	886.22	538.43	96.98	0.44	0.02
0.45	2.3	0.0	2.0	0.1	35.2	13.5	1650	1352.0	6.9	5.2	1037.3	665.2	56.6	0.1	0.0

Member II, Wuhe section, Guizou Province, South China—Lower Slope (Sahoo et al., 2012)

	Sample No.	Strat. Height (m)	Lithology	TIC (Wt %)	C_{org} (Wt %)	DOP	C_{Org}/S_{PY}	$\delta^{34}S_{PY}$ (‰)	Fe_{Mag} (Wt %)	Fe_{Oxide} (Wt %)	Fe_{Carb} (Wt %)	Fe_{PY} (Wt %)	Fe_{HR} (Wt %)	Fe_T (Wt %)	Fe_{HR}/Fe_T	Fe_{PY}/Fe_{HR}
Doushantuo Fm. Member II	WH09-2.4	2.4	Black Shale	0.0	0.72	0.17	4.1		0.0	0.2	0.0	0.2	0.4	2.2	0.17	0.41
	WH09-2.7	2.7	Black Shale	0.0	0.61		3.6	-17.2	0.1	0.3	0.0	0.1	0.5	1.7	0.29	0.29
	WH09-3	3.0	Black Shale	0.2	0.83		1.3	-32.3	0.0	0.1	0.1	0.6	0.8	1.9	0.39	0.73
	WH09-3.2	3.2	Black Shale	0.0	0.94	0.68	0.7	-32.8	0.0	0.0	0.0	1.2	1.3	2.6	0.49	0.97
	WH09-3.5	3.5	Black Shale	0.0	0.80		3.8	-34.6	0.2	0.4	0.0	0.2	0.8	2.1	0.40	0.23
	WH09-3.7	3.7	Black Shale	0.0	1.25		0.6	-33.7	0.1	0.1	0.1	1.7	2.0	3.2	0.63	0.87
	WH09-4	4.0	Black Shale	0.1	0.91		1.1	-32.8	0.0	0.1	0.0	0.7	0.9	2.3	0.38	0.85
	WH09-4.3	4.3	Black Shale	0.0	1.19		0.5	-34.9	0.0	0.0	0.1	1.9	2.1	3.9	0.54	0.91
	WH09-4.6	4.6	Black Shale	2.1	0.77		0.6	-29.1	0.0	0.1	0.7	1.1	2.0	3.2	0.62	0.57
	WH09-4.8	4.8	Black Shale	0.2	1.16		1.8	-30.6	0.0	0.1	0.1	0.6	0.8	2.6	0.30	0.72
	WH09-5.0	5.0	Calcareous Shale	7.5	0.47	0.25	0.3	-26.8	0.4	0.0	2.0	1.3	3.7	5.3	0.70	0.34
	WH09-5.4	5.4	Black Shale	1.4	1.29		0.7	-32.4	0.0	0.0	0.4	1.6	2.0	3.1	0.64	0.79
	WH09-5.6	5.6	Calcareous Shale	3.5	1.12		0.7	-30.5	0.0	0.1	0.9	1.4	2.5	4.0	0.63	0.58
	WH09-5.8	5.8	Calcareous Shale	3.1	0.79		0.4	-29.8	0.0	0.1	0.8	1.5	2.4	3.5	0.69	0.64
	WH09-6.0	6.0	Black Shale	0.0	1.36		0.5	-33.7	0.0	0.0	0.0	2.6	2.6	3.8	0.69	1.00
	WH09-6.3	6.3	Black Shale	0.0	1.39		0.5	-33.5	0.0	0.0	0.0	2.7	2.7	3.8	0.70	0.99
	WH09-6.5	6.5	Black Shale	0.0	1.15		30.2	-32.5	0.0	0.7	0.0	0.0	0.7	2.5	0.29	0.05
	WH09-6.8	6.8	Black Shale	0.0	1.19		0.8	-32.4	0.0	0.0	0.0	1.3	1.4	2.9	0.48	0.97
	WH09-7.0	7.0	Black Shale	0.1	1.15		0.5	-31.1	0.0	0.0	0.1	1.9	2.1	3.4	0.62	0.91
	WH09-7.3	7.3	Black Shale	0.5	1.28	0.31	0.7	-30.0	0.0	0.0	0.3	1.5	1.8	2.9	0.62	0.83
	WH09-8.6	8.6	Black Shale	0.8	1.17		0.5	-31.6	0.0	0.0	0.3	2.2	2.5	3.8	0.67	0.87
	WH09-9.4	9.4	Black Shale	0.5	0.79		0.3	-31.7	0.0	0.1	0.2	2.0	2.3	3.4	0.68	0.86
	WH09-9.7	9.7	Black Shale	0.2	1.27	0.73	0.6	-32.0	0.0	0.0	0.2	1.9	2.1	3.0	0.71	0.91
	WH09-11.6	11.6	Black Shale	0.0	1.25	0.75	0.6	-30.1	0.0	0.0	0.1	1.9	2.0	3.0	0.67	0.95
	WH09-13.7	13.7	Calcareous Shale	4.0	0.60	0.60	0.3	-21.0	0.0	0.0	0.7	1.6	2.2	2.5	0.91	0.70
			Average	0.97	1.02	0.50	2.23	-30.71	0.04	0.10	0.29	1.35	1.78	3.06	0.56	0.72
			STDEV	1.8	0.27	0.2	5.9	4.1	0.1	0.2	0.5	0.8	0.8	0.8	0.2	0.3

S_{PY} (Wt %)	Al (Wt %)	Fe/Al	Al_2O_3	TiO_2	Mo (ppm)	Mo/TOC (ppm/Wt%)	V (ppm)	V/TOC (ppm/Wt%)	U (ppm)	U/TOC (ppm/Wt%)	Re (ppb)	Re/TOC (ppb/Wt%)	Cr (ppm)	Ti (Wt %)	Cr/Ti (ppm/ppm)
0.18	10.4	0.2	19.70	0.75	1	0.8	4438	6124	13.4	18.4	547	754	201	0.45	0.0449
0.17	8.7	0.2	16.44		9	14.2	1824	2994	12.3	20.2	229	376			
0.63	8.4	0.2	15.92	0.65	4	4.6	584	707	14.0	16.9	732	887	56	0.39	0.0145
1.41	8.6	0.3	16.23	0.53	38	40.5	489	522	13.8	14.7	703	750	63	0.32	0.0198
0.21	9.4	0.2	17.68	0.64	2	3.0	390	485	13.8	17.2	5	6	53	0.38	0.0139
1.98	9.0	0.3	17.06	0.62	62	49.7	333	266	15.8	12.6	24	19	57	0.37	0.0151
0.86	8.7	0.3	16.40	0.64	8	8.6	324	356	14.0	15.4	64	70	57	0.39	0.0149
2.20	9.4	0.4	17.81	0.66	172	144.9	288	242	12.6	10.6	26	22	59	0.40	0.0149
1.29	6.6	0.5	12.52	0.54	11	14.6	208	272	9.8	12.8	13	17	49	0.32	0.0153
0.65	8.5	0.3	16.10	0.62	13	11.6	241	208	10.0	8.6	15	13	58	0.37	0.0156
1.46	3.4	1.5	6.51	0.20	40	84.7	171	367	5.5	11.9	22	48	25	0.12	0.0203
1.82	8.5	0.4	16.00	0.58	41	32.0	185	144	6.4	5.0	38	29		0.35	
1.65	7.0	0.6	13.29	0.49	42	37.9	199	178	5.9	5.3	31	28		0.30	
1.77	6.6	0.5	12.55	0.48	22	27.7	213	270	4.3	5.4	37	47		0.29	
2.97	10.0	0.4	18.87	0.72	30	22.0	212	156	4.8	3.5	23	17		0.43	
3.05	10.1	0.4	19.13	0.70	27	19.6	213	153	4.3	3.1	41	30		0.42	
0.04	9.3	0.3	17.63	0.69	58	50.4	184	160	4.7	4.1	24	21		0.41	
1.55	9.6	0.3	18.20	0.74	38	31.5	207	173	5.8	4.8	25	21		0.44	
2.24	9.2	0.4	17.30	0.70	26	22.6	221	192	4.1	3.5	36	32		0.42	
1.73	8.2	0.4	15.55	0.67	13	9.9	174	136	5.7	4.4	30	24	55	0.40	0.0136
2.50	8.6	0.4	16.34	0.67	24	20.5	170	145	3.2	2.8	16	14		0.40	
2.31	7.8	0.4	14.83	0.62	8	10.1	170	216	5.9	7.5	18	23	50	0.37	0.0135
2.19	7.9	0.4	15.02	0.50	12	9.1	134	106	4.2	3.3	10	8	49	0.30	0.0164
2.18	6.8	0.4	12.82	0.44	12	9.5	143	114	3.6	2.8	8	6	44	0.26	0.0168
1.79	4.2	0.6	7.98	0.39	4	6.5	94	156	3.9	6.5	4	7	38	0.23	0.0163
1.55	8.21	0.41	15.51	0.59	28.66	27.46	472.46	593.61	8.07	8.85	108.95	130.77	61.05	0.36	0.02
0.86	1.7	0.3	3.2	0.1	34.6	31.0	891.5	1284.1	4.3	5.7	214.2	262.1	40.0	0.1	0.0

Member II, Yuanjia Section, Hunan Province, South China—Basinal (Sahoo et al., 2012)

	Sample No.	Strat. Height (m)	Lithology	TIC (Wt %)	C_{org} (Wt %)	DOP	C_{Org}/S_{PY}	$\delta^{34}S_{PY}$ (‰)	Fe_{Mag} (Wt %)	Fe_{Oxide} (Wt %)	Fe_{Carb} (Wt %)	Fe_{PY} (Wt %)	Fe_{HR} (Wt %)	Fe_T (Wt %)	Fe_{HR}/Fe_T	Fe_{PY}/Fe_{HR}
Doushantuo Fm. Member II	WHH-5.6	5.6	Black Shale	0.0	1.74		3.9	-14.2	0.0	0.0	0.0	0.4	0.4	0.7	0.65	0.89
	WHH-5.7	5.7	Black Shale	0.0	1.47		0.8	-26.7	0.0	0.1	0.0	1.6	1.7	2.4	0.72	0.94
	WHH-5.9	5.9	Black Shale		1.60									1.9		
	WHH-6.3	6.3	Black Shale	0.0	2.45		1.3	-30.3	0.0	0.1	0.2	1.7	1.9	2.7	0.72	0.88
	WHH-6.4	6.4	Black Shale	0.0	2.67		1.1	-31.7	0.0	0.1	0.1	2.1	2.3	3.1	0.73	0.93
	WHH-6.8	6.8	Black Shale	0.0	3.01		1.2	-35.5	0.0	0.0	0.2	2.3	2.5	2.9	0.84	0.92
	WHH-6.9	6.9	Black Shale	0.0	2.08		0.7	-25.2	0.0	0.0	0.1	2.8	2.9	4.2	0.69	0.95
	WHH-6.95	6.95	Black Shale	0.0				-10.4	0.0	0.0	0.2	5.0	5.2			0.96
	WHH-7.2	7.2	Black Shale	0.0	2.70		0.7		0.0	0.0	0.1	3.5	3.7	4.2	0.86	0.96
	WHH-7.4	7.4	Black Shale	0.0	3.62		0.9	-30.2	0.0	0.0	0.1	3.5	3.7	4.5	0.81	0.97
	WHH-7.6	7.6	Black Shale	0.0	4.06		32.0	-21.4	0.0	0.1	0.0	0.1	0.2	0.6	0.26	0.67
	WHH-9.1	9.1	Black Shale	0.0	0.60		40.1	-7.0	0.0	0.0	0.0	0.0	0.1	0.6	0.11	0.20
	WHH-9.5	9.5	Black Shale	0.0	0.82		15.5		0.0	0.1	0.0	0.0	0.1	0.7	0.16	0.42
			Average	0.0	2.24		8.91	-23.27	0.01	0.05	0.07	1.93	2.05	2.39	0.59	0.81
			STDEV	0.0	1.06		14.2	9.7	0.0	0.0	0.1	1.6	1.6	1.5	0.3	0.3

S_{PY} (Wt %)	Al (Wt %)	Fe/Al	Al_2O_3	TiO_2	Mo (ppm)	Mo/TOC (ppm/Wt%)	V (ppm)	V/TOC (ppm/Wt%)	U (ppm)	U/TOC (ppm/Wt%)	Re (ppb)	Re/TOC (ppb/Wt%)	Cr (ppm)	Ti (Wt %)	Cr/Ti (ppm/ppm)
0.45	9.9	0.1	18.65	0.99	13	7.7	6417	3680	10	6	1819	1043		0.59	
1.88	9.6	0.3	18.05	0.90	64	43.8	2767	1884	18	12	26	18	171.4	0.54	0.0316
	9.4	0.2	17.74		120	75.1									
1.95	8.8	0.3	16.62	0.86	136	55.6	1193	488	20	8	405	165	86.42	0.51	0.0168
2.44	8.7	0.4	16.53	0.84	148	55.3	847	317	20	7	140	52	85.83	0.50	0.0171
2.59	7.6	0.4	14.28	0.73	97	32.3	497	165	13	4	28	9	72.5	0.43	0.0167
3.19	8.6	0.5	16.30	0.91	25	12.1	370	178	11	5			85.98	0.55	0.0157
											238				
4.05	7.1	0.6	13.32	0.66	37	13.8			9	3	25	9	62.48	0.40	0.0158
4.07	7.4	0.6	14.00	0.70	37	10.1	336	93	10	3	38	11	65.63	0.42	0.0156
0.13	8.5	0.1	16.07	0.91	11	2.6	458	113	9	2	86	21	86.98	0.55	0.0159
0.01	6.2	0.1	11.70	0.63	0	0.1			8	13	75	126	48.23	0.38	0.0127
0.05	6.2	0.1	11.79	0.66	0	0.1	256	313	8	10	52	64	51.78	0.40	0.0130
1.89	8.16	0.30	15.42	0.80	57.42	25.72	1460	803	12.30	6.79	266.67	151.93	81.73	0.48	0.02
1.55	1.2	0.2	2.4	0.1	54.4	25.8	2017	1215	4.6	3.8	527.8	317.7	34.7	0.1	0.0

Member II, Jiulongwan Section, Yangtze Geroges, South China—Inner Shelf (Li et al., 2010)

	Sample No.	Strat. Height (m)	Lithology	TIC (Wt %)	C_{org} (Wt %)	C_{Org}/S_{PY}	$\delta^{34}S_{PY}$ (‰)	Fe_{Mag} (Wt %)	Fe_{Oxide} (Wt %)	Fe_{Carb} (Wt %)	Fe_{PY} (Wt %)	Fe_{HR} (Wt %)	Fe_T (Wt %)	Fe_{HR}/Fe_T	Fe_{PY}/Fe_{HR}	S_{PY} (Wt %)	Al (Wt %)	Fe/Al	Al_2O_3	Mo (ppm)	Mo/TOC
Doushantuo Fm. Member II	JS-17	6	Shale/Carbonate	7.1	0.50	0.3	17.4	0	0.1	0.1	1.5	1.8	2.3	0.8	0.8	1.80	1.7	1.4	3.21	1.7	3.3
	JS-18	8	Shale/Carbonate	6.5	1.20	0.9	18.7	0.1	0.2	0.1	1.2	1.5	2.4	0.6	0.8	1.40	2.1	1.1	3.97	1.3	1.1
	JS-21	16	Shale/Carbonate	5.5	1.80	1.7	11.7	0	0	0.1	0.9	1.1	1.9	0.6	0.8	1.10	1.9	1.0	3.59	1.1	0.6
	JS-24	19.7	Shale/Carbonate	4.2	2.90	2.3	23.6	0.1	0.1	0.1	1.1	1.3	2.5	0.5	0.8	1.30	2.6	1.0	4.91	1.6	0.6
	JS-26	25	Shale/Carbonate	7.4	0.70	2.8	3.2	0	0.2	0.1	0.2	0.6	1.2	0.5	0.4	0.30	0.9	1.3	1.70	0.2	0.3
	JS-29	30	Shale/Carbonate	5.8	1.20	31	8.7	0.1	0.9	0.1	0	1.1	1.9	0.6	0	0.00	1.7	1.1	3.21	0.3	0.3
	JS-34	35	Shale/Carbonate	5.8	0.90	29.3	16.6	0	0.1	0.1	0	0.2	0.2	0.9	0.1	0.00	0.2	1.0	0.38	0.1	0.1
	JS-37	38	Shale/Carbonate	5.8	0.80	19	20.1	0	0.8	0.1	0	1	1.6	0.6	0	0.00	1.2	1.3	2.27	0.4	0.5
	JS-40	41	Shale/Carbonate	5.9	1.10	22.4	-12.6	0.1	1.2	0	0	1.4	2.5	0.6	0	0.10	2.7	0.9	5.10	0.4	0.4
	JS-42	49	Shale/Carbonate	6.4	0.90	0.9	4.7	0.1	0.1	0.1	0.8	1.2	2.3	0.5	0.7	0.90	2.0	1.2	3.78	0.8	0.9
	JS-45	52	Shale/Carbonate	7.9	0.70	1.5	9.5	0.1	0.1	0.1	0.4	0.7	1.1	0.6	0.6	0.50	0.9	1.2	1.70	0.4	0.5
	JS-48	56	Shale/Carbonate	7.1	1.00	1.7	3.4	0.1	0.1	0.1	0.5	0.8	1.7	0.4	0.7	0.60	1.4	1.2	2.65	0.3	0.3
	JS-51	59	Shale/Carbonate	7.6	0.60	1	7.4	0	0.1	0.2	0.5	0.8	1.4	0.6	0.6	0.60	1.0	1.4	1.89	0.4	0.6
	JS-56	64	Shale/Carbonate	6.0	0.60	0.6	5.3	0.1	0.1	0.1	1	1.2	2.4	0.5	0.8	1.20	2.3	1.0	4.35	0.5	0.8
	JS-60	70	Shale/Carbonate	5.3	1.60	2.1	14.9	0.1	0.1	0.1	0.7	0.9	1.8	0.5	0.8	0.80	2.2	0.8	4.16	0.9	0.5
	JS-64	75	Shale/Carbonate	6.2	1.60	2.7	17	0.1	0.2	0.1	0.5	0.8	1.5	0.6	0.6	0.60	1.4	1.1	2.65	1.1	0.7
	JS-68l	79	Shale/Carbonate	6.2	0.80	1.1	0.3	0.1	0.1	0.1	0.6	0.8	1.6	0.5	0.7	0.70	1.6	1.0	3.02	0.5	0.6
			Average	6.28	1.11	7.14	9.99	0.06	0.26	0.10	0.58	1.01	1.78	0.58	0.54	0.70	1.64	1.12	3.09	0.71	0.71
			STDEV	0.9	0.60	10.8	9.0	0.0	0.3	0.0	0.5	0.4	0.6	0.1	0.3	0.54	0.7	0.2	1.3	0.5	0.7

Member II, Zhongling Section, Yangtze Geroges, South China—Shelf Margin (Li et al., 2010)

	Sample No.	Strat. Height (m)	Lithology	TIC (Wt %)	C_{org} (Wt %)	C_{Org}/S_{PY}	$\delta^{34}S_{PY}$ (‰)	Fe_{Mag} (Wt %)	Fe_{Oxide} (Wt %)	Fe_{Carb} (Wt %)	Fe_{PY} (Wt %)	Fe_{HR} (Wt %)	Fe_T (Wt %)	Fe_{HR}/Fe_T	Fe_{PY}/Fe_{HR}	S_{PY} (Wt %)	Al (Wt %)	Fe/Al	Al_2O_3	Mo (ppm)	Mo/TOC
Doushantuo Fm. Member II	SH-13	7.5	Shale/Carbonate	5.3	0.10	0.1	9.1	0.1	0.1	0.4	1.7	2.3	2.6	0.9	0.7	2.00	3.6	0.7	6.80	0.7	5.2
	SH-15	9.1	Shale	0.0	0.50	2.6	-15.1	0	1.3	0	0.2	1.6	2.4	0.7	0.1	0.20	6.6	0.4	12.47	4.4	9.4
	SH-16	12.8	Shale	0.0	1.00	103.2	1.7	0	0.5	0	0	0.6	1.7	0.3	0	0.00	6.4	0.3	12.09	4.2	4.0
	SH-18	14.5	Shale	0.0	2.00	0.6	-17.2	0	0.2	0.2	2.9	3.3	3.9	0.8	0.9	3.30	5.1	0.8	9.64	12.4	6.1
	SH-20	17	Shale	0.0	3.00	1.3	-17.2	0	0.8	0.3	1.9	3.1	4.1	0.7	0.6	2.20	5.1	0.8	9.64	6	2.0
	SH-23	19.5	Shale	0.0	2.90	1.3	-11.2	0	0.2	0.4	2	2.7	3.7	0.7	0.8	2.30	5.7	0.6	10.77	12.7	4.3
	SH-24	27	Shale	0.3	3.80	1.3	-11.2	0.2	0.5	0.1	2.5	3.4	4.1	0.8	0.7	2.90	5.4	0.8	10.20	9.6	2.5
	SH-26	29	Shale	0.4	0.70	0.4	-9	0.1	0.2	0.2	1.3	1.9	2.8	0.7	0.7	1.50	5.1	0.5	9.64	4.7	7.1
	SH-28	31	Shale	0.0	3.40	59.3	-10.6	0	0.3	0.1	0	0.4	1.1	0.4	0.1	0.10	5.5	0.2	10.39	8.9	2.6
	SH-31	33.5	Shale	0.0	0.20			0.1	0.9	0	0	1	5.1	0.2	0	0.00	6.5	0.8	12.28	0	0.1
	SH-34	37	Shale	0.5	0.80	7.7	7.2	0.9	0.5	0.9	0.1	2.4	4.3	0.6	0	0.10	6.2	0.7	11.71	0.2	0.2
	SH-38	73.5	Shale	1.6	0.10	2.9	21.1	0	0.3	0.4	0	0.7	6.7	0.1	0	0.00	4.1	1.6	7.75	0.1	1.2
	SH-37	75	Shale	0.1	0.10	3.1	23.4	0.2	0.1	0.2	0	0.5	7.7	0.1	0.1	0.00	4.5	1.7	8.50	0.1	1.3
	SH-35	77.6	Shale	1.5	0.20	4.4	30.1	0	0.5	0.3	0	0.8	5.2	0.2	0	0.00	4.5	1.2	8.50	0.2	0.9
	SH-40	81	Shale/Carbonate	11.6	0.30	4.8	23.5	0	0	0.1	0.1	0.2	0.2	1	0.3	0.10	0.1	2.0	0.19	0.1	0.4
	SH-78	108	Shale/Carbonate	8.5	1.20	15.1	33.2	0	0.3	0	0.1	0.4	0.5	0.9	0.2	0.10	0.5	1.0	0.94	0.6	0.5
	SH-76	112	Shale/Carbonate	7.6	1.80	34.9	29.4	0	0.5	0.1	0	0.6	0.9	0.7	0.1	0.10	0.9	1.0	1.70	0.8	0.5
	SH-73	124	Shale/Carbonate	10.8	0.10	0.8	26.7	0	0	0	0.1	0.2	0.1	1	0.7	0.10	0.1	1.0	0.19	0.3	2.9
	SH-72	126	Shale/Carbonate	11.0	0.10	1.4	35.9	0	0.1	0	0.1	0.2	0.1	1	0.4	0.10	0.1	1.0	0.19	0.2	1.8
			Average	3.12	1.17	13.62	8.32	0.08	0.38	0.19	0.68	1.38	3.01	0.62	0.34	0.79	4.00	0.90	7.56	3.48	2.79
			STDEV	4.4	1.26	27.0	19.7	0.2	0.3	0.2	1.0	1.1	2.3	0.3	0.3	1.15	2.4	0.5	4.5	4.4	2.6

Member IV, Rongxi section, Hunan Province, South China—Shelf Margin (This Study)

	Sample No.	Strat. Height (m)	Lithology	TIC (Wt %)	C_{org} (Wt %)	DOP	C_{Org}/S_{PY}	$\delta^{34}S_{PY}$ (‰)	Fe_{Mag} (Wt %)	Fe_{Oxide} (Wt %)	Fe_{Carb} (Wt %)	Fe_{PY} (Wt %)	Fe_{HR} (Wt %)	Fe_T (Wt %)	Fe_{HR}/Fe_T	Fe_{PY}/Fe_{HR}
Doushantuo Fm. Member IV	RX09-56.5	56.5	Black Shale	0.0	2.7		7.4		0.2	0.0	0.0	0.3	0.6	0.92	0.65	0.52
	RX09-57.0	57.0	Black Shale	0.0	3.2		6.2		0.1	0.0	0.1	0.5	0.6	0.53	1.17	0.74
	RX09-57.6	57.6	Black Shale	0.0	4.1		2.3	-15.8	0.1	0.2	0.2	1.5	2.1	2.81	0.73	0.75
	RX09-58.0	58.0	Black Shale	0.0	4.8		2.7	-17.0	0.8	0.4	0.2	1.5	2.9	4.65	0.63	0.52
	RX09-58.8	58.8	Black Shale	0.0	6.8		3.0	-15.6	0.2	0.1	0.1	2.0	2.4	2.86	0.85	0.82
	RX09-59.5	59.5	Black Shale	0.0	7.8		8.3	-14.0	0.6	0.6	0.3	0.8	2.4	3.03	0.79	0.34
	RX09-60.2	60.2	Black Shale	0.0	11.3		6.1	-17.1	0.3	0.1	0.2	1.6	2.2	2.58	0.84	0.74
	RX09-60.8	60.8	Black Shale	0.0	10.9		13.2		0.2	0.1	0.3	0.7	1.3	1.63	0.83	0.53
	RX09-61.2	61.2	Black Shale	0.0	11.7		6.3		0.2	0.2	0.2	1.6	2.2	2.06	1.00	0.72
	RX09-61.8	61.8	Black Shale	0.0	15.3		46.6		0.3	0.3	0.5	0.3	1.3	0.91	1.00	0.21
	RX09-62.5	62.5	Black Shale	0.0	7.3		34.0		0.2	0.2	0.0	0.2	0.6	0.55	1.15	0.30
			Average	0.01	7.82		12.37	-15.92	0.30	0.20	0.19	1.01	1.71	2.05	0.88	0.56
			STDEV	0.0	4.1		14.4	1.3	0.2	0.2	0.1	0.7	0.8	1.3	0.18	0.21

Al (Wt %)	Fe/Al	S_{PY} (Wt %)	Mo (ppm)	Mo/TOC (ppm/Wt%)	V (ppm)	V/TOC (ppm/Wt%)	U (ppm)	U/TOC (ppm/Wt%)	Re (ppb)	Re/TOC (ppb/Wt%)	Re/Mo (ppb/ppm)	Cr (ppm)	Ti (Wt %)	Cr/Ti (ppm/ppm)	Al_2O_3	TiO_2
Al (Wt %)	Fe/Al	S_{PY} (Wt %)	Mo (ppm)	Mo/TOC (ppm/Wt%)	V (ppm)	V/TOC (ppm/Wt%)	U (ppm)	U/TOC (ppm/Wt%)	Re (ppb)	Re/TOC (ppb/Wt%)	Re/Mo (ppb/ppm)	Cr (ppm)	Ti (Wt %)	Cr/Ti (ppm/ppm)	Al_2O_3	TiO_2
5.84	0.16	0.4	44	16	1214	457	7	3	257	97	5.9	121	0.29	0.0419	11.03	0.48
6.53	0.08	0.5	72	22	1378	424	7	2	60	19	0.8	147	0.32	0.0459	12.33	0.53
5.65	0.50	1.8	95	23	947	230	8	2	10	2.4	0.1	92	0.26	0.0349	10.68	0.44
5.66	0.82	1.8	37	8	1071	224	7	2				111	0.29	0.0386	10.69	0.48
5.77	0.50	2.3	69	10	1066	156	8	1	33	4.9	0.5	102	0.3	0.0355	10.90	0.48
5.47	0.55	0.9	81	10	374	48	13	2	3	0.4	0.0	77	0.3	0.0273	10.33	0.47
4.08	0.63	1.8	35	3	137	12	11	1	9	0.8	0.3	59	0.2	0.0276	7.72	0.36
3.77	0.43	0.8	26	2	142	13	11	1	7	0.6	0.3	56	0.2	0.0270	7.13	0.35
4.45	0.46	1.9	47	4	179	15	13	1	6	0.6	0.1	71	0.2	0.0302	8.41	0.39
4.64	0.20	0.3	27	2	221	14	19	1	3585	234	133.9	88	0.3	0.0320	8.76	0.46
2.89	0.19	0.2	12	2	215	29	8	1	37	5.0	3.1	47	0.2	0.0306	5.47	0.26
4.98	0.41	1.16	49.38	9.32	631.23	147.55	10.30	1.50	400.80	36.42	14.51	88.30	0.26	0.03	9.40	0.43
1.1	0.23	0.8	26.1	8.0	497.5	167.4	3.9	0.5	1121.6	75.5	42.0	30.3	0.0	0.0	2.1	0.1

Member IV, Taoying section, Guizou Province, South China—Upper Slope (This Study)

	Sample No.	Strat. Height (m)	Lithology	TIC (Wt %)	C_{org} (Wt %)	DOP	C_{Org}/S_{PY}	$\delta^{34}S_{PY}$ (‰)	Fe_{Mag} (Wt %)	Fe_{Oxide} (Wt %)	Fe_{Carb} (Wt %)	Fe_{PY} (Wt %)	Fe_{HR} (Wt %)	Fe_T (Wt %)	Fe_{HR}/Fe_T	Fe_{PY}/Fe_{HR}
Doushantuo Fm. Member IV	TY09-47.0	47.0	Black Shale	0.0	5.7	0.44	45.9		0.0	0.0	0.0	0.1	0.1	0.27	0.52	0.78
	TY09-48.0	48.0	Black Shale	0.0	4.6		21.7		0.1	0.1	0.3	0.2	0.6	1.00	0.62	0.30
	TY09-49.0	49.0	Black Shale	0.0	4.2	0.19	35.5		0.0	0.1	0.2	0.1	0.4	1.18	0.36	0.24
	TY09-50.0	50.0	Black Shale	0.0	4.9		87.1	40.6	0.1	0.1	0.4	0.0	0.7	0.55	1.22	0.07
	TY09-51.0	51.0	Black Shale	0.0	5.8	0.36	47.4	39.7	0.0	0.1	0.0	0.1	0.2	0.55	0.33	0.59
	TY09-52.0	52.0	Black Shale	0.0	7.0	0.12	53.0		0.2	0.8	0.0	0.1	1.1	0.26	1.00	0.10
	TY09-53.0	53.0	Black Shale	0.0	5.7	0.41	46.0		0.0	0.0	0.0	0.1	0.2	0.49	0.31	0.71
	TY09-55.0	55.0	Black Shale	0.0	7.8	0.18	56.7		0.0	0.4	0.0	0.1	0.5	0.96	0.53	0.24
	TY09-57.0	57.0	Black Shale	0.0	2.9	0.10	21.4		0.1	0.5	0.1	0.1	0.8	2.94	0.27	0.14
	TY09-59.0	59.0	Black Shale	0.0	2.4	0.18	19.0		0.0	0.4	0.0	0.1	0.5	0.76	0.63	0.23
			Average	0.01	5.11	0.25	43.37	40.16	0.04	0.25	0.10	0.11	0.51	0.90	0.58	0.34
			STDEV	0.0	1.7	0.1	20.6	0.6	0.1	0.3	0.2	0.0	0.3	0.8	0.3	0.26

Al (Wt %)	Fe/Al	S_{PY} (Wt %)	Mo (ppm)	Mo/TOC (ppm/Wt%)	V (ppm)	V/TOC (ppm/Wt%)	U (ppm)	U/TOC (ppm/Wt%)	Re (ppb)	Re/TOC (ppb/Wt%)	Re/Mo (ppb/ppm)	Cr (ppm)	Ti (Wt %)	Cr/Ti (ppm/ppm)	Al_2O_3	TiO_2
2.29	0.12	0.1	2	0.4	62	11	2.58	0.45	6.7	1.2	2.9	83	0.123	0.0673	4.33	0.21
7.51	0.13	0.2	17	4	246	54	7.09	1.54	16.7	3.6	1.0				14.18	
9.12	0.13	0.1	2	1	304	72	8.99	2.13	23.3	5.5	9.4	368	0.630	0.0585	17.24	1.05
8.17	0.07	0.1	9	2	1511	309	14.85	3.03	12.8	2.6	1.4				15.43	
6.43	0.09	0.1	4	1	175	30	7.81	1.34	13.5	2.3	3.2	219	0.416	0.0528	12.15	0.69
2.26	0.12	0.1	2	0.3	61	9	2.54	0.36	3.7	0.5	1.6	82	0.121	0.0673	4.26	0.20
5.75	0.09	0.1	3	1	158	28	7.49	1.31	12.9	2.3	4.1	185	0.389	0.0475	10.87	0.65
4.49	0.21	0.1	5	1	127	16	5.52	0.71	5.1	0.6	1.0	162	0.306	0.0529	8.48	0.51
12.36	0.24	0.1	5	2	268	94	9.26	3.23	7.0	2.4	1.5	470	0.743	0.0633	23.36	1.24
3.99	0.19	0.1	2	1	89	37	3.10	1.27	2.1	0.9	1.3	108	0.229	0.0471	7.53	0.38
6.24	0.14	0.13	5.18	1.11	300.18	65.78	6.92	1.54	10.37	2.20	2.74	209.67	0.37	0.06	11.78	0.62
3.2	0.06	0.04	4.6	1.0	433.9	89.6	3.8	1.0	6.6	1.5	2.6	140.9	0.2	0.0	6.0	0.4

Member IV, Wuhe section, Guizou Province, South China—Lower Slope (Sahoo et al., 2014)

	Sample No.	Strat. Height (m)	Lithology	TIC (Wt %)	C_{org} (Wt %)	DOP	C_{Org}/S_{PY}	$\delta^{34}S_{PY}$ (‰)	Fe_{Mag} (Wt %)	Fe_{Oxide} (Wt %)	Fe_{Carb} (Wt %)	Fe_{PY} (Wt %)	Fe_{HR} (Wt %)	Fe_T (Wt %)	Fe_{HR}/Fe_T	Fe_{PY}/Fe_{HR}
Doushantuo Fm. Member IV	WH09-114.5	114.5	Black Shale	1.4	1.1	0.76	1.5	-7.3	0.0	0.0	0.0	0.7	0.7	1.00	0.70	0.98
	WH09-115.3	115.3	Black Shale	0.7	3.8	0.78	2.4	-23.3	0.0	0.0	0.1	1.4	1.5	2.47	0.60	0.95
	WH09-115.5	115.5	Black Shale	0.8	1.5		0.8	-15.1	0.1	0.0	0.1	1.6	1.8	2.45	0.74	0.90
	WH09-115.9	115.9	Black Shale	0.6	2.9		1.6	-23.2	0.1	0.0	0.1	1.6	1.7	2.39	0.72	0.90
	WH09-116.3	116.3	Black Shale	1.5	1.9		1.6	-21.6	0.0	0.0	0.2	1.0	1.2	1.90	0.65	0.84
	WH09-116.8	116.8	Black Shale	0.6	5.0		3.8	-21.5	0.1	0.0	0.1	1.2	1.3	1.80	0.73	0.88
	WH09-117.4	117.4	Black Shale	1.3	5.2		1.9	-15.9	0.1	0.0	0.1	2.4	2.7	3.19	0.83	0.92
	WH09-117.8	117.8	Black Shale	0.8	8.5	0.87	3.5	-14.2	0.0	0.0	0.1	2.1	2.3	3.43	0.67	0.94
	WH09-118.3	118.3	Black Shale	0.8	9.3		4.1	-15.0	0.0	0.0	0.2	2.0	2.2	2.63	0.84	0.90
	WH09-118.9	118.9	Calcareous Shale	4.0	7.0	0.79	5.6	-11.7	0.0	0.0	0.2	1.1	1.2	1.35	0.92	0.87
	WH09-119.5	119.5	Calcareous Shale	3.2	7.1		5.7	-12.7	0.0	0.0	0.2	1.1	1.3	1.45	0.88	0.85
	WH09-120.0	120.0	Calcareous Shale	4.7	4.1	0.76	7.3	-9.9	0.0	0.0	0.1	0.5	0.6	0.84	0.67	0.86
			Average	1.70	4.79	0.79	3.31	-15.96	0.03	0.00	0.11	1.39	1.54	2.08	0.75	0.90
			STDEV	1.4	2.7	0.0	2.1	5.3	0.0	0.0	0.0	0.6	0.6	0.8	0.10	0.04

Al (Wt %)	Fe/Al	S_{PY} (Wt %)	Mo (ppm)	Mo/TOC (ppm/Wt%)	V (ppm)	V/TOC (ppm/Wt%)	U (ppm)	U/TOC (ppm/Wt%)	Re (ppb)	Re/TOC (ppb/Wt%)	Re/Mo (ppb/ppm)	Cr (ppm)	Ti (Wt %)	Cr/Ti (ppm/ppm)	Al_2O_3	TiO_2
2.82	0.35	0.8	2	1.3	92	81	3.0	2.6	15	13	10.0	59	0.14	0.0432	5.33	0.23
7.09	0.35	1.6	68	18.1	2956	785	18.4	4.9	1063	282	15.6	508	0.34	0.1476	13.40	0.57
7.39	0.33	1.9	76	52.2	966	666	13.6	9.4	74	51	1.0		0.44		13.96	0.73
7.98	0.30	1.8	126	43.5	1693	584	13.9	4.8	432	149	3.4		0.47		15.07	0.79
7.11	0.27	1.2	66	33.9	1089	564	11.1	5.8	21	11	0.3		0.43		13.44	0.71
5.67	0.32	1.3	79	15.8	773	154	8.8	1.8	184	37	2.3		0.31		10.71	0.52
5.25	0.61	2.8	95	18.1	278	53	20.4	3.9	51	10	0.5		0.31		9.92	0.51
5.18	0.66	2.5	61	7.2	126	15	20.2	2.4	15	2	0.2	64	0.27	0.0243	9.79	0.44
3.59	0.73	2.3	34	3.7	138	15	13.7	1.5	8	1	0.2	69	0.18	0.0388	6.78	0.30
1.98	0.68	1.2	35	5.1	100	14	31.5	4.5	12	2	0.3	28	0.12	0.0239	3.74	0.20
2.38	0.61	1.2	33	4.7	177	25	19.4	2.7	42	6	1.3	54	0.12	0.0452	4.49	0.20
2.25	0.37	0.6	22	5.5	396	97	18.5	4.5	66	16	2.9	72	0.12	0.0586	4.26	0.21
4.89	0.47	1.59	58.11	17.41	732.06	254.43	16.04	4.06	165.19	48.27	3.19	122.22	0.27	0.05	9.24	0.45
2.2	0.2	0.68	34.5	17.0	863.9	299.4	7.1	2.2	307.2	84.5	4.8	170.8	0.1	0.0	4.2	0.2

Member IV, Jiulongwan Section, Yangtze Geroges, South China—Inner Shelf (Li et al., 2010)

	Sample No.	Strat. Height (m)	Lithology	TIC (Wt %)	C_{org} (Wt %)	DOP	C_{Org}/S_{PY}	$\delta^{34}S_{PY}$ (‰)	Fe_{Mag} (Wt %)	Fe_{Oxide} (Wt %)	Fe_{Carb} (Wt %)	Fe_{PY} (Wt %)	Fe_{HR} (Wt %)	Fe_T (Wt %)	Fe_{HR}/Fe_T	Fe_{PY}/Fe_{HR}	Al (Wt %)	Fe/Al	S_{PY} (Wt %)	Mo (ppm)	Mo/TOC (ppm/Wt%)
Doushantuo Fm. Memb	HN-23	154	Shale/Carbonate	1.1	15.1		6.8	-13.5	0	0.1	0.2	1.9	2.3	3.3	0.7	0.8	5.3	0.6	2.2	181	12
	HN-21	152	Shale/Carbonate	3.7	5.2		4.4	-15.7	0	0	0.1	1	1.1	2.7	0.4	0.9	4.5	0.6	1.2	136	26.3
	HN-18	149	Shale/Carbonate	1.6	6.4		5.8	-13.8	0	0	0.1	1	1.1	2.3	0.5	0.9	4.5	0.5	1.1	111	17.3
	HN-15	146	Shale/Carbonate	1.8	5		3.1	-10.9	0	0	0.1	1.4	1.5	2.7	0.5	0.9	5.4	0.5	1.6	161	32.6
	HN-13	144	Shale/Carbonate	1.1	4.8		4.1	-7.7	0	0	0.1	1	1.1	2.9	0.4	0.9	5.5	0.5	1.2	72	15.1
	HN-09	144	Calcareous Shale	0.9	4.6		2.1	-7.4	0	0.1	0.1	1.9	2.2	2.8	0.8	0.9	4.5	0.6	2.2	114	24.6
	HN-12	143	Calcareous Shale	0.8	5.1		2.1	-6.1	0	0.1	0.1	2.1	2.3	3.1	0.8	0.9	4.4	0.7	2.4	125	24.5
	HN-11	142.2	Calcareous Shale	0.6	2		0.8	-10.7	0	0.1	0.1	2.1	2.2	3.2	0.7	0.9	5.3	0.6	2.4	122	61.5
			Average	1.45	6.03		3.65	-10.73	0.00	0.05	0.11	1.55	1.73	2.88	0.60	0.89	4.93	0.59	1.79	127.74	26.74
			STDEV	1.0	3.9		2.0	3.5	0.0	0.1	0.0	0.5	0.6	0.3	0.17	0.04	0.5	0.1	0.6	33.0	15.6

Member IV, Zhongling Section, Yangtze Geroges, South China—Shelf Margin (Li et al., 2010)

	Sample No.	Strat. Height (m)	Lithology	TIC (Wt %)	C_{org} (Wt %)	DOP	C_{Org}/S_{PY}	$\delta^{34}S_{PY}$ (‰)	Fe_{Mag} (Wt %)	Fe_{Oxide} (Wt %)	Fe_{Carb} (Wt %)	Fe_{PY} (Wt %)	Fe_{HR} (Wt %)	Fe_T (Wt %)	Fe_{HR}/Fe_T	Fe_{PY}/Fe_{HR}	Al (Wt %)	Fe/Al	S_{PY} (Wt %)	Mo (ppm)	Mo/TOC (ppm/Wt%)
IV	SH-42	286	Shale/Carbonate	4	0.1		0.1	22	0	0	0	0.8	0.8	0.9	0.8	1.0	0.7	0.8	0.9	0	4.2
	SH-79	284.5	Black Shale	0	0.6		4.2	16.8	0	0	0	0.1	0.2	0.2	1	0.8	5.1		0.2	0	0.1
	SH-44	282	Shale/Carbonate	7			0.1	22.3	0	0	0	0.1	0.1	0.1	1	0.7	0.1	1.0	0.1	0	
			Average	3.47	0.35		1.47	20.37	0.00	0.00	0.00	0.33	0.37	0.40	0.93	0.83	1.97	0.89	0.40	0.20	2.15
			STDEV	3.4	0.4		2.4	3.1	0.0	0.0	0.0	0.4	0.4	0.4	0.12	0.15	2.7	0.16	0.4	0.2	2.9

Table 2 Micro Probe data for two selected Member II samples.

1. Member II Wuhe section (Sample no. WH09-4.3)

A. Shale matrix

Element	Ca	Si	Mn	S	K	Na	Mg	Al	Fe	Ti	V	Mo	Cr
Spot	wt%	wt%	wt%	wt%	wt%	wt%	wt%	wt%	wt%	ppm	ppm	ppm	ppm
4-71		30.21		0.01	13.00	0.12		9.90	0.10	83		9	140
4-72	0.01	46.76		0.00	0.03	0.00	0.00	0.04	0.05	18	33		93
5-73	0.14	23.04	0.01	0.17	6.32	0.09	1.63	14.09	2.64	4924	334	74	71
5-74	0.09	27.28	0.01	0.03	5.71	0.07	1.10	11.74	1.51	1666	329	16	165
5-75	0.09	25.95	0.01	0.04	7.26	0.12	1.01	13.41	1.48	1957	295		48
5-76	0.08	28.69	0.01	0.01	6.22	0.08	0.98	11.06	1.48	964	362	49	39
5-77	0.09	27.08	0.01	0.28	5.71	0.10	1.21	12.44	1.92	1350	288	83	219
5-78	0.08	27.23		0.03	6.43	0.10	1.06	12.56	1.50	1133	391	62	77
5-79	0.09	26.79	0.02	0.05	5.78	0.14	1.18	12.17	1.59	9067	489		317
5-80	0.08	26.41	0.01	0.24	6.37	0.10	1.05	12.31	1.57	758	252	38	
5-81	0.09	27.42		0.27	6.11	0.09	0.95	11.72	1.32	1154	410	29	453
5-82	0.09	28.03	0.02	0.08	5.74	0.07	1.10	11.61	1.37	1741	283	13	49

B. Pyrite framboids and crystals

Element	Ca	Si	Mn	S	K	Na	Mg	Al	Fe	Ti	V	Mo	Cr
Spot	wt%	wt%	wt%	wt%	wt%	wt%	wt%	wt%	wt%	ppm	ppm	ppm	ppm
8-83		0.10	0.13	51.68			0.01	0.05	45.57		35	6704	57
8-84		0.11	0.02	51.72				0.04	45.07	107		6642	
8-85		0.24	0.02	52.35			0.00	0.08	45.17	296		6841	
8-86		0.21		52.30			0.01	0.06	44.77	451		6685	
8-87		0.23		52.00			0.01	0.06	44.79	121		6574	
10-88		1.57	0.02	43.78			0.05	1.07	37.62	71		6243	156
10-89		1.63		45.40			0.07	1.38	38.78	162		6235	
10-90	0.04	3.93	0.04	39.36			0.25	2.36	34.94	77		5581	
11-91		0.42	0.01	50.16			0.02	0.25	43.34	81		6702	182

2. Member II Yuanjia section (Sample no. WHH-6.4)

A. Shale matrix

Element	Ca	Si	Mn	S	K	Na	Mg	Al	Fe	Ti	V	Mo	Cr
Spot	wt%	wt%	wt%	wt%	wt%	wt%	wt%	wt%	wt%	ppm	ppm	ppm	ppm
14-95	0.04	28.64	0.03	0.15	4.59	0.09	0.75	9.53	0.86	3276	1211	144	
14-96	0.06	30.42		0.09	4.29	0.09	0.70	10.11	0.74	1180	1003	224	26
14-97	0.05	30.30		0.05	3.14	0.07	0.48	7.92	0.68	16835	922	78	43
14-98	0.06	26.39	0.00	0.08	4.63	0.11	0.71	11.80	0.99	3113	1247		
14-99	0.02	34.57		0.06	3.77	0.06	0.57	7.73	0.65	1543	888	93	
14-100	0.09	31.59	0.04	0.06	3.78	0.08	0.61	10.41	0.67	1532	1070	95	
14-101	0.03	33.84	0.00	0.16	3.31	0.05	0.54	6.87	0.69	4462	941	106	
14-102	0.04	34.41		0.05	2.49	0.06	0.39	6.75	0.55	936	708	55	
14-103	0.02	32.13		0.05	4.83	0.07	0.75	9.69	0.82	2465	1112	41	93
14-104	0.08	26.49	0.00	0.08	1.22	0.05	0.25	14.26	0.80	1099	301	58	127
36-135	0.01	0.08						0.05	0.12	9953			212
37-139	0.08	0.91		0.02			0.02	0.16	0.20	9630	1226		170
37-140	0.00	0.13	0.02	0.01				0.06	0.11	9903	2407	10	454
39-141		47.04		0.00	0.03	0.00	0.00	0.05	0.07	13			
39-142	0.00	46.71		0.00	0.07	0.00	0.00	0.17	0.04	180		61	257

B. Pyrite framboids and crystals

Element	Ca	Si	Mn	S	K	Na	Mg	Al	Fe	Ti	V	Mo	Cr
Spot	wt%	wt%	wt%	wt%	wt%	wt%	wt%	wt%	wt%	ppm	ppm	ppm	ppm
12-92		0.13	0.01	52.68				0.04	45.14	96		6874	
12-93		0.28		52.24				0.06	44.99	244	15	6702	130
13-94	0.05	1.86		41.73			0.02	0.71	35.74	104	68	8158	38

Table 3. Molybdenum concentration sensitivity test

Sample	Phase	Measured	Average Mo [c]	Calculated Mo	Bulk Sample Mo [f]	Min | Max	Whole Rock Mo [g]
		wt%	wt%	ppm	ppm	ppm	ppm
WH09-4.3	Pyrite [a]	2.2	6467	142 [d]	182	132 | 185	172
	Shale Matrix [b]	97.8	41	40 [e]			
WHH-6.4	Pyrite [a]	2.4	7245	177 [d]	263	173 | 396	148
	Shale Matrix [b]	97.6	88	86 [e]			

a The percentage of pyrite from titration
b The percentage of matrix = 100% – percentage of pyrite.
c Average Mo measured in pyrite; see Table
d Mo calculated in pyrite = (average Mo measured in pyrite x percentage of pyrite)/100.
e Mo calculated in matrix = (average Mo measured in matrix x percentage of matrix)/100.
f Mo calculated in bulk sample = Mo calculated in pyrite + Mo calculated in matrix.
g Mo calculated in whole rock from ICP analysis; see Table

CURRICULAM VITA

Graduate College
University of Nevada, Las Vegas

Swapan Kumar Sahoo
swapan.sahoo@bp.com

Degrees:

-MS., Earth and Environmental Sciences, 2006, Tulane University, USA
-M.Sc., Applied Geology, 2003, University of Calcutta, India
-B.Sc., Geological Sciences, 2001, University of Calcutta, India

Special Honors and Awards:

- GSA, Research Grant (Outstanding Mention), 2013
- Sigma Xi, Grants-in-Aid of Research, 2013
- SEPM, Student Assistance Grants, 2013
- Academic Achievement Award, 2013
- GPSA Research Forum, Outstanding Presentation, 2013
- Goldschmidt Conference, Travel Grant, 2012
- Graduate Student Professional Association Research Funding, 2011, 2012, 2013
- UNLV Access Grant,
- Edwards & Olswang & Bernada E. French Scholarship in Geology, 2009 – 2012
- International Programs Student Grant, 2011, 2012
- Lawrence L. Sloss Summer Research Award, Northwestern University, 2006 – 2008
- N.N. C Memorial Grant: Geological, Mining and Metallurgical Society of India, 2002
- National Scholarship, Calcutta University, GMMS, India, 2001

Publications:

-Sahoo, K.S., et al., 2014, Oxidation events in the Ediacaran, Geology, *in review*.
-Sahoo, K.S., et al., 2012, Ocean oxygenation in the wake of the Marinoan glaciation, Nature, v. 489, p. 546-549.
-Sahoo, K.S., et al., 2011, An oxygen window for early Ediacaran animal life, Mineralogical Magazine, v. 75, p. 1778.
-Sahoo, K.S., et al., 2010, Geospatial integration of hazards, infrastructure and resources in an assessment of potential disasters and effects of climate change in Clark County, Nevada—Workshop on Natural Resource Needs.
-Sahoo, K. S., 2007, Tectonic Horst: Field Evidence from the South Purulia Shear Zone, India; GSA Annual Meeting.
-Sahoo, K. S., 2003, Thesis: Deformational patterns in the rocks around Jharbagda near Manbazar, West Bengal, India, Dept. of Geology, University of Calcutta.

Professional Experience:

-Applied Geologist – BP America (BP AMERICA ILC), *Current*
--Field Geologist – Geological Society of India, Bangalore, India, 2003 – 2004